THE EFFECTS OF THE IONOSPHERE ON RADIO TRANSMISSIONS FROM EARTH SATELLITES

by

I. A. Parkin, B.Sc.(Hons)

A Thesis

presented for the degree of

DOCTOR of PHILOSOPHY

at the

UNIVERSITY of ADELAIDE

(Physics Department)

February 1967

"The Effects of the Ionosphere on Radio Transmissions from Earth Satellites"

This thesis is made available for loan, or for photo-copying, with my consent.

To my wife, Rosemary.

CONTENTS

SUMMARY

PREFACE

ACKNOWLEDGEMENTS

CHAPTER 1 A SHORT SURVEY OF RADIO METHODS 1

1.1 Historical 1

1.2 Comparison of Methods 4

1.3 Background to Theory 5

1.4 Conclusion 6

CHAPTER 2 THE THEORY OF RADIO STAR AND SATELLITE SCINTILLATIONS 7

2.1 Introduction 7

2.2 The Nature of the Theoretical Treatment 8

2.3 Review of the Theory of the Thin Phase Screen 16

2.4 Weak Scattering by a Thick Screen 21

2.5 Randomly Phased Angular Spectra 42

2.6 Satellite Applications of the Thick Screen Formulation 47

2.7 Conclusion 57

CHAPTER 3 THE APPLICATION OF THEORETICAL TREATMENTS 59

3.1 Introduction 59

3.2 The Zenith Angle Variation of Scintillation Depth 66

3.3 Applications of the Power Spectrum of Amplitude Fluctuations 78

3.4 The Correlation Function of Amplitude Fluctuations at the Ground 88

CHAPTER 4 THE FARADAY EFFECT 95

4.1 Introduction 95

4.2 Theory 95

4.3 Determination of the Total Electron Content 96

CHAPTER 5 INTRODUCTION TO EXPERIMENTAL STUDIES 99

CHAPTER 6 EQUIPMENT AND METHODS 105

6.1 The Satellites 105

6.2 Ground-based Equipment 106

6.3 Computer Programs 111

CHAPTER 7 THE OCCURRENCE CHARACTERISTICS OF SCINTILLATION 115

7.1 Definition of Scintillation Index 115

7.2 Diurnal and Seasonal Variations 116

7.3 Correlation with Spread-F 118

7.4 Correlation with Sporadic-E 120

7.5 Correlation with Magnetic Activity 121

7.6 Variations with Latitude 122

7.7 The Horizontal Distribution of Irregularities 124

CHAPTER 8 ZENITH ANGLE EFFECTS 126

8.1 Effects Average in Azimuth 126

8.2 The Ratio of Scintillation Depths 130

8.3 The Effects of Anisotropy of the Irregularities 132

CHAPTER 9 DETAILED ANALYSES OF SCINTILLATION PATTERNS 140

9.1 Preparation of Data 140

9.2 Spectral Analyses 141

9.3 Correlation Analyses -- Determination of Height, Shape, and Size of Irregularities 142

CHAPTER 10 DEDUCTIONS FROM STUDIES OF THE FARADAY EFFECT 147

10.1 Analyses of Data 147

10.2 The Relationship between Scintillations and Irregularities in Total Content 148

10.3 The Diurnal and Seasonal Variation of Electron Content 149

CHAPTER 11 CONCLUSIONS 151

BIBLIOGRAPHY 156

APPENDIX I The Reflecting Sphere 164

APPENDIX II The validity of: $|\rho_p(\xi)|^2 = \rho a^2(\xi)$ 165

APPENDIX III Reprint of paper: "On the Variation of Radio Star and Satellite Scintillations with Zenith Angle." J.Atmos.Terr.Phys., 1963, 25, 339

APPENDIX IV Reprint of letter: Comments on paper by Lawrence, J.D., and Martin, J.D., J.Geophys.Res., 69, 4186, 1964.

APPENDIX V Reprint of paper: "The study of Ionospheric Irregularities by the use of Signals from Satellites." J.Instn.Telecomm.Engrs., 10, 299, 1964.

SUMMARY

This thesis is concerned with observations of the effects of the ionosphere on radio waves received from earth satellites. Deductions are made about the integrated electron content of the ionosphere, and about the irregularities of electron density which are frequently present.

The first part of the thesis is concerned with the theory required in the interpretation of the observations. The theory of the propagation of radio waves through a medium containing random variations of electron density is first reviewed; the assumption is made that the scattering is "weak". Applications of the theory to practical observations are then considered. It is shown that, in principle, observations of amplitude fluctuations of the received radio waves can be used to determine the following statistical properties of the ionospheric irregularities: (i) the size and axial ratio of the irregularities (ii) the mean height of the layer in which the irregularities exist, and (iii) the thickness of this layer. In some cases several independent methods are available for the determination of these quantities. A particularly interesting prediction of the theory is that the amplitude fluctuations (or "scintillation depth") should be a maximum when the radio waves propagate parallel to the direction of the earth's magnetic field. This arises from the fact that the ionospheric irregularities are elongated and have their long

axis in the direction of the field. The amount of this enhancement is greater the larger the axial ratio of the irregularities. The theoretical section of the thesis concludes with a brief review of the theory of the Faraday effect, and of the method by which this effect can be used to determine the integrated electron content of the ionosphere.

The second part of the thesis describes the equipment used, the observations which were made, and the results obtained. Only the more interesting and unexpected results will be summarized here. It is found that at Adelaide, appreciable scintillation occurs by day as well as by night: the day-time effect is probably due to irregularities in the E-region with a size less than 0.5 km. The enhancement of scintillation depth when the satellite is close to the direction of the magnetic field is observed, but appears to be of a different nature from that predicted by the theory. Unexpectedly, there is often scintillation when the ray path is within a few degrees of the field direction, even when there is no scintillation at all elsewhere on the record for the transit concerned. A tentative explanation for this phenomenon is advanced; it is suggested that extremely long weakly ionised "filaments" must exist in the upper part of the F-region, aligned with the earth's field. This effect is observed only by night. Studies of fluctuations in the total electron content, as observed by the Faraday method, show that these are not related to the

"patches" of small scale irregularities which often occur in the F-region. This fact is an important piece of evidence in deciding between the many theories of irregularity formation which have been advanced. The seasonal dependence of total electron content of the F-region showed no "seasonal anomaly"; it was considerably larger in summer than in winter.

To the best of the author's knowledge this thesis contains no material previously published or written by another person, except where due reference is made. It contains no material which has been accepted for the award of any other degree or diploma in any University, except where due reference is made.

(Ian A. Parkin)

Adelaide University

24/2/67

ACKNOWLEDGEMENTS

The work described in this thesis was carried out in the Physics Department of the University of Adelaide under the supervision of Dr. B.H.Briggs. The author is grateful to Dr. Briggs for help and encouragement throughout the course of the work. Some of the work of Chapter 3 was carried out in collaboration with Dr. Briggs and published in papers under joint authorship. The extent of this joint work is indicated in the text and by the contents of the published papers which are included as Appendices to the thesis.

Many of the author's colleagues in the Upper Atmosphere and Meteor groups of the Physics Department have given invaluable assistance from time to time in the carrying out of the project. The author would particularly like to mention the help received frpm Mr. John Smith and Miss Elizabeth Doyle. Mr. Lindsay Hettner was responsible for much of the mechanical work required in connection with the erection of aerials.

The analysis of the records, involving much tedious work, was carried out by Mrs. Judy Laing, Miss Marilyn Bartlett, and Miss Janice Gordon. The author is also grateful to Mrs. Laing and Miss Bartlett for their careful drawing of the diagrams.

Finance for the project was provided by a grant from the United States Air Force (Grant AFOSR-298-63) and by the University of Adelaide Research Grant. The National Aeronautics and Space

Administration assisted with a loan of two satellite receivers. The author is grateful to the University of Adelaide for the award of a Research Studentship.

CHAPTER 1.

A SHORT SURVEY OF RADIO METHODS

1.1 Historical

The exploration of the ionosphere by the use of radio waves began with the work of Appleton in the 1930's.

An early advance, the use of pulsed transmissions, was pioneered by Breit and Tuve in America and taken up by Appleton in England. The method led to the development of the ionosonde with which a series of heights in the ionosphere are explored by means of a progressive change of radio frequency. Only with the recent development of electronic computers has the full potential of this apparatus been realised, for the conversion of the ionogram, a plot of group delay versus frequency, into a curve showing electron density as a function of height, requires elaborate computations. These computations are now carried out on a routine basis at many stations, and have been applied to the data from both ground-based ionosondes and the so-called "topside sounders" carried in satellites. By combining records obtained from both sources, complete "electron density profiles" can be obtained, showing how the electron density varies with height throughout the whole ionosphere. The study of these results is providing new information about the "large-scale" behaviour of the ionosphere.

While sounding methods were being developed, interesting facts related to the "fine-scale" structure of the ionosphere were noted. It was observed that the echo pulse returned from

the ionosphere was often much longer in duration than the transmitted pulse, and that the different parts of the lengthened echo varied randomly in strength, in a manner suggesting a scattering process. For echoes returned from the F-region of the ionosphere, the phenomenon was particularly marked, and it came to be known as "spread-F".

It was also found that successive members of a series of echo pulses often varied in strength, in a random way, even if the echoes were not "spread". This phenomenon, known as "fading", was studied extensively by Ratcliffe and Pawsey in the late 1930's. Studies using spaced receivers showed that the reflection process in the ionosphere is best thought of in terms of a "random scattering screen" which moves and changes under the action of winds and turbulent motions. These spaced receiver methods are similar in conception to those to be discussed later in this thesis.

The development of radio-astronomy in the 1950's allowed, for the first time, the study of the effects of the ionosphere on a radio wave transmitted right through it. The intensity of radio-stars was found to vary randomly (a phenomenon analogous to the "twinkling" of visible stars) and workers at Cambridge and Jodrell Bank showed the effect to be due to irregularities of ionisation in the ionosphere. "Radio-star scintillation" was found to be present mainly at night, but did not occur every night; a close correlation was established with the occurence of spread-F echoes, suggesting that the same irregularities

were responsible for both phenomena. Further work at Cambridge showed these F-region irregularities to be highly anisotropic, having the form of elongated clouds with their long axes aligned along the geomagnetic field. Such irregularities would be expected to produce "back-scattering" of a radio wave, provided it was incident perpendicular to their long axes; workers at Stanford demonstrated that such "aspect-sensitive" echoes could in fact be observed at frequencies of about 20 Mc/s.

In 1957 the Soviet Union launched the first artificial satellite, Sputnik I, which carried radio transmitters at frequencies of 20 Mc/s and 40 Mc/s. Workers whose interests had lain in the study of radio-star scintillation recognised at that time that such a satellite provided a signal source with advantages not held by a radio-star. Since then, many papers have appeared which discuss "satellite scintillation", and a study of the phenomenon forms the major portion of the present thesis.

The use of transmitting satellites also permitted the determination of the "total electron content" (the total number of electrons in a column of unit area between the observer and the satellite) by a measurement of the total angle of rotation of the plane of polarisation of a radio wave in its passage through the ionosphere. The method, which is known as the Faraday method (the rotation phenomenon was first demonstrated by Faraday in the laboratory), has proved to be a useful supplement to the use of ionosondes. Some results

obtained by the Faraday method are described in this thesis.

1.2 Comparison of Methods

Since the work to be reported here is principally concerned with the study of irregularities, it is appropriate to summarise, in a general way, the advantages and disadvantages of the methods available.

The study of spread-F echoes has the disadvantages that only a part of the ionosphere is sampled - that part which lies below the level of reflection of the wave. Statistics related to the occurrence of spread-F, the daily and seasonal variations and correlations with other geophysical phenomena, are suspect because of this selection effect. Spurious correlations may be introduced by changes in the reflection level due to variation of the mean, or "ambient", electron density. From this point of view, studies of radio-star and satellite scintillations, in which the whole of the ionosphere is involved, are preferable.

The "whole of the ionosphere" property of scintillation observations would itself be a disadvantage if the height at which irregularities occur was unknown. Fortunately, in the case of satellite studies, a method is available for determining the height, and this is explained in a later Chapter.

The study of fading echoes provides some information regarding the shapes and sizes of irregularities if spaced receiver methods are used. However, the appropriate theory is complex, for the scattering which occurs near the reflection level of the wave is inevitably strong. In contrast, radio-star

and satellite methods permit the choice of operating frequencies which are so high that the effects of the ionosphere on the wave are slight, and a weak scattering theory can be used. Under these conditions, the scale of the signal irregularities observed by spaced receivers is simply related to the scale of irregularities in the ionosphere.

The use of a satellite as a radio source, rather than a radio-star, has some advantages and some disadvantages. One important advantage is that the satellite can be regarded as having negligible angular diameter; effects arising from the finite size of the source can be neglected. Also, since the satellite moves rapidly from horizon to horizon and passes over a large region of the ionosphere, it is especially useful in locating irregularities which are confined to more or less localised "patches". A disadvantage lies in the high speed of the satellite source, compared with which, drift speeds of ionospheric irregularities are very small; these cannot be measured by satellite methods as they can when a radio-star is used. A compensating advantage is found here, however, in the satellite method for determination of irregularity height.

1.3 Background to Theory

The first half of these thesis is concerned with the treatment of some theoretical problems and it may be useful to review briefly the background to these.

The basic theory of radio wave propagation in an ionised gas in the presence of a magnetic field was developed by Appleton

and Hartree and based on Lorentz's "Theory of Electrons". The "magneto-ionic" theory provides a complicated expression for the refractive index under very general conditions, and this has been the key to the understanding of many complex phenomena taking place in the ionosphere.

In the present work, the only aspect requiring the full theory is that relating to the Faraday effect where the presence of the earth's magnetic field is essential. For the rest of the work, relating to the scattering of high frequency radio waves by irregularities of electron concentration, it can be shown that the earth's magnetic field has negligible effect. The formula for the refractive index becomes very simple and depends only on the number of free electrons per unit volume and the wave frequency.

Much of the theory relating to random diffraction is quite general and is not restricted to radio applications. Extensive use is made of Fourier methods and correlation functions, as pioneered by Ratcliffe at Cambridge, especially in connection with spaced receiver experiments.

1.4 Conclusion

This chapter is intended to provide a broad survey of the general background to the work to be discussed. More detailed surveys, with references, are given at appropriate points in the thesis.

CHAPTER 2.

THE THEORY OF RADIO STAR AND SATELLITE SCINTILLATIONS

2.1 Introduction

In this chapter and the next a review is given of the theory relevant to studies of radio star and satellite scintillations. The division into two chapters follows the distinction between what may be called "pure" theory, in which diffraction by an irregular screen is discussed in fairly general terms, and "applied" theory, in which results previously obtained are made specific to the real ionosphere and observational practice.

The discussion of these chapters is applicable to both radio star and, with slight modification, satellite observations of scintillation. The two-fold context is therefore maintained in the theory although the experimental work described in later chapters involved only satellite studies.

The formation of amplitude patterns only is considered as the amplitude of a received signal as the quantity most easily and most often observed. None but amplitude observations were made in the work described later.

The discussion of the present chapter is divided into five sections. In Section 2.2 the type of theoretical treatment appropriate to scintillation studies is

outlined. This is, very often, a "weak scattering" treatment and the remainder of the chapter describes situations in which the scattering of radiation is assumed to be weak. Diffraction by a thin screen is considered in Section 2.3 and the treatment of a thick screen is given in Section 2.4. This has a bearing on the properties of "randomly phased spectra" which are discussed in Section 2.5. In Section 2.6 it is shown how the thick screen theory applies to the motion of the amplitude pattern on the ground when the radio source moves across the sky.

2.2 The Nature of the Theoretical Treatment

2.2.1 The Refractive Index of the Irregular Ionosphere

At the radio frequencies commonly used for observations of radio star or satellite scintillations the Appleton-Hartree expression for the refractive index becomes simple in all regions of the ionosphere. "Magneto-ionic" and "collision" terms in the expression become, to the first order, negligible and the radio frequency is well removed from the plasma frequency. The refractive index may be written then:

$$n \doteq 1 - \frac{\lambda^2 r_e N}{2\pi}, \qquad (2.1)$$

where λ is the radio wavelength, N is the electron density and r_e is a constant equal to the classical electron radius.

Since the refractive index deviates little from unity the ray path between a radio source and a receiver can usually be taken to be a straight line; in particular, the ray path is straight in a region containing weak irregularities of ionization. Within such a region the mean refractive index (averaged over a volume containing many irregularities) may be given a value of unity without serious error, and the small fluctuations about the mean are given by

$$\Delta n = - \frac{\lambda^2 r_e \Delta N}{2\pi} \qquad (2.2)$$

Equation (2.1) gives a real value for n indicating that, at the frequencies of interest, a wave passes through the ionosphere without appreciable absorption. A thin irregular region behaves as a phase-modulating screen which produces no amplitude fluctuation in a wave emergent from it. Over a short distance ℓ in such a screen, the change of phase suffered by a wave, relative to that of an unmodulated wave experiencing the same mean refractive index, is

$$\begin{aligned} \phi &= \frac{2\pi}{\lambda} \int_0^{\ell} \Delta n \, d\ell \\ &= - r_e \lambda \int_0^{\ell} \Delta N \, d\ell \ , \end{aligned} \qquad (2.3)$$

the integral being taken, as suggested previously, along a rectilinear ray path through the medium. Since Δn

is small, so is the deviation of phase, ϕ. It is assumed in fact throughout this chapter, that ϕ, as obtained by integrating right through a region of irregularity, does not exceed, at any point of the wave front, a value of about one radian. This is in effect the assumption that scattering by the irregular medium is weak. Cases where the assumption is not valid are considered in Chapter 3.

Ionospheric irregularities are usually much larger in size than the radio wavelengths used in scintillation studies. (Compare the scales, of the orders of kilometres, mentioned in Chapter I, with wavelengths of tens of metres).

Scattering of radiation occurs, therefore, over a very small range of angles. This, and the fact that equation (2.1) contains no terms relating the refractive index to the geomagnetic field*, imply that both in propagation, and when summed at any point, the scattered wave field may be treated in a scalar fashion.

---

* Yeh (1965) has considered the magneto-ionic splitting of scattered components of a wave field. His results indicate that the effect has no relevance to scintillation studies in the Earth's ionosphere.

(This is not so when second-order terms are included in the expression for the refractive index. The Faraday effect, to which this point has relevance, is discussed in Chapter 4.)

2.2.2. Statistical measures

The fluctuations of electron content which produce scintillations are irregular to the extent that interest is not usually shown in their detailed structure, but in their structure in the mean. Exceptions occur in the discussions of single "lenses" of Warwick (1964) and Dagg (1957) and others, but these structures are usually of a larger scale than those considered here. The requirement of specifying the behaviour of irregularly varying quantities has led to the adoption of several statistical measures which, for completeness, are defined here.

The averaging process, implicit in most statistical measures, can be performed in two ways. If $\underset{\sim}{f}(x)$ is a complex random function (the symbol '~' will henceforth denote a complex, or more generally, a vector quantity), its spatial average is given by:

$$\lim_{x_0 \to \infty} \frac{1}{2x_0} \int_{-x_0}^{x_0} \underset{\sim}{f}(x)\,dx$$

The assembly average, $\overline{\underset{\sim}{f}(x_1)}$ is defined as the value of $\underset{\sim}{f}$ at the point x_1, averaged over an assembly of such

functions $\underset{\sim}{f}$, all of which arise in the same stationary random process.

The notations of, in one case the integral form and, in the other, the bar, will be used in the following work to distinguish the two types of average.

The variance, or mean squared deviation, of $\underset{\sim}{f}$, defined by

$$\sigma^2_{\underset{\sim}{f}} = \lim_{x_0 \to \infty} \frac{1}{2x_0} \int_{-x_0}^{x_0} |\underset{\sim}{f}(x) - \underset{\sim}{f}_0|^2 \, dx \quad ,$$

where $\underset{\sim}{f}_0$ is the spatial mean of $\underset{\sim}{f}$, is a well known measure of the depth of fluctuation of $\underset{\sim}{f}(x)$. An analogous definition in terms of the assembly average can be written.

The spatial cross-correlation function of two functions $\underset{\sim}{f}(x)$ and $\underset{\sim}{g}(x)$, with spatial means $\underset{\sim}{f}_0$ and $\underset{\sim}{g}_0$ is

$$\rho_{\underset{\sim}{f},\underset{\sim}{g}}(\xi) = \frac{\int_{-\infty}^{\infty} [\underset{\sim}{f}(x) - \underset{\sim}{f}_0][\underset{\sim}{g}(x+\xi) - \underset{\sim}{g}_0]^* \, dx}{\left\{ \int_{-\infty}^{\infty} |\underset{\sim}{f}(x) - \underset{\sim}{f}_0|^2 \, dx \cdot \int_{-\infty}^{\infty} |\underset{\sim}{g}(x) - \underset{\sim}{g}_0|^2 \, dx \right\}^{\frac{1}{2}}}$$

where the symbol '*' denotes complex conjugation. Again, a definition in terms of the assembly average can be written.

When applied to one function alone, the auto-correlation function $\rho_{\underset{\sim}{f},\underset{\sim}{f}}$ takes a value of unity for

$\xi = 0$ and decreases in absolute value as the "shift", ξ, increases. The value of ξ for which the absolute value falls to some specified level, like 0.5 or e^{-1}, gives a measure of the spatial scale of the fluctuations of f.

The measures of a random function $f(x)$ which are most representative of the process in which it arises are those defined in terms of assembly averages. In practice, however, and in scintillation studies in particular, spatially defined measures are often more easily obtained and two assumptions must be made: firstly, that $f(x)$ is a stationary random variable (Briggs (1961) has described a case where this assumption cannot be made); secondly, the ergodic assumption, that in the assembly average, spatially defined measures tend in value to their assembly-average-defined analogues.

A full discussion of the validity of these assumptions is not merited as the accuracy of experimentally determined measures is limited in other respects. Recordings of satellite scintillations are made as the satellite moves across the sky. As time passes the geometry of the scattering process, and the nature of the effective part of the ionosphere, change and the temporal record is not statistically stationary. To achieve a

degree of stationarity the record must be broken into short lengths and this may preclude the taking of an accurate spatial average. The work of Awe (1964) and that of McGee (1960) show the differences that can arise between correlation functions derived from short data samples and the assembly-averaged values of these functions.

The theory discussed in the following pages is derived in terms of assembly-averaged values of spatially defined quantities. When, later in this thesis, experimental results are discussed, the matter of their approximation to the assembly-average will again be taken up.

2.2.3 Mathematical method

In discussing aspects of ionospheric diffraction the "Fourier" approach will be used. This, as opposed to the "scattering" method in which spherical scattered wavelets are simply summed at a receiver, has the advantage of showing, via the "angular spectrum", the way in which structure impressed on the wavefront is carried to the receiver. The question: "How is the ionosphere imaged on the ground?", is thereby answered in a direct way.

In order to simplify the treatment, several abbreviations are used; these are outlined below:

The temporal phasor of the wave field, $\exp\{iwt\}$, is omitted throughout.

Complex and vector quantities are denoted by an under-written "~"; the context makes clear which type of quantity is intended.

The limits of all integrations are to be taken as $-\infty$ and $+\infty$ unless otherwise specified. The order of integration in multiple integrals is frequently changed without reference to the fact; the integrands involved will normally be well-behaved functions.

The limiting notation involved in defining the spectrum of a function which itself is defined in an infinite space is omitted. Thus:

$$\underset{\sim}{F}(X,Y,Z) = \lim_{\substack{x_o\to\infty \\ y_o\to\infty \\ z_o\to\infty}} \frac{1}{8x_o y_o z_o} \int_{-x_o}^{x_o}\int_{-y_o}^{y_o}\int_{-z_o}^{z_o} \Delta N(x,y,z) \times \exp\{2\pi i[xX+yY+zZ]\}dxdydz ,$$

will be written

$$\underset{\sim}{F}(X,Y,Z) = \iiint \Delta N(x,y,z)\exp\{2\pi i[xX+yY+zZ]\}dxdydz$$

and may be further abbreviated to:

$$\underset{\sim}{F}(\underset{\sim}{R}) = \int \Delta N(\underset{\sim}{r})\exp\{2\pi i\ \underset{\sim}{r}\cdot\underset{\sim}{R}\}d\underset{\sim}{r}$$

where $\underset{\sim}{r}\cdot\underset{\sim}{R}$ denotes a scalar product.

In thinking of Fourier transform space it is convenient to consider the X,Y,Z axes to be parallel

to the x,y,z axes of real space. $\underset{\sim}{P}(\underset{\sim}{R})$ is then the complex amplitude of the real wave whose wavelength is $1/|\underset{\sim}{R}|$ and whose wave normal is parallel to $\underset{\sim}{R}$.

2.3 Review of the Theory of the Thin Phase Screen

2.3.1 The Angular Spectrum:

Consider the geometry of Figure (2.1). A thin layer of ionospheric irregularities, infinite in x and y and described by $\Delta N(x,y)$, lies in the (0,x,y) plane of a Cartesian axial frame. The layer, of thickness (dz) is at a height h above the ground in which the origin O' is fixed.

A plane v.h.f. wave of unit amplitude and wavelength λ is incident normally on the layer and emerges phase-modulated; its phase deviation is, by equation (2.3),

$$\phi(x,y) = -r_e \lambda \Delta N(x,y) dz. \qquad (2.4)$$

If ΔN has the two dimensional spectrum

$$\underset{\sim}{Q}(X,Y) = \iint \Delta N(x,y) \exp\left\{2\pi i[xX + yY]\right\} dxdy, \qquad (2.5)$$

then the spectrum of ϕ is:

$$- r_e \lambda dz \underset{\sim}{Q}(X,Y).$$

It is assumed, in accordance with the discussion of Section 2.2.1, that no component of the spectrum of ϕ exceeds one radian in amplitude. The thin scattering layer then behaves as an ideal "thin phase screen" and

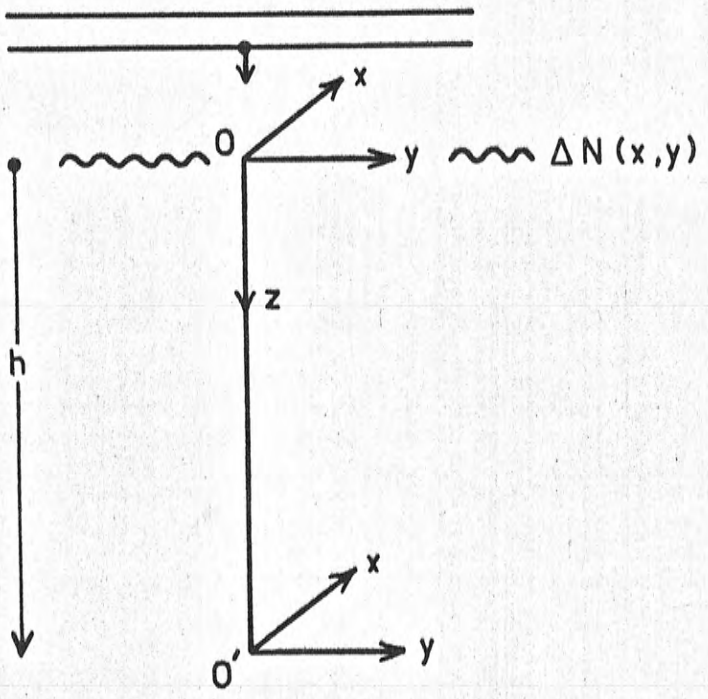

Figure (2.1). The geometry for normal, plane wave illumination of a thin scattering screen.

the angular spectrum of scattering is linearly related to the spectrum of ϕ. The angular spectrum is given by:

$$\underset{\sim}{F}(\nu) = \delta(\nu_x, \nu_y) - ir_e\lambda dz\underset{\sim}{Q}(\nu_x, \nu_y) \qquad (2.6)$$

where $|\underset{\sim}{\chi}| = 1/\lambda$. The term $\delta(\nu_x, \nu_y)$ indicates the presence of a strong unscattered component in the emergent wave field. With the assumption above, that the scattered field is weak, the delta function may be given unit amplitude without serious error.

2.3.2 Propagation of the Spectrum

Hewish (1951), Ratcliffe (1956) and Bowhill (1961a) have described the manner in which the angular spectrum of equation (2.6) propagates through the distance h to the ground. The wavefront at first only phase-modulated, develops an amplitude modulation, the spatial spectrum of which is given at the ground by:

$$\underset{\sim}{A}(X,Y) = - r_e\lambda dz\underset{\sim}{Q}(X,Y)\sin[\pi h\lambda(X^2 + Y^2)]. \qquad (2.7)$$

The corresponding assembly-averaged power spectrum of amplitude fluctuations is

$$V(X,Y) = (r_e\lambda dz)^2\,\overline{|\underset{\sim}{Q}(X,Y)|^2}\sin^2[\pi h\lambda(X^2 + Y^2)]. \qquad (2.8)$$

These equations apply for normal illumination of the screen. Budden (1965) has given the expression for V(X,Y) when the illumination is oblique and a similar expression is derived in Section 2.4.4.

2.3.3 The Amplitude Pattern at the Ground

All the important properties of the amplitude diffraction pattern at the ground can be derived from the spectra expressed above. The mean amplitude is determined by the unscattered, "specular" component of the angular spectrum and has a value of unity in the present treatment. The deviation of amplitude from the mean is given by:

$$a(x,y) = \iint \mathcal{A}(X,Y)\exp\left\{-2\pi i(xX + yY)\right\}dXdY. \qquad (2.9)$$

The application of Parseval's theorem to this relationship gives an expression for the variance of $a(x,y)$; thus, in the assembly-average

$$\sigma_a^2 = \iint \overline{a^2(x,y)}\,dxdy = \iint V(X,Y)\,dXdY \qquad (2.10)$$

This quantity, when normalised by the value of the mean amplitude, is used as a measure of scintillation depth. Hewish (1952) and P.W.James(private communication) have derived expressions for σ_a^2 in special cases and that of James is used extensively in Section 2 of Chapter 3.

The two-dimensional auto-correlation function of the amplitude fluctuations, $\rho_a(\xi,y)$, is related to the power spectrum V by

$$\rho_a(\xi,\eta) = \frac{1}{\sigma_a^2}\iint V(X,Y)\exp\left\{-2\pi i[X\xi+Y\eta]\right\}dXdY \qquad (2.11)$$

Bowhill (1961a) has used this relationship to derive a functional form for the correlation function in a special case; its properties are considered briefly in Section 4 of Chapter 3.

2.3.4 The Power Spectrum of Amplitude Fluctuations

The amplitude power spectrum $V(X,Y)$ of equation (2.8) deserves study in its own right; in some respects it describes the diffraction process in a more straightforward manner than do the quantities derived from it. The most important feature of the expression for V is the relative isolation of the terms $|\underset{\sim}{Q}(X,Y)|^2$, which describes the scattering of radiation, and $\sin^2 \pi h\lambda(X^2 + Y^2)$ which describes the subsequent diffraction. The effects on the power spectrum of changes in either process can be simply studied if the other is held constant. The simplicity is lost if attention is turned to quantities like σ_a^2 or ρ_a which are derived from V. Under Fourier transformation the product of the terms above becomes a convolution which is not so easily visualised.

Figure (2.2) shows the behaviour of the power spectrum V (in X-section) as distance, h, from the thin screen, increases. The "fringe function", $\sin^2\left\{\pi h\lambda X^2\right\}$ moves inward towards the origin of transform space with a consequent increase, from zero to a limiting

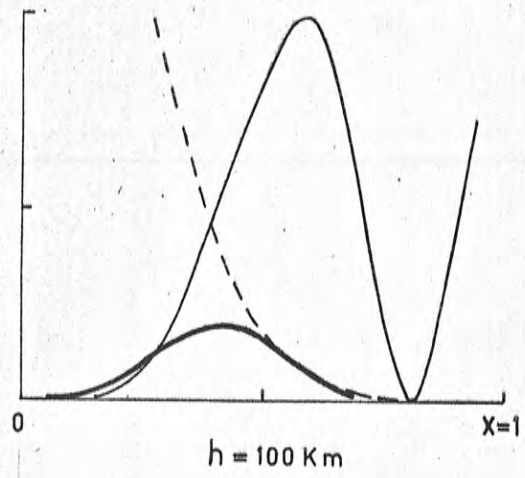

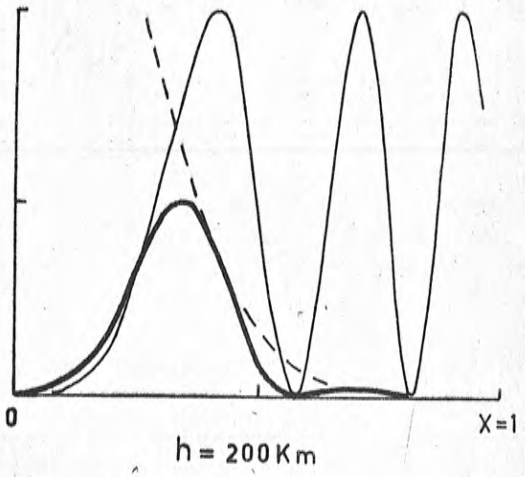

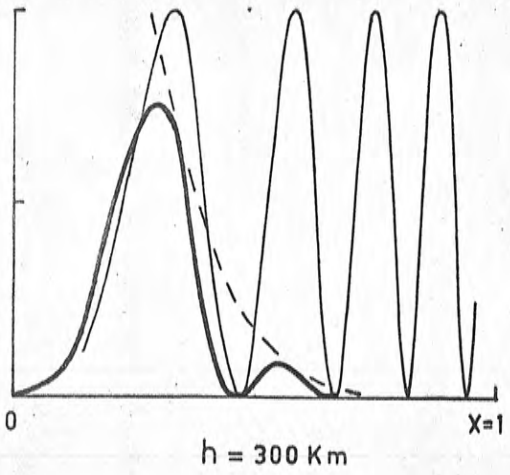

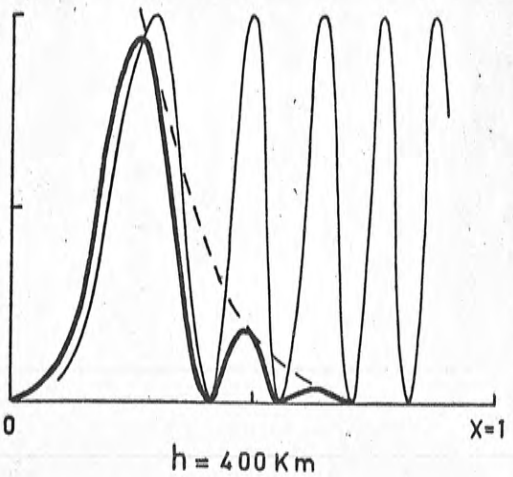

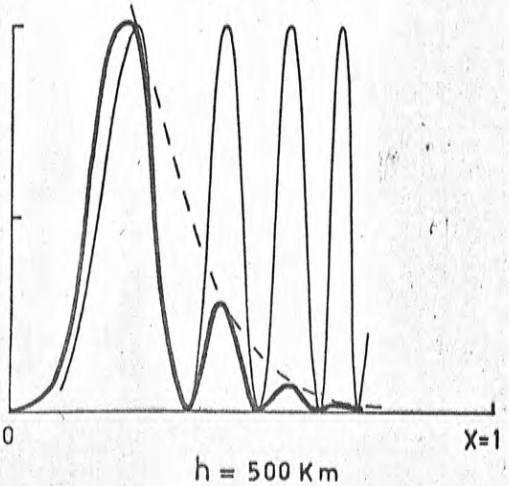

Figure (2.2) Showing the variation of the X-section of the spectrum V (heavy line), with height h. (X in Km^{-1}). The plots are for normal illumination at 20 Mc/s, and the power spectrum of the screen (dashed line) has the form $\exp(-\pi^2 r_o^2 X^2)$, with r_o = 1Km. The "fringing function" is shown to half scale by the light line.

value, of the area under the curve for V. Now this area is related in an obvious manner to the variance of amplitude fluctuations σ_a^2 (see equation (2.10)) its behaviour reflects the increase of scintillation depth with increasing distance from the screen. The growth in spatial scale of the amplitude correlation function ρ_a, described by Kaiser (1956) and Bowhill (1961a) can likewise be seen in terms of the decreasing frequencies at which the power in V is concentrated.

An instance of the application of the simple properties of the amplitude power spectrum is a method described variously by Hewish (1951) and Briggs and Parkin (1964), determining the height of a scattering layer: note is taken of the positions of the fringe zeros in the spectrum and these lead directly to a value for h in the argument of the fringe function. The method is fully discussed in Section 3 of Chapter 3.

In considering this method it becomes clear that if the scattering layer were to thicken (while remaining weakly scattering), a number of overlapping fringe functions would arise in the amplitude power spectrum. The apparent effect would be a "filling in" of the fringe zeros of the thin screen. This may destroy the "visibility" of the fringes, rendering impossible the method outlined above, or if not so marked, may

provide another measure, that of layer thickness.

Budden (1965) has examined the situation in a special case and has verified these possibilities. It has been the interest of the present author to derive the thick screen's amplitude power spectrum in a form more easily visualised than Budden's expressions allow, and to give in particular, an explicit relationship between the visibility of the fringe system and the layer thickness; this last Budden did not do. The treatment is given in the following section.

2.4 Weak Scattering by a Thick Screen

2.4.1 Description of the Screen

Reference is now made to Figure (2.3) in which the axial frames are the same as those previously defined.

Consider first an ionosphere infinite in three dimensions containing statistically stationary fluctuations of electron density $\Delta N(x,y,z)$; 0 is the origin of coordinates. Let ΔN have the spatial spectrum $\underset{\sim}{P}(X,Y,Z)$; the assembly-average power spectrum is

$$W(X,Y,Z) = \overline{\underset{\sim}{P}(X,Y,Z)\underset{\sim}{P}^{*}(X,Y,Z)}. \qquad (2.12)$$

The assembly-average correlation function of the medium is

$$\rho_N(\xi,\eta,\zeta) = \frac{1}{\sigma_{N^2}}\iiint W(X,Y,Z)\exp\left\{-2\pi i(\xi X+\eta Y+\zeta Z)\right\}dXdYdZ \qquad (2.13)$$

where the variance of ΔN is

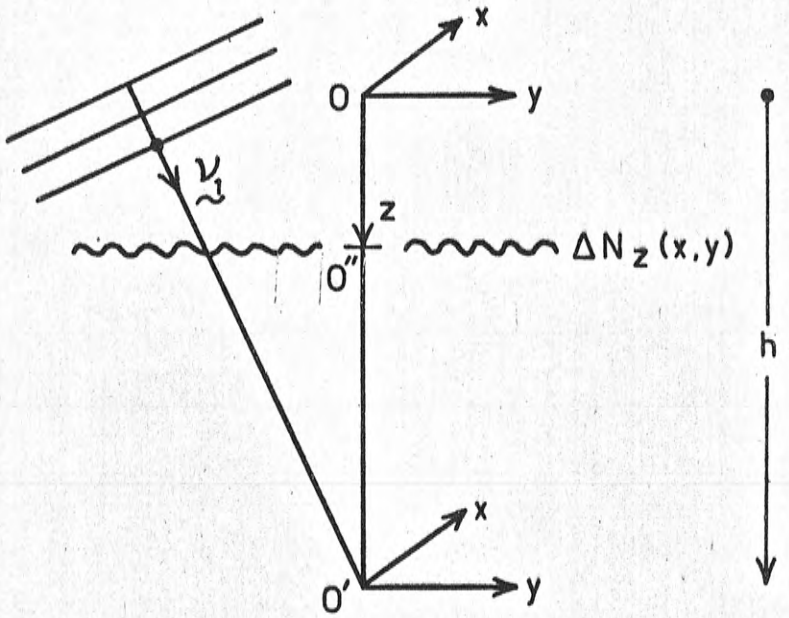

Figure (2.3). The geometry for oblique, plane wave illumination of a thick scattering screen.

$$\sigma_N^2 = \iiint W(X,Y,Z)dXdYdZ.$$

A thin screen of the type previously discussed is obtained by taking a horizontal section of the three dimensional distribution. The thin layer at a distance z below O is

$$\Delta N_z(x,y) = \Delta N(x,y,z)$$

and has a spatial spectrum

$$\underset{\sim}{Q}_z(X,Y) = \int \underset{\sim}{P}(X,Y,Z)\exp\left\{-2\pi i Z z\right\}dZ \qquad (2.14)$$

when expressed relative to the origin O" within the thin layer.

The thick scattering screen is created by modulating $\Delta N(x,y,z)$ with the vertically varying profile function $s(z)$ where

$$0 \leq s(z) \leq 1$$

When assembly averages are taken it is assumed that $s(z)$ is constant over the assembly of thick screens.

This formulation of the thick screen is effectively that given by Budden (1965).

2.4.2 Scattering by the Thick Screen

The scattered spectrum arising from illumination of the thick screen is obtained by summing the spectra produced in a succession of thin screens of the type described by ΔNz. It is again assumed that the wave emergent from the thick screen contains a specular part

which is large compared with the scattered components. This is in effect the Born approximation for it implies that none of the elementary thin screens scatters strongly and therefore, that second order scattering is negligible.

Consider as in Figure (2.3) a plane wave of unit amplitude, wavelength λ and wave normal ν_1 (where $|\nu_1| = \frac{1}{\lambda}$) incident on the thin screen at a distance z below O. If at O the wave has zero phase, it is described at O" by

$$\exp\left\{-2\pi i z\, \underset{\sim}{\nu}_1 . \underset{\sim}{k}\right\}$$

where $\underset{\sim}{k}$ is the unit vector in the z direction. The angular spectrum arising in the thin screen is then, expressed phase-relative to O":

$$F_z(\underset{\sim}{\nu}) = \frac{-ir\,e\,dz}{\underset{\sim}{k}.\underset{\sim}{\nu}_1} \mathcal{G}_z(\underset{\sim}{\nu}-\underset{\sim}{\nu}_1)\exp\left\{-2\pi i z \underset{\sim}{\nu}_1 . \underset{\sim}{k}\right\}$$

and, phase-relative to O:

$$F_z(\underset{\sim}{\nu}) = \frac{-ir\,e\,dz}{\underset{\sim}{k}.\underset{\sim}{\nu}_1} \mathcal{G}_z(\underset{\sim}{\nu}-\underset{\sim}{\nu}_1)\exp\left\{-2\pi i z (\underset{\sim}{\nu}_1-\underset{\sim}{\nu}).\underset{\sim}{k}\right\}. \qquad (2.15)$$

The delta function $\delta(\underset{\sim}{\nu}-\underset{\sim}{\nu}_1)$, describing the unscattered wave, has for convenience been omitted from these expressions. The preceding constants in the expressions contain reference to the slant thickness of the screen in the form $dz/(\lambda \underset{\sim}{k}.\underset{\sim}{\nu}_1)$.

2.4.3 The Angular Spectrum of an Infinite Medium

It is of interest first to consider the angular spectrum of an infinite three-dimensional medium.

Substituting in the last expression above, for Qz from equation (2.14), and integrating through the medium, gives

$$\underset{\sim}{G}(\underset{\sim}{\nu}) = iC\int\int \underset{\sim}{P}[(\underset{\sim}{\nu}-\underset{\sim}{\nu}_1)_x,(\underset{\sim}{\nu}-\underset{\sim}{\nu}_1)_y,Z]\exp\left\{+2\pi iz[(\underset{\sim}{\nu}-\underset{\sim}{\nu}_1)_z-Z]\right\}dZdz$$

where C is a real constant and

$$(\underset{\sim}{\nu}-\underset{\sim}{\nu}_1)_z = (\underset{\sim}{\nu}-\underset{\sim}{\nu}_1).\underset{\sim}{k}$$

is the Z-component of $(\underset{\sim}{\nu}-\underset{\sim}{\nu}_1)$.

Then

$$\underset{\sim}{G}(\underset{\sim}{\nu}) = iC\int \underset{\sim}{P}[(\underset{\sim}{\nu}-\underset{\sim}{\nu}_1)_x,(\underset{\sim}{\nu}-\underset{\sim}{\nu}_1)_y,Z]\delta[Z-(\underset{\sim}{\nu}-\underset{\sim}{\nu}_1)_z]dZ$$

$$= iC\underset{\sim}{P}(\underset{\sim}{\nu}-\underset{\sim}{\nu}_1). \qquad (2.16)$$

This is essentially the result obtained by Bowhill (1961b) by a more complicated method. It illustrates the fact, not mentioned by Bowhill, that when the Born approximation is valid, the angular spectrum of scattering is obtained by sampling the spatial spectrum of scattering material on the "Reflecting Sphere". This sphere, often used in studies of X-ray scattering [James (1948), Ratcliffe (1956)] is of radius $1/\lambda$ and is centred at $-\underset{\sim}{\nu}_1$ in Fourier transform space, $\underset{\sim}{\nu}_1$ being, of course, the illuminating wave vector. The concept is mentioned here as it has

application in the work to follow.

2.4.4 The Spectrum of Amplitude Fluctuations on the Ground

After propagating through the height h, the angular spectrum of equation (2.15) is given at the point $\underset{\sim}{r} = (r_x, r_y)$ in the ground plane by:

$$\underset{\sim}{F}'_z(\underset{\sim}{\nu}) = \frac{-ir_e dz}{\underset{\sim}{k}\cdot\underset{\sim}{\nu}_1} \cdot \mathcal{Q}_z(\underset{\sim}{\nu}-\underset{\sim}{\nu}_1)\exp\left\{-2\pi i(z\underset{\sim}{\nu}_1\cdot\underset{\sim}{k} + (h-z)\underset{\sim}{\nu}\cdot\underset{\sim}{k} + \underset{\sim}{\nu}\cdot\underset{\sim}{r})\right\}$$

At the same point, the unscattered wave is

$$\delta(\underset{\sim}{\nu}-\underset{\sim}{\nu}_1)\exp\left\{-2\pi i(h\underset{\sim}{\nu}_1\cdot\underset{\sim}{k} + \underset{\sim}{\nu}_1\cdot\underset{\sim}{r})\right\} .$$

Since the unscattered wave is of much larger amplitude than the scattered components, the amplitude fluctuation at the ground is given by those parts of the wave field which are in phase with the unscattered wave. These parts are extracted by expressing $F'_z(\underset{\sim}{\nu})$ phase-relative to the unscattered wave at each point $\underset{\sim}{r}$ and then taking the real part of the signal resulting from the "rephased" spectrum. This signal is

$$\underset{\sim}{f}_z(\underset{\sim}{r}) = \frac{-ir_e dz}{\underset{\sim}{k}\cdot\underset{\sim}{\nu}_1}\int \mathcal{Q}_z(\underset{\sim}{\nu}-\underset{\sim}{\nu}_1)\exp\left\{-2\pi i[(h-z)\underset{\sim}{k}+\underset{\sim}{r}]\cdot(\underset{\sim}{\nu}-\underset{\sim}{\nu}_1)\right\}d\underset{\sim}{\nu} \quad (2.17)$$

the integral being taken over all $\underset{\sim}{\nu}$ for which $|\underset{\sim}{\nu}| = 1/\lambda$. The amplitude fluctuation is given by the real part of this, namely:

$$a_z(\underset{\sim}{r}) = \tfrac{1}{2}[\underset{\sim}{f}_z(\underset{\sim}{r}) + \underset{\sim}{f}^*_z(\underset{\sim}{r})] \quad (2.18)$$

and the spatial spectrum of amplitude fluctuations by

$$\underset{\sim}{A}_z(X,Y) = \int a_z(\underset{\sim}{r}) \exp\left\{ 2\pi i (Xr_x + Yr_y) \right\} d\underset{\sim}{r} \qquad (2.19)$$

The expression for $\underset{\sim}{A}_z(X,Y)$ is obtained by substituting equation (2.17) into equation (2.18), and that into equation (2.19). The algebra of these steps is cumbersome and is omitted. When the integrations are performed in a manner similar to those of Section 2.4.3 the expression is obtained:

$$\underset{\sim}{A}_z(X,Y) = \frac{-ir_e dz}{2(\underset{\sim}{k}\cdot\underset{\sim}{\nu}_1)} \underset{\sim}{Q}_z(X,Y)\left\{ \exp[-2\pi i(h-z)Z_1] - \exp[2\pi i(h-z)Z_1'] \right\} \qquad (2.20)$$

In writing this, the equality $\underset{\sim}{Q}^*(-X,-Y) = \underset{\sim}{Q}(X,Y)$ has been used, reflecting the fact that $\Delta N(x,y)$ is a real function and the screen produces a phase-modulated wave. Were an amplitude-modulating screen considered, the working to this point would follow that given above, but the analogue of this last equality would contain a negative sign on the right hand side (or, equivalently, the imaginary unit i would not appear in the expression for $\underset{\sim}{A}_z(X,Y)$).

The quantity Z_1 appearing in the expression for $\underset{\sim}{A}_z(X,Y)$ is the Z-coordinate of the point on the reflecting sphere of $\underset{\sim}{\nu}_1$ whose X- and Y- coordinates are the X and Y of the expression. This geometry is shown in Figure (2.4). Z_1' has a similar meaning when the X- and Y- coordinates

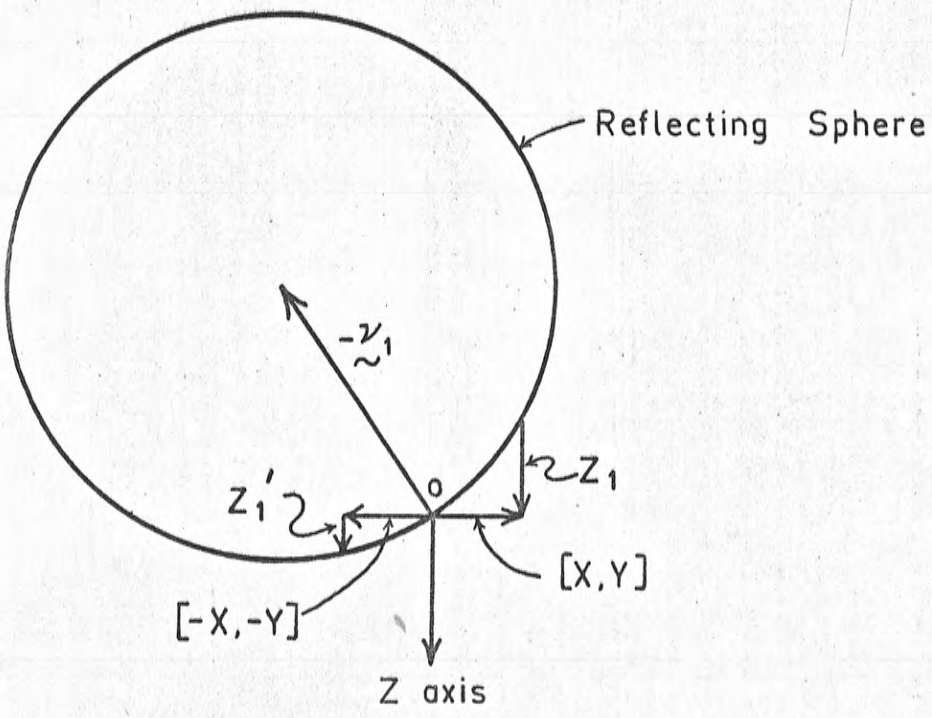

Figure (2.4). A section through the reflecting sphere which is associated with the wave vector $\underset{\sim}{\nu}_1$ in Fourier transform space. Z_1 and Z_1' are the ordinates of the points on the sphere whose horizontal coordinates are [X,Y] and [-X,-Y] respectively.

are -X and -Y. It should be noted that Z_1 and Z_1' are not independent variables but functions of both $\underset{\sim}{\varrho}_1$ and coordinates (X,Y). The functional relationship between these quantities is given in Appendix I, but for the sake of simplicity the Z_1, Z_1' notation is maintained in the following work.

Equation (2.20) is the extension to oblique illumination of the amplitude spectrum given for normal illumination in equation (2.7).

2.4.5 Extension to the Thick Screen

The assembly-averaged cross-spectrum is now expressed for the case when the thick screen is illuminated by two wave vectors $\underset{\sim}{\varrho}_1$ and $\underset{\sim}{\varrho}_2$. This cross-spectrum is the Fourier transform of the (unnormalised) cross correlation function of the two amplitude patterns arising from the illumination. The extension to the thick screen is achieved by integrating $A_z(X,Y)$, modulated by the profile function s(z), with respect to z. The integral is taken over $-\infty,+\infty$ on the assumption that the scattering layer lies wholly between the source of radiation and the ground. Although s(z) was defined in terms of the scattering medium it may be applied to the spectrum $\underset{\sim}{A}_z(X,Y)$ since the relationship between $\underset{\sim}{Q}_z(X,Y)$ and $\Delta N_z(x,y)$ is linear.

The amplitude cross-spectrum is, then:

$$\underset{\sim}{\Gamma}_{12}(X,Y) = \frac{re^2}{4(\underset{\sim}{k}\cdot\underset{\sim}{\nu}_1)(\underset{\sim}{k}\cdot\underset{\sim}{\nu}_2)} \iint s(z_1)s(z_2)\,\overline{\underset{\sim}{\varrho}_{z_1}(X,Y)\underset{\sim}{\varrho}^{*}_{z_2}(X,Y)}$$

$$\times \Big[\exp\Big\{-2\pi i[(h-z_1)z_1-(h-z_2)Z_2]\Big\}$$

$$+ \exp\Big\{2\pi i[(h-z_1)z_1'-(h-z_2)Z_2']\Big\}$$

$$- \exp\Big\{-2\pi i[(h-z_1)Z_1+(h-z_2)Z_2']\Big\}$$

$$- \exp\Big\{2\pi i[(h-z_1)Z_1'+(h-z_2)Z_2]\Big\}\Big] dz_1\,dz_2 \qquad (2.21)$$

where z_1 and z_2 are two z-like variables.

Writing $z_2 = z_1 + \zeta$, (2.22)

and making use of equation (2.14) gives

$$\overline{\underset{\sim}{\varrho}_{z_1}(X,Y)\underset{\sim}{\varrho}^{*}_{z_2}(X,Y)} = \iint \overline{\underset{\sim}{P}(X,Y,\Psi)\underset{\sim}{P}^{*}(X,Y,\Psi+\psi)}$$

$$\times \exp\Big\{2\pi i(z_1\psi+\zeta\Psi+\zeta\psi)\Big\} d\Psi\, d\psi$$

where $\underset{\sim}{P}$ is the three-dimensional spectrum of the medium. Now, since the irregularities of the medium are random and statistically stationary in space, there is no correlation between different components of $\underset{\sim}{P}$. That is

$$\overline{\underset{\sim}{P}(X,Y,\Psi)\underset{\sim}{P}^{*}(X,Y,\Psi+\psi)} = \begin{cases} \overline{|P(X,Y,\Psi)|^2}, & \text{for } \psi=0, \\ 0, & \text{for } \psi \neq 0. \end{cases}$$

The ψ-integrand takes non-zero values only at $\psi=0$, the variable z_1 disappears (reflecting the spatial stationarity) and

$$\overline{\underset{\sim}{\varrho}_{z_1}(X,Y)\underset{\sim}{\varrho}^{*}_{z_1+\zeta}(X,Y)} = \int W(X,Y,\Psi)\exp\left\{2\pi i\zeta\Psi\right\}d\Psi, \qquad (2.23)$$

the power spectrum $W(X,Y,\Psi)$ being substituted from equation (2.12).

The profile function, $s(z)$, may be expressed in terms of its Fourier transform, $S(\sigma)$, thus:

$$s(z) = \int \underset{\sim}{S}(\sigma)\exp\left\{-2\pi i\sigma z\right\}d\sigma. \qquad (2.24)$$

The phase origin of $\underset{\sim}{S}(\sigma)$ is the origin 0, at which $s(z)$ is defined.

When equations (2.22), (2.23) and (2.24) are substituted into the expression (2.21) for $\underset{\sim}{\gamma}_{12}$ the variables z_1 and ζ only occur in factors of an exponential form. The integrations over these variables are easily performed and lead to the equation:

$$\underset{\sim}{\gamma}_{12}(X,Y) = \frac{re^2}{4(\underset{\sim}{k}\cdot\underset{\sim}{\nu}_1)(\underset{\sim}{k}\cdot\underset{\sim}{\nu}_2)} \times$$

$$\left\{\exp[-2\pi ih(Z_1-Z_2)]\int \underset{\sim}{S}(Z_1-\Psi)\underset{\sim}{S}^{*}(Z_2-\Psi)W(X,Y,\Psi)d\Psi\right.$$

$$+ \exp[2\pi ih(Z_1'-Z_2')]\int \underset{\sim}{S}(-Z_1'-\Psi)\underset{\sim}{S}^{*}(-Z_2'-\Psi)W(X,Y,\Psi)d\Psi$$

$$- \exp[-2\pi ih(Z_1+Z_2')]\int \underset{\sim}{S}(Z_1-\Psi)\underset{\sim}{S}^{*}(-Z_2'-\Psi)W(X,Y,\Psi)d\Psi$$

$$\left.- \exp[2\pi ih(Z_1'+Z_2)]\int S(-Z_1'-\Psi)S^{*}(Z_2-\Psi)W(X,Y,\Psi)d\Psi\right\}. \qquad (2.25)$$

This is the required form for the cross-spectrum of amplitude fluctuations.

2.4.6 The Power Spectrum

The power spectrum of amplitude scintillations

is obtained from the equation above by putting $\chi_1 = \chi_2$; when this is done,

$$\underset{\sim}{V}_{11}(X,Y) = \frac{re^2}{\pi(\underset{\sim}{k}.\underset{\sim}{\nu}_1)} \left\{ \int |\underset{\sim}{S}(Z_1-\Psi)|^2 W(X,Y,\Psi)\,d\Psi \right. \qquad - (A)$$

$$+ \int |\underset{\sim}{S}(-Z_1'-\Psi)|^2 W(X,Y,\Psi)\,d\Psi \qquad - (B)$$

$$- \exp\{-2\pi i h(Z_1+Z_1')\} \int \underset{\sim}{S}(Z_1-\Psi)\underset{\sim}{S}^*(-Z_1'-\Psi)W(X,Y,\Psi)\,d\Psi. \qquad (C)$$

$$\left. - \exp\{2\pi i h(Z_1+Z_1')\} \int S(-Z_1'-\Psi)S^*(Z_1-\Psi)W(X,Y,\Psi)\,d\Psi \right\}. \qquad (D)$$

(2.26)

The sources of the various terms in this equation are of considerable interest. In describing them reference is made to the diagrams of Figure (2.5) which show portions of the reflecting sphere intercepting the power spectrum W. W is represented by one of its contours, which is drawn as an ellipse, but no particular form is intended.

The term (A) of equation (2.26) describes the convolution of $W(X,Y,\Psi)$ with the function $|\underset{\sim}{S}(-\Psi)|^2$ centred on Z_1; so as X and Y vary, the latter function "moves" over the surface $Z_1(X,Y)$, which is the reflecting sphere of χ_1. The hatched area of Figure (2.5a) represents the portion of W which is "sampled" by this movement.

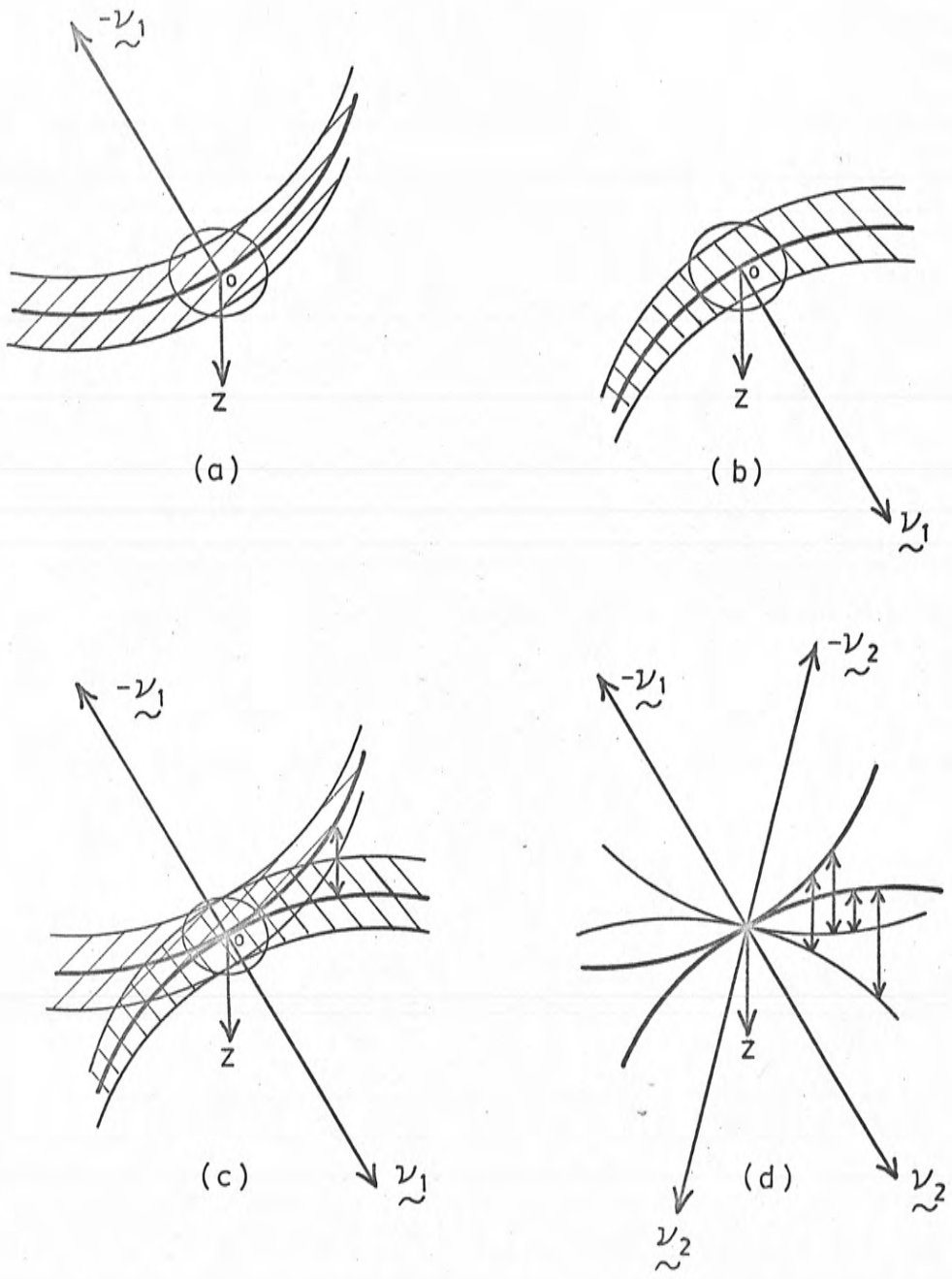

Figure (2.5). The "sources" of the terms in equation (2.26). In (a), (b) and (c) the power spectrum of the medium (elliptical contour) is sampled in various ways by the transformed profile function moving over reflecting spheres. (d) shows the four "interactions" appropriate to illumination by two different wave vectors.

The term (B) arises from a similar convolution with $|\underset{\sim}{S}(-\Psi)|^2$ centred on $-Z_1'(X,Y)$. Now $Z_1'(X,Y) = Z_1(-X,-Y)$, so the surface $-Z_1'(X,Y)$ is obtained by reflecting $Z_1(X,Y)$ in the vertical Z axis and then in the (X,Y) plane; it is in fact the reflecting sphere of $-\underset{\sim}{\chi}_1$, centred at $\underset{\sim}{\chi}_1$ in transform space. Figure (2.5b) shows the geometry appropriate to term (B).

Terms (C) and (D) are now seen to arise in the region of overlap of the parts of W involved in the preceding terms. This region is shown by cross hatching in Figure (2.5c). The "interaction" between the two reflecting spheres is also indicated by the double-headed arrow in this figure. The exponential factors in terms (C) and (D) are associated with the "fringe function" of the type seen previously.

The form of the expression (2.26) for $\underset{\sim}{V}_1$ is not obvious; it might be expected, when the infinite medium is shaped by the profile function, that the convolution of $W(X,Y,Z)$ and $|\underset{\sim}{S}(Z)|^2$ would be sampled by the reflecting sphere. This is not the case; rather is W sampled by the convolution of the sphere with $|\underset{\sim}{S}(Z)|^2$. The appearance of the second reflecting sphere is also an unexpected feature.

In conclusion of this section attention is directed to Figure (2.5d) where the interactions involved

in the formation of the cross spectrum $\underset{\sim}{Y}_{12}$ (equation 2.25) are indicated. Four reflecting spheres, those of $\underset{\sim}{\rho}_1$ and $\underset{\sim}{\rho}_2$, $-\underset{\sim}{\rho}_1$ and $-\underset{\sim}{\rho}_2$ are shown in the diagram.

2.4.7 Applications of the Expression for the Power Spectrum

The Thin Screen

The thin screen is simulated by putting

$$s(z) = \delta(z);$$

$\underset{\sim}{S}(\Psi)$ is then independent of Ψ and takes a value of unity. Equation (2.26) then gives:

$$\underset{\sim}{Y}_{11}(X,Y) = \frac{re^2}{2(\underset{\sim}{k}\cdot\underset{\sim}{\nu}_1)^2}\left[\int W(X,Y,\Psi)d\Psi\right]\left\{1-\cos 2\pi h(Z_1+Z_1')\right\} \qquad (2.27)$$

which is easily shown to be equivalent to the expression (2.20) for the amplitude spectrum of the thin screen at oblique incidence. The factor

$$\int W(X,Y,\Psi)d\Psi$$

is the power spectrum of an infinitely thin, horizontal sample of the medium whose power spectrum is $W(X,Y,Z)$ (compare equation (2.23)).

The Infinitely Thick Screen

If the screen is considered to be infinitely thick,

$$\underset{\sim}{S}(\Psi) = \delta(\Psi).$$

The overlap region of Figure (2.5.c) disappears except at the origin, and

$$V_{11}(X,Y) = C\left\{W(X,Y,Z_1) + W(X,Y,-Z_1') - 2W(0,0,0)\right\} \qquad (2.28)$$

where C is some real constant. The spectrum is sampled on the reflecting sphere only and the fringing of the amplitude power spectrum disappears.

At $X=Y=0$, $Z_1=Z_1'=0$ and $V_{11}(0,0)=0$ corresponding to removal of the specular component in Section 2.4.4. This zero at the origin point is not an important feature of the spectrum; it would not appear in fact if V was derived in terms of a screen of finite horizontal size, the size subsequently tending to infinity. No "point" structure can exist in the spectrum of a screen of non-infinite aperture.

The Screen of Finite Thickness

Consideration is now given to an important case lying between the two extremes just described. Two assumptions are made:

(i) that the screen is thick enough to contain a number (of the order of ten or more) of typical

irregularities in its vertical extent. The scale of the transformed profile, $\underset{\sim}{S}$, is then several times smaller than the Z-dimension of W. If W(X,Y,Z) is a smoothly-varying function of Z it is approximately constant in Z throughout the region sampled by $\underset{\sim}{S}(Z)$, and may be set equal to its value on the appropriate reflecting sphere.

(ii) that the wavelength λ is much smaller than the scales typical of the irregularities of the medium and, as a result, the radius of the reflecting sphere ($\frac{1}{\lambda}$) is much larger than the values of X and Y for which W is appreciable. Figure (3.1) illustrates the situation for a case to be described later. The two reflecting spheres (of $\underset{\sim}{\nu}_1$ and $-\underset{\sim}{\nu}_1$) approximate their common tangent plane near the origin and for given X and Y, the value of W, as sampled by either sphere, may be taken to be that on the tangent plane. That is, to a sufficient approximation, the value $W[X,Y,(Z_1-Z_1')/2]$.

With these assumptions, the amplitude power spectrum may be written:

$$V_{11}(X,Y)=\frac{re^2}{2(\underset{\sim}{k}\cdot\underset{\sim}{\nu}_1)^2}\,W[X,Y,(Z_1-Z_1')/2]\left[\int|\underset{\sim}{S}(\Psi)|^2\,d\Psi\right]$$

$$\times\Big\{1-\tfrac{1}{2}\exp[-2\pi ih(Z_1+Z_1')]\;\underset{\sim}{\rho}S(Z_1+Z_1')$$

$$-\tfrac{1}{2}\exp[2\pi ih(Z_1+Z_1')]\;\underset{\sim}{\rho}^{*}S(Z_1+Z_1')\Big\}$$

$$=\frac{re^2}{2(\underset{\sim}{k}\cdot\underset{\sim}{\nu}_1)^2}\,W[X,Y,(Z_1-Z_1')/2]\left[\int|\underset{\sim}{S}(\Psi)|^2\,d\Psi\right]$$

$$\times \left\{1-\cos[2\pi h(z_1+z_1')]R[\underset{\sim}{\rho}S(z_1+z_1')] - \sin[2\pi h(z_1+z_1')]\Im[\underset{\sim}{\rho}S(z_1+z_1')]\right\} \qquad (2.29)$$

where $\underset{\sim}{\rho}S$ is the auto-correlation function of the profile function $\underset{\sim}{S}$:

$$\underset{\sim}{\rho}S(z) = \frac{\int \underset{\sim}{S}(z-\Psi)\underset{\sim}{S}^*(-\Psi)d\Psi}{\int |\underset{\sim}{S}(-\Psi)|^2 d\Psi}, \qquad (2.30)$$

and R and $\Im$ indicate real and imaginary parts.

The function $\underset{\sim}{\rho}S$ is proportional to the Fourier transform of the square of the profile function; that is, of $s^2(z)$, and the real and imaginary parts of $\underset{\sim}{\rho}S$ are related respectively to the even and odd parts of $s^2(z)$ about z=o. Now $s^2(z)$ cannot be purely odd, the profile s(z) being purely real, so it is assumed for simplicity that s(z) (and $s^2(z)$) are purely even. Then $\underset{\sim}{\rho}S$ is purely real and

$$V_{11}(X,Y) = \frac{re^2}{2(\underset{\sim}{k}\cdot\underset{\sim}{\chi}_1)^2} W[X,Y,(z_1-z_1')/2]\left[\int |S(\Psi)|^2 d\Psi\right] \times \left\{1-\cos 2\pi h(z_1+z_1')\cdot\rho S(z_1+z_1')\right\} \qquad (2.31)$$

Comparison of this form with that for the thin screen (equation (2.27)) shows directly the effect of screen thickness on the "fringe function" which is given by the last factor in each expression. For the thick screen the minima of this function do not take the value

zero (compare Figure (2.2)) but lie on the curve $(1-\rho S)$. This constitutes the "filling-in" of the zeros alluded to previously.

Figure (2.6) is a plot of the section $V_{11}(X)$ (equation (2.31)) showing the effect. It is drawn for the following situation: A plane wave, of wavelength 15 metres, is normally incident on an "ionospheric" scattering layer of mean height 1000 km. The profile of this layer is given by $s(z)=\exp(-z^2/L^2)$, where $L = 100$ km. The corresponding function ρS, expressed as a function of X by means of the result derived in Appendix I, is shown by a dashed curve. The horizontal section $W(X)$, of the power spectrum W, has the form $\exp(-\pi^2 r_0^2 X^2)$ where $r_0 = 1$ km (corresponding to "gaussian" irregularities of typical radius 1 km). This section is also shown by a dashed curve. The curves are plotted on an arbitrary vertical scale and reference to the constant $\int |\underset{\sim}{S}(\Psi)|^2 d\Psi$ is omitted.

The (heavy) curve for V_{11} is seen to oscillate between the envelope curves $\frac{1}{2}W(X)[1+\rho S(X)]$ and $\frac{1}{2}W(X)[1-\rho S(X)]$ at a rate determined by the argument of the cosine term in equation (2.31). Were such a plot to be obtained experimentally, the following information could be derived: the envelope curves could be drawn in, tangent to the fringes of V_{11}; the

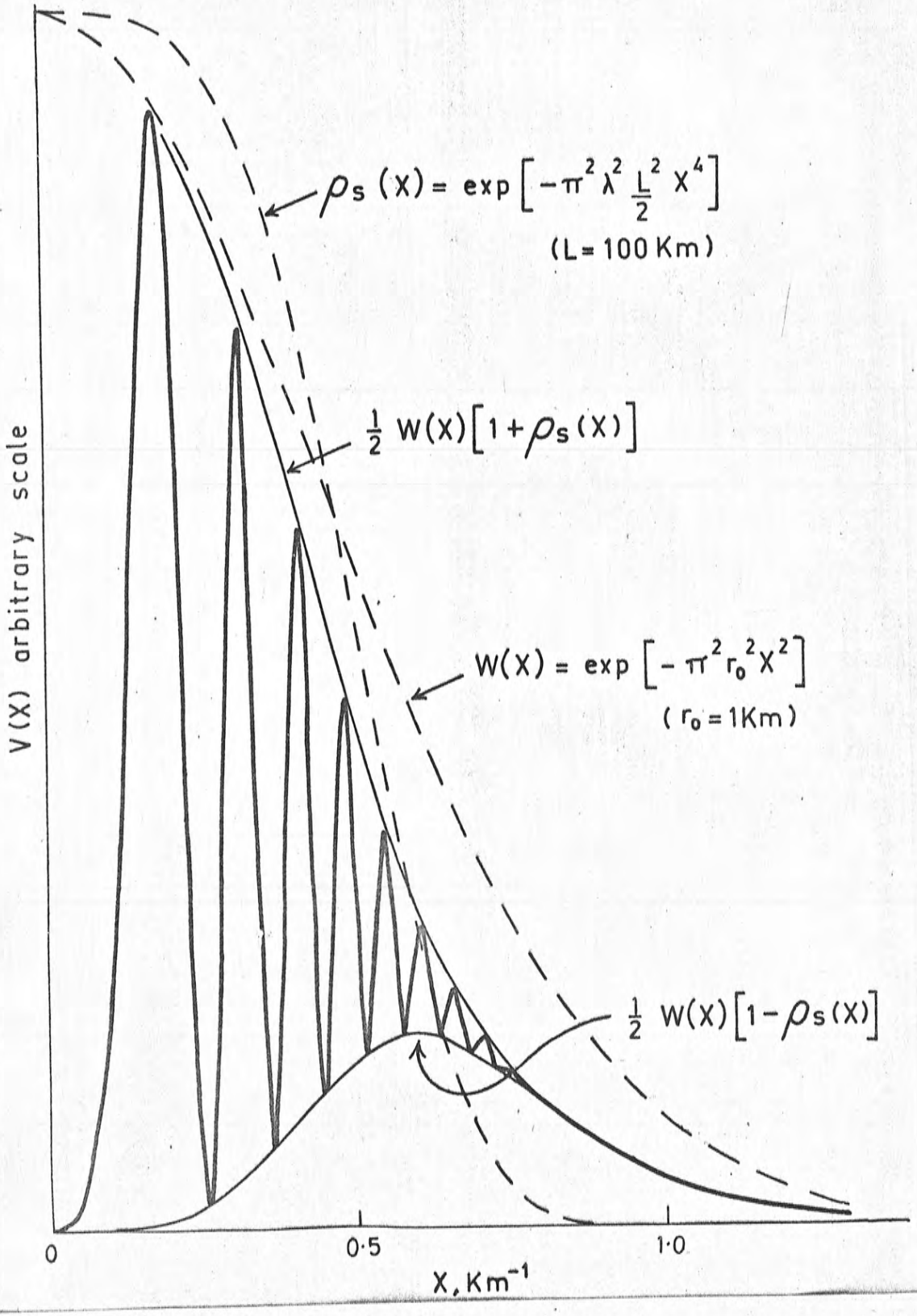

Figure (2.6). The amplitude power spectrum at the ground (heavy line) for normal illumination of a thick screen, and the functions from which it derives. Details are given in the text.

sum, at each X, of these has the form of W(X), and the difference, of $W(X).^{\rho}S(X)$; both functions could be determined, one describing the irregularities of the medium ($^{\rho}N$), and the other the layer profile ($s^2(z)$); the effects of these functions on the fringe function could be removed and the mean height of the scattering layer derived from the (varying) periodicity of the fringes.

The layer height of 1000 km. for which Figure (2.6) is drawn is too large to be typical of the irregular ionosphere. Adequate illustration of the discussion requires a large number of fringes in the spectrum and a large value was therefore assumed for the height. In application to the real ionosphere the procedure outlined above may suffer since fewer fringes will be available to define the envelope curves. This matter is further discussed in Section 3.3 of Chapter 3.

As was suggested earlier, the "filling-in" of the spectral fringe minima can be seen in the summation of a series of thin-screen fringes whose periodicities depend on the heights at which they arise in the thick screen. It was proposed that a measure of screen thickness could be obtained from the power spectrum and this has been done for a fairly general case - the

measure is $^{\rho}S$.

A different approach to the formation of the power spectrum, and a particular meaning for $^{\rho}S$, is given in the next section.

2.4.8 The Visibility of Thick-Screen Spectral Fringes

When, in the classical "Young's double slit" experiment, two narrow slits are illuminated with coherent wave fields, an intensity distribution of the form $1 + \cos\phi$ appears on a distant screen; ϕ is the phase difference of the two waves arriving at the general point of the screen. If the wave fields at the slits are not perfectly coherent, the intensity distribution takes the form $1 + v\cos\phi$ where the quantity v, called the visibility, is less than unity in absolute value.

The "fringe function" of equation (2.31) has a very similar form and the visibility of the spectral fringes is, by analogy, given by the correlation function $^{\rho}S$. The analogy drawn has further significance for the visibility of the double slit fringes can also be expressed in terms of a correlation function. If the wave fields at the slits are $\mathfrak{f}_1$ and $\mathfrak{f}_2$, their visibility is given by

$$v = |\mathfrak{f}\mathfrak{f}| = \frac{|\overline{\mathfrak{f}_1\mathfrak{f}_2^*}|}{(|\mathfrak{f}_1|^2\,|\mathfrak{f}_2|^2)^{\frac{1}{2}}} \qquad (2.32)$$

The similarity between the formulations is now examined.

The analogy can be traced to a point early in the preceding treatment. In Section 2.4.4 the thin-screen spectra $\underset{\sim}{Q}_z(X,Y)$ and $\underset{\sim}{Q}_z^*(-X,-Y)$ were combined on a propagation-phase basis to give the amplitude spectrum $\underset{\sim}{A}_z(X,Y)$ of equation (2.20). For given X and Y this process is formally the same as combining, on a propagation-phase basis, the wave fields of two slits. The operative "slits", $\underset{\sim}{Q}_z(X,Y)$ and $\underset{\sim}{Q}_z^*(-X,-Y)$, in the thin-screen case, give rise to fringe structure of unit visibility. For, since $\underset{\sim}{Q}_z$ is the spectrum of the real function $\Delta N_z(x,y)$,

$$\underset{\sim}{Q}_z^*(-X,-Y) = \underset{\sim}{Q}_z(X,Y),$$

and applying the "definition" of equation (2.32),

$$v = \frac{|\underset{\sim}{Q}_z(X,Y)[\underset{\sim}{Q}_z^*(-X,-Y)]^*|}{|\underset{\sim}{Q}_z(X,Y)| \cdot |\underset{\sim}{Q}_z^*(-X,-Y)|} = \frac{\underset{\sim}{Q}_z(X,Y)\underset{\sim}{Q}_z^*(X,Y)}{|\underset{\sim}{Q}_z(X,Y)|^2}$$

$$= 1 ,$$

for all X and Y. The unit visibility and perfect zeros of the thin-screen amplitude spectrum (and amplitude power spectrum) have already been noted.

The "slit" $\underset{\sim}{Q}_z(X,Y)$ is related, by infinite integration over Ψ, to all the points $\underset{\sim}{p}(X,Y,\Psi)$ of the

spectrum $\mathcal{P}$(equation (2.14)); $\mathcal{Q}_z^*(-X,-Y,)$ is, similarly, related to all the points $\mathcal{P}(-X,-Y,-\Psi)$. The result established above could in fact have been shown by using the relationship:

$$\mathcal{P}^*(-X,-Y,-\Psi) = \mathcal{P}(X,Y,\Psi),$$

which holds since $\Delta N(x,y,z)$ is real. The result, or this relationship, shows that $\mathcal{P}$ contributes equally to the "slits" $\mathcal{Q}_z(X,Y)$ and $\mathcal{Q}_z^*(-X,-Y)$.

Now as the thin screen becomes thicker, the transformed profiles $\mathcal{S}[Z_1(X,Y)-\Psi]$ and $\mathcal{S}^*[Z_1(-X,-Y)+\Psi]$ (which is $\mathcal{S}^*[Z_1^{-1}(X,Y)+\Psi]$) become narrower in their Ψ-distributions and sample less than an infinite range of $\mathcal{P}(X,Y,\Psi)$ and $\mathcal{P}^*(-X,-Y,-\Psi)$ respectively. The situation is depicted in Figure (2.7). The samples, which are now the operative "slits" are not disposed symmetrically relative to the origin of transform space so each contains some points of $\mathcal{P}$ not contained by the other. The coherence of the "slits" therefore falls, as does the visibility of the fringes produced. The function $^{\rho}S$ in equation (2.31) measures this effect, being large when $\mathcal{S}(Z_1-\Psi)$ and $\mathcal{S}^*(-Z_1^{-1}-\Psi)$ are greatly "overlapped" and the "slits" have many points in common, and vice versa.

In the limiting case of the infinitely thick screen, $S(\Psi) = \delta(\Psi)$, $^{\rho}S(Z_1+Z_1^{-1}), = \delta(Z_1+Z_1^{-1})$

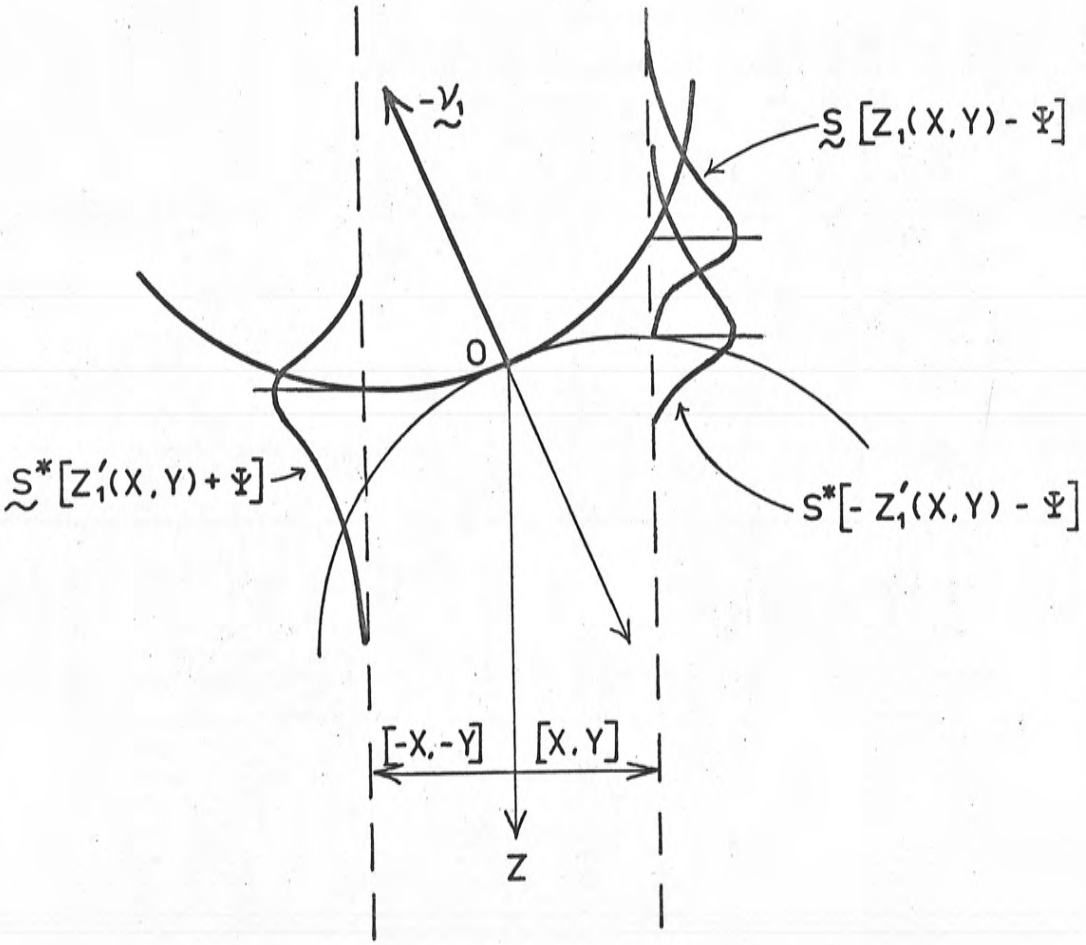

Figure (2.7). Showing the locations, in transform space, of the samples taken by the functions $S[Z_1 (X,Y) - \Psi]$ and $S^*[Z_1 (X,Y) + \Psi]$. These samples, which are not disposed symmetrically, one to another, about the origin O, "interfere" to give fringe structure in the amplitude power spectrum at the ground. The visibility of the structure is determined partially by the size of the region where $S(Z_1 - \Psi)$ and $S^* (-Z_1 - \Psi)$ (the reflection of $S^*(Z_1 + \Psi)$ in O) overlap.

and $\mathcal{E}$ is sampled only on the reflecting sphere. The "slits" $\mathcal{E}(X,Y,Z_1)$ and $\mathcal{E}(-X,-Y,Z_1')$ have no symmetry relationship connecting them and are unrelated. The fringes vanish as was shown in the earlier treatment of this screen.

The interpretation given applies to the fringes formed for given X and Y as the mean height of the screen h, changes. For a fixed height, visibility may change with X and Y. In Figure (2.5c) the area of overlap of the functions $\mathcal{S}(Z_1-\Psi)$ and $\mathcal{S}^*(-Z_1'-\Psi)$ is seen to decrease with increasing distance from the origin; a corresponding decrease in fringe visibility with increasing X is seen in the spectrum of Figure (2.6).

Equation (2.31) was the starting point of the preceding discussion. The interpretation does not however depend on the assumptions which led to this equation and equations (2.25) and (2.26) are statements of the same process; in fact the "interactions" between the reflecting spheres, which are depicted in Figure (2.5), are just interactions between "slits". In the more general cases the visibility depends not only on ρ_S but also on the form of the power spectrum W.

The discussion of visibility in spectra has relevance to a deeper problem in diffraction theory which is discussed in the next section.

2.5 Randomly Phased Angular Spectra

An angular spectrum of scattering is said to be "randomly phased" if the phase of its general component is a random variable over the angular range of the spectrum and over an assembly of such spectra. A considerable body of theory, based on the concept, has been developed (Booker, Ratcliffe and Shinn(1950), Ratcliffe (1956)), one result of which is: If the angular spectrum derived from any type of scattering screen is randomly phased, and if the spectrum contains a strong unscattered component (as assumed in previous pages), then

$$\rho_a(\xi,\eta) \doteq \rho_{\mathfrak{f}}(\xi,\eta) \qquad (2.33)$$

where $\rho_a(\xi,\eta)$ is the correlation function of amplitude fluctuations at the ground and $\rho_{\mathfrak{f}}$ is the correlation function of the scattered wave field. (Bramley (1951), Ratcliffe (1956)).

Now it is well known that $\rho_{\mathfrak{f}}$ is independent of distance from the scattering screen and it has been seen in, for example, the case of the thin phase screen that the power spectrum V, which is (proportional to) the Fourier transform of ρ_a, is dependent on this distance. The angular spectrum of the random, phase-modulating screen is, by deduction, not randomly phased. The argument applies equally to a purely amplitude-

modulating screen and to the thick scattering screen discussed in this chapter, which produces both phase and amplitude modulation in an emerging wave. The question arises: in what sense are the angular spectra produced in these random screens not randomly phased?

The question has received considerable attention (Briggs, Ratcliffe, private communication) and Ratcliffe (1956 § 8.2) has stressed its importance. The work of the preceding section suggests a general answer.

Consider an angular spectrum $\underset{\sim}{F}(S)$ which arises in a one-dimensional screen of any type; S is the direction cosine, attached to an axis which is parallel to the screen, of the wavenormal of a typical component of $\underset{\sim}{F}$. Let the screen be infinite in aperture and let $\underset{\sim}{F}(S)$ be randomly phased so that the phases of any two discrete components $\underset{\sim}{F}(S)$ and $\underset{\sim}{F}(S + \sigma)$, $\sigma \neq 0$, are independent random variables over an assembly of screens.

Then,

$$\overline{\underset{\sim}{F}(S)\underset{\sim}{F}^{*}(S + \sigma)} = \begin{cases} \overline{|F(S)|^2}, & \text{for } \sigma = 0, \\ 0, & \text{for } \sigma \neq 0, \end{cases}$$

for all S. (2.34)

The left hand side of this equation is a well known measure of correlation in the spectrum. The angular spectrum arising in a random phase-or amplitude-modulating screen is easily shown to satisfy the equation.

A second condition, arises from, and is therefore necessary to, the randomly phased nature of $\underset{\sim}{E}(S)$. This is:

$$\overline{\underset{\sim}{E}(S)\underset{\sim}{E}(S+\sigma)} = 0, \text{ for all } S \text{ and } \sigma. \qquad (2.35)$$

This equation is most often trivially true when applied to randomly oriented vectors; but it is not so when a relationship like

$$\underset{\sim}{E}(S+\sigma) = \underset{\sim}{E}^*(S), \text{ for some } \sigma,$$

may exist. For then,

$$\overline{\underset{\sim}{E}(S)\underset{\sim}{E}(S+\sigma)} = \overline{\underset{\sim}{E}(S)\underset{\sim}{E}^*(S)} \neq 0, \text{ in general}$$

by equation (2.34).

Such relationships occur for the types of screens mentioned above; for the phase-modulating screen,

$$\underset{\sim}{E}^*(-S) = -\underset{\sim}{E}(S),$$

and for the amplitude-modulating screen

$$\underset{\sim}{E}^*(-S) = \underset{\sim}{E}(S),$$

so for both of these screens,

$$\overline{\underset{\sim}{E}(S)\underset{\sim}{E}(-S)} \neq 0$$

To the extent then that equation (2.35) is not satisfied, the angular spectra of these screens are not randomly phased. The importance of the condition (2.35) has not been stressed in the past.

Any angular spectrum which satisfies equation

(2.34) can fail to satisfy equation (2.35) only when the left hand side of the latter is of the form $\overline{\underset{\sim}{F}(S)\underset{\sim}{F}(-S)}$, unless the spectrum is of a very special nature. Further consideration can be restricted to this form alone.

It is easily shown that the propagation phasor associated with $\underset{\sim}{F}(S)$ disappears in the term $\overline{\underset{\sim}{F}(S)\underset{\sim}{F}^*(S)}$ (thereby establishing the distance - independent property of the angular power spectrum), but survives in combination with the term $\underset{\sim}{F}(S)\underset{\sim}{F}(-S)$. Condition (2.35) may therefore be regarded as the requirement that any quantity which formally depends on the latter term should not actually depend on distance from the scattering screen.

It is not at first obvious why the product $\underset{\sim}{F}(S)\underset{\sim}{F}(-S)$ should appear formally; it may be seen as follows. If any enquiry is made into the properties of the amplitude or phase distribution arising from scattering in any type of screen, the relationship between $\underset{\sim}{F}(S)$ and $\underset{\sim}{F}^*(-S)$ is immediately brought into question. (See, for example, the treatment of Section 2.4.4). The correlation coefficient of these quantities, which is often important to the discussion, is proportional to

$$\overline{F(S)[F^*(-S)]^*} = \overline{F(S)F(-S)},$$

which has the required form.

Now, the left hand side of this last equality is, in absolute value, and when normalised, the measure

of visibility of equation (2.32), as applied to the "slits" $\mathcal{E}(S)$ and $\mathcal{E}^*(-S)$. The condition (2.35) is not satisfied unless this visibility is zero. The present treatment is, in fact, suggested by the manner in which the visibility measure, and the height dependence, of the amplitude power spectrum of the thick screen, disappear together in the limiting case of the very (infinitely) thick screen.

The non-satisfaction of equation (2.33) in the cases previously cited is now adequately explained. The deductions made above are further verified in Appendix II, by discussion of the validity of the equality:

$$\rho a^2(\xi,\eta) \doteq |\rho \mathcal{E}(\xi,\eta)|^2$$

(Bramley (1951), Ratcliffe (1956)).

(This equation applies when the angular spectrum is randomly phased and does not contain a strong unscattered component). The Fourier transforms of the quantities in the equation are shown to be unequal when equation (2.35) is not satisfied. These transforms, which are power spectra, differ by a distance-dependent quantity whose magnitude is expressible in a form like the visibility measure discussed above.

In conclusion it may be noted that the measure of visibility does not, in modulus, depend on distance

from the screen; the angular spectrum does not become more, or less, randomly phased as it propagates. Bowhill (1961a)has shown that equation (2.33) is true for the amplitude distribution formed at a great distance from a thin phase-modulating screen (but not, as has been seen, at lesser distances). Fejer (1965, App.§ II.7) suggests that this is due to the randomly phased nature of the angular spectrum. This is not so; at all distances the visibility of the fringes in the amplitude power spectrum is unity (see Figure (2.2)
The fringes do, however, become very "rapid" at great distances and sample their envelope curve in many points. The Fourier transforms of the spectrum and the envelope function are then very similar, and these transforms are ρ_a and $\underset{\sim}{\rho_f}$ - this is Bowhill's result.

2.6 Satellite Applications of the Thick Screen Formulation

2.6.1 Spherical Wave Illumination.

When the radio source is a satellite at a finite height above the ground, the wavefront incident on the ionosphere is not plane but spherical and the treatment given previously must be modified. If the satellite is a distance of many times the radio-wavelength from the scattering region the modification is achieved by a simple transformation of the diffraction geometry

(Ratcliffe (1956), Bowhill (1961), Budden (1965)).

Let the satellite be at (z-h) = -H, above the ground, reference being made to Figure (2.8). In terms of the co-ordinates [x,y,z-h], referred to the origin O' on the ground, a new space is defined by

$$\left.\begin{aligned}[x',y',(z-h)'] &= [\alpha x,\ \alpha y,\ \alpha(z-h)] \\ \text{where } \alpha &= \frac{H}{H-(z-h)}\end{aligned}\right\} \qquad (2.36)$$

Under this transformation the ground plane ($\alpha=1$) is unaltered but all other points are changed; in particular the satellite, at (z-h) = -H in real space, is at a height (z'-h') = $-\infty$ in "α-transformed" space. Ray paths are parallel and wavefronts are planar in the new space, and the treatment of previous pages may be applied there.

For convenience, the treatment will be written in terms of the spatial variables x,y,z,X,Y, and Z used previously; where they appear in expressions for power spectra they will refer to "α-transformed" space. Any result obtained must undergo the inverse α-transformation before being applied to the real space of Figure (2.8).

2.6.2 Behaviour of the Amplitude Pattern at the Ground

To complete the description of the thick-screen formulation a brief demonstration is given of its

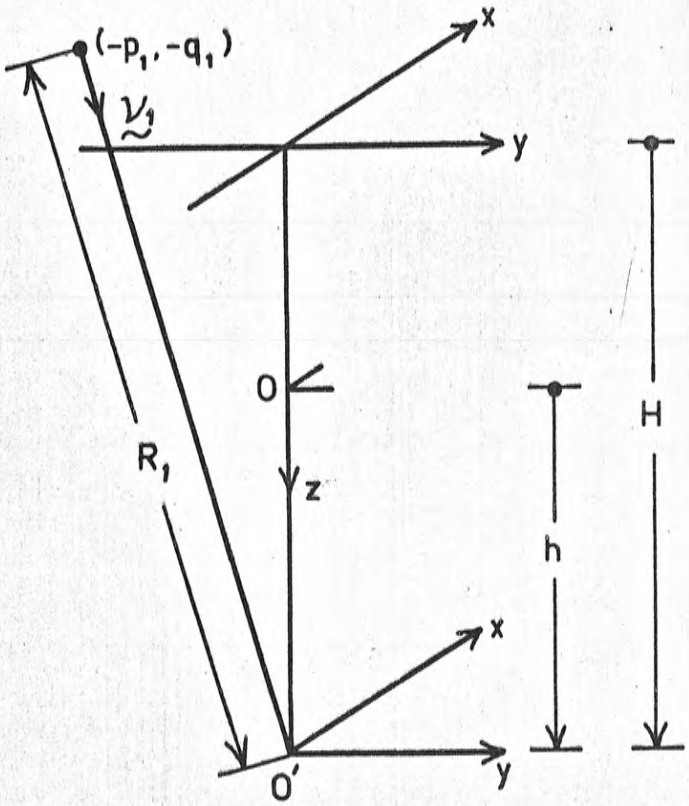

Figure (2.8). The geometry of the scattering problem when the radio source is a satellite.

relevance to the behaviour of the amplitude pattern at the ground, when the radio source is a moving satellite.

Let a satellite, radiating at a wavelength λ, and travelling at a constant height H, above the ground, take successively the positions $(-p_1,-q_1)$ and $(-p_2,-q_2)$ in the horizontal plane. The direction cosines of the ray through the ground origin 0' from, for example, the first position, are

$$\frac{p_1}{R_1}, \frac{q_1}{R_1}, \frac{H}{R_1}$$

where R_1 is the distance of the satellite from 0'. (Figure (2.8)). Being defined at the ground, these quantities are unaffected by "α-transformation" and become the direction cosines of the wavenormal in "α-transformed" space.

In writing the expression for the cross-spectrum of amplitude fluctuations, $\underline{Y}_{12}$, it is convenient to separate the quantities Z_1, Z_1', Z_2 and Z_2' into parts which contain the spatial frequencies X and Y to the first and second powers. Thus, making reference to Appendix I, for the first satellite position,

$$Z_1 = Z_{1a} + Z_{1b}$$

$$Z_1' = -Z_{1a} + Z_{1b} ,$$

and, inserting the values of the wavenormal direction

cosines,

$$Z_{1a} = -\left(\frac{P_1}{H}X + \frac{q_1}{H}Y\right)$$

$$Z_{1b} = -\frac{1}{2}\frac{\lambda R_1}{H}[X^2 + Y^2 + Z_{1a}^2]$$

Similar relations apply for Z_2 and Z_2' which pertain to the second position of the satellite.

The cross-spectrum V_{12} is now expressed in terms of the profile function $s(z)$ and the correlation function of the scattering medium $\rho N(\xi', \eta', \zeta')$, these being defined in "α-transformed space". This is achieved by straightforward Fourier transformation of the integrands in equation (2.25). Using the notation defined above:

$$V_{12} = c\int_{-\infty}^{\infty}\int s(z_1)s(z_2)\rho N(\xi', \eta', z_1 - z_2)\exp\left\{2\pi i(\xi' X + \eta' Y)\right\}$$

$$\times \exp\left\{-2\pi i[(h' - z_1)Z_{1a} - (h' - z_2)Z_{2a}]\right\}$$

$$\times \sin[2\pi(z_1 - h')Z_{1b}]\sin[2\pi(z_2 - h')Z_{2b}]dz_1 dz_2 d\xi' dy'$$

where c is a constant and all parameters refer to "α-transformed" space.

The Motion of the Amplitude Pattern

The amplitude patterns, which exist at the ground when the satellite is in each of the positions "1" and "2", are spatially cross-correlated to give the function $\rho a_{12}(\xi, \eta)$. The point of maximum value of ρa_{12} is displaced from the origin of correlation space by a

vector distance equal to the distance which the pattern moves, consequent to the motion of the satellite. This distance will not be determined but, what is a close approximation to it, for small movements of the satellite, the distance of the "mean" position or "centre of mass" of ${}^{\rho}a_{12}$ from the origin of correlation space.

$\underset{\sim}{Y}_{12}$ and ${}^{\rho}a_{12}$ are related by Fourier transformation:

$$K\iint {}^{\rho}a_{12}(\xi,\eta)\exp\left\{2\pi i(\xi X+\eta Y)\right\}d\xi d\eta = \underset{\sim}{Y}_{12}(X,Y)$$

where K is a constant. This relationship is differentiated with respect to X and normalised, and the limit as X and Y tend to zero is taken. This gives

$$\xi_0 = \frac{\iint \xi\,{}^{\rho}a_{12}(\xi,\eta)\,d\xi d\eta}{\iint {}^{\rho}a_{12}(\xi,\eta)\,d\xi d\eta} = \lim_{\substack{X\to 0\\ Y\to 0}} \frac{1}{2\pi i}\left[\frac{\partial \underset{\sim}{Y}_{12}(X,Y)}{\partial X}\Big/\underset{\sim}{Y}_{12}(X,Y)\right]$$

which is the ξ-coordinate of the centre of mass of ${}^{\rho}a_{12}$. The η-coordinate, η_0, is similarly expressed in terms of the Y-derivative.

Substituting for $\underset{\sim}{Y}_{12}$ from above and expressing $Z_1 a$, $Z_2 a$, et cetera in terms of X and Y gives, after some algebraical steps:

$$\xi_0 = h'\left(\frac{p_1}{H} - \frac{p_2}{H}\right) + \frac{\int_{-\infty}^{\infty}\int (-z_1\frac{p_1}{H} + z_2\frac{p_2}{H} + \xi')T(z_1, z_2, \xi', \eta')dz_1 dz_2 d\xi' d\eta'}{\int_{-\infty}^{\infty}\int T(z_1, z_2, \xi', \eta')dz_1 dz_2 d\xi' d\eta'}$$

where $T(z_1, z_2, \Xi', \eta') = s(z_1)s(z_2)\rho N(\xi'\eta', z_1 - z_2)$;

and a similar expression for η_0 in terms of $\frac{q_1}{H}$ and $\frac{q_2}{H}$.

This expression can be analysed as follows:

(i) ρN is necessarily centrosymmetric (since $\Delta N(x,y,z)$ is real). If it is assumed that the profile $s(z)$ is symmetric about $z = 0$, it is easily shown that the numerator of the second term vanishes and

$$\xi_0 = h'\left(\frac{p_1}{H} - \frac{p_2}{H}\right), \quad \eta_0 = h'\left(\frac{q_1}{H} - \frac{q_2}{H}\right).$$

Performing the inverse "α-transformation" on h' gives $h' = \frac{Hh}{H-h}$, by equation (2.36). (The layer has been assumed symmetric about the height h' in "α-transformed" space; it is very nearly so about h in real space if the layer thickness is small compared with the height of the satellite). The displacement of ρa_{12}, and the distance moved by the amplitude pattern, are then

$$\xi = \frac{h}{H-h}(p_1 - p_2), \quad \eta_0 = \frac{h}{H-h}(q_1 - q_2),$$

when the satellite moves through $(p_2 - p_1, q_2 - q_1)$. The motion of the pattern is that of the shadow on the ground of a point at the height h. The result is

equivalent to that of James (1962) and Liu (1966) who studied special cases of symmetrical layers. The present derivation is quite general.

(ii) If the layer is not symmetrical about $z = o$, the second term in the expression for ξ_o describes, in an obvious way, the process of finding the centres of mass of the profile function and the correlation function ρ_N. If $s(z)$ is symmetrical about $z = \delta$, the second term subtracts δ from h' in the first.

Additional terms arise if $s(z)$ is not symmetric. The parameter ξ', where it occurs, not as the argument of a function, specifies the ξ'-coordinate of the centre of mass of $\rho_N(\xi',\eta')$, averaged over the portions of $\rho_N(\xi',\eta',\zeta')$ sampled by $s(\zeta')$, as seen from the two viewing positions ("1" and "2"). An effect analogous to that measured here is the movement of the centre of mass of the shadow when an unsymmetrical opaque body is rotated about its centre of mass in a stationary beam of light.

Such effects contribute negligibly to the translational motion of the amplitude pattern in the ionospheric case. The satellite and the observer are usually so far removed from the scattering layer that the aspect presented by the typical irregularity, to an observer moving with the pattern, changes little in the

time that the pattern moves a distance many times the scale of the irregularity.

The Form of the Correlation Function

The effects of the motion of $\rho_{a_{12}}$ can be removed by expressing the spectrum Y_{12} phase-relative to the moving centre of mass. Applying the result obtained above for the motion, the "rephased" spectrum is

$$Y_{12} = Y_{12} \exp\left\{2\pi i h'(Z_1 a - Z_2 a)\right\}$$

where h' is the height of the centre of mass of the (squared) profile in "α-transformed" space. Y_{12}' describes the cross-correlation function expressed relative to its centre of mass, in which form it is written $\rho_{\dot{a}_{12}}$.

The sine terms in the expressions for Y_{12} and Y_{12}' produce considerable complexity in a general expression for the correlation function. In order to keep the discussion simple it is assumed that all parts of the scattering layer are at large distances from the ground (in "α-transformed" space) so that the sine terms, which represent fringe functions, may be omitted and replaced by a numerical constant. (Compare the discussion, in Section 2.5, of the equality : $\rho_a = \rho_f$, established by Bowhill (1961a)).

With this approximation, V_{12} may be Fourier transformed to give:

$$\rho'_{a_{12}}(\xi,\eta) = \frac{1}{(\sigma_{a_1}^2\sigma_{a_2}^2)^{\frac{1}{2}}} \iint s(z_1)s(z_2) \times {}^{\rho}N\left(\xi - \frac{z_1p_1}{H} + \frac{z_2p_2}{H}, \eta - \frac{z_1q_1}{H} + \frac{z_2q_2}{H}, z_1 - z_2\right)dz_1dz_2 \quad (2.37)$$

where $\sigma_{a_1}^2$, $\sigma_{a_2}^2$ are the variances of amplitude fluctuations in the patterns "1" and "2".

The auto-correlation function of the amplitude pattern, ${}^{\rho}a_{11}$ (or ${}^{\rho}a_{22}$), is obtained by putting: $p_1 = p_2$, $q_1 = q_2$. The double integral then represents the projection of each horizontal section ${}^{\rho}N(\xi',\eta')$ (of ${}^{\rho}N(\xi',\eta',\zeta')$, as sampled by the profile function) in the direction of the wavenormal "1"; in particular, when the profile function is of greater vertical extent than ${}^{\rho}N$ and the latter is little modified by the former, ${}^{\rho'}a_{11}$ is the "shadow" of ${}^{\rho}N$ in the plane wave illumination of "a-transformed" space; the spatial dimensions of ${}^{\rho'}a_{11}$ are weighted averages of the corresponding dimensions of the ${}^{\rho}N(\xi',\eta')$. Under the inverse "a-transformation" appropriate to the mean height $h' = \frac{Hh}{H-h}$ of the scattering layer, the spatial dimensions are found to be $\frac{H}{H-h}$ times larger than the corresponding averaged horizontal dimensions of ${}^{\rho}N$ in real space.

The last point to be considered is the decrease

in the maximum value of $\rho'_{a_{12}}$ as the patterns "1" and "2", on moving apart, become less similar. For small movements the variances $\sigma_{a_1}^2$ and $\sigma_{a_2}^2$ of the amplitude fluctuations may be considered to be equal and, therefore, constant. The maximum value of $\rho'_{a_{12}}$, which is taken to be the value at the centre of mass, is then:

$$\rho'_{a_{12}}(0,0) \propto \iint s(z_1)s(z_2) \times \rho_N\left(-\frac{z_1 p_1}{H} + \frac{z_2 p_2}{H}, -\frac{z_1 q_1}{H} + \frac{z_2 q_2}{H}, z_1 - z_2\right) dz_1 dz_2 .$$

The expression on the right is most simply described in terms of an intuitive picture given by McClure and Swenson (1964). These authors show that $\rho'_{a_{12}}(0,0)$ varies like the volume of scattering material common to two cylinders whose radii are equal to the radius of the first Fresnel zone (as seen by an observer on the ground), and whose axes, which intersect at the centre of the scattering layer, are directed along the wavenormals "1" and "2". The expression above is a formal statement of a similar picture and indicates that ρ_N weights the common volume. No reference to the Fresnel zone size appears in the expression since diffractive effects have been removed in limiting attention to behaviour at large distances from the scattering screen. As McClure and Swenson have shown,

these effects do not greatly influence the value of ${}^{\rho\prime}a_{12}(0,0)$.

The relative change of the common volume alluded to, for a given change in direction of the wavenormals, is greater in a thicker layer; it does not change at all in an infinitely thin layer. The thickness of the layer can therefore be determined from the rate of change of ${}^{\rho\prime}a_{12}(0,0)$ with respect to changes in, say, p_2 and q_2. James (1962) first demonstrated this possibility and McClure and Swenson (1964) have generalised his results. The application of the method is considered in Section 3.4 of the next chapter.

2.7 Conclusion

A review has been given of the theory basic to studies of weak scattering in irregular media and new work has been introduced which, if not always directly applicable to ionospheric studies, has interest in more general optical contexts.

The results obtained are not summarised here but it is pointed out that a simple central "model" has been given, the cross-spectrum χ_{12} from which all results concerning weak scattering can be derived.

The simplicity inherent in working in Fourier transform space, the usefulness of the concept of the

"reflecting sphere" and the value of the Fourier transformation as an operation upon a geometrical, rather than a mathematical, situation, have been tacitly stressed. None of these aspects is new but there is, in the literature, a tendency to derive purely mathematical results based on particular formulations of the properties of the scattering layer. Such derivations often give no indication of the often simple relationship between "object" and "image" and are therefore of little value to the student or, on occasion, apparently, the practical experimenter. The preceding discussion has been regarded, inter alia, as a study in giving geometrical interpretations in either real or Fourier transform space, and in preserving "descriptive" functions such as the auto-correlation function of the medium and the layer profile function, in their general forms, to the final stages of each development.

CHAPTER 3

THE APPLICATION OF THEORETICAL TREATMENTS

3.1 Introduction

The discussion in this chapter concerns the application of diffraction theory as previously considered, to practice, to the extraction of useful information regarding the irregular ionosphere from available scintillation data.

Preparatory to this discussion, values typical of ionospheric irregularities are assigned to various theoretical quantities in Section 3.1.1 and the nature of the effective ionospheric scattering screen is described in Section 3.1.2. Three main topics are then discussed: in Section 3.2, the behaviour of the depth of amplitude scintillations as the zenith angle of a radio source changes; in Section 3.3, the practicability of obtaining information from the power spectrum of amplitude scintillations; in Section 3.4, the important properties of the correlation function of amplitude fluctuations at the ground.

3.1.1 Measures Characteristic of Ionospheric Irregularities

By way of making the following considerations more definite, various parameters will be assigned

values which are typical of the irregular ionosphere. The appropriate findings are summarised here.

The irregularities responsible for radio star and satellite scintillations are often found to lie at F-region heights of about 300 km. E-region irregularities which may become important when a radio source is at low elevations, occur around 100 km. height. In the absence of precise knowledge the profile of scattering layers may be taken to be Gaussian; a typical value for the half-thickness of such a layer in the F-region would appear to be 30 km.

F-region irregularities are aligned along the geomagnetic field. Their spatial dimensions show considerable variation but characteristic values, expressed as the distances in which the correlation function of the medium falls to e^{-1}, are, transverse to the field, 1 km., and along the field, 5 km.

Few observations of suitable definition have been made with E-region irregularities. General considerations suggest that they would be smaller than those in the F-region. Backscatter observations indicate that, on some occasions at least, they too are field aligned.

3.1.2 The Effective Ionospheric Screen

Given the characteristics described above the scattering process in the ionosphere may be formalised as follows. The correlation function of the irregular medium is taken to have the Gaussian form:

$$\rho_N(r,s) = \exp\left[-\frac{r^2}{r_0^2} - \frac{s^2}{(\alpha r_0)^2}\right] \qquad (3.1)$$

where s and r are spatial coordinates measured along, and radial to, the geomagnetic field respectively. The "characteristic" contour, on which $\rho_N = e^{-1}$ is a spheroid of revolution about the field direction. Its radius radial to the field is r_0, typically 1 km. and its "axial ratio" is α (≥ 1), typically of value 5.

The profile function of the scattering layer is written:

$$s(z) = \exp\left(-\frac{z^2}{L^2}\right), \qquad (3.2)$$

which falls to e^{-1} in the distance L which is typically 30 km. The coordinate z is, as previously, measured vertically downward.

Now the half-thickness L of the profile function is several times larger than the radii typical of ρ_N, and the radio wavelengths used for scintillation studies, of the order of 10 metres, are

one hundred times smaller than these radii. These are just the conditions assumed in discussing the screen of finite thickness in Section 2.3.7 of Chapter 2. In Fourier transform space (see Figure (3.1)) the transformed profile $\underset{\sim}{S}(z)$ is narrow in distribution compared with the vertical section, $W(0,0,Z)$, of the power spectrum of the medium and the spectrum is effectively sampled on the tangent plane to the reflecting sphere at the origin.

Under these conditions, and if the scattering be weak, the expression (2.31) for the power spectrum of amplitude fluctuations at the ground may be adopted. Thus:

$$V_{11}(X,Y) = \frac{r_e^2}{2(\underset{\sim}{k}\cdot\underset{\sim}{\rho}_1)^2} W[X,Y,(Z_1-Z_1')/2]\left[\int |\underset{\sim}{S}(Z)|^2 dZ\right] \times \left\{1 - \cos[2\pi h(Z_1+Z_1')]\right\} {}^{\rho}s(Z_1+Z_1')$$

Since ${}^{\rho}N$ has a smaller dimension of ~ 1 km., X and Y do not exceed ~ 1 km^{-1} within the region where W takes appreciable values. Within this region, then, for a wavelength λ of ~ 0.01 km, the vertical separation of the reflecting spheres is:

$$Z_1 + Z_1' \sim \lambda(X^2 + Y^2), \qquad \text{(Appendix I)}$$

which does not exceed ~ 0.01 km^{-1}. This value is several times smaller than the half-width of $\underset{\sim}{S}(Z)$

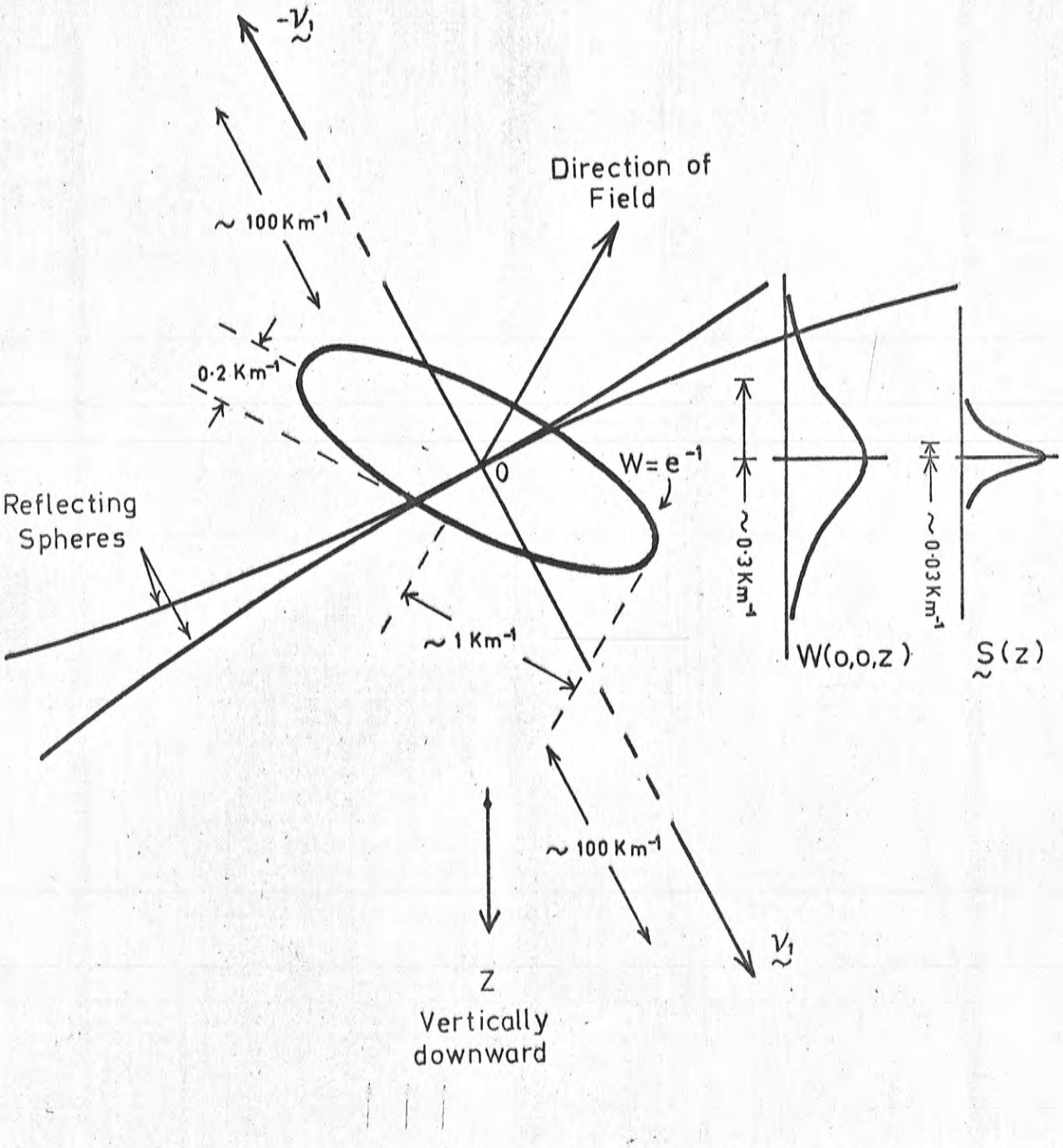

Figure (3.1). The geometry of Fourier Transform space for v.h.f. illumination of F-region irregularities. Typical scale sizes are shown for the radii of the reflecting spheres, for the contour on which the spectrum W(X,Y,Z) falls to e^{-1} and for the half-width of the transformed profile function S(Z). The curvatures of the reflecting spheres are exaggerated.

which is ~ 0.03 km^{-1}, so the visibility function, $\rho_S(Z_1 + Z_1')$, may be put equal to unity for all X and Y. The amplitude power spectrum then takes the form:

$$V_{11}(X,Y) = \frac{r_e^2}{(\underset{\sim}{k}\cdot\underset{\sim}{\varrho}_1)^2} W[X,Y,(Z_1-Z_1')/2] \left[\int |\underset{\sim}{g}(z)|^2 dz\right] \times \sin^2\left[\pi h(Z_1 + Z_1')\right]. \qquad (3.3)$$

The fact that ρ_S is unity indicates that the scattering layer, though physically thick, behaves in diffraction as a thin phase-modulating screen.

Comparison of equation (3.3) with that originally given for the thin screen, equation (2.8), shows that the factor:

$$\frac{r_e^2}{(\underset{\sim}{k}\cdot\underset{\sim}{\varrho}_1)^2} \left[\int |\underset{\sim}{g}(z)|^2 dz\right] W\left[X,Y,(Z_1 - Z_1')/2\right], \qquad (3.4)$$

describes the power spectrum of phase fluctuations in the wavefront emerging from the layer. Now the sampling of W on the plane perpendicular to the wave-normal (see Figure (3.1)) corresponds to the integration of its Fourier transform, ρ_N, along lines parallel to the wave normal; it corresponds in fact, in real space, to the integration of phase along the ray path.

The matter may be formalised thus: the Fourier relationship between W and ρ_N (equation (2.13)) is

written, for brevity:

$$W(X,Y,Z) \;<\!\!-\!\!>\; \sigma_N^2 \; \rho_N(\xi,\eta,\zeta).$$

Sampling W on the plane perpendicular to the wavenormal $\underset{\sim}{\nu}_1$, and multiplying by $r_e^2\lambda^2$, gives:

$$\frac{r_e^2\lambda^2}{\underset{\sim}{k}\cdot\hat{\underset{\sim}{\nu}}_1} W[X,Y,(Z_1-Z_1')/2] \;<\!\!-\!\!>\; r_e^2\lambda^2\sigma_N^2\int\rho_N(\xi',\eta',\zeta')d\zeta' \qquad (3.5)$$

where ζ' is measured parallel to the wavenormal and ξ' and η' orthogonal to it. The factor $\underset{\sim}{k}\cdot\hat{\underset{\sim}{\nu}}_1$, where $\hat{\underset{\sim}{\nu}}_1 = \lambda\underset{\sim}{\nu}_1$ is the unit vector parallel to $\underset{\sim}{\nu}_1$, arises in the rotation of axes from (ξ,η,ζ) to (ξ',η',ζ'). The left-hand side here is similar in form to the expression (3.4) but contains no reference to layer thickness; it is the power spectrum of phase fluctuations per unit distance of propagation, and may be written:

$$\frac{r_e^2\lambda^2}{\underset{\sim}{k}\cdot\hat{\underset{\sim}{\nu}}_1} W[X,Y,(Z_1 - Z_1')/2] \;<\!\!-\!\!>\; \phi_0^2 \; \rho_\phi(\xi',\eta') \qquad (3.6)$$

where ϕ_0^2 is the variance of phase per unit distance, and ρ_ϕ is the auto-correlation function of phase, in the wavefront.

Equating the right-hand sides of relationships (3.5) and (3.6) gives:

$$\phi_0^2 = r_e^2\lambda^2\sigma_N^2\int_{-\infty}^{\infty}\sigma_N(0,0,\zeta')d\zeta' \;, \qquad (3.7)$$

as given by Chernov (1960), and

$$\rho_\phi(\xi',\eta') \;\alpha\int_{-\infty}^{\infty}\rho_N(\xi',\eta',\zeta')d\zeta'. \qquad (3.8)$$

These equations and the fact that wave phase can be meaningfully integrated through the medium, apply whenever the irregularities of the medium are much larger than the radiation wavelength, the scattering is weak and the scattering region is not so thick that $^{\rho}S \neq 1$.

The term $\frac{1}{\underset{\sim}{k}\cdot\hat{\underset{\sim}{\iota}}_1}\int|\underset{\sim}{S}(Z)|^2 dZ$ in (3.4), as yet undescribed, gives the distance over which the variance of phase must be summed. Applying Parseval's theorem and substituting from equation (3.2),

$$\int|\underset{\sim}{S}(Z)|^2 dZ = \int s^2(z)dz = \int_{-\infty}^{\infty}\exp(-2z^2/L^2)dz = (\tfrac{\pi}{2})^{\frac{1}{2}}L$$

which is the effective vertical thickness of the scattering layer. The "slant" thickness increases like $\frac{1}{\underset{\sim}{k}\cdot\hat{\underset{\sim}{\iota}}_1}$, that is, like sec(i), where i is the angle of incidence of the wavenormal, when the illumination is oblique.

Briggs and Parkin (1963) have carried out the integrations of equations (3.7) and (3.8) in the case where $^{\rho}N$ has the form of equation (3.1). Their results, when applied to the present discussion, give, for the variance of phase in the wavefront emerging from the scattering layer:

$$\phi_o^2 = (\tfrac{\pi}{2})^{\frac{1}{2}} r_e^2 \lambda^2 L \sec(i) \sigma_N^2 \frac{\alpha}{\beta} r_o, \qquad (3.9)$$

and for the correlation function of phase:

$$\rho_{\phi}(\xi',\eta') = \exp\left[-\frac{\xi'^2}{r_o^2} - \frac{\eta'^2}{(\beta r_o)^2}\right], \qquad (3.10)$$

where β is a new "axial ratio" given by:

$$\beta = (\alpha^2 \sin^2\psi + \cos^2\psi)^{\frac{1}{2}} \qquad (3.11)$$

In these equations, the η' axis which, with the ξ' axis, lies in the plane of the wavefront, is also assumed to lie in the plane containing the wavenormal and the geomagnetic field vector; ψ is the angle between these two vectors.

The expressions for ϕ_o^2 and ρ_{ϕ} have been derived because they are the starting point for many discussions of diffraction in the ionosphere. Their derivation from the thick screen formulation has not previously been given in the literature.

The weak scattering situation has been considered here. Bramley (1954) has shown that phase may be integrated along the ray when multiple scattering takes place. The sampled spectrum is then multiply self-convoluted (Fejer (1953)) and equations (3.7) and (3.8) must be replaced by more complex ones.

3.2 The Zenith Angle Variation of Scintillation Depth.

The work to be reviewed now has been published by Briggs and Parkin (1963). Only the main points and those which apply to the experimental work to follow, are mentioned here.

3.2.1 Theory

Several authors (Hewish (1952), Booker (1958)) have given approximate expressions for the expected variation of the depth of amplitude scintillations as the zenith angle of a radio source changes. The results given below are derived on the basis of a full diffraction theory.

A suitable measure of the depth of amplitude fluctuations is the quantity:

$$S = \left\{ \overline{(R^2 - \overline{R^2})^2} \right\}^{\frac{1}{2}} \Big/ \overline{R^2} \ , \qquad (3.12)$$

where R is the total signal amplitude at the ground and the bar (——) denotes, for brevity, a spatial average. By a method outlined in Section 2.3.3, P.W.James (private communication) has derived an expression for S for the case where scattering is weak and the auto-correlation function of phase in the emerging wavefront has the form of equation (3.10). In terms of the quantities defined in the last section, S is given, at a distance z' from the scattering layer in the direction of the wavenormal, by:

$$S = \sqrt{2}\phi_0 \left\{ 1 - [\cos U_1 . \cos U_2]^{\frac{1}{2}} \cos[\tfrac{1}{2}(U_1 + U_2)] \right\}^{\frac{1}{2}} \qquad (3.13)$$

where: $\tan U_1 = 2\lambda z'/\pi r_0^2$ and $\tan U_2 = 2\lambda z'/\pi\beta^2 r_0^2$.

S is obviously proportional to the root-mean-square phase fluctuation ϕ_0. Its dependence on the

parameters $\lambda z'/r_0^2$ and β is important and is shown in Figure (3.2) where the function $F = (S/\sqrt{2}\phi_0)$ is plotted against $\lambda z'/r_0^2$ for various values of β. As a function of the distance z', F increases approximately linearly from zero at $z' = 0$ until the point for which $\lambda z'/r_0^2 \doteq 1$ is reached. Thereafter, F is approximately constant and distance-independent. Briggs and Parkin have called the two regions delineated by the change in behaviour of F, the "near zone" ($\lambda z'/r_0^2 <\sim 1$) and the "far zone" ($\lambda z'/r_0^2 > \sim 1$).

The effect of anisotropy in ρ_ϕ is seen in the behaviour of the curves of Figure (3.2) as the axial ratio β increases from unity. The curves tend rapidly to a limiting form, the curve for $\beta = 5$ closely approximating that for $\beta \to \infty$. This shown that as soon as anisotrppy is appreciable, the diffraction process depends mainly on the smaller dimension r_0 of ρ_ϕ and is almost independent of the larger dimension βr_0.

Mercier (1962) has derived an expression for the quantity S which applies whether scattering be weak or strong. He finds, however, that when the scattering is strong ($\phi_0 > \sim 0.7$ radians), the form of the dependence of S on z' changes as ϕ_0 changes. Since this behaviour does not permit the presentation of

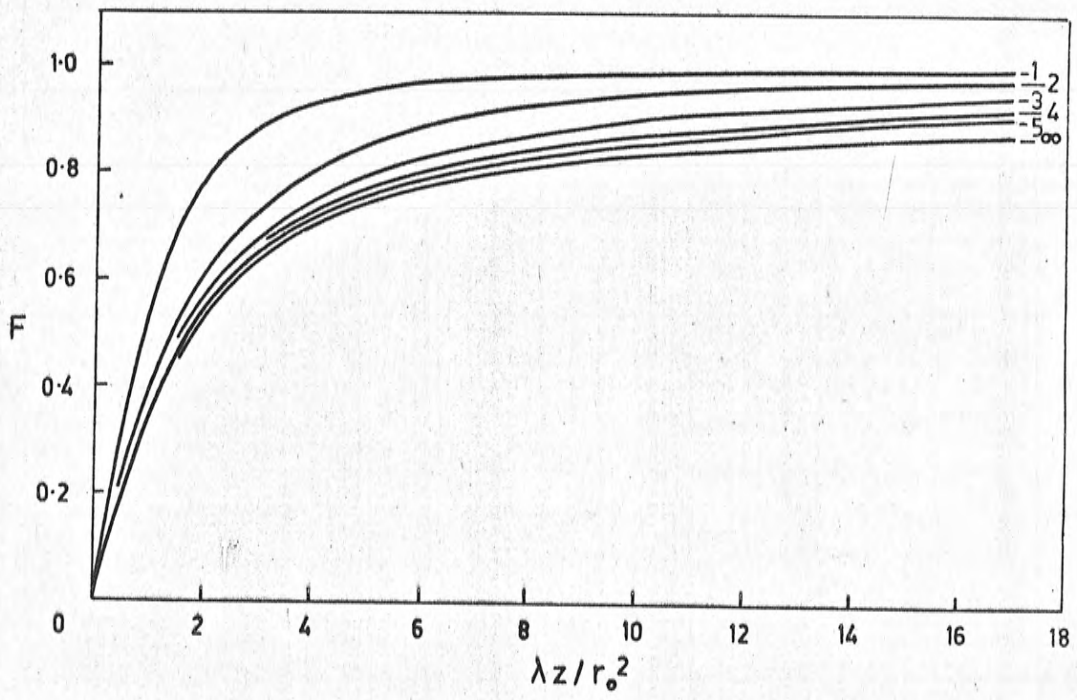

Figure (3.2). The function $F = S/\sqrt{2}\phi_0$ as a function of $\lambda z/r_0^2$ for an anisotropic phase screen. The curves are for different values of the axial ratio β.

general curves for the zenith angle variation of scintillation depth, subsequent discussion is restricted to cases where scattering is weak and the expression (3.13), with its simple dependence on ϕ_0, is valid.

The summary of the theory being complete, attention is given to curves showing the zenith angle variations typical of satellite scintillations.

In deriving these, geometrical expressions are required which relate the quantity z' and the angles i and ψ (of the equations (3.9) and (3.11) for ϕ_0 and β) to the zenith angle of the satellite, its height and the height of the scattering layer. These are given by Briggs and Parkin (1963) and are omitted here. It is pointed out, however, that allowance must be made for the spherical nature of the incident wave from the satellite. This is done by substituting for z' in equation (3.13) with:

$$z' = \frac{z_1' \cdot z_2'}{z_1' + z_2'} , \qquad (3.14)$$

where z_1' and z_2' are the slant ranges along the ray from the layer to the satellite, and to the observer, respectively. This modification is a variant of the "α-transformation" of Section 2.6.1, defined so that the plane at the mean height of the layer is unchanged

by the transformation. The radius r_o is, therefore, not modified (see Budden (1965)).

3.2.2 Isotropic Irregularities

First to be considered is the case of isotropic irregularities for which the axial ratio α of ρ_N is unity. The zenith angle variation of the scintillation depth S, does not depend on the orientation of the geomagnetic field and arises from: (i) the dependence of ϕ_o on the slant thickness of the scattering layer; which is, from equation (3.9):

$$\phi_o \alpha \sec^{\frac{1}{2}}(i)$$

(ii) the variation of the effective slant range z' from the layer to the observer (equation (3.14)), as it affects the function F of Figure (3.2).

Two sets of curves showing the variation of S with change of zenith angle are given in Figure (3.3). The curves are normalised to unity at the zenith and are drawn for layer heights (h) of 300 km. (heavy lines) and 100 km. (light lines). The satellite height is 1000 km. Briggs and Parkin give such curves for different values of λ/r_o^2 but in Figure (3.3) the wavelength λ has been set at 7.5 metres (40 Mc/s) and the radius r_o takes the values listed (in kms.) in the columns on the right.

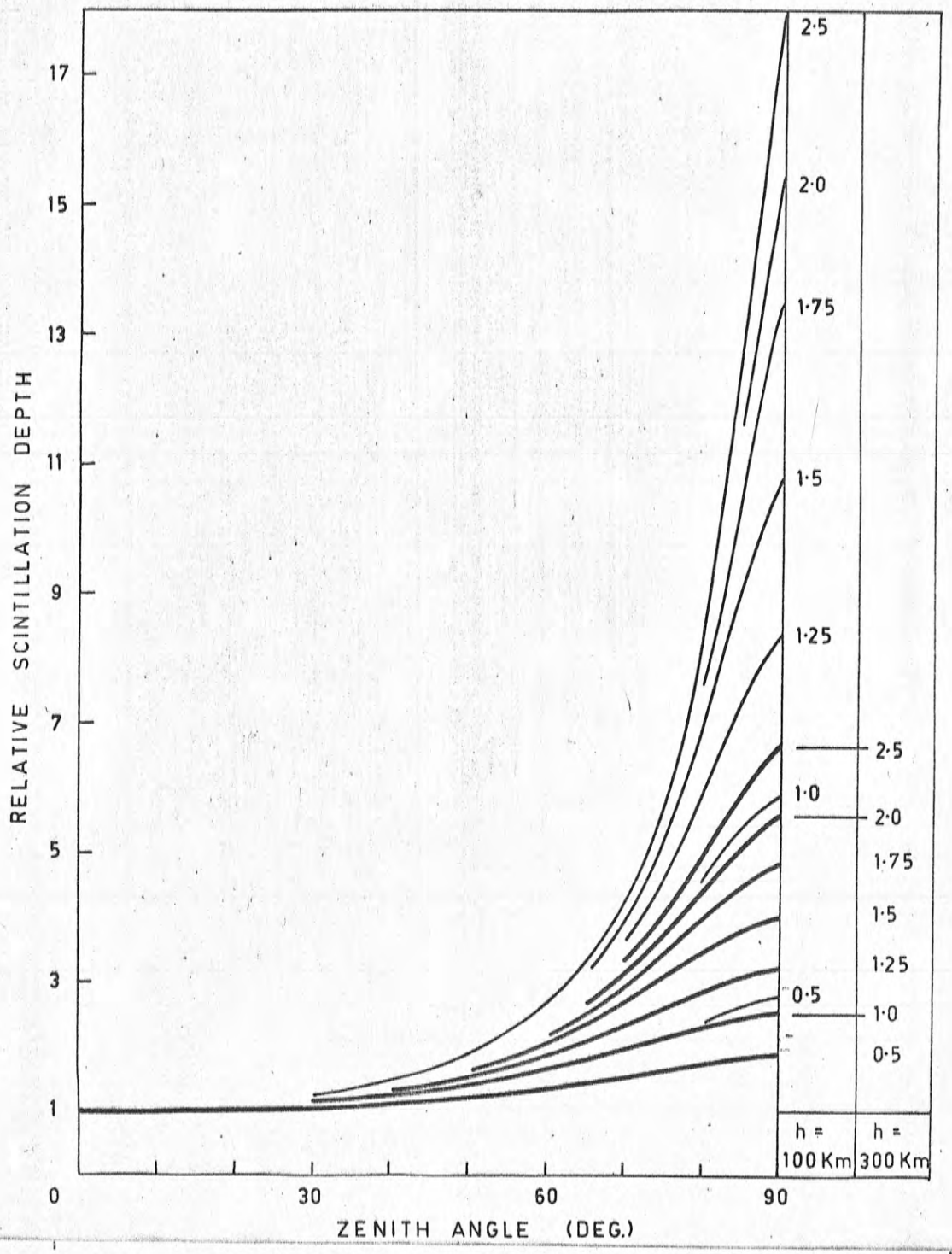

Figure (3.3). The scintillation depth at 40 Mc/s (normalised to unity at the zenith) as a function of zenith angle, when the source is a satellite at a height of 1000 Km. The irregular layer is at a height of 300 Km. (heavy lines) or 100 Km. (light lines). The radius r_o (Km.) appropriate to each curve is shown on the right.

The quantity λ/r_0^2 determines the value of z' for which the conditions of diffraction go from those of the near zone to those of the far zone. If λ/r_0^2 is small, the observer is in the near zone for all zenith angles, the function F is proportional to z', and $S \propto z' . \sec^{\frac{1}{2}}(i)$. Since both z' and sec(i) increase with zenith angle, the scintillation depth shows a large variation. The curve for h = 100 km, r_0 = 2.5 km illustrates this. If λ/r_0^2 is large, the appropriate conditions are those of the far zone: F is approximately constant, $S \propto \sec^{\frac{1}{2}}(i)$, and the variation of S is much reduced. The curve for h = 100 km, r_0 = 0.5 km. is typical.

Attempts have been made in the past to determine the height of a scattering layer on the assumption that the scintillation depth varies like $z' . \sec^{\frac{1}{2}}(i)$. The discussion above shows that typical values of λ and r_0 do not necessarily lead to such near zone behaviour and that a family of dissimilar curves can be associated with a given height. Figure (3.3) shows moreover that such families overlap extensively, making a determination of layer height impossible in the absence of an accurate knowledge of r_0 (and λ) .

The curves are, in fact, more sensitive to changes in r_0 than to those in height, for r_0 enters

the controlling parameter $\lambda z'/r_o^2$ to the second power while the distance z' appears to the first. If the height of a layer is known to a reasonable relative accuracy, r_o can be determined to about twice that accuracy.

3.2.3 Anisotropic Irregularities

If the irregularities of the scattering medium are anisotropic, the zenith angle variation of scintillation depth depends not only on the parameters h, λ and r_o, but also on the dip angle of the geomagnetic field, on the axial ratio α of $^{\rho}N$ and on the azimuth of the radio source.

The variations of most of these parameters must be restricted in presenting illustrative curves. Figure (3.4) is drawn for observations made in the magnetic meridian at the magnetic latitude of Adelaide (dip angle 66°). A satellite source at 1000 km. height illuminates a layer at 300 km. height on frequencies of 40 Mc/s (heavy lines) and 20 Mc/s (light lines). The curves, which are normalised to unity at the zenith, are drawn for various values of the axial ratio α and the radius r_o takes the fixed value of 1 km.

For $\alpha = 1$ (isotropic irregularities) the scintillation depth varies with zenith angle in the manner described in the last section. When $\alpha \neq 1$

additional variations arise. Firstly, the axial ratio β of ${}^{\rho}\phi$ changes (as ψ of equation (3.11) changes) with consequent variation in the function F discussed in Section 3.2.1. As is seen in Figure (3.2) this variation cannot exceed the limits set by the curves for $\beta = 1$ and $\beta \to \infty$. Secondly, the integral along the ray, $\int {}^{\rho}N(0,0,\zeta')d\zeta'$ of equation (3.7), changes as the ray moves, producing a variation in ϕ_0. This takes a maximum value when the ray direction coincides with that of the longer dimension of ${}^{\rho}N$, that is, with the geomagnetic field direction.

The second process is the more important and produces the peaks in the curves for $\alpha \neq 1$ in Figure (3.4).

Equation (3.9) shows that the dependence of ϕ_0 on α has the form $(\alpha/\beta)^{\frac{1}{2}}$. In the "along the field" configuration where the angle ψ is zero, β is independent of α, and ϕ_0 and hence S, are proportional to $\alpha^{\frac{1}{2}}$. This simple relationship is somewhat modified in Figure (3.4) by the (α-dependent) normalisation at the zenith, but the sensitivity of the peaks to changes in α is obvious. If the layer height and the radius r_0 are known to a reasonable accuracy, the peak value observed "along the field" can be used as a practical measure of the ratio α.

Note must be made of the behaviour of the curves

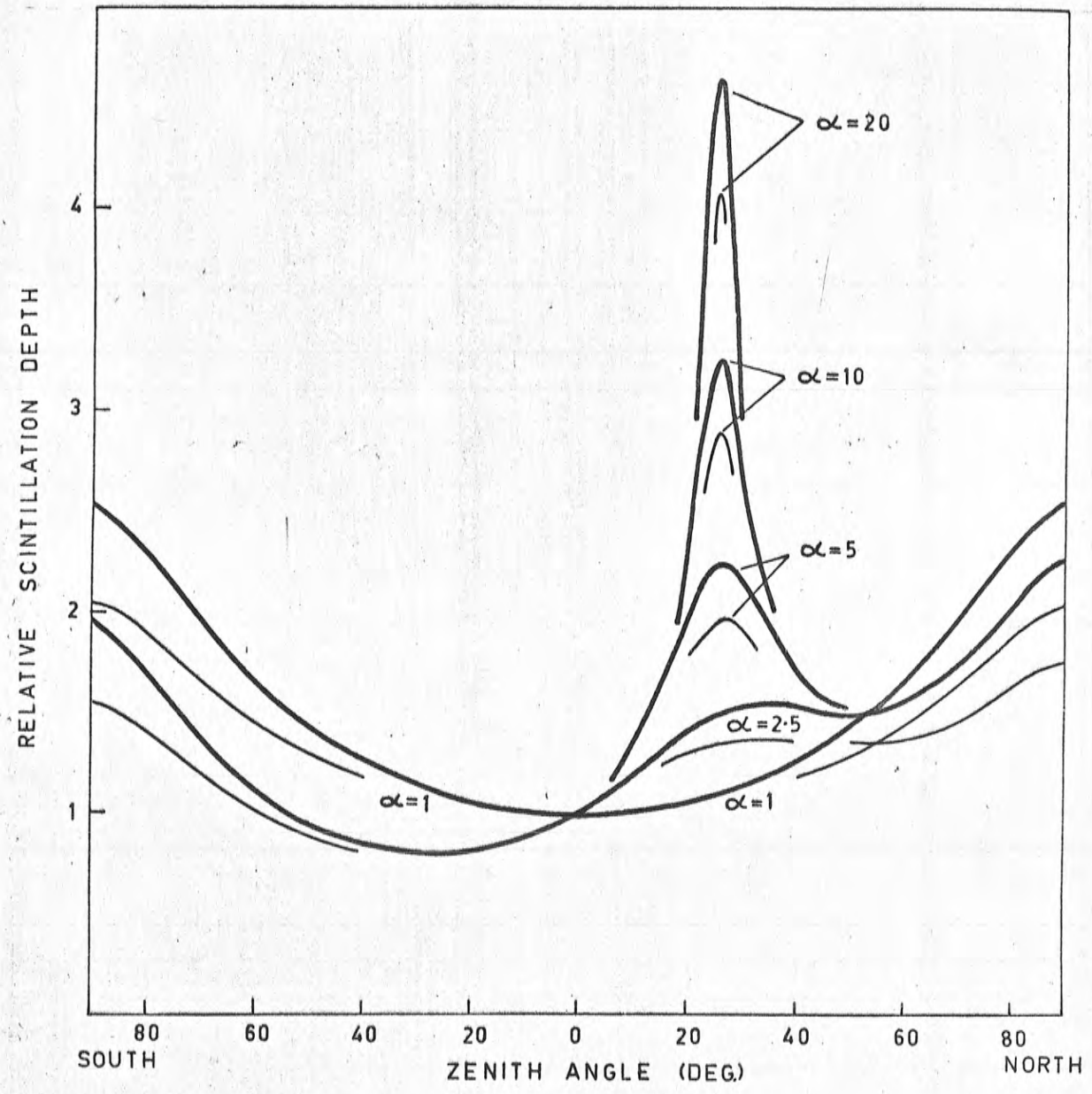

Figure (3.4). The zenith angle variation in the magnetic meridian for scintillation of signals from a satellite at a height of 1000Km, observed at Adelaide. The curves, which are drawn for observations at both 40 Mc/s (heavy line) and 20 Mc/s (light line), are for different values of the axial ratio α, and for irregularities at a height of 300 Km. The curves are normalised to unity at the origin.

in Figure (3.4) at zenith angles removed from that corresponding to illumination in the direction of the field. Except at the zenith where they are normalised to unity, the curves for a given radio frequency, for $\alpha \neq 1$, are depressed below that for $\alpha = 1$. This is not a general result but occurs at magnetic latitudes at which the peak "along the field" appreciably overlaps the zenith, and zenithal values of the scintillation depth are enhanced. If, in determining the mean variation of scintillation depth with zenith angle, an average is taken over many occasions and over all azimuths of the radio source, the field-aligned peak will tend to disappear because it occupies a relatively small area of the field of view. The enhancement of the zenithal values is not lost in the average-in-azimuth, and the mean variation, when normalised to unity at the zenith, takes, elsewhere, values lower than those for isotropic irregularities with the same values of r_o and h. This effect must be taken into account when an attempt is made to determine r_o from the form of the mean variation.

3.2.4 The Ratio of Scintillation Depths on Two Frequencies

To this point in the discussion of zenith angle variations it has been tacitly assumed that the distribution of scattering material across the sky is uniform. Now, in reality, ionospheric irregularities often occur in

"patches" and may show persistent latitudinal variations in their distribution, and the straight forward application of the results given above is not possible; a measure is required which is independent of the degree of irregularity of the ionosphere. Such a measure is now discussed.

The "degree of irregularity" as it affects the depth of scintillation S, depends on both the variance of electron density fluctuation in the scattering layer and the thickness of the layer, the factors σ_N^2 and L in the expression (3.9) for ϕ_0^2. It is clear that if the scattering is weak, so that S depends linearly on ϕ_0, the effects of these factors cancel out in a ratio of the scintillation depths found on two frequencies at a given zenith angle. In fact, all the quantities upon which ϕ_0 depends, except the wavelength λ, cancel out.

Therefore, for observations, at wavelengths λ_1 and λ_2, of isotropic irregularities, (i) if both observations are made entirely within the far zone, where the function F is (approximately) constant and independent of λ (Figure (3.2)), the ratio of scintillation depths takes the constant value,

$$\frac{S(\lambda_1)}{S(\lambda_2)} = \frac{\lambda_1 F(\lambda_1)}{\lambda_2 F(\lambda_2)} = \frac{\lambda_1}{\lambda_2} ,$$

for all zenith angles; (ii) if the observations are

entirely within the near zone where $F \propto \lambda z/r_0^2$, the ratio takes the constant value,

$$\frac{S(\lambda_1)}{S(\lambda_2)} = \frac{\lambda_1 F(\lambda_1)}{\lambda_2 F(\lambda_2)} = \left(\frac{\lambda_1}{\lambda_2}\right)^2 ,$$

for all zenith angles. For observations in which the conditions move from those of one zone to those of the other, as the zenith angle changes, the variation of the ratio lies between these two limiting values.

Figure (3.5) shows the way in which the ratio of the scintillation depth at 20 Mc/s to that at 40 Mc/s varies with zenith angle when a satellite at a height of 1000 km illuminates a layer at 300 km. The curves are given for various values of the radius r_0 of isotropic irregularities. It can be seen that in the near zone (r_0 large) the plotted ratio approximates a constant value of 4, and in the far zone (r_0 small), a value of 2; these are the values expected, following the discussion above, when the frequency ratio is 2:1.

The ratio of scintillation depths is a function not only of r_0, but also of the height of the scattering layer. It is found by trial (Briggs and Parkin (1963)) that curves such as those of Figure (3.5) are, in the "between zones" region, about twice as sensitive to relative changes in r_0 as to those in height. They are best used in determining r_0 if the height of the

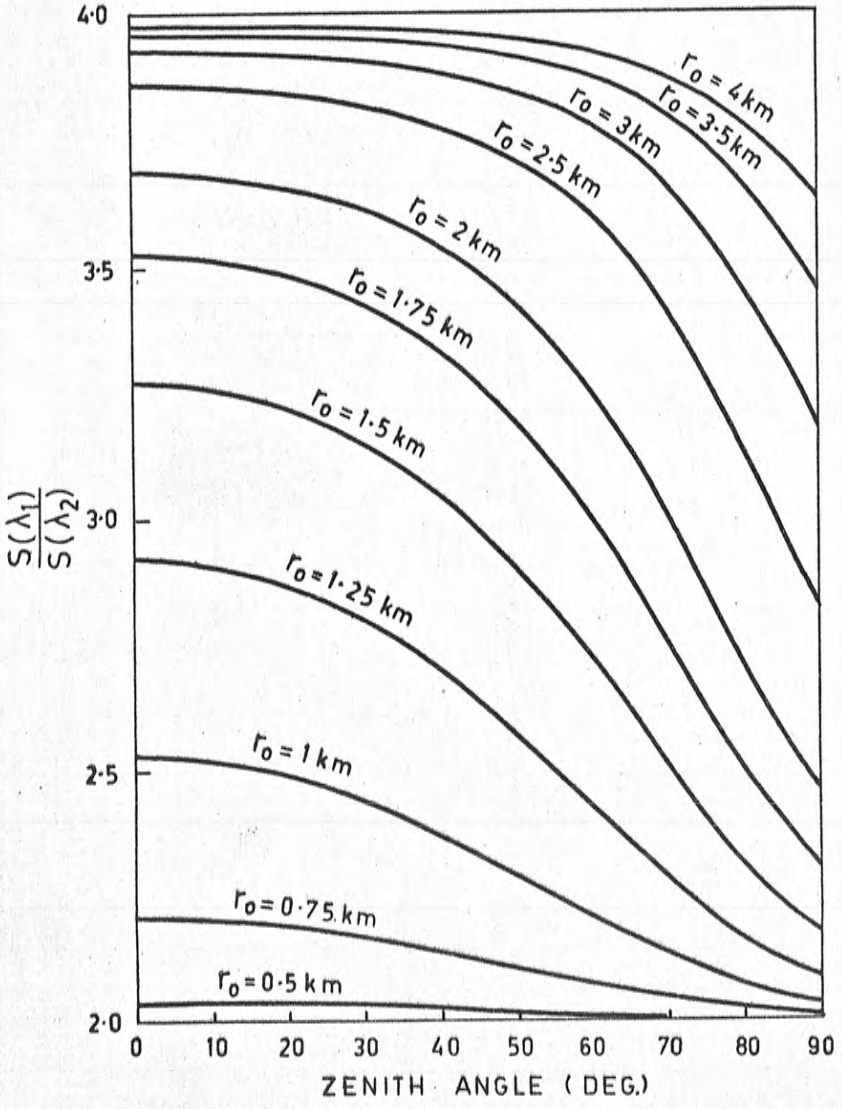

Figure (3.5). The ratio of the scintillation depth at 20 Mc/s to the scintillation depth at 40 Mc/s as a function of zenith angle, when the source is a satellite at a height of 1000Km. Irregularities at 300Km.

layer is known fairly accurately. An equivalent result was found in Section 3.2.2.

It may be noted that taking the ratio of scintillation depths removes from the quantity ϕ_o the factors which depend on the relative orientation of the ray and the geomagnetic field; anisotropy of the scattering irregularities can only effect curves like those of Figure (3.5) through the slight variation of the function F with β (Figure (3.2)). In the use of such curves the irregularities may therefore be regarded as isotropic.

3.2.5 Other Measures of Scintillation Depth

The measure of scintillation depth S, defined by equation (3.12) is suitable for theoretical enquiries but its repeated evaluation in practice requires a considerable computational effort. In satellite scintillation studies a record of signal amplitude is obtained and a more suitable measure is:

$$S' = \overline{|R - \bar{R}|}/\bar{R} \,, \qquad (3.15)$$

where, again, R is the total signal amplitude and the bar denotes a spatial average over the record.

It is difficult to discover theoretically the relationship between the measures S and S' (Mercier (1962)) but Briggs and Parkin (1963) show, by a test of scintillation data obtained at Adelaide, that they may,

for practical purposes, be taken to be linearly related. This assumption is made in the discussion of experimental work in later pages and the results given above in terms of S, will be applied to the measure S'.

3.3 Applications of the Power Spectrum of Amplitude Fluctuations

3.3.1 Determination of Layer Height

Hewish (1951) and Briggs and Parkin (1964) have described methods whereby the height of a scattering layer may be deduced from the spectrum of amplitude fluctuations at the ground. A variant of their methods is now described which allows the height to be determined from recordings of satellite scintillations made at a single receiving site.

Consider, for simplicity, a thin weakly scattering layer at a height h which varies in the x-direction only. Let a satellite, at a height H vertically above the receiving site, illuminate the layer at wavelength λ, and let the power spectrum of phase fluctuations in the wave emergent from the layer be W(X). Then the spatial power spectrum of amplitude fluctuations at the ground varies in the X-direction only, and is given by:

$$V(X) = W(X) \sin^2 \left(\pi\lambda \frac{Hh}{H-h} X^2\right).$$

The "α-transformation" of Section 2.6.1 has been applied to the quantity h.

Let the satellite have a horizontal speed v in the x-direction. From the result of Section 2.6.2, pertaining to motion of the amplitude pattern on the ground, it is easily shown that the pattern has a speed, in the negative x-direction, given by:

$$u = \frac{h}{H-h} v.$$

The observer obtains a temporal power spectrum of amplitude fluctuations in which the temporal frequency f is related to the spatial frequency X by:

$$X = f/u = (H-h)f/hv \quad ;$$

the temporal spectrum has the form:

$$W\left[(H-h)f/hv\right] \sin^2\left[\pi\lambda \frac{(H-h)H}{h}\left(\frac{f}{v}\right)^2\right].$$

The positions, on the frequency axis, of the zeros of the sine-squared fringe function are dependent on the (presumably known) quantities H and v, and on the height h of the scattering layer. A practical determination of the position of one such zero, other than that at the origin, would enable the height h to be deduced.

The relationship between fringe position and layer height has been indicated in previous pages. The

treatment above principally shows that the velocity of the amplitude pattern over the ground need not be known explicitly, in determining the layer height.

3.3.2 The Two-Dimensional Power Spectrum

The generalisation of the preceding discussion to oblique incidence is straightforward, and more general directions of the velocity of the satellite are easily treated; but the extension to a screen which varies in two directions is not simple.

The record obtained when an amplitude pattern drifts in the x-direction, say, past a single receiver, can only provide a section, ${}^{\rho}a(\xi,o)$, of the two-dimensional auto-correlation function ${}^{\rho}a(\xi,\eta)$. (A temporal auto-correlation function is, in fact, obtained; this is taken, for the present, to be equivalent to the section described). Since the Fourier transform of ${}^{\rho}a(\xi,\eta)$ is proportional to the amplitude power spectrum $V(X,Y)$, the transform of ${}^{\rho}a(\xi,o)$ is proportional to $\int V(X,Y)dY$. The latter function, which is the power spectrum of the recorded amplitude scintillations, will not, in general, show a fringe structure like that of $V(X,Y)$.

Having regard to the considerable amount of information which may be carried by the fringe structure (see Section 2.3.7), and in view of the simplicity of the method outlined in the preceding section, consideration

is given to situations in which the fringes can be observed.

Consider normal illumination of a thin phase screen at height h, by a plane wave of wavelength λ. Let the power spectrum of phase fluctuations in the emerging wave be:

$$W(X,Y) = \exp\left\{-\pi^2\left[r_0^2X^2+(\beta r_0)^2Y^2\right]\right\}, \qquad (3.16)$$

which corresponds to a phase correlation function, ${}^{\rho}\phi$, of the form of equation (3.10). If the scattering is weak, the amplitude power spectrum at the ground is:

$$V(X,Y)= \exp\left\{-\pi^2\left[r_0^2X^2+(\beta r_0)^2Y^2\right]\right\}\sin^2\left[\pi h\lambda(X^2+Y^2)\right] \qquad (3.17)$$

and the spectrum $\int V(X,Y)dY$ can be shown to have the form:

$$\exp\left[-\pi^2 r_0^2X^2\right] \quad \times$$
$$\times\left\{\frac{\pi^{-\frac{1}{2}}}{\beta r_0}-\frac{1}{\left[4\lambda^2z^2+\pi^2(\beta r_0)^4\right]}\cos\left[2\pi\lambda zX^2+\tfrac{1}{2}\tan^{-1}\left(\frac{2\lambda z}{\pi(\beta r_0)^2}\right)\right]\right\}.$$

Using these functions the properties of the spectra can be compared; as a basis for comparison the section $V(X,0)$ of $V(X,Y)$ is plotted in Figure (3.6) for the parameter values: λ = 15 metres, h = 250 km. and r_0 = 0.5 km.

Consider first the case in which $\beta = 1$, so that $W(X,Y)$ is circularly symmetric. The fringe function is circularly symmetric (at normal incidence) and so, therefore, is $V(X,Y)$; it is generated by rotating the curve for $V(X,0)$ about the X = 0 axis. The function

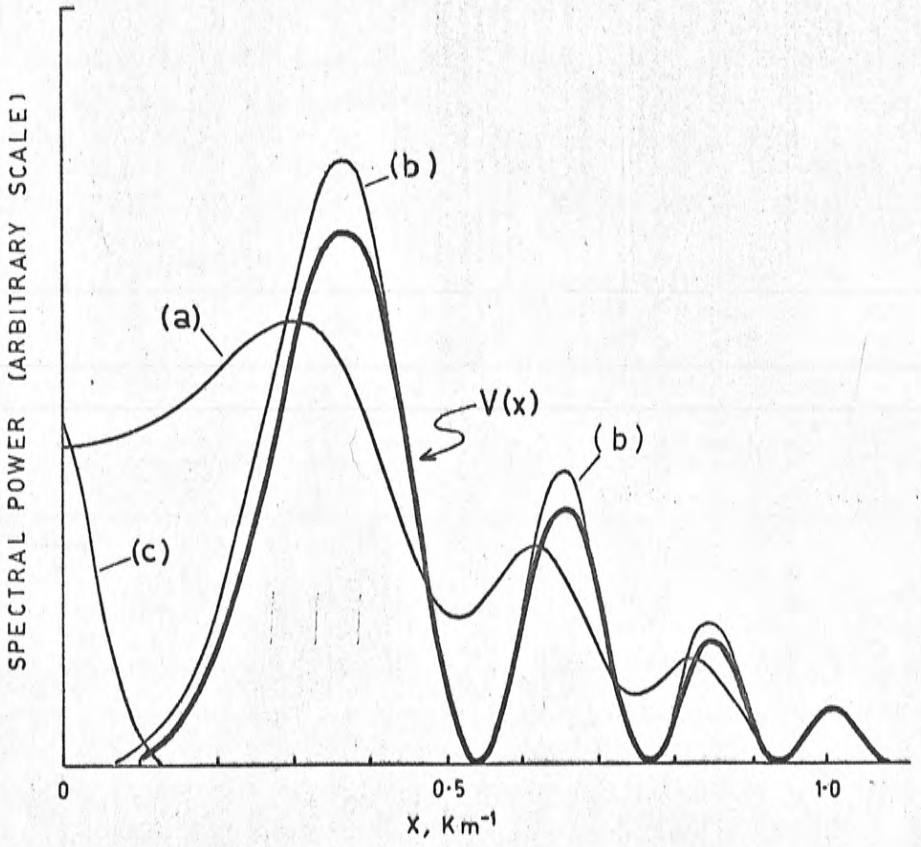

Figure (3.6). V(X) (heavy line) is a cross section typical of the power spectra of two-dimensional amplitude patterns at the ground. The curves (a), (b) and (c), which are derived in various ways from V(X), show types of scintillation spectra which may arise when the patterns drift past an observer. Details are given in the text.

$\int V(X,Y)dY$ appropriate to this case is given by the curve (a) of Figure (3.6). It is typical of the spectra to be found in many situations of more general geometry in that it does not strongly reflect the fringed nature of $V(X,Y)$. The fringe positions could not be accurately determined by direct observation if the spectrum was at all "noisy".

In the case of circular symmetry the form of $V(X,0)$ can, in fact, be derived from $\int V(X,Y)dY$; the two functions are related by Fourier-Bessel transformation (Budden (1965)): but most often (when $\beta \neq 1$ or when the illumination is oblique), the spectrum $W(X,Y)$ and the fringe function have different symmetrics, and $V(X,Y)$ has none (apart from its basic centre-symmetry); no special transforms then apply.

One case does arise in which the spectrum of recorded scintillations closely resembles a section through the two-dimensional spectrum of amplitude fluctuations. This occurs when the spectrum W is greatly elongated in the direction of motion of the amplitude pattern and is narrow at right angles to it, and the fringe function is effectively sampled in that direction; more explicitly, W has the form of equation (3.16) for large β, the pattern motion being in the X-direction, and:

$$\int V(X,Y)dY \doteq \int W(X,0)\delta(Y)\sin^2[\pi h\lambda(X^2 + Y^2)]dY = V(X,0).$$

In such a case, the use of the exact expression for $\int V(X,Y)dY$ with the same parameter values as before, but with $\beta = 10$, gives the curve (b) in Figure (3.6). The fringe structure of $V(X,0)$ is seen to be accurately reproduced in the derived spectrum.

It may be noted that the configuration just considered is that in which the correlation function of amplitude fluctuations, ${}^{\rho}a(\xi,\eta)$, is elongated at right angles to the motion of the amplitude pattern; it is that in which the situation on the ground is most similar to the one arising in the one-dimensional screen described in the last section.

3.3.3 The "Usefulness" of Spectral Fringe Zeros.

It is clear that little useful information regarding the diffraction process can be obtained from the amplitude power spectrum unless at least one fringe zero, other than the one at the origin, appears in the spectrum. The conditions under which this occurs are considered briefly here.

Reference to the expression (3.17) shows that, in the X-direction, the first fringe zero of interest occurs at $h\lambda X^2 = 1$; that is, at $X^2 = 1/h\lambda$. The value of the enveloping function $W(X,Y)$ at this point is $\exp(-\pi^2 r_o^2/h\lambda)$, and if it be taken as a criterion of the "usefulness" of the zero that it occurs at points where

W is not less than, say, e^{-2} ($\doteq 0.15$), the criterion can be written:

$$\frac{\lambda h}{\pi^2 r_0^2} \gtrsim \frac{1}{2} \qquad (3.18)$$

The condition that the first zero in the Y-direction is useful is, similarly:

$$\frac{\lambda h}{\pi^2 r_0^2} \gtrsim \frac{\beta^2}{2}$$

When values typical of scintillation studies are inserted (for example, $\lambda = 0.015$ km. (20 Mc/s), $h = 300$ km., $r_0 = 1$ km., so that $\frac{\lambda h}{\pi^2 r_0^2} \doteq 0.45$), the former criterion is found to be satisfied marginally. The latter criterion is not satisfied for any β appreciably greater than unity.

The equation (3.17) referred to above, applies to plane wave illumination; if satellite sources are to be considered, the derived criteria must be modified by "α-transformation" of h and r_0 (Section 2.6.1). The condition (3.18) becomes:

$$\frac{\lambda h}{\pi^2 r_0^2} \gtrsim \frac{\alpha}{2} , \qquad (3.19)$$

where $\alpha = \frac{H}{H-h} \doteq 1.4$, when the values $H = 1000$ km., $h = 300$ km., for the satellite and scattering layer heights respectively, are inserted. This criterion is even more stringent than that of (3.18).

It appears, then, that attempts to observe fringe

structure in spectra of ionospheric scintillation will be only marginally successful, especially when satellite sources are used; the information in the spectrum regarding layer height and form of layer profile (Section 2.3.7) must remain largely unused.

Note is made, nevertheless, of the conditions under which fringe structure is most likely to be seen. These are:

(i) when the height of the scattering layer is greatest, in reality, or in effect (when the radiation is incident obliquely), and when the ionospheric irregularities are smallest;

(ii) when the lowest radio frequency compatible with the weak scattering condition is used;

(iii) when the observer samples the narrower, rather than the wider, section of the amplitude correlation function on the ground (so that r_o, rather than βr_o, enters the appropriate critical measure). This condition is the same as that for least "filling in" of the spectral zeros, as discussed in the last section. Its two-fold merit is seen in a comparison of curves (b) and (c) of Figure (3.6). The details appropriate to curve (b) have been given; the spectrum of curve (c) is obtained from a section through the amplitude pattern orthogonal to that from which (b) is derived. It can be seen that, regardless

of "filling in", the spectrum (c) falls too rapidly to include any useful fringe zeros.

3.3.4 Further Notes Concerning Spectra

It was assumed earlier in this discussion that the temporal auto-correlation function of amplitude scintillations, from which the scintillation power spectrum is derived in practice, has the same form as a section through the spatial auto-correlation function of the drifting amplitude pattern. If the pattern changes as it moves, this assumption is not fully valid and components appear in the temporal spectrum in addition to those which have been described above. Such effects are not further considered here, but note is made of the work of Fooks (1965) in relating the additional Fourier components to the changes which occur in the cross-correlation function $\rho'_{a_{12}}$, as described in Section 2.6.2.

In conclusion of the present discussion, reference is made to the practical investigations of scintillation spectra by several authors. Hewish (1951), using the signal from a radio star, attempted to determine the height of a scattering layer by comparing spectral fringe positions at different radio wavelengths (3.7 and 6.7 metres). Being unable to detect significant differences between the scintillating signals and, therefore, between their spectra, he assigned an upper limit

of about 1000 km. to the layer height, on the basis of a criterion like (3.18).

Gruber (1961) derived theoretically the relationship between the spectra of amplitude and phase scintillations of a radio star, as observed with an interferometer system. As a starting point Gruber adopted the results of Booker, Ratcliffe and Shinn (1950) which apply to randomly phased angular spectra, and assumed the two-dimensional amplitude and phase spectra at the ground to have identical forms. This assumption is not valid. At the radio frequencies used by Gruber (50 Mc/s and 200 Mc/s) the ionosphere does not produce randomly phased angular spectra (see Chapter 2), and the power spectra of amplitude and phase fluctuations show different fringe structures. The sine-squared amplitude fringe has a zero at the origin and the complementary cosine-squared "phase" fringe (not previously discussed here) does not.

It may be noted that the scintillation power spectra actually obtained by Gruber do not show these contrasting forms, although his theory, when corrected, and his supposition that the observed patterns were drifting eastward or westward and had north-south - elongated correlation functions, both indicate that structure at the origin should not have been "filled in".

Jespersen and Kamas (1964) have obtained power spectra from recordings of satellite amplitude scintillations. These show a zero at the lowest frequencies, which the authors attribute directly to the zero at the origin in the two-dimensional amplitude spectrum. The lack of a zero in such curves as (a) and (c) of Figure (3.6), and in the curves of Gruber (1961) (cited by these authors), indicates that this is insufficient argument. The additional logical step probably lies in the fact that Jespersen and Kamas selected for study, occasions on which the auto-correlation function was elongated orthogonally to the motion of the amplitude pattern.

The spectra of Gruber (1961) and Jespersen and Kamas (1964) show interesting structure, but it cannot be identified with diffractive fringing; no report of observations of the latter has yet been made.

3.4 The Correlation Function of Amplitude Fluctuations at the Ground

In this section the properties of the amplitude correlation function at the ground, which were outlined in Section 2.6.2, are more closely defined. This is done in preparation for later discussions of experimental work, and emphasis is placed on applications to satellite studies.

It is convenient at this stage to express explicitly the temporal nature of movements and changes in the correlation function, and to write the function as:

$$\rho_a(\xi,\eta,\tau) = \frac{1}{\sigma_a(t)\sigma_a(t+\tau)} \iint a(x,y,t)a(x+\xi,y+\eta,t+\tau)dxdy, \quad (3.20)$$

where $a(x,y,t)$ is the deviation of signal amplitude from the mean at the time t, at the point (x,y) on the ground, and $\sigma_a^2(t)$ is the variance of this deviation. The auto-correlation function of the amplitude pattern at any instant t, referred to as $\rho_{a,1}(\xi,\eta)$ in Section 2.6.2, is now written $\rho_a(\xi,\eta,0)$, and the cross-correlation function of two patterns, previously written $\rho_{a,2}(\xi,\eta)$, becomes $\rho_a(\xi,\eta,\tau)$ if observations of the patterns are separated in time by the interval τ.

The Auto-Correlation Function

It was shown in Section 2.6.2 that, when scattering is weak, $\rho_a(\xi,\eta,0)$ behaves at large distances from the scattering screen like the "shadow" of the three-dimensional auto-correlation function of the medium, ρ_N. Under conditions typical of scintillation studies, the integration in equation (2.37) is very similar to that for ρ_ϕ in equation (3.8), indicating that the spatial dimensions of the distant shadow, like those of ρ_ϕ in equation (3.10), are related to the radii of ρ_N by simple ray-optical projection.

Closer to the screen this is not so and corrections must be applied to dimensions measured at the ground before an interpretation in terms of ionospheric scales is made. Bowhill (1961a) has investigated the matter and his results are most easily applied to the auto-correlation function of amplitude fluctuations in the wavefront at the ground. This function, which is written ${}^{\rho}a(\xi',\eta')$ can be approximated near the origin by

$$ {}^{\rho}a(\xi',\eta') = \exp\left\{ -\frac{\xi'^2}{r_o'^2} - \frac{\eta'^2}{(\beta' r_o')^2} \right\} \qquad (3.21) $$

It is the relationship between the radii r_o' and $\beta' r_o'$, so defined, and the corresponding radii r_o and βr_o of ${}^{\rho}\phi(\xi',\eta')$ in equation (3.10), which is of present interest.

In practice it suffices to use one of the special cases given by Bowhill, that for $\beta \to \infty$. Under this condition the ratio of minor axes r_o'/r_o has the variation shown in Figure (3.7) when plotted against the quantity $d = \frac{2\lambda z'}{\pi r_o^2}$, z' being the distance along the ray from the scattering screen to the ground; at $d = 0$, $r_o'/r_o = \frac{1}{\sqrt{5}} (\doteq 0.45)$ and $r_o' \to r_o$ as $d \to \infty$. The ratio of major axes $\beta' r_o'/\beta r_o$ takes the value unity for all d.

Whenever β is appreciably greater than unity the behaviour is effectively that just described. If, for example, $\beta = 3$, the ratio r_o'/r_o has the value 0.46 at

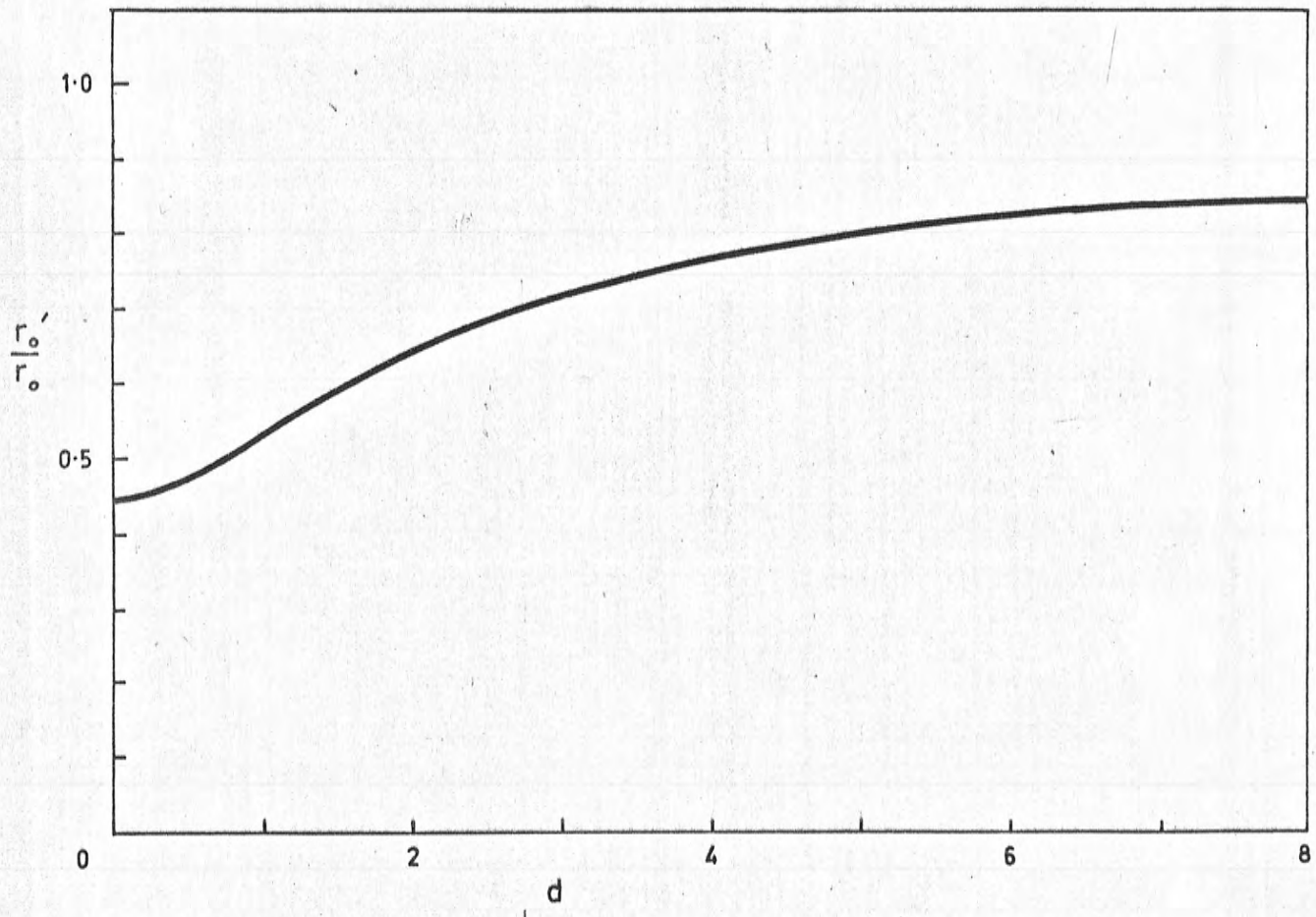

Figure (3.7). The ratio of the correlation radius measured in the wavefront at the ground to that measured in the wavefront at the ionosphere, as a function of the distance - dependent parameter d (defined in the text); for a one-dimensional screen ($\beta \to \infty$)

$d = 0$; the ratio $\beta' r_0'/\beta r_0$ is equal to 0.9 at $d = 0$ and increases rapidly to unity as d increases.

Since the formation of a nearly isotropic phase distribution ($\beta \doteq 1$) is a rare event, the behaviour appropriate to this case need not be described here.

The results quoted above apply for weak scattering of a plane wave. When the illuminating wave is spherical two modifications must be made:

(i) the quantity z' upon which the parameter d depends must be redefined in terms of the distances z_1' and z_2', measured along the ray from the scattering layer to the ground, and to the radio source, respectively. Equation (3.14) gives the appropriate definition.

(ii) the linear magnification of all spatial quantities measured at the ground, as described in Section must be taken into account. The magnification factor, previously found to be $\frac{H}{H-h}$, is more suitably expressed as $\frac{z_1' + z_2'}{z_2'}$ when curved-earth geometry is to be applied to the diffraction process.

When strong scattering takes place, spatial scales measured at the ground depend upon the root-mean-square deviation of phase ϕ_0 in the scattering layer. No precise curves are available but Hewish (1951) and Ratcliffe (1956) show, for plane wave illumination, that when $\phi_0 >> 1$, the

quantities r_o and r_o' used above are related by

$$\frac{r_o'}{r_o} \doteq \frac{1}{\phi_o} \qquad (3.22)$$

The projection of the elliptical contours of the function ${}^{\rho}a(\xi',\eta')$, defined in the wavefront at the ground, into those of ${}^{\rho}a(\xi,\eta,0)$, defined in the ground plane, presents a simple geometrical problem. It will not be discussed here.

The Correlation Function in Space and Time

The correlation function ${}^{\rho}a(\xi,\eta,\tau)$ may be approximated near the origin by:

$${}^{\rho}a(\xi,\eta,\tau) = \exp\left\{-[A(\xi-V\tau)^2 + B\eta^2 + 2C(\xi-V\tau)\eta + D\tau^2]\right\}. \qquad (3.23)$$

This formulation describes the main characteristics of the function, which are:

(i) the "characteristic ellipse",

$$A\xi^2 + B\eta^2 + 2C\xi\eta = 1,$$

upon which ${}^{\rho}a(\xi,\eta,0) = 1/e$. This is the projection upon the ground of the similarly defined contour of ${}^{\rho}a(\xi',\eta')$.

(ii) the translational motion, of speed V (in the direction of which the ξ-axis has been defined to lie). By the work of Section 2.6.2, V is related to the satellite's horizontal speed U, thus:

$$V = \frac{h}{H-h} U. \qquad (3.24)$$

Drift speeds of the ionospheric scattering medium, which are found to be about two orders of magnitude smaller than

the orbital speed of a near-earth satellite, have been neglected in writing this equation.

(iii) the temporal decay expressed by the term $-D\tau^2$. Of the changes in the cross-correlation function discussed in Section 2.6.2, this is the first order effect. Using first order theory, James (1962) has investigated its dependence on the thickness of a scattering layer and has shown that the ratio,

$$V_{c_V} = \frac{\text{characteristic radius of } \rho[\xi\ \eta\ 0] \text{ in V-direction}}{\text{decay time constant of } \rho[-(V\tau)^2,\ 0,\ \tau]} = \left(\frac{D}{A}\right)^{\frac{1}{2}}$$

is given by

$$V_{c_V} = \frac{H\ L}{(H-h)^2}\ \frac{U}{2}\ , \qquad (3.25)$$

where U is the satellite speed and L is the half thickness of the layer profile as defined by equation (3.2). The more rigorous treatment of McClure and Swenson (1964) leads to essentially the same result.

Temporal decay of the correlation function is also produced by change of the characteristic shape, or by rotation, of the irregularities in the amplitude pattern at the ground. These effects, which are not mentioned by McClure and Swenson, can be discussed in terms of the formulations of Section 2.6.2 but the working is not given here. Most often the corrections involved are negligible but they can become important when the ray path passes close to the direction of elongation of the ionospheric irregularities and the geometry of projection changes very rapidly.

The application of equation (3.25) is not, then, justified.

Compared with the changes in the correlation function already mentioned, those produced by random motions of the irregularities in the ionosphere are negligible and need not be further discussed.

It may be noted that results which are given above in terms of the parameters H and h are made applicable to curved earth geometry by making the substitutions, $z_1' + z_2'$ for H, and z_1' for h, as was done earlier in this section.

As it is written in equation (3.23), $\rho a(\xi,\eta,\tau)$ has the form assumed for the correlation function in the correlation analysis of Briggs, Phillips and Shinn (1950) and Phillips and Spencer (1955). The application of this analysis to satellite scintillation records, and the subsequent evaluation of various ionospheric parameters by the use of the theory outlined above, are reported in Chapter 9.

CHAPTER 4.

THE FARADAY EFFECT

4.1 Introduction

An outline of the theory of the Faraday effect and its application to the determination of ionospheric electron content is given in this chapter. Reference to this discussion will be found in Chapter 10 where relevant experimental findings are reported.

4.2 Theory

The most commonly used formulation of the Faraday effect is that based upon the quasi-longitudinal approximation the refractive index of the ionosphere, which leads to the equation (Browne et al. (1956)):

$$\Omega = \frac{K}{f^2} MI,$$

where $$M = H\cos(\psi)\sec(i),$$

and $$I = \int_0^{h_s} N dz.$$

Here Ω is the total angle of rotation experienced by the plane of polanisation of a wave of frequency f in passing through the ionosphere from a satellite to the ground. The quantity $H\cos(\psi)$ is the component of the geomagnetic field in the direction of the ray and i is the angle of the ray to the horizontal.

Along the ray the product $H\cos(\psi)\sec(i)$ varies only slowly throughout the regions of greatest electron content, and a mean value of M is usually used appropriate to the height of

the centroid of the electron density distribution.

The quantity I, the value of which is determined in the analysis, is the columnar electron content, i.e.; the electron density N integrated vertically through the ionosphere from the ground to the height of the satellite h_s. In the horizontel plane its value is associated with the co-ordinates of the point at which M is evaluated.

K is a basic constant of value 0.0297 in m.k.s. units.

Both I and M are functions of spatial position (and therefore functions the one of the other). As a plane polarised radio source crosses the sky, Ω changes continuously and an observer on the ground, receiving the signal on a simple dipole, records a temporal trace in the form of a rectified sine wave. The distinctive "nulls", or points of zero signal, indicate successive half rotations of the plane of polarisation. If the motion of the satellite is known, the determination of spatial changes of M is straight-forward.

In associating changes in Ω with changes in I, ionospheric drift speeds may be neglected in comparison with the speed of the satellite.

4.3 Determination of the Total Electron Content

Since the total angle Ω can not usually be determined directly, resort must be made to differential methods for the evaluation of I. The author has used two such methods, each

complementing the other. They are now described briefly:

If the first of the equations (4.1) is differentiated with respect to M, the result is obtained:-

$$\frac{d\Omega}{dM} = \frac{K}{f^2}\left(I + M\frac{dI}{dM}\right) \qquad (4.2)$$

A value of I is obtained in terms of $\frac{d\Omega}{dM}$, therefore, if it can be assumed that $\frac{dI}{dM}$ is zero; that is, if I does not change across the sky.

Many authors have used this method. Garriott and Mendonca (1963), working at 54 Mc/s compared its accuracy with that of a highly accurate Doppler-Faraday hybrid method. They find that in the presence of a gradient of total content over their site ($\frac{dI}{dM} \neq 0$) the differential method over-estimates the value of I by 20 % in the mean. The results also show a wide scatter, only 50 % of their number lying within 10 % of their mean value.

For the second method of evaluating I, in which the differential of Ω with respect to radio frequency is used, waves of frequencies f_1 and f_2, which differ by a small amount, are employed. For simplicity they will be assumed to be transmitted with the same polarisation and received on dipoles having the same orientation.

A type of "Vernier" measure is used, the "coarse" ruling being provided by "coincidences", i.e.; the points along the ray at which the polarisation planes of the two transmissions, which rotate at different rates, regain parallelism. The "fine" measure is obtained as follows (Figure (4.1)): if, at the time that a

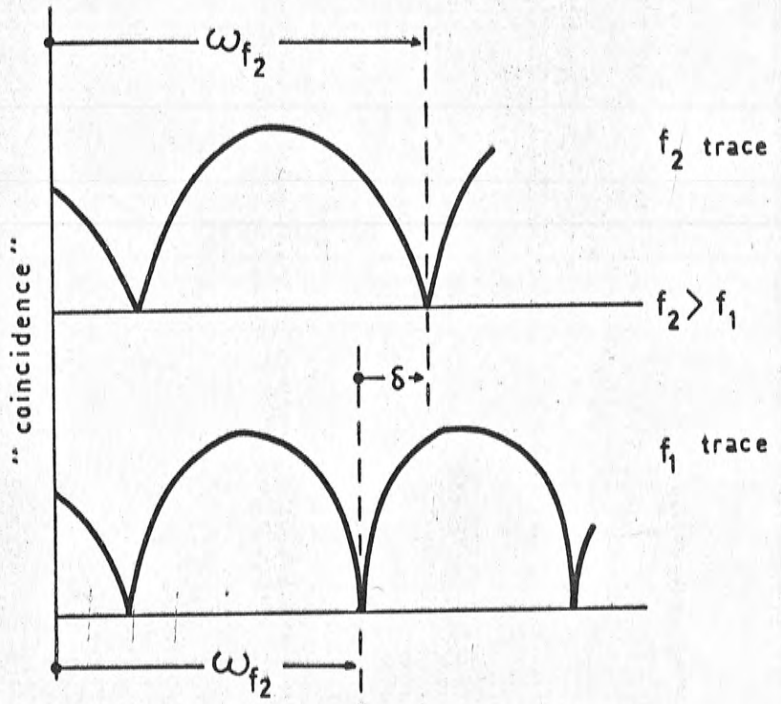

Figure (4.1). Illustrating the "Vernier" method of finding the angle of rotation of the plane of polarisation when two radio frequencies are used.

recorded null occurs at the higher frequency, f_2 say, the plane of polarisation at frequency f_1, has rotated through an angle δ $(0 \leq |\delta| < \pi)$ from its preceding null position, the angle:

$$\omega_{f_2} = \frac{\delta}{\left(\frac{f_2^2}{f_1^2} - 1\right)} \qquad (4.3)$$

is the amount by which Ω_{f_2} exceeds the value it took at the last coincidence.

Equation (4.3) which is derived from the relationship $\Omega \propto \frac{1}{f^2}$ (4.1), indicates in particular that the coincidences are given by:

$$\Omega_{f_2} = \frac{n\pi}{\left(\frac{f_2^2}{f_1^2} - 1\right)} \quad , \quad n = 0, 1, 2, \ldots \qquad (4.4)$$

As it stands the frequency differential method is ambiguous as to the value of the integer n in equation (4.4). If, however, f_1 and f_2 are chosen to be so nearly equal that a change of unity in n produces a large change in the right hand side of equation (4.4), the correct value of n can be determined by comparing the possible values of I with that obtained from the method described earlier. The author has found, using frequencies of 40.01 and 41.01 Mc/s for f_1, and f_2, that only one value of n can usually be accepted as reasonable.

No information is available regarding the accurancy of the frequency differential method; since it makes no assumptions about the gradient of total electron content it will not, on the average, give a biassed result.

CHAPTER 5.

INTRODUCTION TO EXPERIMENTAL STUDIES

The principal purpose of the experimental work reported in this thesis was to apply to observations of scintillations at a middle latitude southern hemisphere station such as Adelaide is, the more definitive methods of investigation which have become available in recent years.

The following brief review outlines the progress of Australian studies of scintillation to the time of commencement of the work reported.

Australian observations of radio-star scintillations were first made by Mills and Thomas (1951) shortly after the first discovery by British workers that the scintillations were imposed by irregularities in the terrestrial ionosphere (Smith (1950), Little and Lovell (1950)). These observations, and those that shortly followed (Bolton, Slee and Stanley (1953)) were principally concerned with correlations of scintillation occurrence with that of E and F layer parameters, but Wild and Roberts (1956) performed spaced-receiver analyses of the drifting amplitude pattern. These authors found the irregularities of the pattern had widths of between 1.5 and 8 km, and that they exhibited anisotropy, but no specific interpretation was made in terms of the effective ionospheric irregularities. More recent Australian studies of radio-star scintillation have dealt mainly with occurrence properties: Slee (1962) studied the relationship with geomagnetic activity and Smerd and Slee (1966) determined the seasonal and diurnal variations of the phenomenon, and its dependence on solar angular distance.

An early study of satellite scintillations in Australia was that of Slee (1958) who established a correlation with radio-star scintillations, and who showed that the irregularities producing scattering must be below an altitude of 350 km., this being the height of the satellite at the time of observation. Singleton and Lynch (1962a) discussed the diurnal variation of satellite scintillation and its relationship with E- and F-region parameters. They gave theoretical curves for the variation of scintillation depth with zenith angle (the validity of which is questioned by Briggs and Parkin (1963)), and from them established the height of scattering irregularities to be between 200 and 500 km. Singleton and Lynch (1962b) and Singleton, Lynch and Thomas (1961) showed the existence of a peak of scintillation activity for observations made in the direction of the geomagnetic field and established, thereby, the field aligned anisotropy of the scattering irregularities. Munro (1963) investigated the sizes of patches of irregularities over south-eastern Australia and showed, by a method of triangulation, that the irregularities occurred at heights near 300 km.

This outline clearly shows that comparatively few definitive investigations have been made in Australia regarding the heights, shapes and sizes of the irregularities which produce scintillation. Suitable methods of investigation are available and have been applied at various locations. They are now reviewed briefly.

The mean height of ionospheric irregularities is most simply determined by comparison of the velocity of drift of a satellite scintillation

pattern over the ground with the velocity of the satellite itself. The appropriate theory is that given in Section 2.6.2. and by James (1962) and Liu (1966). Experimental methods differ in the manner of measurement of the drift velocity of the pattern at the ground.

In the simplest method, the passage of an abrupt and obvious "transition" in scintillation depth is observed at receivers which are spaced in the direction of satellite motion. The method was first used at College, Alaska (Parthasary, Basler and deWitt (1959), Basler and deWitt (1962)) and indicated irregularity heights from 100 to 1000 km. Similar measurements at Urbana yielded heights of from 320 to 430 km. (Yeh, Swenson and McClure (1963)).

When obvious transitions of scintillation depth do not occur, the motion of the signal fluctuations in the pattern at the ground must be determined. This can be done by timing the passage of individual fades of distinctive shape (the Mitra method, see Mitra (1949)) or, more accurately, by noting the lag in the temporal cross-correlation function of signal fluctuations observed at spaced receivers. Many investigators have used these methods. Measurements by Frihagen and Troim (1960 and 1961) at Kjeller in Norway indicated heights of irregularities between 300 and 400 km. Hook and Owren (1962), working at College, Alaska, found irregularities from 100 to 275 km. Heights between 330 and 540 km. were found by de Barber (1963) at Pennsylvania and measurements made at Gorki State University (Yerukimov (1962)) yielded heights between 270 and 390 km. The most extensive study to date, that of McClure and Swenson (1964) at

Urbana involving 130 height measurements, gives heights between 250 km. and 600 km. for night-time irregularities and around 100 km. for day-time irregularities.

The correlation analysis which is used by most of the authors mentioned above can also provide accurate determinations of the sizes and shapes of the irregularities. From satellite observations, McClure and Swenson (1964) and Frihagen and Troim (1960) have shown the characteristic radii of the irregularities transverse to the geomagnetic field to be of the order of 1 or 2 km., in agreement with results of radio-star observations (Jones (1960)). Field aligned anisotropy is observed by Frihagen and Troim (1960), who find the irregularities to have an axial ratio of about 2. Irregularities whose minor radii are between 0.5 and 1.0 km. and whose axial ratios vary between 1.4 and 8 are found in the Cambridge observations of Margaret E. Clarke (1964).

The applications of the correlation analysis to spaced receiver recordings made at Adelaide are discussed in Chapter 9.

The methods of investigation which have been described in Section 3.2 are capable of yielding accurate determinations of irregularity size and shape. Their use has not yet been reported in the literature. A discussion of the application of these methods is given in Chapter 8.

In Chapter 7 the occurrence properties of satellite scintillations, and the correlation of scintillations with other geophysical

phenomena are discussed. In this chapter, estimates of the heights of irregularities are obtained for use in the discussion of Chapter 8. These estimates have been used, rather than the values obtained in Chapter 9, to make obvious the simplicity of the determinations of Chapter 8.

The results of the analysis of Faraday fading are presented in Chapter 10. The main aim of this study was to investigate a possible clue to the nature of the source of ionospheric irregularities. There are three types of theory regarding this source. The first type proposes an irregularly ionising source such as energetic ions (Peterson et al. (1955)) or protons (Herman (1966)). Irregularities produced by such a source would be associated with an increase in the mean electron content. The second type of theory suggests that observed irregularities are associated with turbulent eddies (Piddington (1964)); these would not cause any change in the mean electron content. The same would be true if the irregularities were caused by any type of hydromagnetic wave. The third type of theory proposes a streaming of molecular nitrogen from the E-region to the F-region where it produces irregular regions of increased electron recombination (King and Roach (1961)). The recombination would produce a decreased mean content. In Section 10.1 the relationship between patches of scintillation and irregularities in the total ionised content of the ionosphere is investigated with a view to deciding between these theories.

In Section 10.2 the diurnal and seasonal variations of total electron content at Adelaide are discussed.

CHAPTER 6.

EQUIPMENT AND METHODS

6.1 The Satellites

In experimental observations the author made use of the S-66 Ionosphere Beacon satellites BE-B(6464a) and BE-C(6532a). Being intended for use in world-wide ionospheric studies, these were placed in stable circular orbits at heights of about 1,000 km., above the major portion of the ionospheric electron content and the irregular regions of greatest interest.

The orbits of these satellites are inclined to the equator at angles of 80°(BE-B) and 41°(BE-C) with the result that both north-south and east-west scans of the sky are observed at a middle latitude station. Both satellites have orbital periods of about 100 minutes and a typical useful pass lasts about 15 minutes from rise to set at a given observing site.

An important feature of the satellites' behaviour is the slow movement of their pass times through the twenty-four hour day. At Adelaide, groups of two or three successive observations of BE-B are separated by a twelve-hour interval. The groups occur slightly earlier each day to the extent that after 90 days they have interchanged temporal positions within the day. BE-C is observed during four or five consecutive passes, the group of passes advancing through twenty-four hours in about 60 days. Because of these properties it is necessary to combine the results of three months observations to reveal the diurnal variation of any phenomenon being studied.

Both of the satellites provide plane-polarised

transmissions of 250 milliwatts power at frequencies of 20.005, 40.01 and 41.01 Mc/s. Since the satellites are stabilised against tumbling motions, it can be assumed, for the purpose of Faraday rotation analysis, that the initial direction of polarisation of the transmissions is fixed throughout any one observing period.

6.2 Ground-based Equipment

6.2.1 Configuration of Equipment

Observations of the satellites were made at the field station operated by the University of Adelaide at St. Kilda ($34^{\circ}43'S$, $138^{\circ}35'W$), north of Adelaide, South Australia.

Two distinct receiving systems were used. The first of these was operated daily for the continual monitoring of scintillation and Faraday effects. Its aerials consisted of simple half-wave dipoles, each mounted horizontally at a height of one quarter wave-length above the ground. Fitted with balancing and matching transformers, these fed receivers in the nearby recording station which were tuned to the three satellite radio frequencies mentioned above.

The second system, consisting of three spaced aerial-and-receiver "out-station" combinations, was used in the detailed study of the amplitude scintillation pattern at 40 Mc/s. Each aerial comprised two crossed folded dipoles phased in quadrature so that only circularly polarised radiation was received from the zenith. This arrangement minimised unwanted Faraday fading in the scintillation records. After balanced-to-unbalanced

transformation and matching, the signal was fed to an accumulator - powered transistorised receiver housed near the aerial in a weatherproof, bulletproof canister. Landlines carried the receiver output signals to the central recording station.

The out-stations were initially set up as indicated by the points L,S,W1 in Figure (6.1). The distances between the out-stations were chosen to approximate the expected mean dimension of irregularities in the scintillation pattern at the ground; that is, about 1km.

The operation of the spaced receiver equipment and the subsequent analysis of the scintillation pattern have formed a major portion of the author's work. The project was, however, severely hampered by difficulties in keeping the landlines connecting the system in working order.

Repeated damage to the western line in the vicinity of a civil construction site necessitated time-consuming repair work and eventually forced the withdrawal of the western out-station to the point W2. The shortening of the base line L W so produced, somewhat reduced the resolution of the system in the east-west direction.

A more serious problem was the control of induced mains frequency (50 c/s.) voltages which appeared on the longer lines (those from the southern and western out-stations). This "hum" was removed most effectively, but not completely, by isolating each out-station assembly from the earth, and by reducing the output impedance of each out-station receiver. A stage of

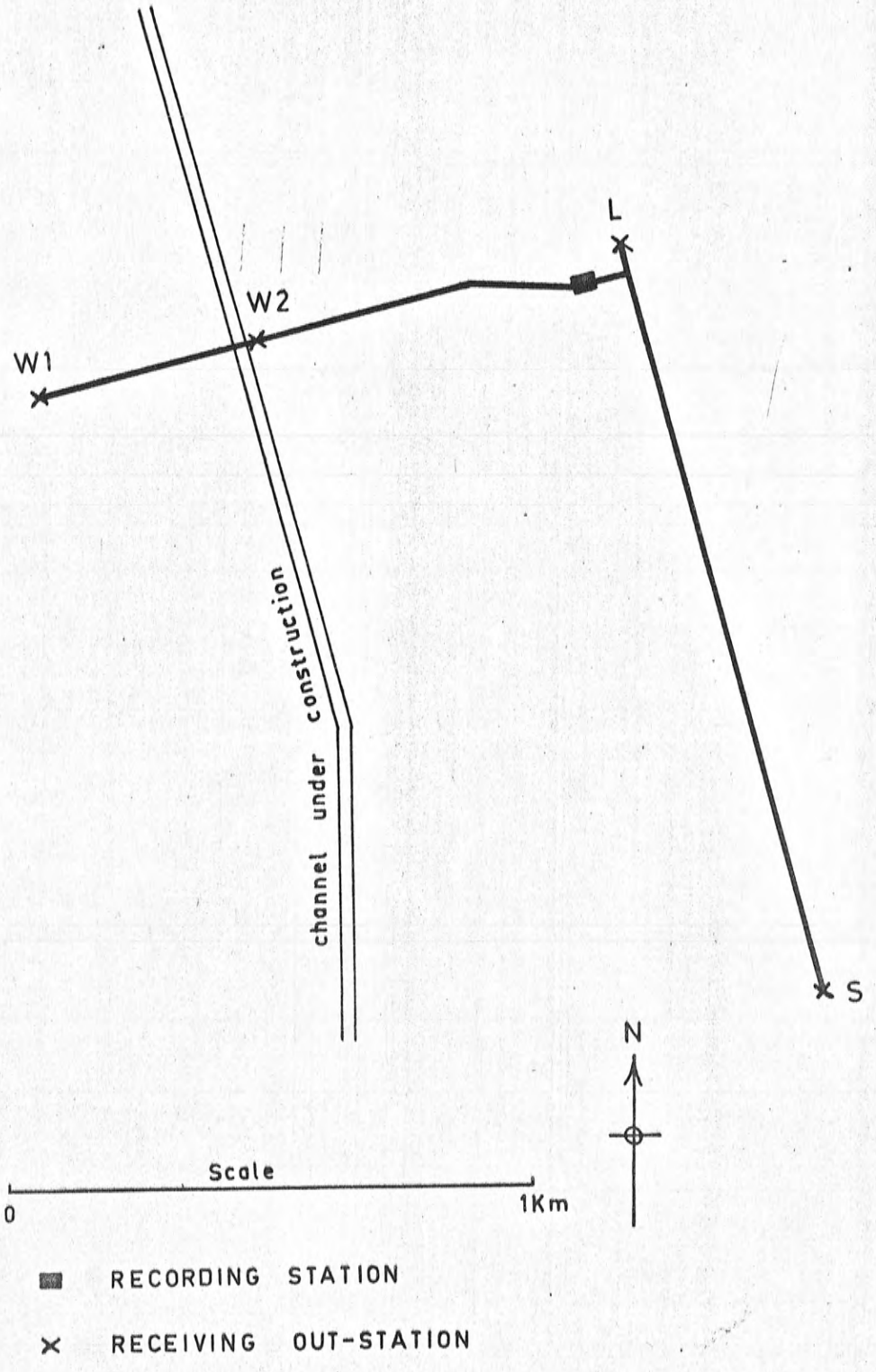

Figure (6.1). Map showing the arrangement of the out-stations used in the spaced receivers experiment at St. Kilda, South Australia.

amplification followed by cascaded buffer (emitter - follower) circuits was included between receiver and landline.

It was not possible for the author to develop or acquire the "modulated carrier" equipment which would most simply circumvent the "hum" problem but, on the author's advice, such equipment is being developed at the time of writing.

6.2.2 Receivers

For the greater number of satellite observations use was made of the "Model B" receivers produced by the Magnavox Company of America. These transistorised, double-conversion receivers, which were designed specifically for satellite studies, are among the most sensitive that can be produced without the use of phase lock or automatic frequency control systems. Their main characteristics are:

Noise Figure : 3db

Bandwidth : 2500 c/s

(The bandwidth must, of course, cover the Doppler frequency variation in the signal from a moving satellite).

As designed, the A.G.C. (automatic gain control) action of the Model B. receiver is such that the output (A.G.C.) voltage is proportional to the logarithm of the income signal amplitude. Beside extending the range of signal levels which, after reception, can be satisfactorily recorded, this action conveniently produces a sharpening of the Faraday fading cusps in the recorded trace; but for scintillation measurements a linear system is preferable. A scintillation record cannot be analysed with consistent accuracy

if the recording gain is not a symmetrical function of signal departure from the mean signal.

For this reason, the operation of the A.G.C. was stopped at scintillation frequencies ($\geqslant$ 1c/s) by increasing the time constant of the A.G.C. circuit. The gain of the receiver then became a function of the mean signal level averaged over several scintillation cycles. The maximum acceptable value of the modified time constant was determined only by the requirement that the A.G.C. should not be completely disabled at the Faraday fading rate ($\leqslant$ 0.3c/s at 20 Mc/s).

In the receivers used for continual monitoring of scintillation and Faraday effects a time constant of 5 seconds was employed; those used for detailed scintillation analysis, the mean output voltages of which were monitored by an operator during use, were modified to have a time constant of 10 seconds.

The performances of the receivers after modification were checked in two ways. Their responses to step increases in input signal were recorded and found to conform with expected behaviour. The scintillation depths of recordings made with both the modified sets and a receiver known to have a linear response were compared. They were found to differ by less than 10 per cent at fading frequencies down to 1.5 c/s.

6.2.3 Recording

The receiver output voltages were applied to directly-coupled amplifiers which drove, in turn, the motor coils of chart recorder pens. With regard to the recording system it need only

be noted that the frequency response of the pen suspension fell to one half at 50 c/s.

6.2.4 Timing

For the routine observations of satellite passes the chart recordings were marked once per minute. The pulses which drove the marker pen were derived from a mains synchronised clock, none more reliable being available. The time given by this clock was checked daily against standard radio transmissions and was found to deviate by less than two seconds from Universal Time. Although a greater accuracy in timing is generally desirable in satellite studies (Swenson (1962)), this error produces no more than a one degree (average) uncertainty in the angular position of a satellite as seen by an observer. It is, therefore, of little consequence in most experimental work.

However, in a detailed analysis of the movement of the signal fading pattern over the ground, a greater timing accuracy is needed. During such observations time was kept by the operator present to an accuracy of 0.2 seconds.

6.2.5 Other Equipment

Several devices were developed by the author which allowed unmanned operation of the receiving and recording equipment. These include a "timer" which can be programmed to start chart recorders at predicted satellite rise times and to stop them after a preset interval. Another device produces a voltage pulse train, which, when "written" on a moving chart, is a binary representation of current clock time.

Although such equipment was important to the acquisition of data, its description is not relevant to the discussion of the results, and it is left at this point.

6.3 Computer Programs

It is not proposed to give detailed analyses or listings of the computer programs used by the author but, in the interests of continuity and conciseness, descriptions of the important operations for which computers were used are collected here.

6.3.1 Geometry of the Satellite-Ionosphere-Observer System

The agency which organised dissemination of information regarding the satellites BE - B and BE - C (National Aeronautical and Space Administration, Maryland, U.S.A.) provided two aids to the analysis of satellite motions. These were, firstly, a listing of the minute-by-minute geographic positions of the satellites and, secondly, a table from which various geometrical quantities, dependent upon the relative positions of satellite and observer, could be obtained.

Since the analysis reported in later pages required the determination of satellite position at upwards of sixty points for each of about 1500 passes, it was considered impractical to carry out repeated interpolations of these tables. Computer programs were written by the author which accomplished the necessary evaluations and the tabulations were only used for the checking of computed results.

(As many experimenters now have access to computing equipment, it would seem to be a simple matter, in future

satellite projects, to provide suitable program listings as an alternative to tabulations. A request by the author for such information went unacknowledged).

A basic set of instructions on the manipulation of vectors in three-dimensional Cartesian frames was included in all "space geometry" programs. This enabled the operative parts of such programs to be written in a very straight-forward manner, in terms of a vector notation.

Satellite Position

Since both satellites BE - B and BE - C have high stable orbits, it was found possible to determine their positions to a sufficient accuracy by the use of first order Newtonian orbit theory. Orbital elements appropriate to fortnightly intervals of time were obtained from the agency mentioned above and were included permanently in the program. A satellites position (accurate to less than half a degree in latitude or longitude) and velocity were made available to any other program as continuous functions of time.

Geometry Relative to an Observer

Programs were written which solve the spherical earth geometry pertaining to obsefvation of a satellite through an intermediate layer. Measures of obvious importance such as the azimuth and elevation angles of the satellite, and the distances along the ray from the layer to the observer, and to the satellite, are evaluated by the programs.

The inclusion of a program for the determination of

the geomagnetic field enabled the factors involved in the quantity M, of equation (4.1), to be evaluated for use in Faraday rotation analysis.

It was found most useful, in the interpretation of the results of the spaced receiver analysis, to have available determinations of:

(i) the expected direction of motion of the scintillation pattern across the ground.

(ii) the expected lengths and orientations of the "shadows" on the ground of unit vectors lying along the geomagnetic field, or at right angles to it in the place of the wavefront.

These evaluations were performed by a specialised "geometry" program.

6.3.2 Correlation Analysis

The correlation analysis introduced by Briggs, Phillips and Shinn (1950) and extended in scope by Phillips and Spencer (1955) has been used extensively in both reflected-wave and radio-star studies of ionospheric irregularities; it has become a standard technique. Most often the analysis is performed by graphical methods but Fooks (1965) has described a computer program which achieves it.

With the aid of advice from Fooks (private communication) the author has written a similar program. Since its description conforms exactly to that given by Fooks (1965), only an outline

of its operation is given here.

The analysis assumes a form like that of equation (3.23) for $\rho_a(\xi,\eta,\tau)$ with the added freedom that the functional form need not be an inverse exponential, but any which, near the origin, decreases monotonically from unity at the origin. The polynomial argument, of ellipsoidal symmetry in (ξ,η,τ) space, is assumed.

The temporal variations of signal amplitude at three spaced receivers are mutually correlated to give, ideally, one auto-correlation function and three cross-correlation functions. These four functions describe the behaviour of $\rho_a(\xi,\eta,\tau)$ along the -axis and along three other lines, parallel to it, and separated from it in the (ξ,η) plane by the vector separations of the receivers. A knowledge of the form of the auto-correlation function and the positions and values of the three cross-correlation maxima is sufficient for complete determination of the "characteristic" ellipsoidal contour on which $\rho_a(\xi,\eta,\tau)$ falls to 1/e. The quantities determined, in fact, are the required coefficents A,B,C,D,V of the appropriate polynomial.

The program logic follows the steps of the earlier graphical procedure. The form of the spatial characteristic ellipse (see Section 3.4) is first obtained. An "apparent velocity" is then determined from a knowledge of the positions of the cross-correlation maxima. Finally, the quantities V and V_c are derived from the "apparent velocity", allowance being made for its dependence on the shape and orientation of the characteristic ellipse.

CHAPTER 7.

THE OCCURRENCE CHARACTERISTICS OF SCINTILLATION

7.1 Definition of Scintillation Index

In reducing the satellite recordings taken at Adelaide to a form suited to the study of scintillation occurrence characteristics, a coarse index of scintillation depth, determined by eye, was assigned to each quarter-minute interval of recording time. Three levels of scintillation, none, weak and strong, were recognised, and were given the weights 0, 1 and 2 respectively. Figure (7.1) shows tracings of scintillations which are typical of the three levels. The scintillation depths of the traces (b) and (c), determined according to the definition of equation (3.15), are .15 and .32 respectively, indicating that the assigned weights (or indices) give an approximately linear measure of depth.

The indexing method described has been used by several authors (Yeh and Swenson (1959), Liszka (1963)) and was adopted by a group of Australian observers of the S-66 satellites at the conference reported by Briggs (1963).

By the use of the satellite position and space geometry programs described in the previous chapter, each quarter-minute reading of scintillation depth was associated with spatial position co-ordinates; these were, for most of the applications of this chapter, the elevation and azimith angles of the satellite relative to the observing station. To separate from other variations those due to the changing zenith angle or ltitude

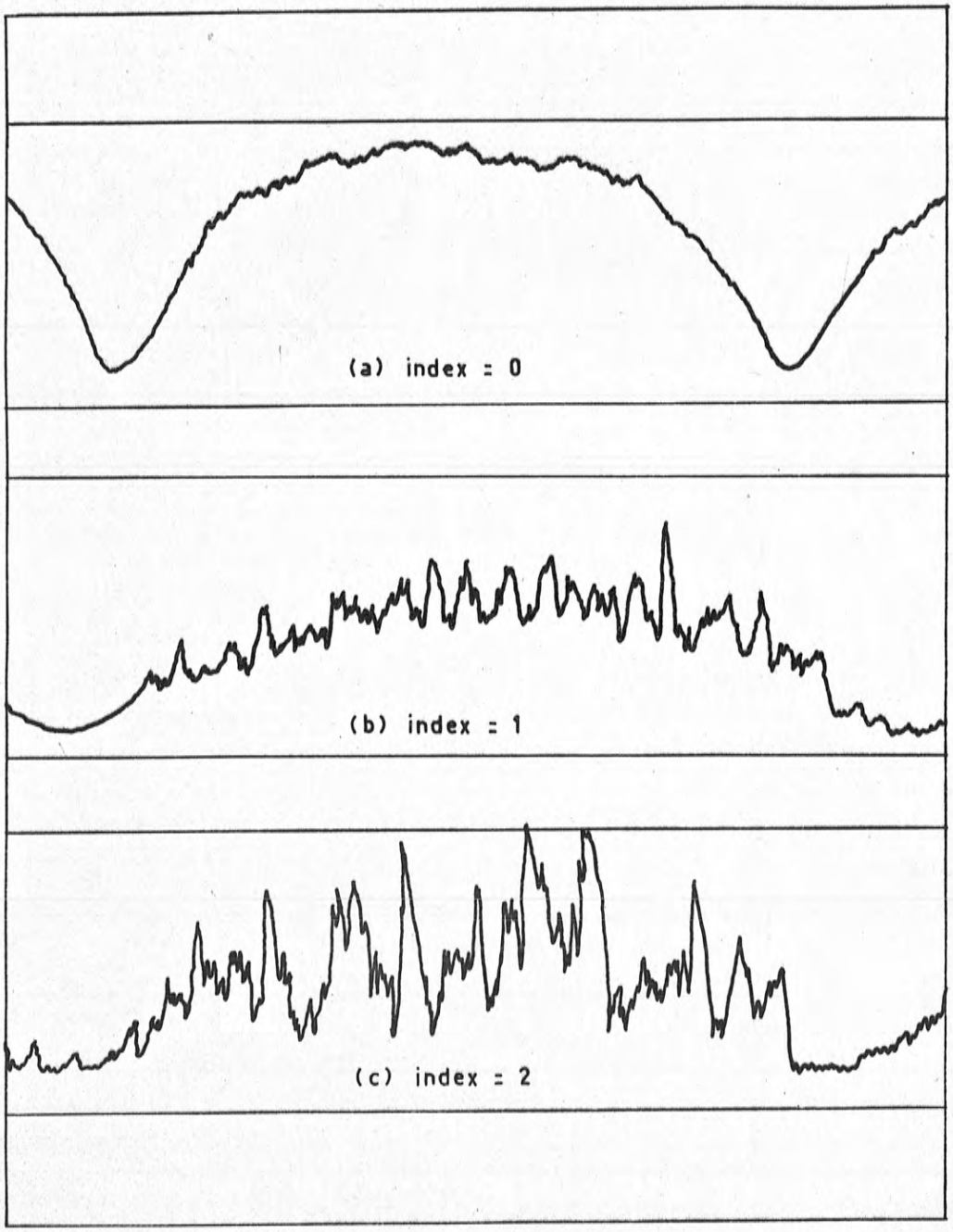

Figure (7.1). Tracings of scintillation recordings typical of the scintillation indices 0, 1, and 2. The scintillation is superimposed upon the slower Faraday fading.

of the source, the data which applied to conditions "overhead" were then selected out on the basis that the elevation angles with which they were associated were greater than 45°. It is these "overhead" data which are referred to in Sections 7.2, 7.3, 7.4 and 7.5.

The results are derived from observations at 40 Mc/s of 1105 satellite passes.

7.2 Diurnal and Seasonal Variations

Figures (7.2) and (7.3) show the diurnal and seasonal variations of the scintillation index at Adelaide for 1965. The results are for four "seasons" which are centred approximately on the equinoxes and solstices, as follows:

Summer:	January, November, December, 1965, and January, 1966.		
Autumn:	February	-	April, 1965.
Winter:	May	-	July, 1965.
Spring:	August	-	October, 1965.

The curves were drawn to connect smoothly the two-hourly means of the average hourly values of scintillation index.

The level of scintillation is at all times low, never greatly exceeding the value of unity.

There are no Australian observations for a year of high sunspot number with which the present results can be compared in a determination of the variation of scintillation depth with solar activity. It is probable that the generally low level of scintillation is due in part to such a variation (the mean sunspot number in 1965 was 12), for decreases of both day and

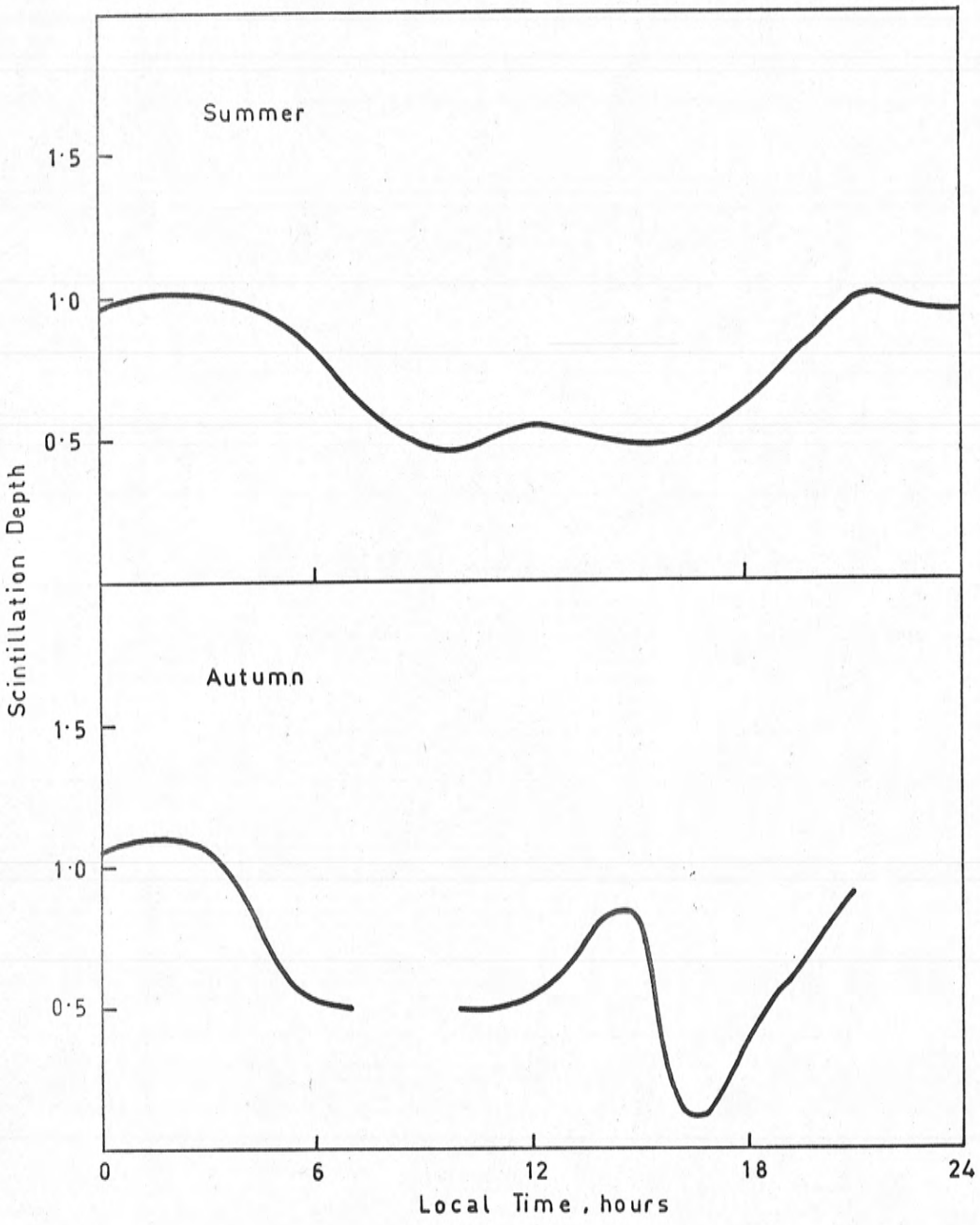

Figure(7.2). The diurnal variations of 40 Mc/s scintillation depth in Summer and Autumn, 1965.

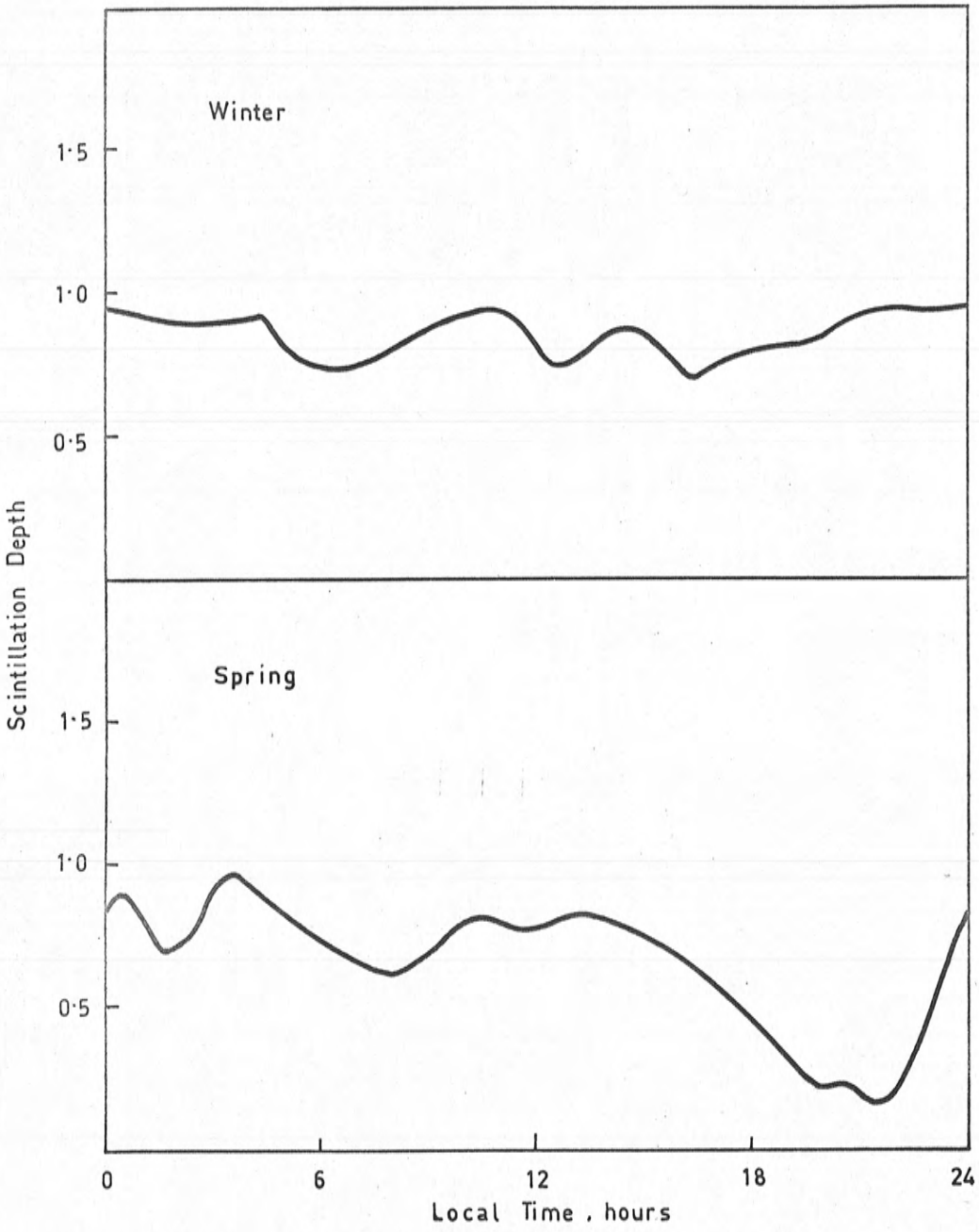

Figure (7.3). The diurnal variations of 40 Mc/s scintillation depth in Winter and Spring, 1965.

night-time scintillation depths with decreasing sunspot number have been found by several authors (Chivers (1960), Koster (1958), Briggs (1964), Yeh and Swenson (1964)). The actual values of scintillation depth found in the present study are very similar to those found at 54 Mc/s in a year of low sunspot number (1962) by Yeh and Swenson (1964).

The diurnal variation of the scintillation index shows, in all seasons, a night-time maximum which is a characteristic common to observations at higher latitudes (Briggs (1964)) and lower latitudes (Koster (1958)).

Day-time scintillation appears in all seasons and shows, to varying degrees, a maximum which is secondary to the night-time maximum. Day-time scintillation is rarely observed by English workers, especially at a time of sunspot minimum (Briggs (1964)), but a day-time maximum was found in Australian observations at low elevation angles by Bolton, Stanley and Slee (1953). More recently Smerd and Slee (1966), working at Sydney at a time of high sunspot number (1955-59) have observed a pronounced day-time maximum at all elevation angles. Munro (1965), who determines, not the level of scintillation, but the fractional amount of each satellite pass which shows scintillation, finds a day-time behaviour similar to that reported here. Day-time scintillation is reported by Yeh and Swenson (1964).

The seasonal variation of the night-time scintillation level is slight, as found by observers at other latitudes

(Briggs (1964), Yeh and Swenson (1964)), but day-time scintillation shows a winter maximum. Munro (1965) finds a similar behaviour as do Yeh and Swenson (1964) for whom, however, the variation is more marked.

In conclusion of this section, special attention is drawn to the general similarity between the present results and those obtained by Yeh and Swenson (1964) at Urbana, Illinois, in a year of low sunspot number. Smerd and Slee (1966) raise the question of whether the maximum in day-time scintillation observed by them, is characteristic of the southern hemisphere alone, or of temperate latitudes in both hemispheres. The similarity noted answers the question in part (for years of low sunspot number). However, the absence of a marked day-time peak in the results of Yeh and Swenson for years of high solar activity does indicate a difference depending on the hemisphere of observation. The matter deserves further investigation.

7.3 Correlation with Spread-F

The close association between radio-star scintillation and spread-F is well known (Ryle and Hewish (1950), Booker (1958), Briggs (1964)), and several workers (Kent (1959), Yeh and Swenson (1959)) have reported a high correlation between spread-F and satellite scintillations. To investigate the relationship at Adelaide, the scintillation index (or its mean for several passes, if they were available) for the night-time hours between mid-night and 0300 has been correlated with an index of spread-F activity. The latter index was determined

from the Ionospheric Data Bulletins for Salisbury, South Australia, (which is approximately five miles from the site of satellite observations), The spread-F index was given the values:

0, if no spreading was observed,

1, if the letter F appeared in the bulletin,

2, if the letters UF appeared, signifying that the critical frequency could not be read from the ionogram because of severe spreading.

To obtain a sufficiently large number of values for the calculation of the correlation co-efficient, results for the whole of 1965 were used. It was considered that the different seasonal variations of the spread-F indices (broad winter maximum) and scintillation indices (little seasonal change) would not, in combination, produce a spuriously high correlation co-efficient; they would, if anything, lower its value.

A correlation co-efficient of .41, with a 5 per cent significance level of .186, was obtained, indicating that a relationship does exist between night-time scintillation and spread-F.

Using this information, an estimate may be made of the height of night-time irregularities for use in determinations carried out in Chapter 8. Throughout 1965 the virtual height of the night-time F-layer took values between 240 km. and 290 km. These values, which are regarded only as guides, suggest heights for the irregularities of between 250 km. and 300 km.

7.4 Correlation with Sporadic-E

The discovery by Wild and Roberts (1956), that a strong correlation exists between sporadic-E echoes and the day-time radio-star scintillations observed in Australia, suggests that the day-time satellite scintillations observed at Adelaide may originate at E-region heights.

An attempt to establish this fact was inconclusive. Ionograms made at Salisbury, South Australia, were not sufficiently clearly resolved to allow a direct measure of the degree of irregularity of the sporadic-E layer to be obtained. Instead, a less meaningful measure, the critical frequency of the sporadic-E layer, was used, and the co-efficient of its correlation with the mean scintillation index for the four hours centred on noon was calculated. A value of no significance (0.1, with a 5 per cent significance level of .21) was obtained. (This may indicate a lack of correlation between the degree of irregularity and the critical frequency of the sporadic-E layer).

To provide an estimate of height for use in the determinations of Chapter 8, it will be assumed, on the basis of the results of Wild and Roberts (1956), that the irregularities responsible for day-time scintillations lie in the E-region at altitudes of about 100 km. The assumption is supported in part by the observations of McClure and Swenson (1964) (reported by Yeh and Swenson (1964)) who find day-time irregularities to occur at this height.

7.5 Correlation with Magnetic Activity

Since the occurrence of night-time irregularities is found to correlate positively with magnetic activity at high latitudes (Little and Maxwell (1952), Hartz (1958), Basler and de Witt (1962)), and negatively at equatorial latitudes (Rao and Rao (1961)), it may be expected that the correlation between the phenomena is small and of either sign at a mid-latitude station. Recently Slee (1962) has found a positive correlation between the planetary K-index and night-time radio-star scintillations observed at Sydney.

In determining the relationship between magnetic activity and the night-time satellite scintillations observed at Adelaide, note was taken of the result found by Briggs (1965), that changes in the occurrence of spread-F echoes tend to lag on changes in the K-index. The lag is about 2 days at a time of sunspot minimum.

The co-efficient of correlation was determined between the mean scintillation index for the hours 0000 to 0300 of each available night of 1965, and the mean K-figure measured at Toolangi, Victoria, for that night, and for the four preceding nights. The five values of the co-efficient are shown with the appropriate lags, in days, in Table 7.1.

TABLE 7.1

Lag in days:	0	1	2	3	4
Correlation co-efficient:	.16	.05	.05	.19	.08

The 5 per cent significance level of each value, taken independently is .186, so the value for a lag of 3 days is

barely significant. Briggs (1965), who obtained similar values of maximum correlation co-efficient, established their significance in the repeated appearance, throughout a solar cycle, of a peak in the lag-correlation function. It is probable that the significance of the present result can only be proved in a similar way.

7.6 Variations with Latitude

A predominant feature of the geographic distribution of spread-F occurrence, as observed at the ground, is the existence of two areas of maximum. One is in equatorial regions, always on the night-time side of the earth, and the other is confined to polar latitudes, mainly in the dark hemisphere but often observed during the day (Shimazaki (1959), Singleton (1960)). Similar latitude dependence is seen in "topside" sounder data (Calvert and Schmid (1964)). Both types of observation shows a dependence on geomagnetic, rather than geographic latitude.

Briggs (1964) finds indications of an increase of radio-star scintillation activity to the north of a latitude of about 56°N (60°geomagnetic), and a similar increase is found in satellite scintillations at several northern hemisphere stations. (Kent (1959), Aarons et al. (1963), Joint Satellite Studies Group (1965)). Yeh and Swenson (1964) find a large increase in night-time satellite scintillation activity to the north of 40°N (geographic) in a year of high sunspot number (1958), but observe only a slight variation in a year of low sunspot number (1962).

In investigating the latitude variation of night-time scintillations at Adelaide, the dependence of the scintillation index on the azimith of the satellite was first determined. Figure (7.4) shows this dependence for both winter and summer observations. The data used were those appropriate to zenith angles between 50° and 60°, as these are not greatly influenced by the effects of anisotropy (see Figure (3.4)).

The curve of Figure (7.4) for winter shows no significant variation, indicating that there is no appreciable dependence of scintillation activity on latitude in winter.

The curve for summer shows a maximum towards the south (which behaviour, it may be noted, is opposed to that expected from anisotropy of the scattering irregularities). When the mean southerly trend of this curve is plotted against the latitude of the effective irregularities (assumed to be at a height of 300 km.), Figure (7.5) results. This shows the latitude variation of the night-time scintillation level in summer; a slight increase of the level towards the south occurs at $35{\cdot}4^{\circ}$S (approximately $44{\cdot}4^{\circ}$S geomagnetic).

The present results may be compared with those of Munro (1955) who found night-time scintillation to lie mainly to the north in winter; and to the south in summer.

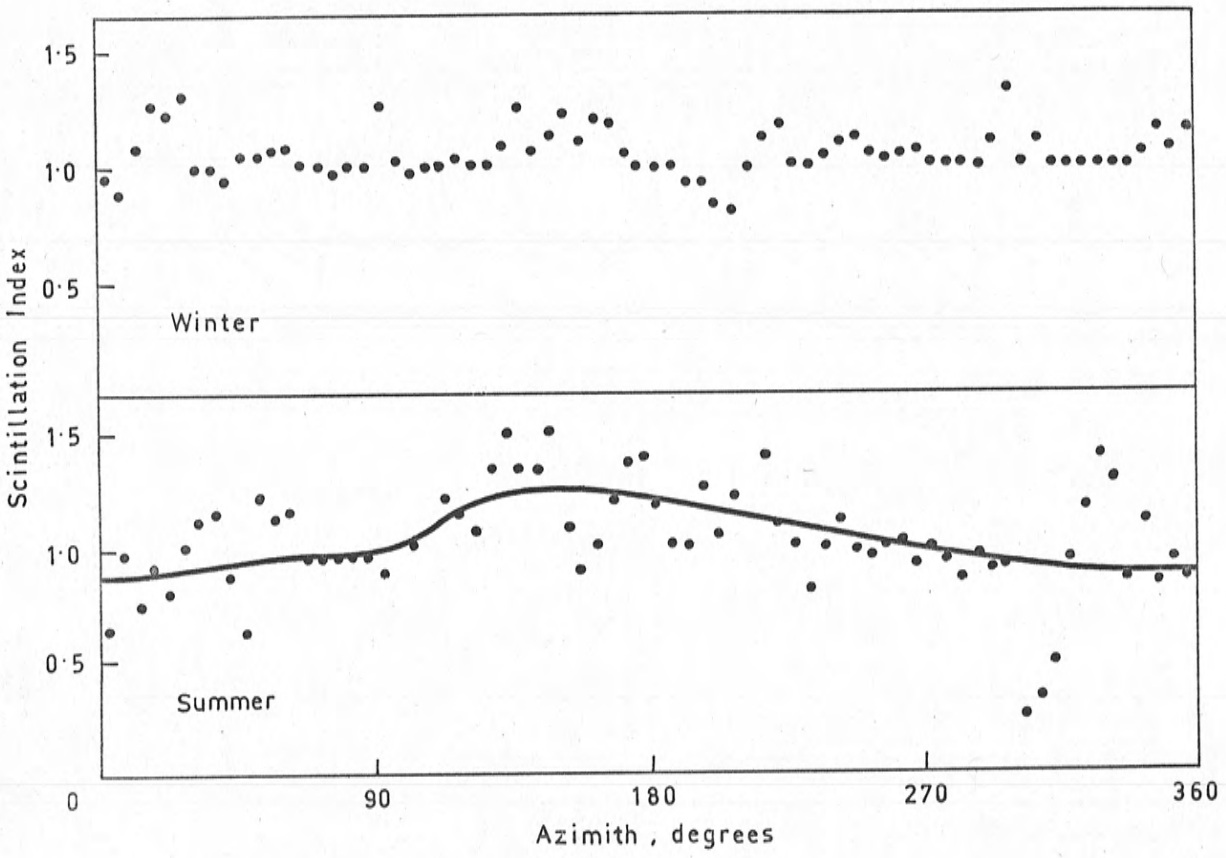

Figure (7.4). The azimith variation of the night-time 40 Mc/s scintillation index for Winter and Summer. The observations were made at a mean zenith angle of 55°.

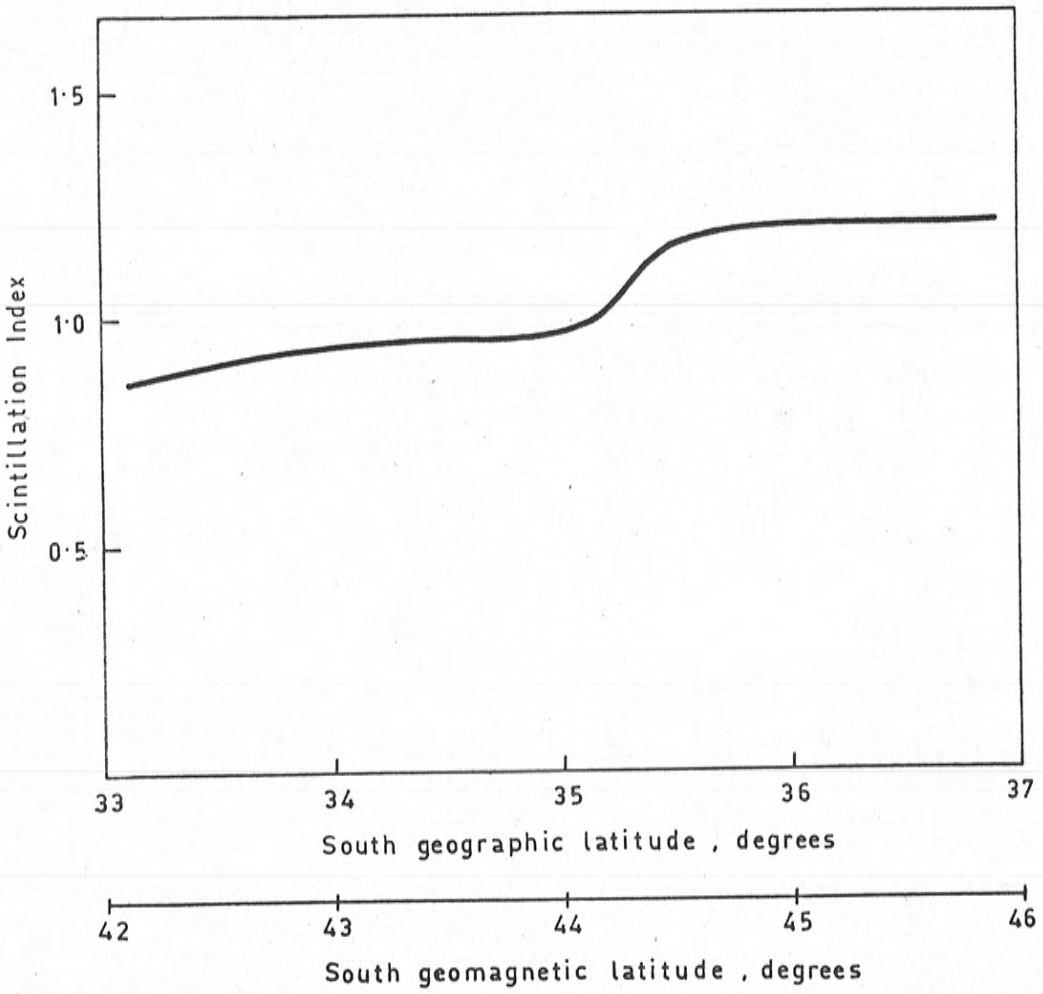

Figure (7.5). Showing the latitude variation of the night-time 40 Mc/s scintillation index in Summer.

7.7 The Horizontal Distribution of Irregularities

It has been found by several authors that irregularities occur in large patches with dimensions of from several hundred, up to one thousand, kilometres. (Calvert and Cohen (1961), Beynon and Jones (1964), Munro (1963), Koster (1963)). The boundary of a patch is recognised in a recording of scintillations as a transistion from conditions of weak scintillation to strong, or vice versa.

Such transitions occurred rarely at Adelaide and only appeared in about 5% of the recordings made. (Yeh and Swenson (1964) report a similar result for 1962). The most usual condition was found to be one of continuous weak scintillation throughout a whole pass.

A rough estimation of the size of patches which produced deep scintillation yielded a value in excess of 500 km., independent of the direction of motion of the satellite.

In the present connection, note may be made of the activities of a group of Australian observers with which the author was associated. Throughout 1965 observations of the S-66 satellites were made at Townsville, Brisbane, Sydney, Camden, Melbourne, Hobart, Adelaide, Woomera and Perth. The results have not yet been fully collated but the possibilities of the survey are illustrated by the preliminary analysis. Figure (7.6) shows the "tracks" on the ionosphere (at a height of 300 km.) of the ray paths connecting the satellite to observing stations at Adelaide, Melbourne, Hobart and Camden. The quarter-minute scintillation indices determined at the stations are marked on the appropriate tracks.

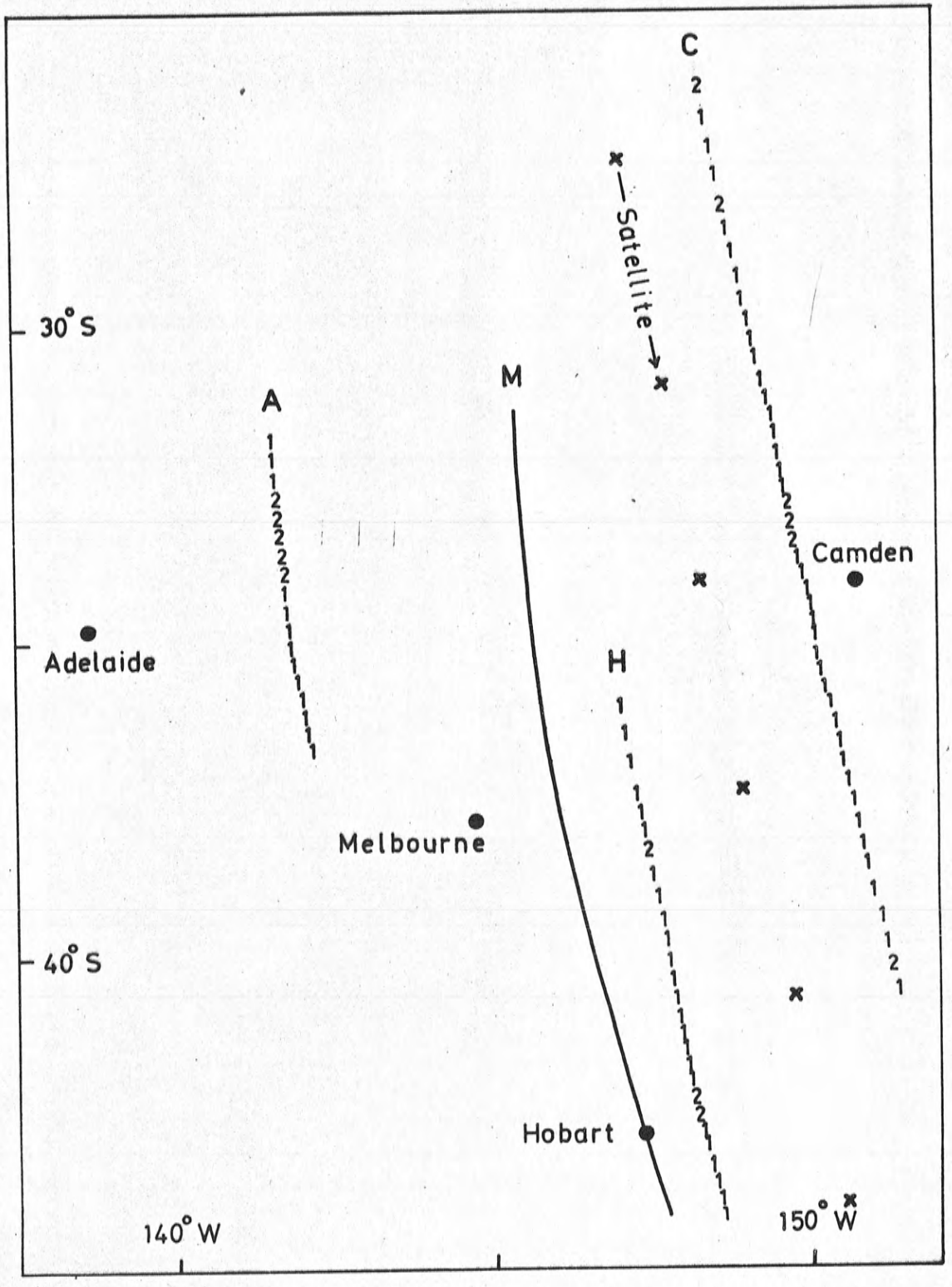

Figure (7.6): Observing stations and associated ionospheric tracks, with scintillation indices, for a pass at 2004, Adelaide time, on 20th Sept. 1965. No scintillation was observed at Melbourne.

The tracks are seen to be spaced sufficiently closely to delineate patches of the sizes commonly observed. When data from all the stations are available, detailed pictures of a large area of the irregular ionosphere will be obtained.

CHAPTER 8.

ZENITH ANGLE EFFECTS

8.1 Effects Average in Azimuth

When the 40 Mc/s scintillation indices described in the previous chapter are averaged in azimuth and plotted against the zenith angle of the satellite, the diagrams of Figures (8.1) and (8.2) result. The separation into seasons, which was employed previously, is again used, and a distinction between night (Figure (8.1)) and day (Figure (8.2)) results is made. Night and day have been taken to be bounded by 0600 hours and 1800 hours, local times.

In fitting the experimental points with smooth curves, diminished weight has been given to points at the extremes of zenith angle since relatively few observations were available to define these. The curves have been extrapolated, regard being given to the trends of the data points and the expected form of the curves.

According to the discussion of Section 3.2.2, estimates of irregularity size may be obtained from these curves if reasonably accurate values for the heights of the irregularities are available. The simplest method is as follows:

(i). from each curve the "zenith angle ratio", the ratio of scintillation depth at the horizon to that at the zenith, is found.

(ii). if the irregularities are known to be anisotropic, the effects of enhancement

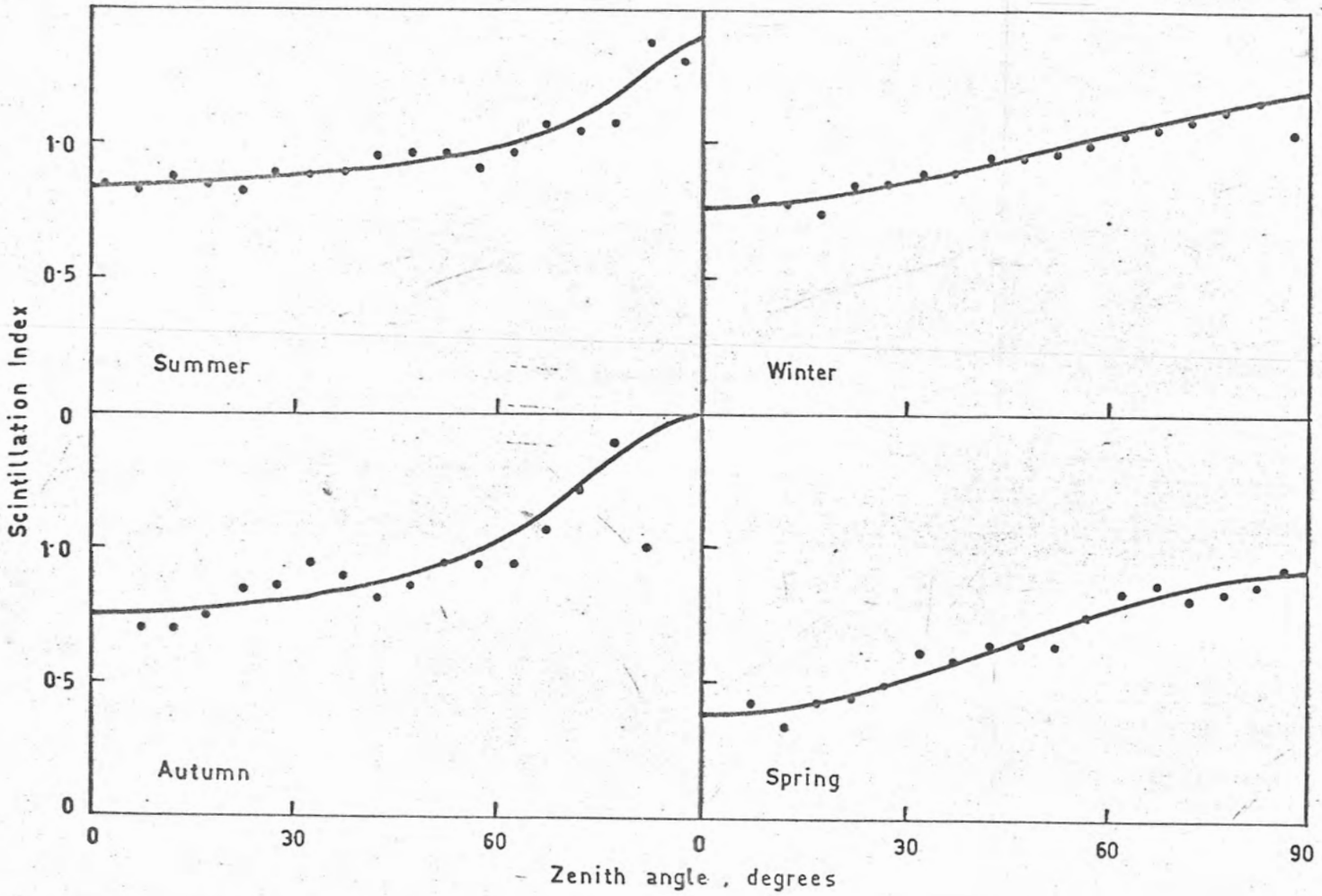

Figure (8.1) The zenith angle variations of night-time scintillation indices for four seasons.

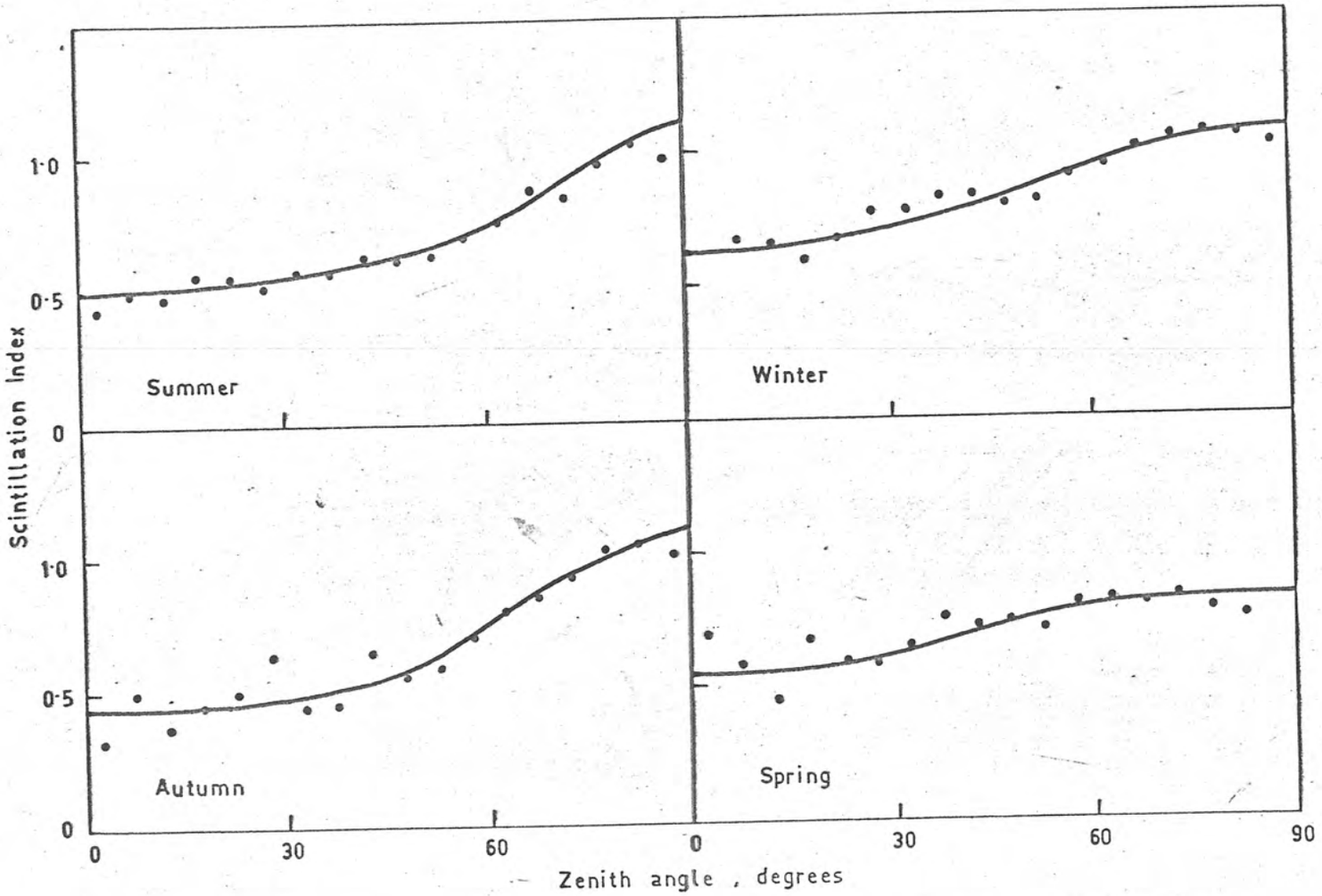

Figure (8.2) The zenith angle variations of day-time scintillation indices for four seasons.

of scintillation at the zenith are removed by multiplication of the ratio in (i) by a suitable factor; the correction has been discussed in Section 3.2.3. The multiplying factor compensates, in the azimuth-average, for the depression of the "anisotropic" scintillation depth at the horizon below the "isotropic" value. (see Figure (3.4)). The factor to be used is determined, therefore, by calculating the extent of the depression for a typical situation of illumination from the horizon. In Adelaide, where the dip angle is high (66°), this situation is the one in which the ray is (approximately) perpendicular to the field direction. Using this fact, and noting that the extent of depression is little affected by change of axial ratio, (so that an infinite ratio may be assumed) the correction factor is easily evaluated. Its value is only weakly dependent on the parameters of irregularity height and size which are used in the calculation, and these need be known only approximately. (Note, for example, at the southern horizon in Figure (3.4),

that the factor only changes from 1.29 to 1.3 as the radio frequency is changed from 40 Mc/s to 20 Mc/s).

(iii). the zenith angle ratio, corrected if necessary, is compared with theoretical values for isotropic irregularities at the estimated height. Such values are available in Figure (3.3). The three steps just described are now applied to the data of Figures (8.1) and (8.2):

TABLE (8.1).

	Summer.	Autumn.	Winter.	Spring.
Zenith angle ratio	1.7	2	1.6	2.2
Corrected ratio	2.2	2.6	2.1	2.8
Radius r_o, km.	3/4	1	3/4	1

The zenith angle ratios obtained from the curves of Figure (8.1) for night-time scintillations are given in the first line of Table (8.1). It is found (Section 8.3.1) that night-time irregularities exhibit anisotropy so these ratios must be corrected. The correction factor appropriate to the experimental conditions is 1.29 (see above), and multiplication by it produces the ratios in the second line of the table. If the height of night-time irregularities is taken to be 300 km. (see Section 7.3 Figure (3.3) (which is drawn for a satellite at 1000 km. height,

transmitting at 40 Mc/s) shows the appropriate values of the characteristic radius r_o to be those in the third line of Table (8.1)).

The accuracy of the method is not so high that the variation of radius seen in Table (8.1) can be accepted as a seasonal one; the four values should be regarded as independent estimates of the radius.

TABLE (8.2).

	Summer.	Autumn.	Winter.	Spring.
Zenith angle ratio	2.2	2.4	1.7	1.5
Corrected ratio	2.9	3.1	2.2	2

The zenith angle ratios of the curves for day-time scintillation (Figure (8.2)) are given in the first line of Table (8.2). A correction factor of 1.3, which is appropriate for irregularities of 0.5 km. radius at a height of 100 km., has been applied to the ratios to give the values in the second line of the table.

Now, results reported in Section 8.3.1 indicate that day-time irregularities are only weakly anisotropic, and it is difficult to decide which of the ratios in Table (8.2) are applicable. The matter is not of great importance however, because reference to the curves of Figure (3.3) for a height of irregularities of 100 km. (see Section 7.4), shows the ratios to be typical of "far zone" conditions. Their values are so low

that determinations of irregularity size cannot reasonably be made. It can only be said that the radius r_o is of value 0.5 km. or less.

8.2 The Ratio of Scintillation Depths on Two Frequencies

The method described in Section 3.2.4 has been applied to the determination of irregularity size.

Short lengths of 20 Mc/s and 40 Mc/s signal traces which corresponded in time were analysed, and their scintillation depths S'_{20} and S'_{40} respectively, were determined according to the definition of equation (3.15). The ratios of scintillation depths, of the form (S'_{20}/S'_{40}), were then plotted as functions of the zenith angle of the satellite to give Figures (8.3) and (8.4). Figure (8.3) is derived from night-time passes observed between 2100 hours and 0300 hours local time; Figure (8.4) represents day-time observations between 0900 hours and 1500 hours local time.

It was not usually feasible to determine the complete zenith angle variation of the ratio of scintillation depths from a single recording of a satellite pass. Several "chains" of points, which are shown in Figure (8.3), were obtained from individual observations but, most often, the accurate evaluation of scintillation depth was hampered by the signal variations arising from the Faraday effect, especially at 20 Mc/s; the points at which evaluations were made could not be chosen at will. Because of this, and to increase (relatively) the number of points associated with small zenith angles (which points were

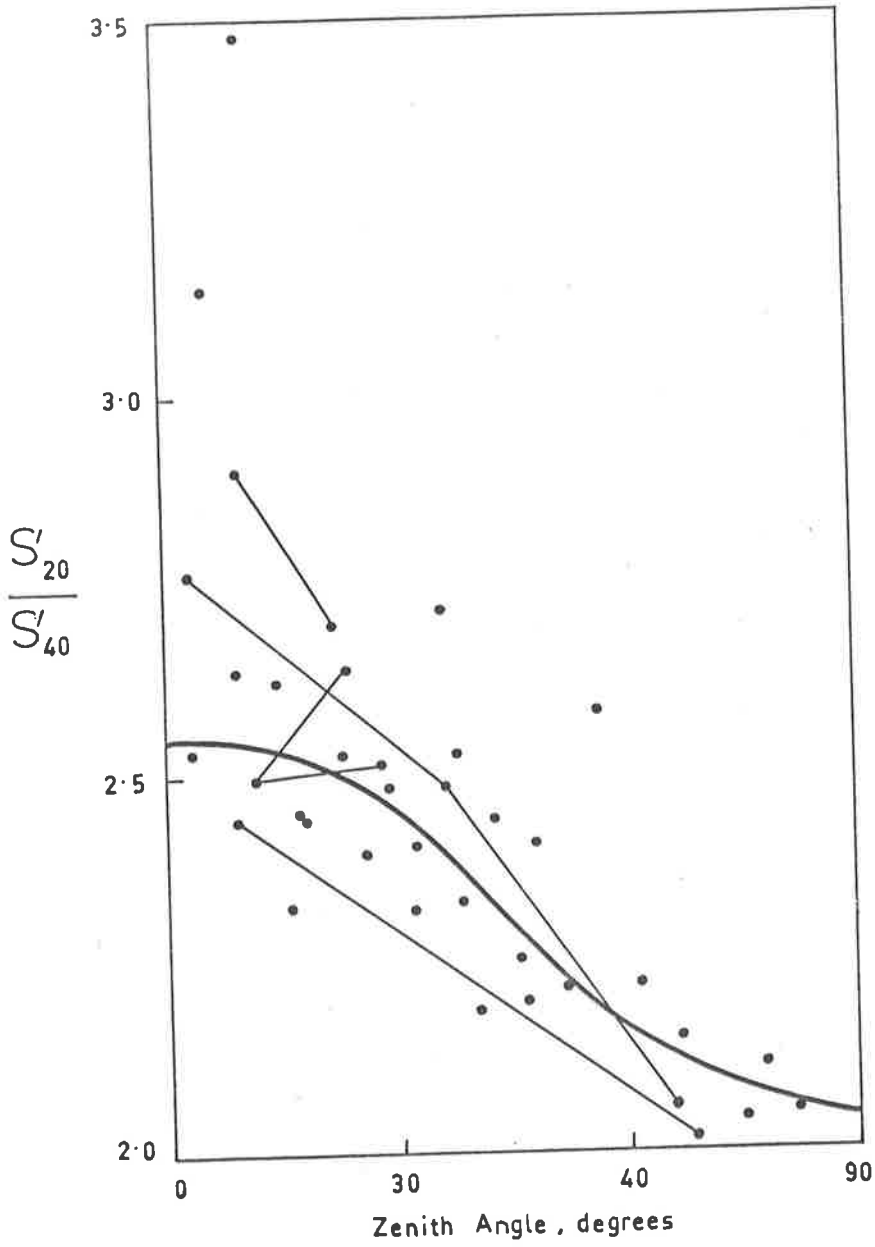

Figure (8.3) The zenith angle variation of the ratio of scintillation depth at 20 Mc/s that at 40 Mc/s, for night-time scintillation.

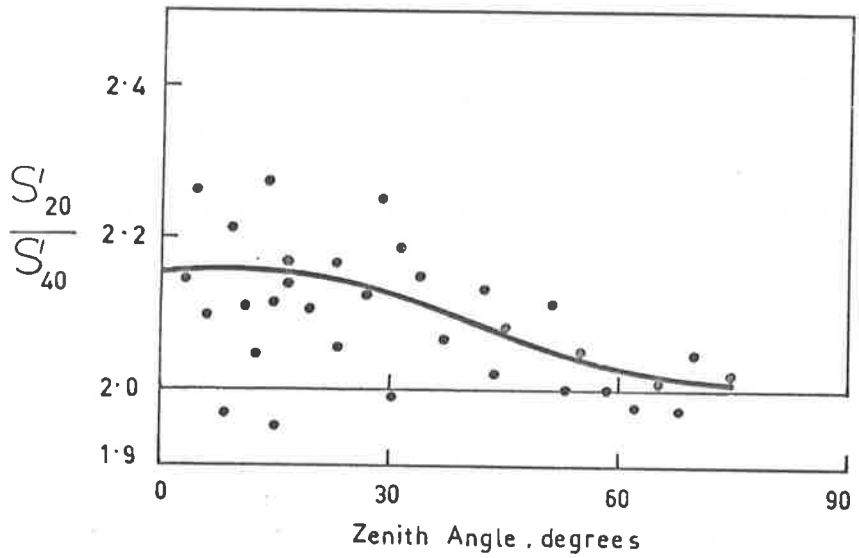

Figure (8.4). The zenith angle variation of the ratio of scintillation depth at 20 Mc/s to that at 40 Mc/s, for day-time scintillation.

found to be the most sensitive indicators of irregularity size), determinations of scintillation depth were obtained from many different records.

Within the scatter of the points in the diagrams, no significant seasonal variation was found, and points appropriate to all seasons have been plotted.

The indications of the method, in terms of irregularity size, are similar to those of the previous section. The curve drawn to follow the mean trend of the points in Figure (8.3) takes a value slightly in excess of 2.5 at the zenith. Reference to Figure (3.5), which is drawn for appropriate conditions of satellite height and radio frequency, and an irregularity height of 300 km, shows this value to correspond to a radius r_o of 1 km. If the height of the irregularities is taken to be 250 km., the theory of Section 3.2 shows the zenithal value of the ratio of scintillation depths to be 2.25 for $r_o = 0.75$ km. and 2.62 for $r_o = 1$ km. A value of r_o lying between 0.75 km. and 1 km. is therefore indicated for night-time irregularities, independent of whatever (reasonable) height is assigned to them.

The points for day-time irregularities in Figure (8.4) again show a tendency towards "far zone" conditions. A curve appropriate to irregularities at 100 km. height, for which r_o has the value .45km, has been drawn (it takes a value of 2.15 at the zenith), and it appears to fit the experimental points. It must be remembered, however, that the curves for all smaller irregularities lie between the curve and the theoretical lower

limit of 2.0, so an accurate estimate of irregularity size cannot be obtained. An upper limit of about 0.5 km. can be assigned to the size; the zenithal value of the ratio of scintillation depths for r_o = 0.6 km. is 2.4 and this value is at the upper limit of variation of the experimental values.

8.3 The Effects of Anisotropy of the Irregularities

8.3.1 General Properties

No strongly marked effects which could be attributed to anisotropy of the scattering irregularities were found in an examination of the scintillation indices appropriate to illumination in the direction of the geomagnetic field. Such effects as are described below were probably masked by averaging processes which were applied to the indices.

A distinctive property was found, however, when a selection was made of recordings of those passes in which the ray passed within ten degrees of the field direction. Especially marked examples are shown in Plate (1): a sudden increase of scintillation depth and, sometimes, of scintillation rate occurs, the event being symmetrically disposed about the time of closest approach of the ray direction to that of the field. That the effect is associated with the field is indicated by this symmetry, by an observed dependence of the intensity of the effect on the closeness of approach, and by the almost complete absence of such "bursts" of scintillation in any other part of the sky.

The behaviour seen in such recordings as those of Plate (1) has not previously been reported in the literature.

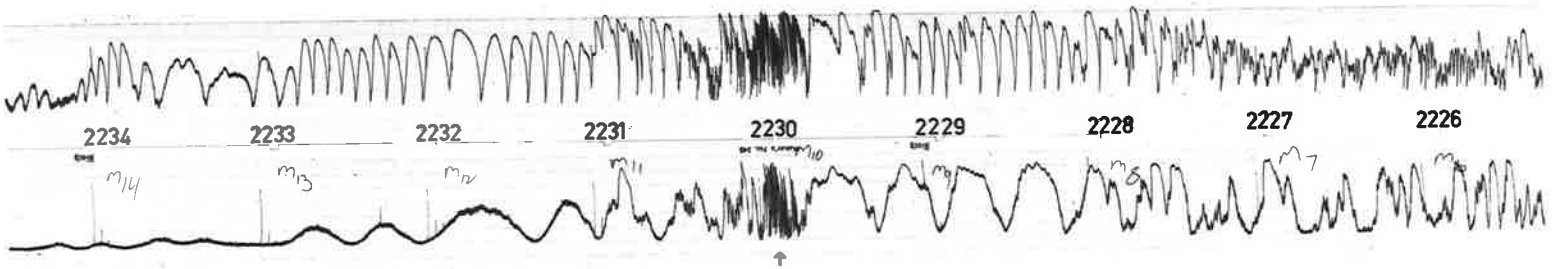

(a) Minimum angle of approach of ray direction to field direction, 1.4 degrees, at 2230.0 on 5th June, 1965. 20 Mc/s trace upper, 40 Mc/s trace lower. Time is marked in minutes, local time.

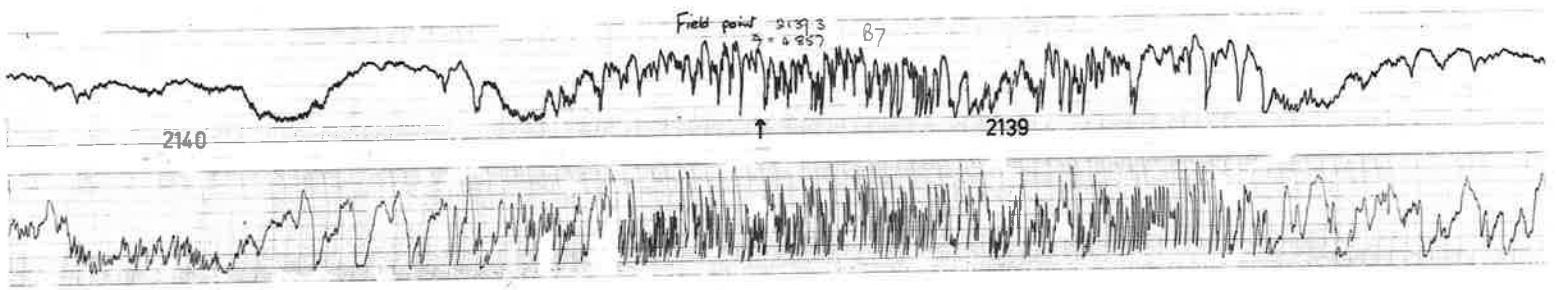

(b) Minimum angle of approach of ray direction to field direction, 4.9 degrees, at 2139.3 on 12th September, 1965. 40 Mc/s trace upper, 20 Mc/s trace lower. Time is marked in minutes, local time.

Plate (1) Two examples of "field-crossing" events observed at Adelaide.

Singleton, Lynch and Thomas (1961) and Singh (private communication) have found a general increase of scintillation depth near the direction of the geomagnetic field but do not report the appearance of complete "field-crossing" events in single recordings. Singleton and Lynch, who do not specify the radio frequency at which their observations were made, found no increase of scintillation rate as the direction of the field was approached.

A study of 115 recordings (selected for passage of the ray within ten degrees of the field direction) showed a diurnal variation in the occurrence of "field-crossing" effects. It is difficult to give a quantitative measure of this result because many of the events, particularly those of the day-time, consisted of no more than a brief appearance of shallow scintillation, at the time of close approach to the field, in an otherwise non-scintillating trace; but, such events being taken as real, the following results were found: of 44 night-time recordings (taken between 1800 and 0600 hours, local time), only 9 showed no "field-crossing" effect, and of 71 day-time observations, 46 showed no effect.

The relative lack of an effect during the day cannot be associated with the generally lower level of day-time scintillation depth for, as record (a) of Plate (1) shows, a "strong" event can occur in a non-scintillating (night-time) trace. Nor, as consideration of Section 3.2.3 indicates, can the lack be attributed to a change in the geometry of the diffraction process. It must be taken that, while field-oriented

anisotropy is the normal condition for night-time (F - region) irregularities, day-time (E - region) irregularities are only very weakly field aligned.

An insufficient number of suitable day-time recordings was available for detailed study of the effects of anisotropy. Results obtained from night-time observations are given in the following sections.

8.3.2 Deductions from the Variation of Scintillation Depth

In determining the form of the variation of night-time scintillation depth for directions near to that of the geomagnetic field it was not usually possible, because of the path taken by the satellite, to normalise results with zenithal values of scintillation depth. The values used for normalisation were, however, for ray directions within about 30° of the zenith and removed by at least 30° from the field direction. So errors arising from an incorrect choice of direction for normalisation are not greater than about 10 per cent (see Figures (3.4) and (8.1)).

Larger errors occurred in the evaluation of the scintillation depth used for normalisation. The scintillation was often very shallow and its depth had to be determined by eye rather than by calculation. In doubtful cases the depth was consciously over-estimated so that an under-estimated value of normalised scintillation depth for the near-field direction resulted. Such a value does not affect the final findings.

The normalised values, which were obtained from

observations at 40 Mc/s, are plotted against angular deviation of the ray from the field direction, in Figure (8.5). Several "chains" of points were obtained from single observations which, like record (b) of Plate (i), had been recorded at a suitably high chart rate; each of the other points was obtained from a different pass.

Comparison of Figure (8.5) with the 40 Mc/s curves of Figure (3.4) shows that the axial ratios of the irregularities under observation are very large, a result which is immediately obvious in such an observation as that of record (a) (in Plate (1)), where the normalised scintillation depth "along the field" is effectively infinite. The scatter of the points in the figure does not allow an accurate estimate to be made of axial ratio (other than, that it exceeds 20), but the point of chief interest is that the values indicated are greatly in excess of those found by spaced receiver methods (see Chapter 9).

The discrepancy implies that it is not F - region irregularities which are observed in a "field-crossing" event but another type, possibly the field-aligned "ducts" which are observed with "top-side" satellite sounders (Lockwood and Petrie (1963)). Existing at higher altitudes than the F - region and being inbedded in a region of lower electron concentration, these would not contribute to scintillation effects for most ray directions; but viewed along their direction of elongation, they may well produce effects which "swamp" those due to irregularities at lower levels.

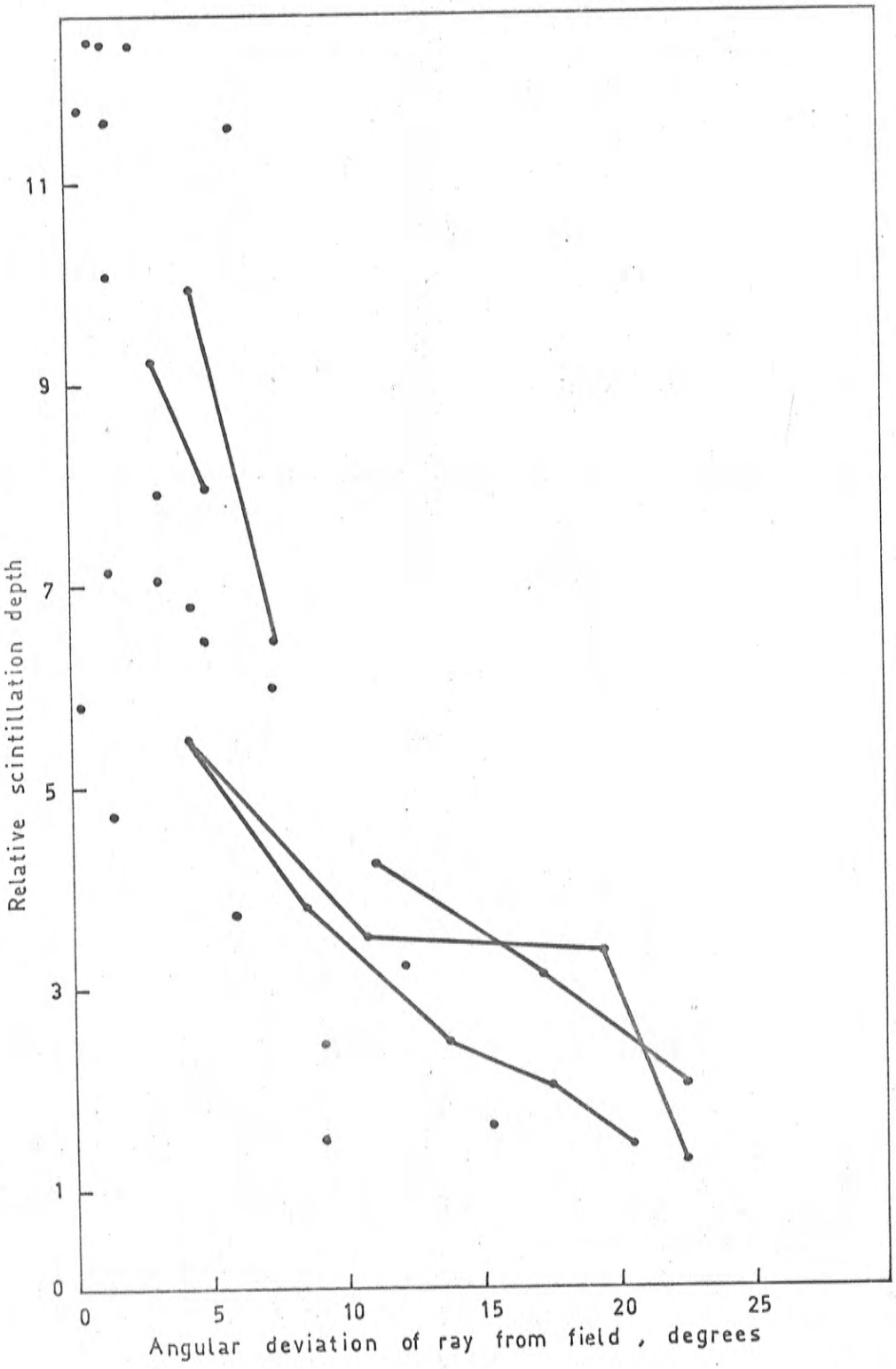

Figure (8.5). The observed variation of normalised scintillation depth at 40 Mc/s in the neighbourhood of the geomagnetic field direction.

In view of the somewhat unexpected nature of the results obtained, it is suggested that the method of this section be used in further investigations. On the basis of present experience, it can be recommended that:

(i). "Field-crossing" events should be predicted, and recording devices should be run at high speeds during an event.

(ii). The angular position of the satellite and the orientation of the geomagnetic field at ionospheric heights should be determined to an accuracy of better than half a degree. The peak in the variation of scintillation depth "along the field" has a very high slope, and if assistance in estimating the height of the peak is to be gained by extrapolation from lower points, these points must be known to a high accuracy. The simplest way of determining the exact orientation of the geomagnetic field may be to average the positions indicated by a number of "field-crossing" events.

8.3.3 Deductions from the Variation of Scintillation Rate

A method of investigation is now briefly described which, although it has not been applied successfully, provides an interesting alternative to the method of the preceding section.

The discussion of Section 3.4 shows that, when the r.m.s. phase deviation ϕ_o is less than unity, the spatial dimensions of signal fluctuations at the ground are equal (to a reasonable approximation) to those of the shadows of the scattering irregularities. If, on the other hand, ϕ_o exceeds unity, spatial dimensions at the ground are approximately $1/\phi_o$ times the corresponding shadow dimensions (equation (3.22)). From this it follows, since temporal fading of a satellite signal is produced mainly by the drift of a spatially irregular pattern that the rate of fading is proportional to ϕ_o, if ϕ_o is greater than unity.

A "worked example" of the application of this logic to the "field-crossing" event of record (b) in Plate (1) follows.

The rates of fading (the numbers of fading maxima or minima per second) of both the 20 Mc/s and 40 Mc/s signals are found for each second of time in the neighbourhood of the time of close approach to the field*. These rates, R_{20} and R_{40}, are plotted, after smoothing, in Figure (8.6).

---

* Using the results of Bowhill (1957), the author has corrected observed fading rates for the effects of the 50 c/s cut-off action of the pen recording system. The correction, which is an effectively linear function of observed rate, amounts to + 2c/s at an observed rate of 9c/s.

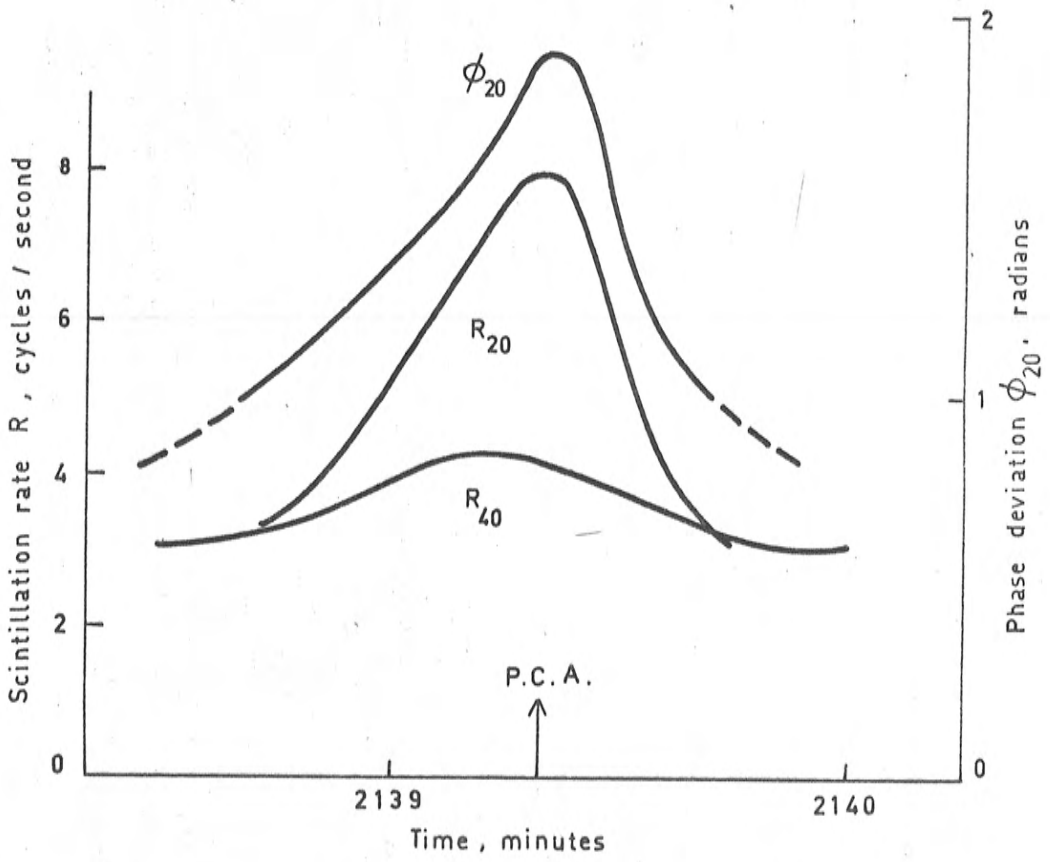

Figure (8.6) The temporal variation of the scintillation rates at 20 Mc/s and 40 Mc/s, and of the r.m.s. phase deviation at 20 Mc/s, as determined from record (b) of Plate (1).

Throughout the event, the rate R_{40} increased little, indicating that the phase deviation at 40 Mc/s, ϕ_{40}, probably did not exceed unity. On the other hand, the rate R_{20} increased markedly, from a value equal to R_{40} to about twice that value, showing that the phase deviation at 20 Mc/s, ϕ_{20}, did exceed unity. Using the theory expressed above, R_{20}, can be normalised against geometrical changes in "shadow" size by division by R_{40}; the resulting ratio is ϕ_{20} and it is plotted in Figure (8.6). (Since the phase deviation is proportional to wavelength (equation (3.9)), and since ϕ_{20} attained the value 2, it follows that ϕ_{40} did attain unity. The value obtained for ϕ_{20} is, therefore, an under-estimate).

The peaked variation of the phase deviation is of interest because, as with the peak it produces in curves like those of Figure (3.4) knowledge of its form allows an evaluation of the axial ratio of the scattering irregularities. Such an evaluation is made difficult, however, by the fact that the phase deviation cannot be known for directions removed from that of the field, for which its value is less than unity; the normalised height of the peak cannot be known: but the shape of the peak can, in principle, be determined and the axial ratio determined from this.

Attempts to discover the shape of the peak have, in fact, met with little success. Figure (8.7), in which the curve for ϕ_{20} is replotted against angular deviation of the ray from the field, illustrates the problem. The slope of

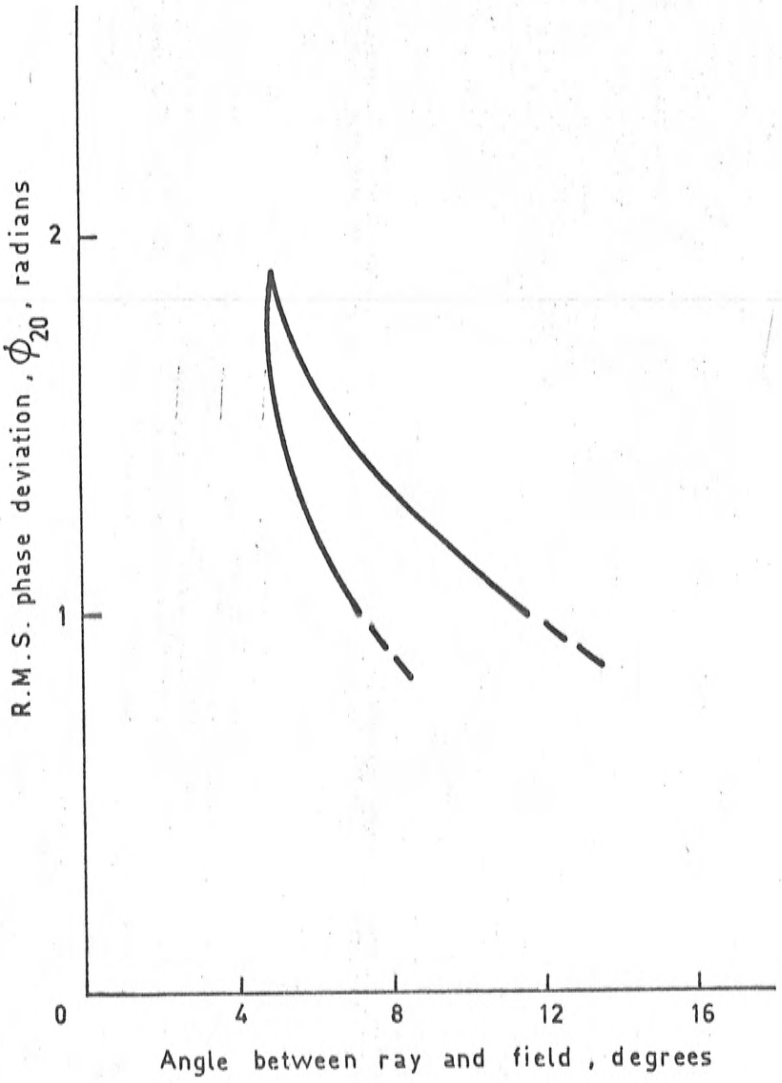

Figure (8.7) The variation of r.m.s. phase deviation at 20 Mc/s in the neighbourhood of the geomagnetic field direction as determined from record (b) of Plate (1).

the curve becomes very high within a few degrees of the field direction and, as was suggested in the previous section, a highly accurate knowledge of both satellite position and field direction is required if the curve is to be extrapolated. A more precise knowledge of the relationship between fading rate and r.m.s. phase deviation is also required.

CHAPTER 9.

DETAILED ANALYSES OF SCINTILLATION PATTERNS

9.1 Preparation of Data

The data used in detailed spectral and correlation analyses of the amplitude pattern at the ground were derived almost exclusively from recordings of the 40 Mc/s signal received by the spaced receiver system described in Section 6.2.1. Because of their "circularly polarised" property, the aerials of this system produced only shallow Faraday fading, and it was possible, in making recordings, to increase the gain of the pen recorder amplifiers until the fluctuations (scintillations) of the signal trace all but filled the available recording track width (40 m.m.). When this was done, the mean signal level was "backed-off" with a steady voltage provided by a dry cell. Recordings were made at a high chart speed, usually 25 mm/sec.

In reducing the observations to numerical values, the amplitude fluctuations of the signal trace were read to an accuracy of 0.25 m.m. The rate of sampling was always chosen to be about 10 times the fading rate of the record.

Long period trends in the data (due to the shallow Faraday fading) were removed by subtraction of the running mean. This mean was determined by convolving the data with a running rectangular "pulse" function, the (temporal) length of which was chosen to be from 5 to 10 times the fading period of the scintillating trace. The presence of a trend had obvious,

and undesirable effects on the shape of the correlation function of scintillation, and its removal was established by stability of the shape against increases in the length of the convolving "pulse".

9.2 Spectral Analyses

All attempts to discover fringe structure in the power spectrum of scintillation recordings, and from this to gain information about the diffraction process (Section 3.3.1), were unsuccessful.

Occasions when the velocity of drift of the amplitude pattern was parallel to the minor axis of the characteristic correlation ellipse were determined using the programs described in Section 6.3.1, and portions of recordings appropriate to these occasions were selected (see Sections 3.3.2 and 3.3.3). The records were read, and long period trends were removed, as described above. The temporal auto-correlation function was determined, usually to a maximum "shift" of 100 times the data sampling interval (that is, of about 10 times the fading period), and the function was Fourier transformed (cosine transform) to give the power spectrum.

Most of the results were obtained from recordings of night-time scintillations at 40 Mc/s. Figure (9.1) shows a typical spectrum. Near the origin the spectral power is low because of the "de-trending" process applied to the data. The decrease of power with decreasing frequency, seen at frequencies greater than 0.5 c/s, is characteristic of the original data and is associated with the fringe zero at the origin referred to in Section 3.3.3.

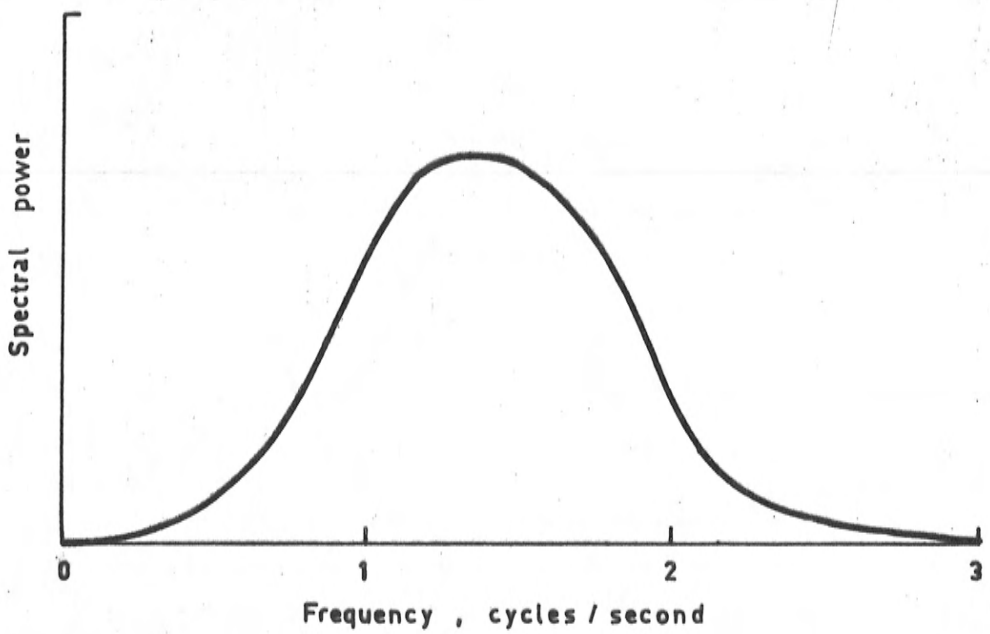

Figure (9.1): Smoothed power spectrum of scintillation at 40Mc/s.

Nothing characteristic of a second fringe zero is to be seen in the spectrum. Using values appropriate to the observation leading to Figure(9.1), and assuming a height of irregularities of 300 km., calculation shows that the second zero should occur at 2.4c/s. The power in the spectrum at this frequency is obviously too low to allow the fringe minimum to be seen.

No spectra appropriate to day-time conditions were obtained. Calculation indicates that the fringe structure would not be seen in day-time observations at 40 Mc/s if the irregularities are of radius 0.5 km. and lie at a height of 100 km.

Attempts to determine the spectra of 20 Mc/s scintillations met with no success. Although a specially constructed "circularly polarised" aerial was used for reception, the data was marred by residual Faraday fading at a rate close to the rate of scintillation fading.

9.3 Correlation Analysis -- Determination of Height, Shape, and Size of Irregularities

In this section the results obtained from the observations on three spaced receivers will be described. The arrangement of the receivers and associated equipment was described in Section 6.2.1.

The recordings of signal fluctuations on 40 Mc/s made with the three receivers were prepared for analysis in the manner described in Section 9.1. The data, with long period trends removed, were then subjected to correlation analysis using the computer program

described in Section 6.3.2. The output from the program gave the auto- and cross- correlation functions, the coefficients of the characteristic ellipse, the "apparent" and true velocities, and the quantity V_c (Fooks (1965)). The correlation functions, the characteristic ellipse, and the velocities, were also plotted directly by the machine. Figure (9.2) is a typical example of these plots. It shows the mean of the three auto-correlation functions of the three records, and the three cross-correlation functions derived by taking the three records in pairs. The spatial characteristic ellipse is shown, and the shorter and longer lines at the centre of the diagram show the directions (but not the magnitudes) of the apparent and true velocities of drift respectively.

Figure (9.3) shows the characteristic ellipses obtained from successive sections of a record made between 0114 and 0134 local time on 10th. February 1966. The local times appropriate to each section are indicated. The rotation and change of shape of the ellipse which occurs as the satellite moves can be seen clearly; these are analogous to the motion of the shadow of the gnomon of a sundial as the sun moves.

The ellipse rotates through an appreciable angle in 6 seconds, and this prompts some consideration of the longest length of record which can be analysed with the assumption that it is statistically stationary. This maximum length is of the order of 6 seconds, but such a record contains only about 10 fading cycles for typical conditions of scintillation. Large errors will occur in the correlation functions

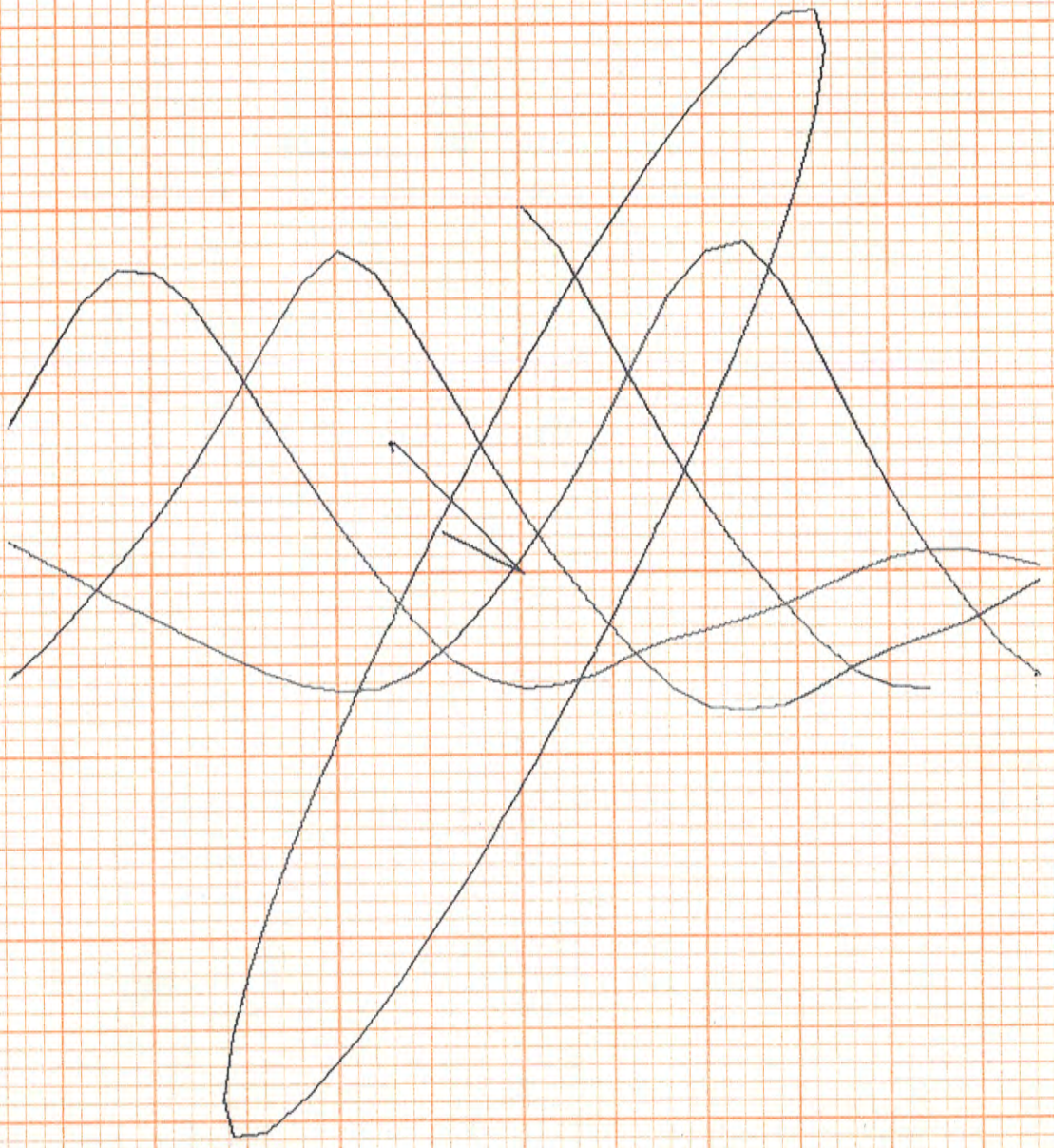

Figure (9.2). The computer-plotted diagram resulting from the correlation analysis of recordings made at 0131.3 local time on 14 Feb. 1966. The horizontal scale for the temporal auto- and cross-correlograms is 0.4 seconds per inch. The spatial characteristic ellipse is plotted to a scale of 1 Km per inch and true north is vertically upwards.

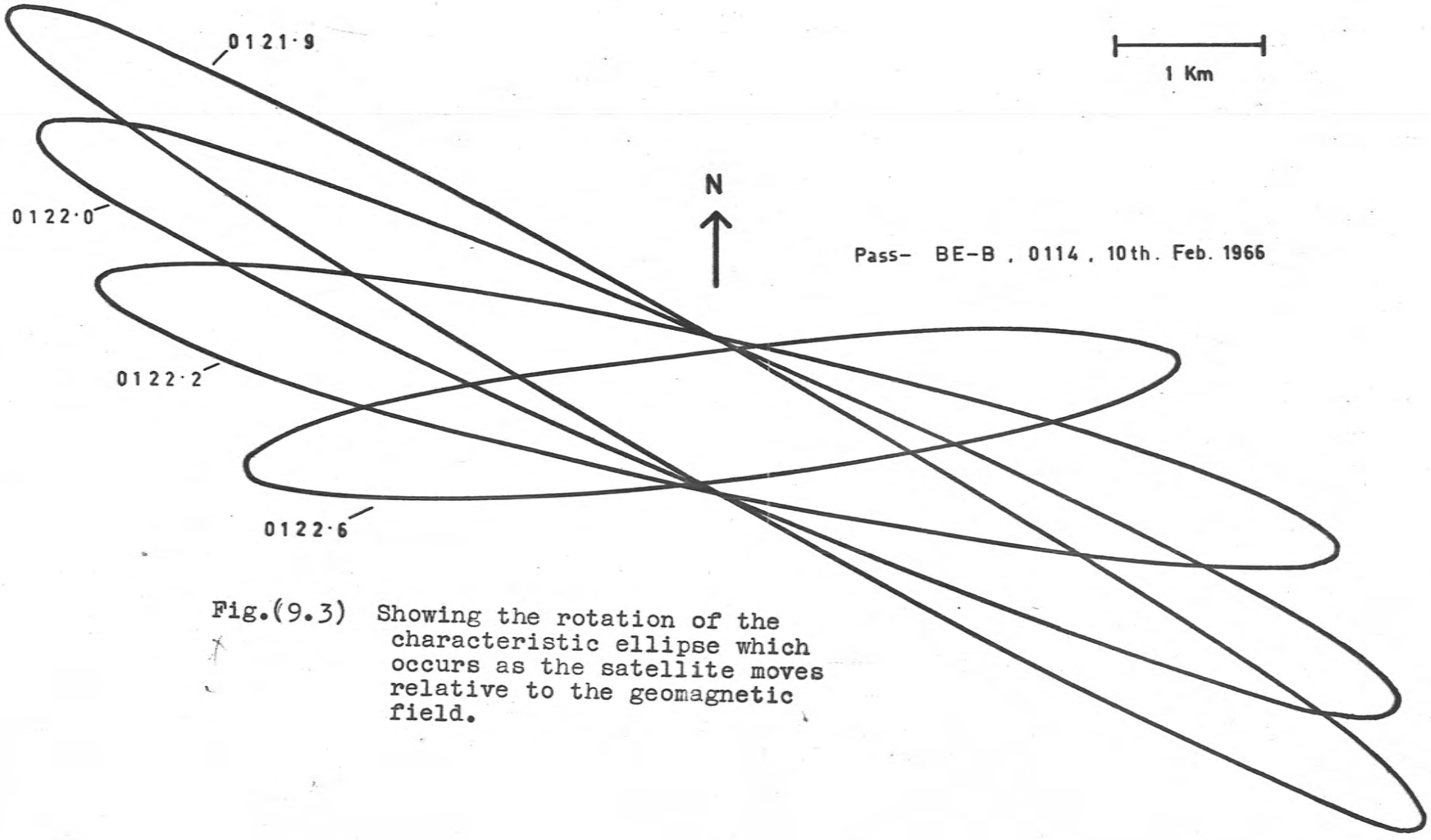

Fig.(9.3) Showing the rotation of the characteristic ellipse which occurs as the satellite moves relative to the geomagnetic field.

for records as short as this (see Fooks and Jones (1961), and Section 2.2.2). The errors involved were studied by comparing the three auto-correlation functions for a given section of record (ideally these would be identical). Typical standard deviations of the correlation values were 5%. The errors in the cross-correlation functions will be of the same order. The error in the mean auto-correlation function will be of the order of $1/\sqrt{3}$ of the error of a single auto-correlation function. At the end of the computation, these typical errors may be expected to produce errors of the order of 5% in the length of the minor axis of the ellipse, but the errors in the major axis may be considerably larger, especially when the axial ratio is large.

A further check on the overall accuracy of the calculations was obtained by comparing the direction of the major axis with that predicted from the satellite position (see Section 6.3.1) assuming that the ionospheric irregularities were aligned along the earth's magnetic field. The mean variation from the predicted direction was about 5°.

The determination of the apparent velocity of the diffraction pattern has a redundancy which enables accurate values to be obtained by the use of a least squares fitting method (Fooks (1965)). However, the derivation of the true velocity from the apparent velocity involves the orientation, axial ratio and size of the ellipse, and the error in the true velocity tends therefore to be larger; errors of the

order of 15% were estimated for this quantity. It is this error in the true velocity which finally determines the error in the height of the irregularities as determined from equation (3.24) of Section 3.4.

The lengths of the major and minor axes of the ellipse were corrected for projection effects by comparison with calculated lengths of projected unit vectors along and across the magnetic field (see Section 6.3.1). They were also corrected for the diffraction effects described in Section 3.4. After these corrections had been applied, the values should give measures of the sizes of the ionospheric irregularities themselves.

An attempt was made to deduce the thickness of the layer of irregularities from the value of V_c using equation (3.25) of Section 3.4. It became apparent, however, that the method in question involves a second order effect and it is doubtful whether the values of V_c obtained are sufficiently accurate to justify the method. Typical values of layer thickness were of the same order as the height of the layer itself. While this result is interesting, and would justify further study, it is considered that the actual values of layer thickness are unreliable, and the detailed results will not be given here.

Discussion of Results

The results obtained for the height of the irregular layer (h) and for the minor axis (r_o) and the axial ratio (α) of the irregularities are given in Table (9.1). Most of the available results are for night.

TABLE 9.1

Date	Time	h(km.)	r_o (km.)*	α
10.2.66	0121.9	326	0.37	13.8
	0122.0	306	0.46	13.2
	0122.1	300	0.48	10.7
	0122.6	307	0.40	10.3
12.2.66	0033.2	389	0.80	9.3
13.2.66	2341.3	297	0.78	3.7
14.2.66	0129.4	275	0.54	2.4
	0130.7	298	0.65	2.0
	0131.3	245	0.53	2.3
19.2.66	0014.5	278	0.36	13.5
	0017.0	299	0.43	2.8
20.2.66	2323.6	307	0.43	26.2
10.6.66	2152.0	240	0.50	1.8
	2156.2	283	0.78	3.6
	2156.7	210	0.93	3.6
	2157.5	196	0.78	5.8
10.8.66	0321.8	334	0.63	11.6
	0322.2	242	0.66	6.7
	0323.1	220	0.55	10.9
19.8.66	2033.0	297	0.62	2.7
	2229.6	343	0.53	3.8
	2230.0	345	0.55	6.8
	2232.1	295	0.52	12.1
20.8.66	2147.9	289	0.61	7.4
	2148.8	244	0.77	7.8
	2343.4	340	0.92	19.8
24.9.66	1121.6	206	1.01	3.5

* In this Table, r_o is defined as the distance at which the correlation has fallen to 1/e.

During the day, scintillations were usually too shallow to permit accurate results to be obtained from the triangle of receivers, owing to residual noise on the land lines.

It will be seen from the table that the heights obtained are in the range 200 km. to 300 km., in fair agreement with the values 230 km. to 300 km. obtained in Chapter 7. The values for the length of the minor axis of the irregularities are generally rather smaller than the values 0.73 km. to 1.0 km. obtained in Chapter 8. The reason for this difference is not known. The axial ratios are generally in the range 2 to 15 with occasional much larger values.

The two sets of day-time results given in Table(9.1) indicate heights near 200 km., and not 100 km. as might have been expected from the discussion of day-time scintillations given in Chapter 7. However the sample is obviously too small for any conclusions to be drawn. Further work on day-time scintillations is needed, and would be possible if the noise level on the lines could be reduced.

CHAPTER 10.

DEDUCTIONS FROM STUDIES OF THE FARADAY EFFECT

10.1 Analysis of the Data

The analysis of Faraday fading data was carried out using a computer and closely followed the steps outlined in Chapter 4.

Each fading null of a 40 Mc/s recording, and one fading null of the associated 41 Mc/s recording, were represented in the basic data by their times of occurrence. These were usually read to a relative accuracy of 0.5 seconds. By the use of the computer programs described in Section 6.3.1, each null was associated with a value of the quantity M of equation (4.1), the value being calculated for a height of 350km. Two types of analysis were then carried out.

In the first, for each pair of successive nulls at 40 Mc/s, the quantity $\frac{d\Omega}{dM}$ was approximated, using the fact that while M increases by dM from one null to the next, Ω increases by π radians. Using the assumptions described in connection with equation (4.2) a value of the total electron content I was calculated and plotted by the computer for a time midway between the times of the appropriate nulls. In this way an "M - derivative" curve for I was obtained.

In the second type of analysis, the "Vernier" measurement described in Section 4.2 was made, the angular position of the 41 Mc/s null with respect to the two closest 40 Mc/s nulls being determined by linear interpolation of their associated values of M. Four values of Ω were determined, corresponding

to the values n= 0,1,2,3 in equation (4.4). From these, four values of Ω were evaluated for each 40 Mc/s null, by addition of multiples of π radians, and all were converted to measures of total electron content I by the use of equation (4.1). Four "frequency - derivative" curves were thus obtained.

Most often one of the "frequency - derivative" curves closely approximated the "M-derivative" curve for parts of the satellite pass which were high in the sky (for which the approximatations leading to equation (4.1) are most nearly valid), and this one was taken to be the appropriate curve for I.

10.2 The Relationship between Scintillations and Irregularities in Total Content

In order to discover if small-scale irregularities in the ionosphere are associated with increased or decreased values of electron density, a correlation was sought between abrupt changes of scintillation depth and irregularities in the curve for total electron content. The study was hampered by the lack of a sufficiently large number of distinctive changes of scintillation depth (see Section 7.7), so the significance of the results may be questioned, but in about forty cases which were examined, no correlation was found between the occurrence of a "patch" of scintillation and a local maximum or minimum of total electron content. Both phenomena occurred together, but independently, in some passes and either was found to occur in the absence of the other in other passes. Unless the fluctuations of electron content

sought were too small to be discovered (quasi-sinusoidal irregularities of amplitude 0.05 x 10^{-16} electrons/square meter column were clearly resolved), the finding suggests that small scale irregularities arise in turbulent processes which do not involve the addition or subtraction of electrons from the local mean electron content.

Note may be made of a tendency, seen in some observations, for a patch of scintillations to occur, not at a maximum or minimum, but at a gradient in the total content. Figures (10.1) and (10.2), which give examples of this behaviour, show the (temporal) variation of total electron content as the satellite moves, together with an indication of the 40 Mc/s scintillation depth. The depth indicated in Figure (10.1) and to the left in Figure (10.2) corresponds roughly to the scintillation index 1 defined in Chapter 7.

The scintillation is seen to be associated with gradients in the electron content, though all gradients are not associated with scintillation (Figure (10.1)). An isolated burst of "lens-like" fading (Warwick (1964)) on the right of Figure (10.2) is probably to be related to the very high gradient of electron content (a "wedge") which occurs at the same time, but no explanation can be given for the other associations seen.

10.3 The Diurnal and Seasonal Variation of Electron Content

Incidental to the study described in the previous section, values of the total electron content over Adelaide

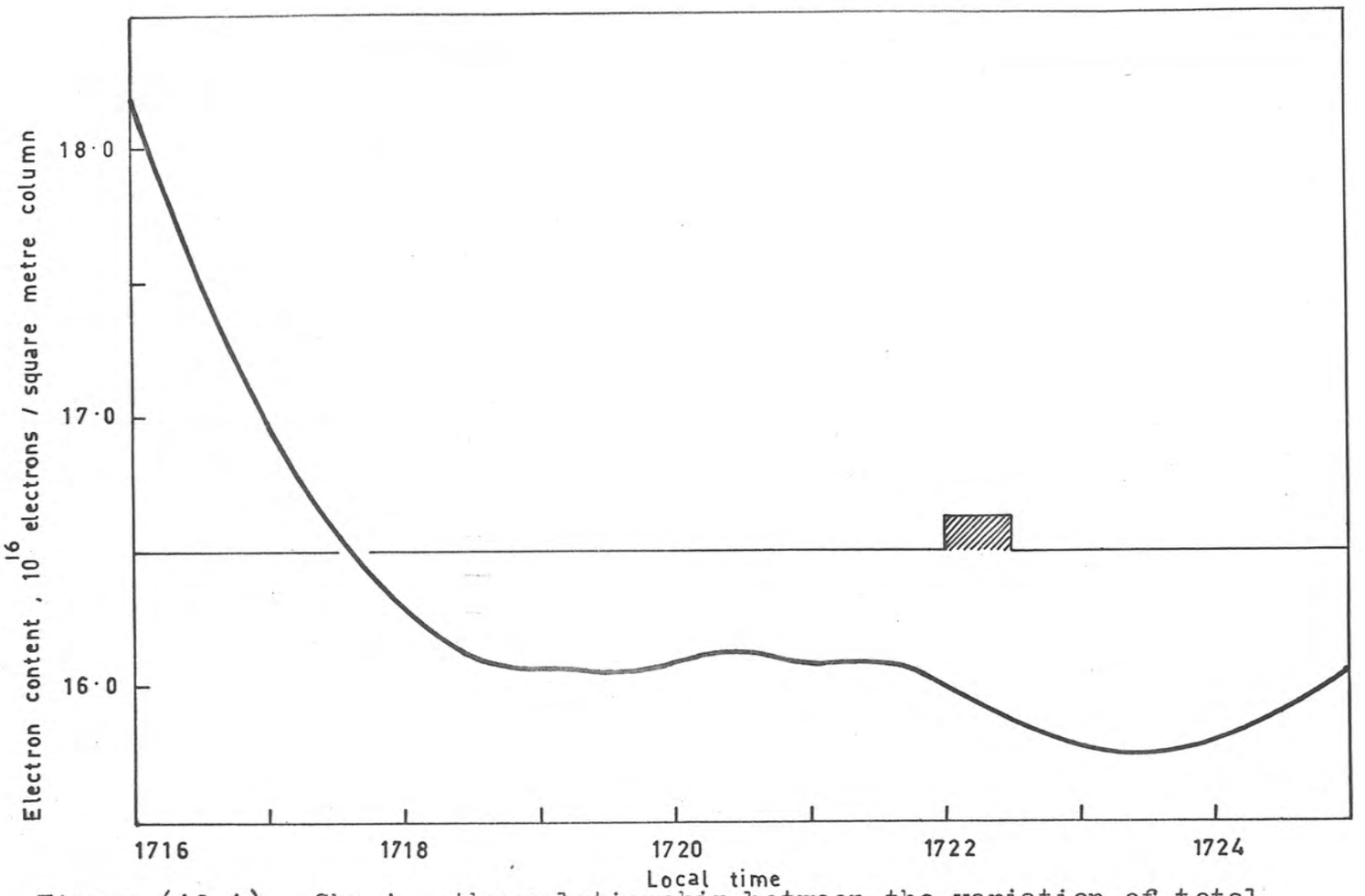

Figure (10.1) Showing the relationship between the variation of total electron content (line) and the occurrence of scintillations at 40Mc/s (hatched area). The observation was made on 19th November 1965.

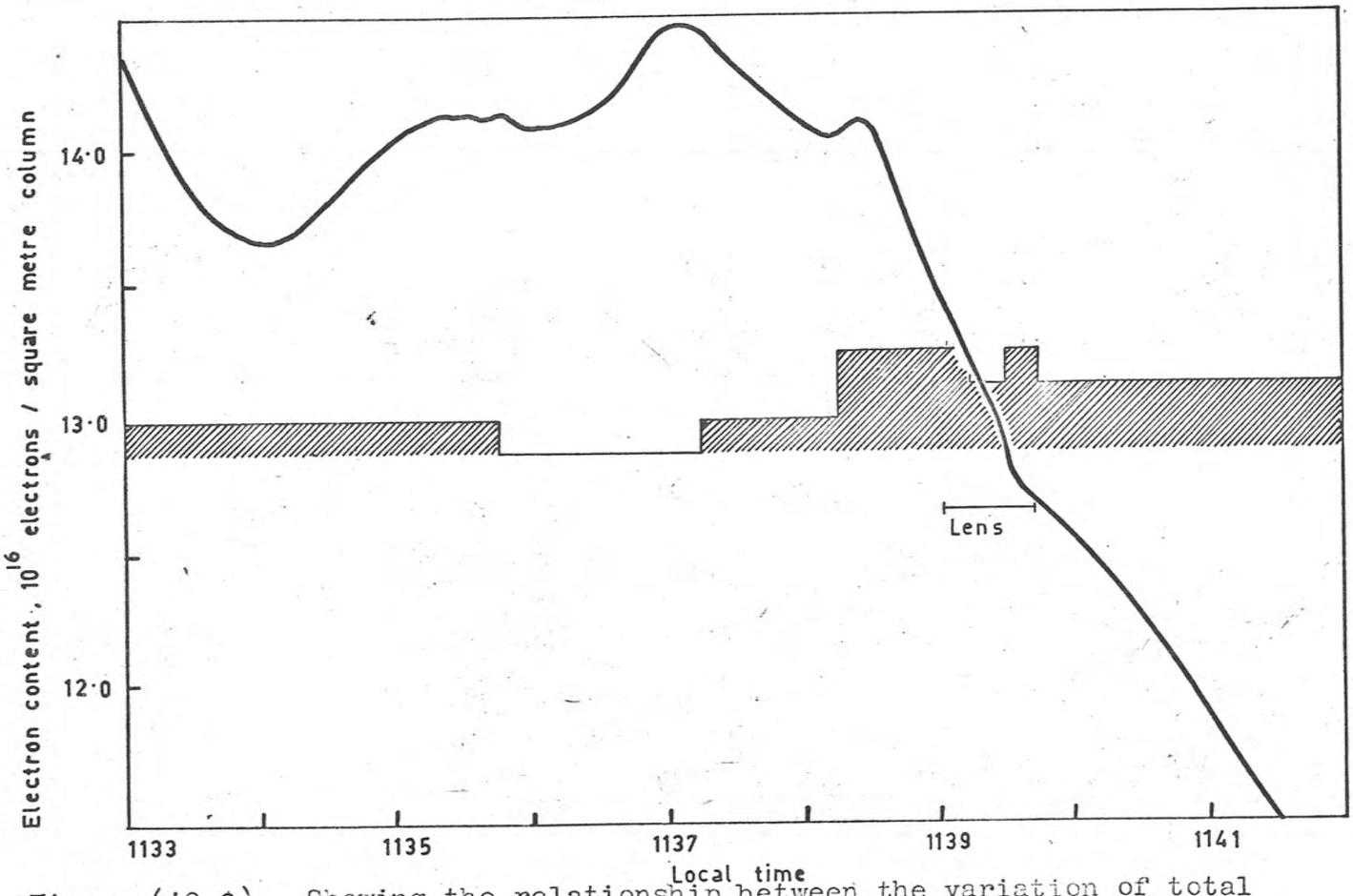

Figure (10.2) Showing the relationship between the variation of total electron content (line) and the occurrence of scintillations at 40Mc/s (hatched area). The observation was made on 21st November 1965.

were obtained from the analysis of Faraday fading. The values were taken from the "frequency-derivative" curves at times appropriate to the satellite's crossing of the latitude of Adelaide, and were plotted against the mean solar time of the point of intersection of the ray with the 350 km. level at that time.

The mean diurnal curves for the four "seasons" of 1965 defined in Section 7.2 are shown in Figure (10.3). In all seasons the diurnal variation exhibits a maximum occurring shortly after mid-day, as found by other authors (Goodman (1966), Yuen and Roelofs (1966)); no marked secondary night-time maximum (Arendt et al (1965)) is found.

The season dependence of the amplitude of the day-time peak is consistent in direction with the predictions of the Chapman theory of electron production. No "winter anomaly" occurred in the total content, as indeed, it did not in the corresponding mean values of F-region critical frequency at noon.

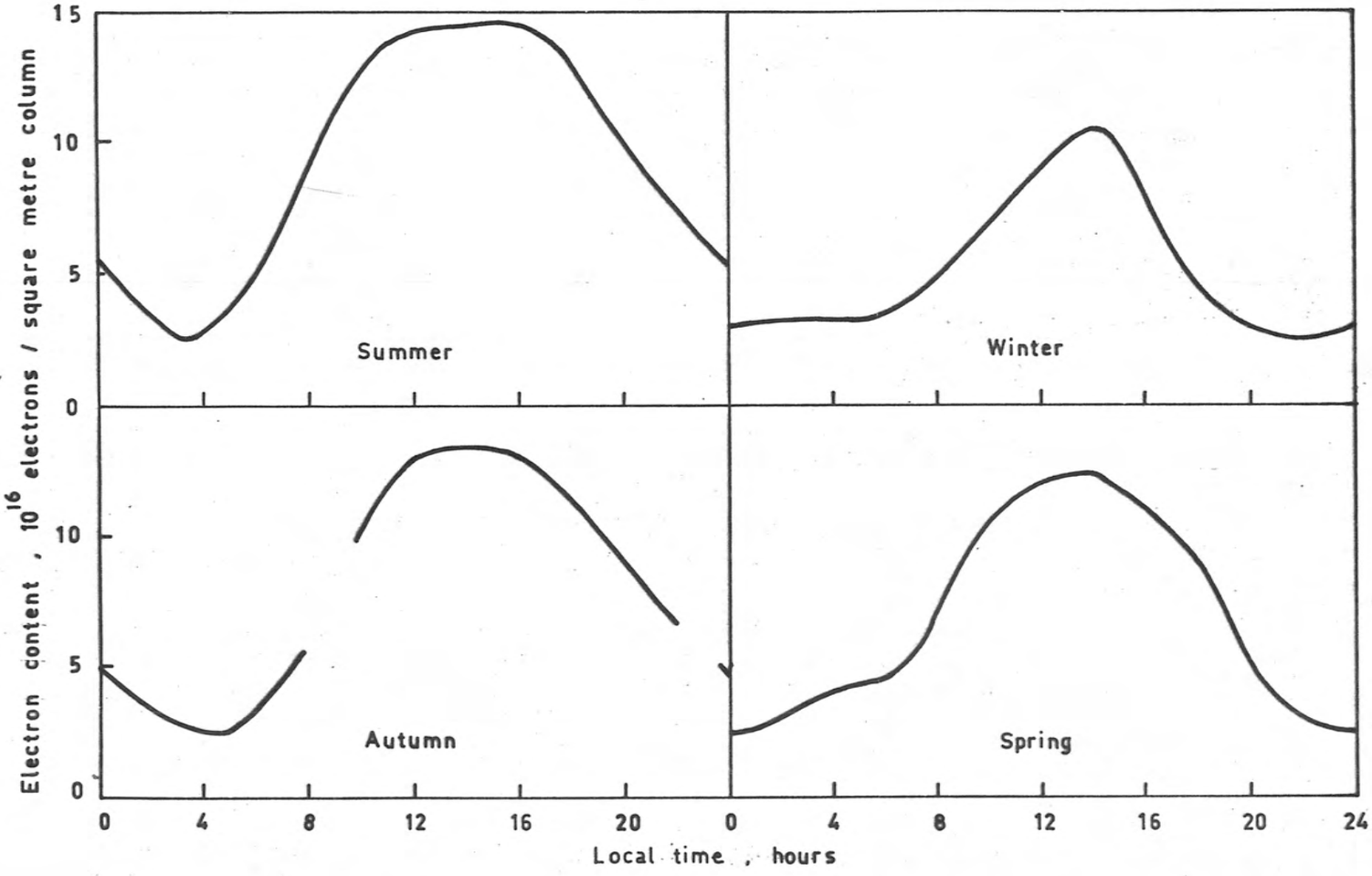

Figure (10.3): The diurnal variation of total electron content for four seasons.

CHAPTER 11

CONCLUSIONS

The main results will now be summarised chapter by chapter, and some suggestions will be made for future work.

Chapter 2. In this chapter a review was given of the basic theory of scattering in irregular media. It was shown that all the results concerning weak scattering can be derived from a simple "geometrical" model which has considerable intuitive appeal, when compared with the highly mathematical treatment given in other formulations. The simplicity obtained by working in Fourier transform space was stressed. It would be interesting to see whether similar ideas could be applied to the more difficult problem of strong scattering from a thick layer of irregular medium.

Chapter 3. This chapter was still concerned with scattering and diffraction theory, but with a more practical emphasis. The object was to show how observations of amplitude scintillations at one or more points on the ground could be used to obtain useful information about the properties of the irregularities in the ionosphere. In particular the variations with zenith angle, the practicability of obtaining useful information from the power spectrum of amplitude scintillations, and the deductions which can be made from spaced observations were considered. It was shown that the size, shape, and height of the irregularities could be determined, often by several independent methods. Formally, the work described in this chapter appears very complete, and it is difficult to imagine how any further information could be extracted from

observations of amplitude alone. However, the work is again limited to the case of weak scattering, and it would be interesting to know how the results would be modified if the scattering became strong; it certainly does become strong on some occasions.

Chapter 4. This chapter contained a survey of the standard theory of the Faraday effect.

Chapter 5. This chapter was mainly a review of existing experimental methods and results. At the end of the chapter the importance of determining whether there is any relationship between scintillation patches and variations in the total electron content was stressed. This could provide a criterion for rejecting some at least, of the many theories of irregularity formation.

Chapter 6. In this chapter the equipment used to make the observations was described. The importance of making some improvements which would eliminate noise and "hum" on the lines was emphasised. The computer programs used in the investigation were also briefly described in this chapter.

It may be worth pointing out here that the same triangle of observing sites could be used to observe a satellite of the "stationary" type. From such observations the drift velocity of the ionospheric irregularities could be determined. If such observations could be made on both orbiting and stationary satellites, perhaps in rapid succession, or better still, simultaneously, a very complete description

of the irregularities and their motion would be obtained.

Chapter 7. The occurrence characteristics of scintillations were described in this chapter. The generally weak character of the scintillations was ascribed to the fact that the observations were made near sunspot minimum. The most interesting result of this chapter is the observation that scintillations are not confined to the night-time. A close association was demonstrated between night-time scintillations and spread-F. No correlation was found between day-time scintillations and sporadic-E occurrence. Only slight variations with latitude were observed.

Chapter 8. Variations of scintillation depth with zenith angle were used in this chapter to show that the irregularities causing scintillations at night have a minor axis (r_o) of the order of 1 km, in general agreement with other observers. For day-time scintillations, all that could be said was that the value of r_o is smaller (probably less than 0.5 km). Similar results were obtained from measurements of the ratio of the scintillation depth on two frequencies.

Recordings of those satellite passes in which the ray passed within ten degrees of the magnetic field often showed a very interesting effect. A sudden increase of scintillation depth and sometimes also of scintillation rate was found, the event being symmetrically disposed about the time of closest approach to the field direction. This effect occurred mainly at night. It is similar to the variation predicted by weak scattering theory for field-aligned irregularities, but much more

pronounced than expected. Sometimes no measurable scintillation occurred on a record except very close to this "field point". The conclusion was reached that it is not F-region irregularities which are observed in these events but another type, possibly associated with the field-aligned ducts observed in the upper F-region and magnetosphere. In view of the unexpected nature of these results it is recommended that field crossing events should be predicted on the basis of orbital data, and recording equipment should be run at high speed in order to obtain good records in which the scintillation characteristics are measurable. A "strong-scattering" theory will probably be needed if useful deductions are to be made from these events.

Chapter 9. Attempts to discover "fringe" structure in the power spectrum of the amplitude fluctuations were unsuccessful. Observations made on spaced receivers gave values for the height, minor axis, and axial ratio of the irregularities. The values obtained from scintillations observed at night were in general agreement with those obtained by other workers. It is suggested that further observations be made by day in order to help elucidate the nature of the irregularities causing day-time scintillations.

Chapter 10. In this Chapter the results obtained by the use of the Faraday method were described. No relation was found between patches of small-scale irregularities and variations in total electron content. This observation lends support to those theories which attribute the

small scale irregularities to a "mixing-up" of the existing ionisation, with no change in the mean, such as theories involving turbulence or hydromagnetic waves. Observations of the seasonal variation of the total electron content of the F-region showed no "seasonal anomaly"; the electron content was larger in summer than in winter.

BIBLIOGRAPHY

Aarons, J., Mullen, J., and Basu, S., 1963, J.Geophys. Res., 68, 3159.

Arendt, P.R., Papayoanov, A. and Soicher, H., 1965, Proc.I.E.E.E., 53, 268.

Awe, O., 1964, J.Atmos.Terr.Phys., 26, 1239.

Basler, R.P., and de Witt, R.N., 1962, J.Geophys.Res., 67, 587.

Beynon, W.J.G., and Jones, E.S.O., 1964, J.Atmos.Terr.Phys., 26, 1175.

Booker, H.G., 1958, Proc.Inst.Radio Engrs., 46, 298.

Booker, H. G., Ratcliffe, J.A., and Shinn, D.H., 1950, Phil.Trans.Roy.Soc.A,242, 579.

Booker, H.G., and Wells, H.W., 1938, J.Geophys.Res., 43, 249.

Bowhill, S.A., 1957, J.Atmos.Terr.Phys., 10, 338.

Bolton, J.G., Stanley, G.J., and Slee, O.B., 1953, Aust.J.Phys., 6, 434.

Bowhill, S.A., 1961a, J.Res.Nat.Bur.Stnds., 65D,275.

Bowhill, S.A., 1961b, J.Atmos.Terr.Phys., 20, 9.

Bramley, E.N., 1951, Proc.Instn.Elect.Engrs, Pt.I, 98, 19.

Bramley, E.N., 1954, Proc.Roy.Soc.A,225, 515.

Briggs, B.H., 1961, Proc.Phys.Soc. LXXVII, 305.

Briggs, B.H., 1963, Nature, 200, 220.

Briggs, B.H., 1964, J.Atmos.Terr.Phys., 26, 1.

Briggs B.H., 1965, J.Atmos.Terr.Phys., 27, 991.

Briggs, B.H., and Parkin, I.A., 1963, J.Atmos.Terr.Phys., 25, 339.

Briggs, B.H., and Parkin, I.A., 1964, J.Instn.Telecom. Engrs., 10, 299.

Briggs, B.H., Phillips, G.J., and Shinn, D.H., 1950, Proc.Phys.Soc.Lond., B63, 106.

Browne, I.C., Evans, J.V., Hargreaves, J.K., and Murray, W.A.S., 1956, Proc.Phys.Soc.B,69, 901.

Budden, K.G., 1965, J.Atmos.Terr.Phys., 27, 155.

Calvert, W., and Cohen, R., 1961, J.Geophys.Res., 66, 3125.

Calvert, W., and Schmid, C.W., 1964, J.Geophys.Res., 69, 1839.

Chernov, L.A., 1960,"Wave Propagation in a Random Medium" (New York : McGraw-Hill), p.29.

Chivers, H.J.A., 1960, J.Atmos.Terr.Phys., 19, 54.

Clarke, M.E., 1964, Ph.D. thesis, University of Cambridge.

Dagg, M., 1957, J.Atmos.Terr.Phys., 11, 118.

de Barber, J.P., Chisholm, G.E., and Ross, W.J., 1963, Proc. of the International Conference on the Ionosphere (London), July, 1962, p.267.

Fejer, J.A., 1953, Proc.Roy.Soc.A,220, 455.

Fejer, J.A., 1965, "Physics of the Earth's Upper Atmosphere" Eds C.O. Hines, I. Paghis, T.R. Hartz, J.A. Fejer, (London : Prentice Hall) : Appendix II.7.

Fooks, G.F., 1965, J.Atmos.Terr.Physc., 27, 979.

Fooks, G.F., and Jones, I.L., 1961, J.Atmos.Terr.Phys., 20, 229.

Frihagen, J., and Troim, J., 1960, J.Atmos.Terr.Phys., 18, 75.

Frihagen, J., and Troim, J., 1961, J.Atmos.Terr.Phys., 20, 215.

Garriott, O.K., 1960, J.Geophys.Res., 65, 1139.

Garriott, O.K., and Mendonca, F., 1963, J.Geophys.Res., 68, 4917.

Goodman, J.M., 1966, J.Geophys,Res., 71, 985.

Gruber, S., 1961, J.Atmos.Terr.Phys., 20, 59.

Hartz, T.R., 1958, R.P.L. Report 23-2-3, Radio Physics Laboratory, Ottawa

Herman, J.R., 1966, Rev. of Geophys., 4, 255.

Hewish, A. 1951, Proc.Roy.Soc.A,209, 81.

Hewish, A.,1952, Proc.Roy.Soc.A,214, 494.

Hook, J.L., and Owren, L., 1962, J.Geophys.Res., 67, 5353.

James, P.W., 1962, J.Atmos.Terr.Phys., 24, 237.

James, R.W., 1948, "The Optical Principles of the Diffraction of X-rays", Chapter 1.

Jespersen, J.L., and Kamas, G., 1964, J.Atmos.Terr.Phys., 26, 457.

Joint Satellite Studies Group, 1965, Planet Space Sci., 13, 51.

Jones, I.L., 1960, J.Atmos.Terr.Phys., 19, 26.

Kaiser, T.R., 1956, Proceedings of a Symposium on Astronomical Optics and Related Subjects, North-Holland, Amsterdam, 1956, p.35.

Kent, G.S., 1959, J.Atmos.Terr.Phys., 16, 10.

King, G.A.M., and Roach, F.E., 1961, J.Res. Nat.Bur.Stnds. D, Radio Prop., 65D, 129.

Koster, J.R., 1958, J.Atmos.Terr.Phys., 12, 100.

Koster, J.R., 1963, J.Geophys.Res., 68, 2571.

Liszka, L., 1963, Arkiv.Geofysik, 4, 211.

Little, C.G., and Lovell, A.C.B., 1950, Nature, 165, 423.

Little, C.G., and Maxwell, A., 1952, J.Atmos.Terr.Phys., 2, 356.

Liu : Chao-Han Liu, 1966, J.Atmos.Terr.Phys., 28, 385.

Lockwood G.E.K., and Petrie, L.E., 1963, Plan Space Sci., 11, 327.

McClure, J.P., and Swenson, G.W. Jr., Beacon Satellite Studies of Small Scale Ionospheric Inhomagenities. Technical Report from Dept. of Electrical Eng., University of Illinois, Urbana, Illinois.

McGee, C.R., 1966, J.Atmos.Terr.Phys., 28, 861.

Mercier, R.P., 1962, Proc.Camb.Phil.Soc., 58, 382.

Mills, B.Y., and Thomas, A.R., 1951, Aust.J.Sci.Res.A, 4, 158.

Mitra, S.N., 1949, Proc.Instn.Elect.Engrs., Pt. III, 96, 441.

Munro, G.H., 1963, J.Geophys.Res., 68, 1851.

Munro, G.H., 1965, Report of the Second Symposium on Radio Astronomical and Satellite Studies of the Atmosphere., October 1965, Boston, Mass. U.S.A.

Patthasary, R., Basler, R.P., and de Witt, R.N., 1959, Proc.Instn.Radio Engrs., N.Y., 47, 1660.

Peterson, A.M., Villard, O.G., Leadabrand, R.L., and Gallagher, P.B., J.Geophys.Res., 60, 497.

Phillips, G.J., and Spencer, M., 1955, Proc.Phys.Soc., B,68, 481.

Piddington, J.H., 1964, Plan.Space Sci., 12, 127.

Potts, B.C., 1963, Report 1116-28, Antenna Laboratory, Ohio State University Research Foundation Columbus.

Rao, M.S.V.G., and Rao, B.R., 1961, J.Geophys.Res., 66, 2113.

Ratcliffe, J.A., 1956, Rep.Progr.Phys., 19, 188.

Ryle, M., and Hewish, A., 1950, Mon. Not. R. Astr. Soc., 110, 381.

Shimazaki, T.A., 1959, J.Radio Res.Lab., Japan, 6, 669.

Singleton, D.G., 1960, J.Geophys.Res., 65, 3615.

Singleton, D.G., and Lynch, G.J.E., 1962a, J.Atmos.Terr. Phys., 24, 353.

Singleton, D.G., and Lynch, G.J.E., 1962b, J.Atmos.Terr. Phys., 24, 363.

Singleton, D.G., Lynch, G.J.E., and Thomas, J.A., Nature, 189, 30.

Slee, O.B., 1958, Nature, 181, 1610.

Slee, O.B., 1962, Aust.J.Phys., 15, 568.

Smerd, S.F., and Slee, O.B., 1966, Aust.J.Phys.,19, 427.

Smith, F.G., 1950, Nature, 165, 422.

Swenson, G.W. Jr., 1962, Bourdeau 1962 Report on S-66 Satellite.

Titheridge, J.E., 1963, J.Geophys.Res., 68, 3399.

Warwick, J.W., 1964, Radio Science J. of Res. NBS/USNC-URSI, 68D, 179.

Wild, J.P., and Roberts, J.A., 1956, J.Atmos.Terr.Phys., 8, 55.

Yeh, K.C., 1965, Preprint N.A.S.A., NsG24-29.

Yeh, K.C., and Swenson, G.W. Jr., 1959, J.Geophys.Res., 64, 2281.

Yeh, K.C., and Swenson, G.W. Jr., 1964, Radio Science, J. of Res. NBS/USNC-U.R.S.I., 68, 881.

Yeh, K.C., Swenson, G.W. Jr., and McClure, J.P., 1963, Spring U.R.S.I. Meeting, Washington, D.C.

Yerukimov, L.M., 1962, Geomagnetism and Aeronomy, 2, 572.

Yuen, P.C., and Roelofs, T.H., 1966, J.Geophys.Res., 71, 849.

APPENDIX I

The Reflecting Sphere

Let $\underline{\kappa}_1$ be the wave normal of plane wave illumination which is weakly scattered by some medium; and let $\underline{\kappa}$ be the wave normal of a typical component of the scattered spectrum. The vectors have lengths given by:

$$|\underline{\kappa}_1| = |\underline{\kappa}| = 1/\lambda.$$

As $\underline{\kappa}$ varies the vector $(\underline{\kappa}-\underline{\kappa}_1)$ generates the "Reflecting Sphere", of radius $1/\lambda$, centred at $-\underline{\kappa}_1$ in Fourier transform space.

An expression is required for the Z-component of the vector $(\underline{\kappa}-\underline{\kappa}_1)$ when its X and Y components are given and the direction cosines of $\underline{\kappa}_1$ are known. The geometry of the situation is shown in Figure (2.5) of Chapter 2

Now

$$\underline{\kappa}-\underline{\kappa}_1 = [X,Y,0] + [0,0,Z] ,$$

so

$$Z^2 = \underline{\kappa}\cdot\underline{\kappa} + \underline{\kappa}_1\cdot\underline{\kappa}_1 + [X,Y,0]^2 + 2\underline{\kappa}_1\cdot[X,Y,0] - 2\underline{\kappa}\cdot(\underline{\kappa}_1 + [X,Y,0]).$$

On resubstituting for $\underline{\kappa}$ in the last term,

$$Z^2 = -[X,Y,0]^2 - 2\underline{\kappa}_1\cdot[X,Y,0] - 2\underline{\kappa}_1\cdot[0,0,Z].$$

If $\underline{\kappa}_1$ has direction cosines ℓ,m,n, this becomes:

$$Z^2 + \frac{2n}{\lambda} Z + (X^2 + Y^2 + \frac{2\ell x}{\lambda} + \frac{2mY}{\lambda}) = 0,$$

whence

$$Z = -\frac{n}{\lambda} \pm \frac{n}{\lambda}\left[1 - \frac{\lambda^2}{n^2}(X^2 + Y^2) - \frac{2\lambda}{n^2}(\ell X + mY)\right]^{\frac{1}{2}}.$$

In most cases of interest and particularly when ionospheric scattering is considered, the spatial frequencies [X,Y] of importance are much smaller than $1/\lambda$. The binomial expansion of the square root occurring above is therefore taken only to the second order in X and Y. The unwanted solution (which gives $|Z| \sim 2/\lambda$) is ignored and

$$Z = -\frac{1}{n}(\ell X + mY) - \tfrac{1}{2}\frac{\lambda}{n}\left[(X^2 + Y^2) + \frac{1}{n^2}(\ell X + mY)^2\right].$$

This is the required expression.

APPENDIX II

The Validity of: $|\rho_{\underset{\sim}{f}}(\xi)|^2 = \rho_{a^2}(\xi)$

Let a wave field of wavelength λ have an angular spectrum $\underset{\sim}{F}(S_1)$ at a height $(h.\lambda)$ above a one-dimensional ground. Let real distance over the ground be measured by $(x.\lambda)$. The parameter S_1 is the sine of the angle between the wave normal of a typical component of the spectrum and the downward normal to the ground. C_1 is the corresponding cosine. (S_2, S_3, S_4 and C_2, C_3, C_4 are similar corresponding quantities which must be distinguished in the multiple integrals which follow).

The wave field at the ground is given by

$$\underset{\sim}{f}(x) = \int \underset{\sim}{F}(S_1) \exp\left\{ - 2\pi i(xS_1 + hC_1) \right\} dS_1,$$

and the intensity, or squared amplitude, by

$$a^2(x) = \iint \underset{\sim}{F}(S_1)\underset{\sim}{F}^*(S_2) \times \exp\left\{ -2\pi i[x(S_1-S_2) + h(C_1-C_2)] \right\} dS_1 dS_2 .$$

The assembly-averaged, un-normalised auto-correlation function of $\underset{\sim}{f}(x)$ is:

$$\underset{\sim}{\rho f}(\xi) = \iiint \overline{\underset{\sim}{F}(S_1)\underset{\sim}{F}^*(S_2)} \times \exp\left\{ -2\pi i[x(S_1-S_2) + h(C_1-C_2) - \xi S_2] \right\} dS_1 dS_2 dx.$$

Integration over x leads to the delta function, $\delta(S_1-S_2)$, which, upon integration over S_2 effects the substitutions:

$$S_2 = S_1$$

and

$$C_2 = C_1.$$

$\underset{\sim}{\rho f}(\xi)$ is therefore height-independent and is given by

$$\underset{\sim}{\rho f}(\xi) = \int \overline{\underset{\sim}{F}(S_1)\underset{\sim}{F}^*(S_1)} \exp\left\{ 2\pi i \xi S_1 \right\} dS_1$$

The squared modulus of $\underset{\sim}{\rho f}$ is:

$$|\underset{\sim}{\rho f}(\xi)|^2 = \iint \overline{\underset{\sim}{F}(S_1)\underset{\sim}{F}^*(S_1)\underset{\sim}{F}^*(S_1+\sigma)\underset{\sim}{F}(S_1+\sigma)} \times \exp\left\{ -2\pi i \xi \sigma \right\} dS_1 d\sigma$$

and the Fourier transform of this is

$$\underset{\sim}{W}_{\rho^2}(\sigma) = \int \overline{\underset{\sim}{F}(S_1)\underset{\sim}{F}^*(S_1)\underset{\sim}{F}^*(S_1+\sigma)\underset{\sim}{F}(S_1+\sigma)} dS_1 .$$

The assembly-averaged, un-normalised auto-correlation function of $a^2(x)$ is:

$$\rho_{a^2}(\xi) = \int\!\!\cdots\!\!\int \overline{\underset{\sim}{F}(S_1)\underset{\sim}{F}^*(S_2)\underset{\sim}{F}^*(S_3)\underset{\sim}{F}(S_4)} \times \exp\left\{-2\pi i[x(S_1-S_2-S_3+S_4)+ h(C_1-C_2-C_3+C_4)]\right\} \times \exp\left\{2\pi i\xi(S_3-S_4)\right\} dS_1 dS_2 dS_3 dS_4 dx.$$

Integration over x leads to the delta function, $\delta(S_1-S_2-S_3-S_4)$ which, upon integration over S_4 effects the substitutions

$$S_4 = -S_1 + S_2 + S_3$$

and $$C_4 = \cos\,[\text{arc sin}\,(-S_1 + S_2 + S_3)].$$

Writing $\sigma = S_2 - S_1$ gives :

$$\rho_{a^2}(\xi) = \iiint \overline{\underset{\sim}{F}(S_1)\underset{\sim}{F}^*(S_1+\sigma)\underset{\sim}{F}^*(S_3)\underset{\sim}{F}(S_3+\sigma)} \times \exp\left\{-2\pi i[h(C_1-C_2-C_3+C_4)+ \xi\sigma]\right\} dS_1 dS_3 d\sigma.$$

The Fourier transform of ρ_{a^2} is then:

$$W_{a^2}(\sigma) = \iint \overline{\underset{\sim}{F}(S_1)\underset{\sim}{F}^*(S_1+\sigma)\underset{\sim}{F}^*(S_3)\underset{\sim}{F}(S_3+\sigma)} \times \exp\left\{-2\pi i h(C_1-C_2-C_3+C_4)\right\} dS_1 dS_3.$$

Now let the phases of $\underset{\sim}{F}(S)$ be random to the extent that:

$$\left.\begin{aligned}\overline{\underset{\sim}{F}(S_1)\underset{\sim}{F}^*(S_2)} &= 0\\ \text{and}\quad \overline{\underset{\sim}{F}(S_1)\underset{\sim}{F}(-S_2)} &= 0\end{aligned}\right\} \text{ for } S_1 \neq S_2$$

These are very general conditions: no random spectrum is likely to have special relationships between components

for which $|S_1| \neq |S_2|$; the quantity $\overline{\underset{\sim}{F}(S)\underset{\sim}{F}^*(S)}$ must be non-zero for some S if the spectrum is to exist at all; the value of $\overline{\underset{\sim}{F}(S)\underset{\sim}{F}(-S)}$ is the important quantity in the following discussion.

Consider the term

$$\overline{\underset{\sim}{F}(S_1)\underset{\sim}{F}^*(S_1+\sigma)\underset{\sim}{F}^*(S_3)\underset{\sim}{F}(S_3+\sigma)}$$

in the integrand of $W_{a^2}(\sigma)$. This is non-zero only if the four factors under the bar are suitably paired like the factors in the conditional equations above. Within the conditions imposed the only possibilities for this are:

$$S_3 = S_1$$

or $$S_3 = -S_1 - \sigma.$$

Using these conditions, and the relationships between C_1, C_2, C_3 and C_4, gives:

$$W_{a^2}(\sigma) = \int\Big[\overline{\underset{\sim}{F}(S_1)\underset{\sim}{F}^*(S_1+\sigma)\underset{\sim}{F}^*(S_1)\underset{\sim}{F}(S_1+\sigma)} + \overline{\underset{\sim}{F}(S_1)\underset{\sim}{F}^*(S_1+\sigma)\underset{\sim}{F}^*(-S_1-\sigma)\underset{\sim}{F}(-S_1)}$$
$$\times \exp\Big\{-2\pi ih\Big[\cos\Big\{\text{arc sin}(S_1)\Big\} - \cos\Big\{\text{arc sin}(S_1+\sigma)\Big\}\Big]\Big\}\Big]dS_1 \ .$$

The first term of the integrand of W_{a^2} is seen to be identical with the integrand of W_{ρ^2} found previously. The second term describes height-dependent structure, the

'visibility' of which is determined by

$$\overline{\underset{\sim}{F}(S_1)[\underset{\sim}{F}^*(-S_1)] * \underset{\sim}{F} * (S_1+\sigma)[\underset{\sim}{F}(-S-\sigma)]} *$$

Comparison with the standard form for the visibility of two-slit interference fringes indicates that the operative 'slits' have the form $\underset{\sim}{F}(S)$ and $\underset{\sim}{F}^*(-S)$. (See the discussion of Section 2.5 of Chapter 2).

When, for all S_1 and σ, the visibility of the height-dependent structure vanishes:

$$W_{a^2}(\sigma) = W_{\rho^2}(\sigma)$$

and the Fourier transforms of these functions are equal. That is,

$$|\underset{\sim}{\rho f}(\xi)|^2 = \rho_{a^2}(\xi)$$

as asserted by Bramley (1951) and Ratcliffe (1956).

Reprinted from

Journal of
ATMOSPHERIC AND
TERRESTRIAL PHYSICS

PERGAMON PRESS
OXFORD • LONDON • NEW YORK • PARIS

Journal of Atmospheric and Terrestrial Physics, 1963, Vol. 25, pp. 339 to 365. Pergamon Press Ltd. Printed in Northern Ireland

On the variation of radio star and satellite scintillations with zenith angle

B. H. Briggs and I. A. Parkin
Department of Physics, University of Adelaide

(*Received* 21 *December* 1962)

Abstract—The theory of the variation of the depth of amplitude scintillations with the zenith angle of the source is considered, for radio waves received from a star or a satellite. It is assumed that irregular phase fluctuations are impressed on the wave in travelling through the ionosphere, and that the amplitude fluctuations develop by a diffraction process as the wave propagates in the free space beneath the ionosphere. Two effects are produced by an increase in the zenith angle of the source. The magnitude of the phase perturbations increases, because the thickness of the ionosphere along the line of sight increases, and the geometry of the diffraction process changes. Theoretical results are given, both for isotropic irregularities and for irregularities elongated along the direction of the earth's magnetic field. The advantages of observing simultaneously on two wavelengths are stressed. Some comparisons with available experimental data are made, and suggestions are made for future experiments. Irregularities at different distances from the observer are not equally effective in producing amplitude scintillations, and some examples of the "weighting function" which determines their effectiveness are given. Various measures of "scintillation depth" are discussed and related to each other.

1. Introduction

Much attention has recently been given to the fluctuations of radio waves from stars and satellites imposed by their passage through irregularities in the ionosphere. These effects depend on the position of the source relative to the observer. When the source is at a large zenith angle, the fluctuations are increased as compared with observations made at the zenith under similar conditions. In this paper the theory of the variation with zenith angle is considered, and the deductions which can be made from experimental observations of this variation are discussed.

Only amplitude fluctuations will be considered because these are much easier to observe than phase fluctuations, and many experimental observations are available for comparison with the theory. For brevity, the amplitude fluctuations will be called "scintillations". A precise measure of the amount of fluctuation will be given in Section 4, and this will be called the "scintillation depth".

In considering the fluctuations imposed on a wave in its passage through an irregular medium there are two possible approaches. In the diffraction method the medium is considered to be equivalent to a certain thin diffracting screen. Because the absorption in the ionosphere is negligible for the frequencies normally used for the observation of scintillations, this screen will produce across the emerging wavefront variations of phase only, with no variations of amplitude. As the wave propagates beyond the screen, fluctuations of amplitude begin to develop, and this part of the problem is essentially a matter of diffraction theory. In the alternative approach, which may be called the scattering method, the wave at the observing point is considered to be the sum of the unscattered wave and waves scattered by the irregularities in the medium. This type of theory has been

used by Wheelon (1959); it is reasonably simple so long as the scattering is weak, but becomes complicated when the scattering is strong. Both methods are equally valid and give identical results, as has been shown for a simple case by Booker (1958).

In the present paper the diffraction method will be used. This is particularly suitable for the consideration of the zenith angle variation because the problem can be divided into two parts which are independent and which can be considered separately. The first part of the problem concerns the way in which the phase variations across the emerging wavefront vary with the angle of incidence of the wave on the irregularities. The second part involves the way in which the geometry of the diffraction process changes with the zenith angle of the source, due to the change in the distance from the irregularities to the observer and, for waves received from a satellite, the change in the distance from the source to the irregularities.

The irregularities in the ionosphere which produce the fluctuations are believed to be mainly in the F-region, at heights near 300 km, and are closely connected with the phenomenon observed in ionospheric sounding known as spread-F echoes (e.g. Ryle and Hewish, 1950; Hartz, 1955; Wright, Koster and Skinner, 1956; Briggs, 1958; Lawrence, Jesperson and Lamb, 1961). When the source is at large zenith angles, approaching 90°, it is possible that irregularities in the E-region, at heights near 100 km, become important (Wild and Roberts, 1956; Chivers and Davies, 1962).

In order to illustrate the theory as it is developed, we shall need typical values for the size and shape of the irregularities in the ionosphere. It was first shown by Spencer (1955) that the irregularities in the F-region are elongated along the direction of the earth's magnetic field. More extensive observations by Jones (1960) gave in more detail the sizes of the irregularities, measured in terms of the separation at which the correlation function of the medium has fallen to one-half. Typical values for these distances are 5 km along the magnetic field, and 1 km transverse to the field, with considerable variations on different occasions. The same observations also show that, to a good approximation, the form of the correlation function is Gaussian. These results were all obtained from observations of the radio star Cassiopeia A made at Cambridge (52°N). There are no similar detailed observations of the irregularities in the E-region. General considerations suggest that they are probably not elongated, and that they may be smaller than the irregularities in the F-region.

The general plan of the paper is as follows. Some geometrical results which are needed in the theory are first obtained in Section 2. Then in Section 3 the phase pattern on the emerging wavefront is related to the properties of the irregular medium. In Section 4 the diffraction aspects of the problem are discussed. The actual results are given in Sections 5 and 6. Section 5 contains the results which apply to observations of waves from a radio star, and Section 6 contains the corresponding results which hold when the source is a satellite. In both cases an approximation is first considered in which the irregularities are assumed isotropic, and afterwards the effects of elongation along the magnetic field are discussed. The ratio of the scintillation depth on two wavelengths is calculated, and

the advantages of observing simultaneously on two wavelengths are stressed. In Section 7 the "weighing function" which determines the effectiveness of irregularities at different distances from the observer is considered. This is important in connection with the determination of the heights of the irregularities by various methods. Finally, in Section 8 we consider various measures of the scintillation depth which have been used, and the way they are related to the quantity calculated in the theory.

2. The Geometry of the Problem

Figure 1 illustrates the geometry of the problem, for observations of signals from a satellite. (For observations of a radio star the source is, of course, at infinity, but otherwise the diagram is the same). It is assumed that the orbit of

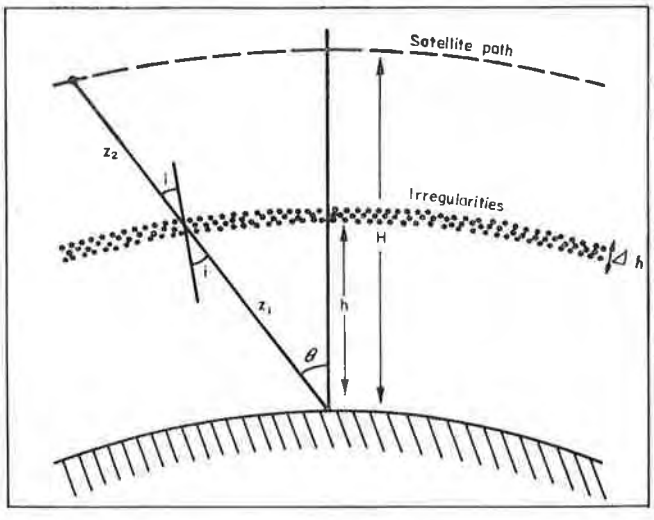

Fig. 1. The geometry of the problem, when the source is a satellite. For a radio star, H and z_2 are infinite.

the satellite is such that the height H may be taken as constant for the range of zenith angles θ involved. The irregularities are assumed to be confined to a layer at a height h, and the thickness of the layer Δh is assumed to be small compared with the height. The angle of incidence of the waves on the layer is i, and z_1 and z_2 are the distances of the irregularities from the observer and the source respectively. Then i, z_1, and z_2 are related to the zenith angle θ by the following expressions

$$i = \sin^{-1}\{R_0 \sin\theta/(R_0 + h)\} \tag{1}$$

$$z_1 = (R_0^2 \cos^2\theta + 2R_0h + h^2)^{1/2} - R_0 \cos\theta \tag{2}$$

$$z_2 = (R_0^2 \cos^2\theta + 2R_0H + H^2)^{1/2} - (R_0^2 \cos^2\theta + 2R_0h + h^2)^{1/2}, \tag{3}$$

where R_0 is the radius of the earth.

For waves received from a radio star, equations (1) and (2) still apply, but H and z_2 are infinite.

It should be noted that effects due to refraction by the regular ionized layers are neglected. At the frequencies normally used these effects are likely to be very small, except possibly for zenith angles which approach 90°.

3. The Relation of the Phase Pattern in the Emerging Wavefront to the Properties of the Irregularities in the Medium

3.1. *The distribution of electron density*

In order to develop the theory it is necessary to make some assumptions about the form of the three dimensional correlation function of the electron density in the ionosphere.

The simplest mathematical representation which fits the observations is the assumption that surfaces of equal correlation have the form of ellipsoids of revolution with their long axes along the direction of the magnetic field and that the variation of the correlation function along any radius is Gaussian. The correlation function of electron density N is therefore taken to be

$$\rho_N(r, s) = \exp\left[-\frac{r^2}{r_0^2} - \frac{s^2}{(\alpha r_0)^2}\right], \tag{4}$$

where r and s are a pair of cylindrical coordinates such that s is measured along the magnetic field and r perpendicular to the field. The quantity r_0 measures the distance at which the correlation falls to $1/e$ in a direction transverse to the field, and αr_0 the corresponding distance along the field. The "axial ratio" is α.

An irregular medium of this type can be thought of as built up by the superposition of electron clouds or "blobs" in a random arrangement (Ratcliffe, 1956). The correlation function of each blob will be the same as that for the medium as a whole. Since the convolution of a Gaussian function with itself is another Gaussian function, but of width $\sqrt{2}$ times that of the original, it follows that an individual blob must have an excess electron density given by

$$\Delta N(r, s) = \Delta N_0 \exp\left[-\frac{r^2}{r_0^2/2} - \frac{s^2}{(\alpha r_0)^2/2}\right], \tag{5}$$

where ΔN_0 is the excess electron density at the centre. If a large number of blobs of this type are assembled in random positions the correlation function of the resulting irregular medium will have the form of equation (4).

In experimental observations it is common to measure the distance at which the correlation falls to $1/e$ (or sometimes to one-half) and to quote this as the "size" of a typical irregularity in the medium. This ignores the factor of $\sqrt{2}$ mentioned above. However this is largely a matter of definition and in order to follow the practice which has become accepted we will not make this distinction in the present paper. Thus the phrase "size of a single irregularity" is taken to mean "distance at which the correlation falls to $1/e$".

3.2. *Propagation of a wave through the medium*

Scintillation observations are most often made on short wavelengths for which the refractive index μ deviates only slightly from unity. For this case we can write

$$\mu - 1 \doteqdot -\frac{\lambda^2 r_e N}{2\pi}, \tag{6}$$

where λ is the wavelength of the radiation and r_e is the classical radius of the electron. The deviation of μ from the mean is then

$$\Delta\mu = -\frac{\lambda^2 r_e}{2\pi}\Delta N, \tag{7}$$

where ΔN is the deviation of N from the mean.

The phase change in travelling a distance l in the medium, relative to the phase change in travelling the same distance in a uniform medium with the same mean electron density, is

$$\begin{aligned}\phi &= \frac{2\pi}{\lambda}\int_0^l \Delta\mu\, dl \\ &= -r_e\lambda\int_0^l \Delta N\, dl.\end{aligned} \tag{8}$$

As the refractive index differs only slightly from unity deviation of the rays will be very small and it is sufficient, in a determination of the phase pattern in the emerging wavefront, to perform the integration of equation (8) along straight lines in the medium. In a sense the three-dimensional medium is "projected" on to a plane normal to the direction of wave propagation.

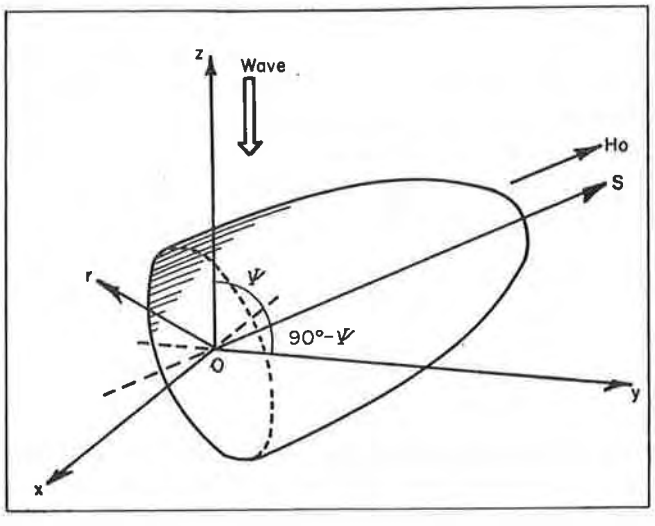

Fig. 2. This illustrates a single "blob", elongated along the magnetic field $\mathbf{H}_0$. The cylindrical co-ordinates r, s are such that Os is in the direction of the field. The Cartesian co-ordinates x, y, z are such that the wave advances in the negative z direction, and $\mathbf{H}_0$ is in the (y, z) plane at an angle ψ to Oz.

In order to carry out the integration of phase for incidence in an arbitrary direction we use the coordinate system shown in Fig. 2. Here a Cartesian system of axes (O, x, y, z) is shown in addition to the cylindrical system (O, r, s). The Cartesian axes are such that the wave advances in the negative z-direction. The (O, y, z) plane contains the magnetic field vector $\mathbf{H}_0$ which is in the (O, s) direction at an angle ψ to (O, z).

Elementary geometry leads to the relations

$$\begin{aligned} s^2 &= (y \sin\psi + z \cos\psi)^2 \\ r^2 &= x^2 + (y \cos\psi - z \sin\psi)^2 \end{aligned} \tag{9}$$

between the coordinates of the two systems of axes.

3.3. *The correlation function of phase*

To derive the correlation function of phase in the emerging wavefront we consider the wave travelling towards O to be incident on the typical blob described by $\Delta N(r, s)$ of equation (5), centred at O. Substituting equations (9) into equation (5) gives the distribution $\Delta N(x, y, z)$ and from equation (8) we find

$$\begin{aligned} \phi(x, y) = -r_e\lambda\Delta N_0 \exp\left[-\frac{x^2}{{r_0}^2/2} - \frac{y^2}{{r_0}^2/2}\left(\cos^2\psi + \frac{1}{\alpha^2}\sin^2\psi\right)\right] \\ \times \int_{-\infty}^{+\infty} \exp\left[\frac{2yz}{{r_0}^2/2}\left(1 - \frac{1}{\alpha^2}\right)\sin\psi\cos\psi - \frac{z^2}{{r_0}^2/2}\left(\sin^2\psi + \frac{1}{\alpha^2}\cos^2\psi\right)\right] dz. \end{aligned}$$

A suitable change of variable and an integration of the type $\int_{-\infty}^{\infty} e^{-t^2}\,dt$ gives

$$\phi(x, y) = -\sqrt{\frac{\pi}{2}}\, r_e\lambda \frac{\Delta N_0 \alpha r_0}{(\alpha^2\sin^2\psi + \cos^2\psi)^{1/2}} \exp\left[-\frac{x^2}{{r_0}^2/2} - \frac{y^2}{({r_0}^2/2)(\alpha^2\sin^2\psi + \cos^2\psi)}\right].$$

The variation in the phase pattern over the (x, y) plane is given by the exponential terms in this expression. If now a number of such phase patterns are superimposed in random positions in the (x, y) plane (corresponding to random occurrence of blobs throughout the medium), the correlation function of the resulting pattern is the same as that for one alone. The latter has the same form as the distribution $\phi(x, y)$ apart from the factors $\sqrt{2}$ discussed previously. Thus the correlation function $\rho_\phi(\xi, \eta)$ of the phase is given by

$$\begin{aligned} \rho_\phi(\xi, \eta) &= \exp\left[-\frac{\xi^2}{{r_0}^2} - \frac{\eta^2}{{r_0}^2(\alpha^2\sin^2\psi + \cos^2\psi)}\right] \\ &= \exp\left[-\frac{\xi^2}{{r_0}^2} - \frac{\eta^2}{(\beta r_0)^2}\right], \end{aligned} \tag{10}$$

where

$$\beta = (\alpha^2\sin^2\psi + \cos^2\psi)^{1/2}. \tag{11}$$

These results show that the phase pattern is anisotropic, the contours of equal correlation being ellipses with an axial ratio of β which is related to the axial ratio of the blobs by equation (11). The smaller dimension of the phase irregularities (i.e. the distance at which correlation falls to $1/e$ measured along the minor axes of the ellipses) is r_0, the same as that for the three dimensional correlation function of the medium.

3.4. *The root mean square fluctuation of phase*

We now proceed to a calculation of the root mean square deviation of phase produced by an extended irregular medium.

CHERNOV (1960) has shown that

$$\phi_0^2 = 4\pi^2 \frac{\overline{(\Delta\mu)^2}}{\lambda^2} L \cdot \int_{-\infty}^{\infty} \rho_\mu(O, O, \zeta)\, d\zeta, \tag{12}$$

where ϕ_0 is the root mean square deviation of phase produced in a wave which travels a distance L through the medium in the z-direction, and $\rho_\mu(O, O, \zeta)$ is the correlation function of refractive index μ in the z-direction.

In the present problem we consider a wave incident at an angle i on a layer of irregularities of thickness Δh (see Fig. 1). The length of its path through the layer is then

$$L = \Delta h \sec i.$$

From the simple relationship between μ and N (equation (6)) it is clear that the three-dimensional correlation function of refractive index, $\rho_\mu(r, s)$, has exactly the same form as that for electron density, $\rho_N(r, s)$(equation (4)). Employing again the equations (9) to give $\rho_\mu(\xi, \eta, \zeta)$ in the (O, x, y, z) frame, we have, on equating ξ, η to zero

$$\rho_\mu(O, O, \zeta) = \exp\left[-\frac{\zeta^2}{r_0^2}\left(\sin^2\psi + \frac{1}{\alpha^2}\cos^2\psi\right)\right].$$

Substituting the values of $\rho_\mu(O, O, \zeta)$ and L into equation (12), and using the expression

$$\overline{(\Delta\mu)^2} = \frac{\lambda^4 r_e^2}{4\pi^2}\,\overline{(\Delta N)^2}$$

derived from equation (7) ,we have

$$\phi_0 = \pi^{1/4} r_e \lambda \frac{(\overline{\Delta N^2}\, \Delta h\, \alpha r_0 \sec i)^{1/2}}{(\alpha^2 \sin^2\psi + \cos^2\psi)^{1/4}}. \tag{13}$$

In applying this result, the only factors which will vary with zenith angle are i and ψ. Since the irregularities are assumed to have similar statistical properties everywhere, the factors $\overline{\Delta N^2}$, Δh, α, and r_0 will all be independent of zenith angle, and in considering relative zenith angle variations these constants may be omitted. For observations on a single wavelength the factor λ could also be omitted. Since, however, we shall sometimes wish to consider the ratio of scintillation depth on two different wavelengths it is necessary to retain this λ in the expression. The simplified expression which is actually used in the calculations is therefore the following

$$\phi_0 \propto \lambda(\sec i)^{1/2}(\alpha^2 \sin^2\psi + \cos^2\psi)^{-1/4}. \tag{14}$$

It may be noted that for the special case of isotropic irregularities, this reduces to

$$\phi_0 \propto \lambda(\sec i)^{1/2}. \tag{15}$$

The expressions (10) and (13) are generalizations to the case of an anisotropic medium of expressions given by Bramley (1954) and Ratcliffe (1956) for an isotropic medium.

4. The Diffraction Theory

The way in which amplitude fluctuations appear, and increase as the wave travels beyond the irregularities, has been considered by Hewish (1952), Wagner (1962b) and Mercier (1962). The work of Hewish and Wagner applies to a "one dimensional" phase screen in which variations exist only in one direction. This is unrealistic when applied to the actual ionosphere, and we shall use the results of Mercier, who considered a two-dimensional phase screen. In Mercier's theory the irregular phase variations are assumed to be isotropic, and to have a Gaussian correlation function. Thus the correlation function of phase is of the form

$$\rho_\phi(\xi, \eta) = \exp\{-(\xi^2 + \eta^2)/r_0^2\}, \tag{16}$$

which is a special case of equation (10). The source of radiation is assumed to be at infinity, and so the results apply directly to the case of a radio star. We shall later show how they can be modified to apply to waves from a satellite. For the present, it should be noted that z, as used by Mercier, is to be taken as equal to z_1 (see Section 2), i.e. it is the distance from the screen to the observer.

The quantity calculated as a measure of the scintillation depth is

$$S^2 = \frac{\overline{R^4} - (\overline{R^2})^2}{(\overline{R^2})^2}, \tag{17}$$

where R is the amplitude of the wave. In his Fig. 1, Mercier shows how S^2 varies with $\sqrt{\lambda z}/r_0$. We prefer to plot S as a function $\lambda z/r_0^2$, since the curves then have a linear portion near the origin, which shows that S is proportional to z in this region. The quantity S will be adopted as a precise measure of the scintillation depth throughout the present paper. (The relation of S to other possible measures of the scintillation depth is discussed in Section 8.) The replotted curves are shown in Fig. 3. The different curves correspond to different values of ϕ_0, the root-mean-square phase deviation.

We shall refer to the region near the origin, where $S \propto z$, as the "near zone". Further from the screen the curves reach a limiting value, so that S no longer increases as the wave travels further. We shall refer to this region, where S is independent of z, as the "far zone". The change over from the near zone to the far zone occurs when $\lambda z/r_0^2 \approx 1$. Mercier has shown that the limiting value of S, far from the screen, is given by

$$S = \{1 - \exp(-2\phi_0^2)\}^{1/2}. \tag{18}$$

The curves of Fig. 1 were obtained by computation using an electronic computer, and there is, in general, no simple analytical expression for them. If, however, ϕ_0 is small there is a useful analytical approximation as follows

$$S = \sqrt{2}\,\phi_0\left(1 + \frac{\pi^2 r_0^4}{4\lambda^2 z^2}\right)^{-1/2}. \tag{19}$$

The limiting value of S far from the screen is, according to this approximation, equal to $\sqrt{2}\,\phi_0$.

In Fig. 3 the form of the approximate expression (19) is shown by the dotted curves. It will be seen that the approximation is very good for values of ϕ_0 up to 0·5 rad and reasonably good up to 0·71 rad. To this approximation, S is proportional to ϕ_0 and this leads to a great simplification, since the form of the variation with zenith angle is then independent of ϕ_0. For this reason the expression (19) will be used, and not the exact curves of Fig. 3. There is no difficulty in calculating zenith angle variations by the use of the exact curves, but the results will depend upon the value of ϕ_0 assumed, so that no general results can be given.

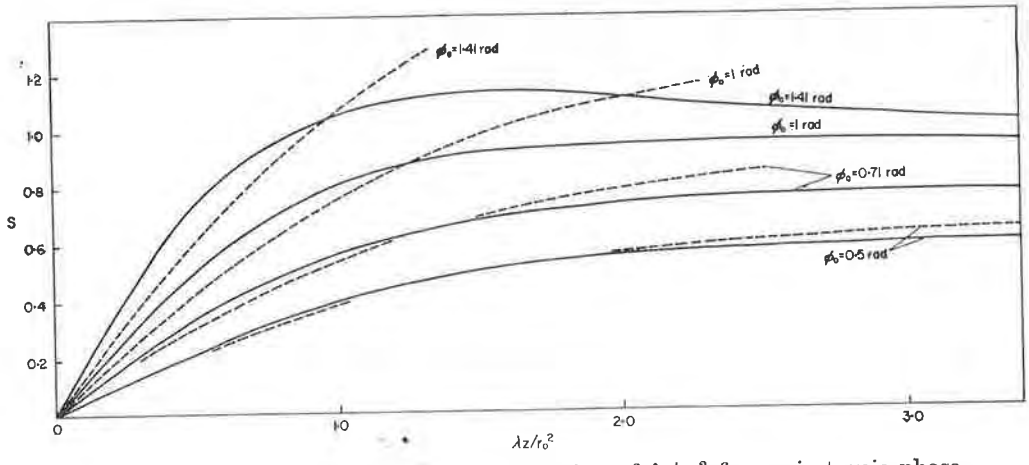

Fig. 3. The scintillation depth S, as a function of $\lambda z/r_0^2$ for an isotropic phase screen. The dotted curves represent the approximation of equation (19).

The theory of MERCIER applies only to isotropic irregularities. In general the phase pattern over the wavefront will be anisotropic and will have a correlation function of the form of equation (10) rather than (16). For this case P. W. JAMES (private communication) has shown that equation (19) must be replaced by

$$S = \sqrt{2}\phi_0\{1 - (\cos u_1 \cos u_2)^{1/2} \cos \tfrac{1}{2}(u_1 + u_2)\}^{1/2}, \tag{20}$$

where $\tan u_1 = 2\lambda z/\pi r_0^2$, and $\tan u_2 = 2\lambda z/\pi\beta^2 r_0^2$.

This function depends only on two parameters, the quantity $\lambda z/r_0^2$, and β, the axial ratio of the phase pattern. Thus we may write

$$S = \sqrt{2}\phi_0 F\left(\frac{\lambda z}{r_0^2}, \beta\right). \tag{21}$$

In Fig. 4 the quantity $F = (S/\sqrt{2}\phi_0)$ is plotted as a function of $\lambda z/r_0^2$, for different values of β. The curve for $\beta = 1$ has, of course, the same shape as the curves of Fig. 3 when ϕ_0 is small. As β increases, there is a progressive change in the curves, but they quickly tend to a limiting form, and the curve for $\beta = 5$ is

very nearly the same as the limiting curve for $\beta \to \infty$. This limit corresponds to diffraction by a "one-dimensional" screen, in which the phase varies in one direction only. The curves show that as soon as the anisotropy is appreciable, the diffraction process depends mainly on the smaller dimension r_0 of the phase pattern, and is almost independent of the larger dimension βr_0.

All the above results apply for a source at infinity. It can easily be shown, however, that any diffraction calculation carried out for a source at infinity can

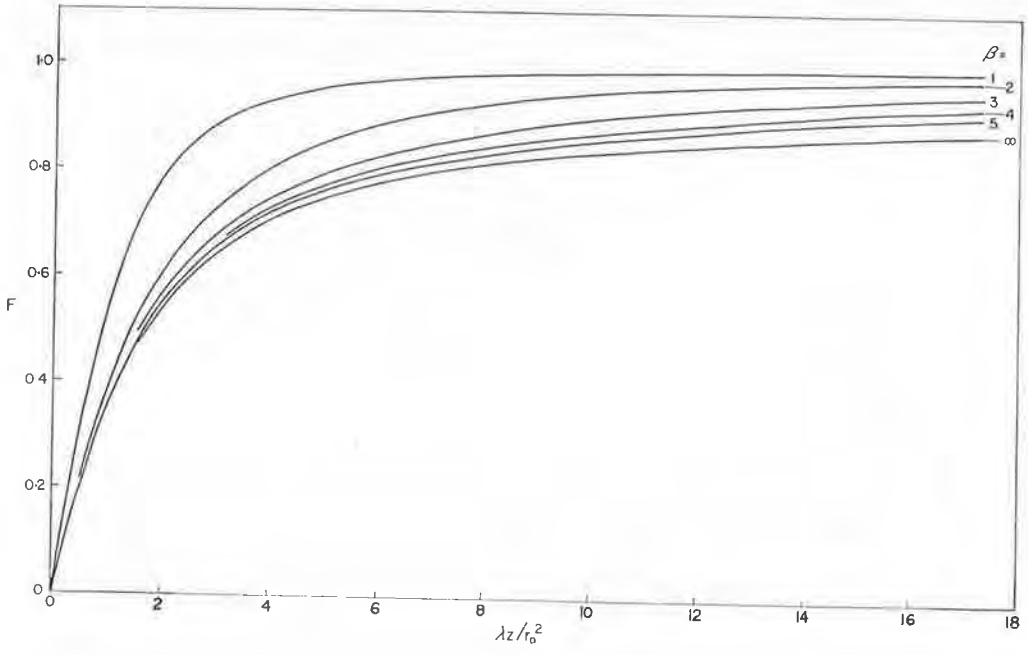

Fig. 4. The function $F = S/(\sqrt{2}\,\phi_0)$ as a function of $\lambda z/r_0^2$ for an anisotropic phase screen. The curves are for different values of the axial ratio β.

be extended to apply to a source at a finite distance by redefining z as follows:

$$\frac{1}{z} = \frac{1}{z_1} + \frac{1}{z_2}, \tag{22}$$

where z_1 and z_2 are the distances of the observer from the screen and the source from the screen respectively. For this result to hold, the angles of diffraction must be small. This condition is well satisfied, as the angles of diffraction are usually less than one degree. Thus all the above results, and in particular equations (19), (20) and (21) can be used when the source of waves is a satellite, provided z is defined by equation (22). As $z_2 \to \infty$, $z \to z_1$ and we go over to the results for a radio star, which now appear as a special case.

By combining the results of Sections 2, 3 and 4, all the necessary theory exists for the calculation of the zenith angle variation of the scintillation depth, both for radio stars and satellites. It should be noted that because the approximate

equations (19) and (20) are used, the results will apply only when the scintillation effects are not too severe (i.e. $\phi_0 < 0{\cdot}7$ rad). The shorter the wavelength, the more likely it will be that this condition will hold.

5. The Zenith Angle Variation for Radio Star Scintillations

5.1. *Isotropic irregularities*

It is useful to consider isotropic irregularities first in order to illustrate the general nature of the results. The difficulty in dealing with anisotropic field-aligned irregularities is that the geometry of the earth's magnetic field is different for each observing station and each radio star, so that only special cases can be worked out. For isotropic irregularities, however, general curves for the variation with zenith angle can be given. For irregularities in the F-region, the assumption of isotropy is a serious oversimplification, as will be shown later. It may be a reasonable assumption, however, for irregularities in the E-region.

In order to calculate the variation of the scintillation depth S with zenith angle, equations (15) and (19) are combined to give

$$S \propto \lambda(\sec i)^{1/2}\left(1 + \frac{\pi^2 r_0^{\,4}}{4\lambda^2 z_1^{\,2}}\right)^{-1/2}. \tag{23}$$

The variation of i and z_1 with zenith angle θ is given by equations (1) and (2). The family of curves shown in Fig. 5 illustrates the results. These curves apply to irregularities at a height of 300 km, and each curve is for a different value of the parameter $\lambda/r_0^{\,2}$. The value of this quantity determines the distance at which the near zone goes over into the far zone. If $\lambda/r_0^{\,2}$ is very small, the observer is situated in the near zone for all zenith angles. Equation (23) shows that S is then proportional to $z_1(\sec i)^{1/2}$. Since z_1 and sec i both increase with zenith angle, there is a large increase in scintillation depth as the zenith angle increases. If $\lambda/r_0^{\,2}$ is larger, observations are made entirely in the far zone, S is independent of z_1, and only the $(\sec i)^{1/2}$ factor remains. The zenith angle variation is therefore much reduced. For intermediate values of $\lambda/r_0^{\,2}$ there is a change over from near zone conditions to far zone conditions as the zenith angle increases.

It has sometimes been suggested that the form of the zenith angle variation might be used to determine the height of the irregularities. The present results show that in general this is not possible, because the curves depend so much on the value of the parameter $\lambda/r_0^{\,2}$. This has not been realized previously, because the assumption has usually been made that the observer is situated in the near zone, so that the zenith angle variation is given by $z_1(\sec i)^{1/2}$. This depends only on the height of the irregularities (from (1) and (2)) and is independent of λ and r_0. However, the assumption that observations are made in the near zone is not justified for the wavelengths normally used. The diffraction process is governed mainly by the smaller dimension of the irregularities (Section 4), and a reasonable estimate of r_0 would be 1 km, for irregularities in the F-region. Thus if $\lambda =$ 8 m, we have $\lambda z/r_0^{\,2} = 1$ for $z = 125$ km. Thus, if the irregularities are at heights near 300 km, it is more nearly true to say that observations are made entirely in the far zone. It is only for very short wavelengths (of the order of 0·3 m for this

example) that observations will be made in the near zone for all zenith angles. At these short wavelengths, scintillation effects will probably be too small to measure except at zenith angles approaching 90°, and here the E-region is likely to take over from the F-region. It seems unlikely, therefore, that the height of

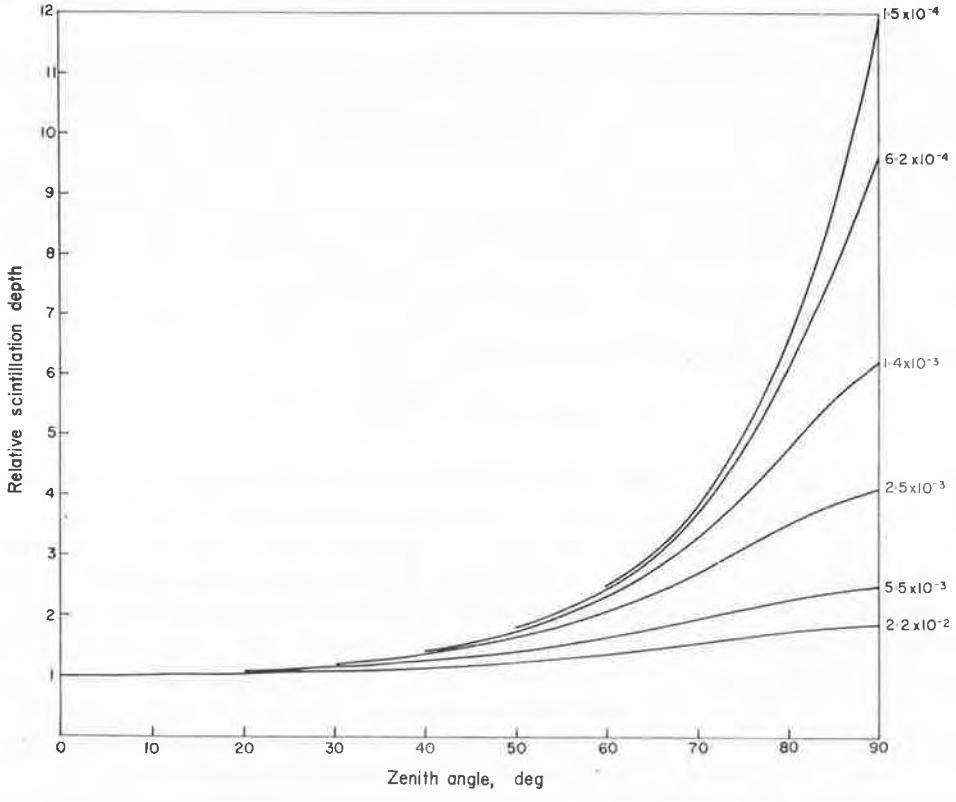

Fig. 5. The scintillation depth S (normalized to unity at the zenith) as a function of zenith angle, for radio star scintillations. Irregularities at a height of 300 km. The curves are for different values of the parameter λ/r_0^2 (km^{-1}).

the irregularities in the F-region can be determined from observations of the zenith angle variation. Also the effects due to anisotropy are important, and this introduces yet another variable.

The only previous work on the zenith angle variation in which the transition to far zone conditions is included appears to be that of Wagner (1962a), which applies to a "one-dimensional" system of irregularities, such that the electron density varies in one direction only. However, the importance of the size of the irregularities (ξ_0 in Wagner's notation) was not emphasized. Figs. 3, 4, 5 and 9 of Wagner's paper must have been calculated for some particular value of ξ_0 and some particular wavelength; the values used are not stated. The curves would be greatly changed by small variations of ξ_0, and it is impossible to determine the height of the irregularities by this method.

It is of interest to consider some recent results obtained by CHIVERS and DAVIES (1962) on 1390 Mc/s ($\lambda = 0{\cdot}22$ m). They observed the variation of the scintillation depth over the range of zenith angles 50° to 86° for the radio sources in Cygnus and Cassiopeia. The observed variation was compared with theoretical curves based on the assumption that observations were made in the near zone, and the conclusion was reached that the irregularities were at a height of 100 km. Now with $r_0 = 1$ km their assumption is justified for this short wavelength. However, there is some uncertainty about the value of r_0 which should be used at the level of the *E*-region, and so it is of interest to examine the results in more detail, in order to see whether the appropriate value of r_0 can be determined. It should first be noted that the height cannot be very different from 100 km. Any greater height will not give a sufficiently large variation with zenith angle for any value of r_0. It is true that the irregularities could, in principle, be lower than 100 km, and the value of r_0 could be adjusted to fit the observations. However, it is extremely unlikely that there would be sufficient ionization below about 90 km to produce any effects. Thus the range of possible heights is extremely limited, and must be close to 100 km. We therefore accept this height, and ask what limitations can be placed on the value of r_0. Figure 6 shows curves of the zenith angle variation calculated from equation (23), with $h = 100$ km and $\lambda = 0{\cdot}22$ m, for various values of r_0. These curves have been normalized to pass through the same point at $\theta = 70°$. The experimental points, similarly normalized, are also shown. It will be seen that r_0 cannot be less than 0·3 km.

5.2. *Anisotropic irregularities*

In general the anisotropy of the irregularities is important, and must be included in the calculation. The scintillation depth then depends on the angle between the line of sight and the magnetic field, so that it is not a function of zenith angle alone, but depends also on the azimuth angle of the source. As the earth rotates the zenith angle and the azimuth angle of a radio star are continually changing. Since there is a unique relation between the two angles, the scintillation depth may be regarded as a function of either angle. The variation can be worked out for any particular source from the results already given, if the geometry of the magnetic field is known.

In order to simplify the discussion, we shall consider only a source which is circumpolar, and instead of working out complete zenith angle curves we shall consider only the ratio of the scintillation depth at lower transit to the scintillation depth at upper transit. The main effects of anisotropy are illustrated by considering this ratio, and since it is a single number, the effects of changing the various parameters can be illustrated without the need to reproduce a very large number of complete curves.

In order to calculate this "zenith angle ratio" for any particular source, the values of the following quantities must first be decided: the height of the irregularities, the value of r_0, and the value of the axial ratio α. The first step is to determine the angle ψ between the line of sight and the magnetic field at upper and lower transit. The field is that in the vicinity of the irregularities, and may be obtained from one of the standard approximations to the earth's field. Then

the axial ratio β of the phase pattern can be determined for upper and lower transit from equation (11). The two values of z_1 are found from equation (2).

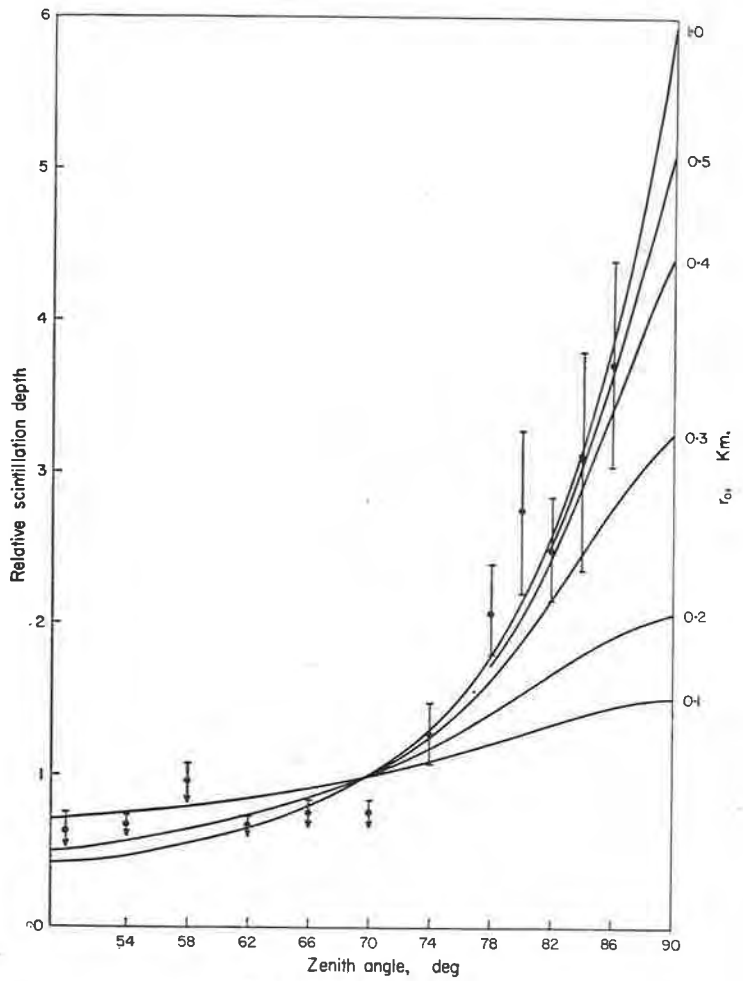

Fig. 6. Zenith angle curves for comparison with Chivers and Davies' observations on 1390 Mc/s. The height of the irregularities is taken as 100 km, and the curves are for different values of r_0.

The zenith angle ratio is then found from equation (21) which gives

$$\frac{S'}{S} = \frac{\phi_0' F(\lambda z_1'/r_0^2, \beta')}{\phi_0 F(\lambda z_1/r_0^2, \beta)}, \tag{24}$$

where the values S, ϕ_0, β, z_1 refer to upper transit and the values S', ϕ_0', β', z_1' to lower transit. The ratio ϕ_0'/ϕ_0 is found from equation (14). In numerical work the curves of Fig. 4 may be used to find the values of the function F.

As a large amount of data is available for the source Cassiopeia A observed at

Cambridge (52°N) on a frequency of 38 Mc/s, the results will be illustrated by considering this example. The source is circumpolar, and the zenith angle has values of 6° and 70° at upper and lower transit. In Fig. 7 the calculated zenith angle ratio is plotted as a function of r_0. Four curves are shown. The dotted curves are for isotropic irregularities ($\alpha = \beta = 1$), and for heights of 200 km and 400 km. The solid curves are for anisotropic irregularities with an axial ratio of 5 and for the same two heights. The effect of the anisotropy is seen to be very important. For example, if the irregularities are at a height of 200 km, the zenith

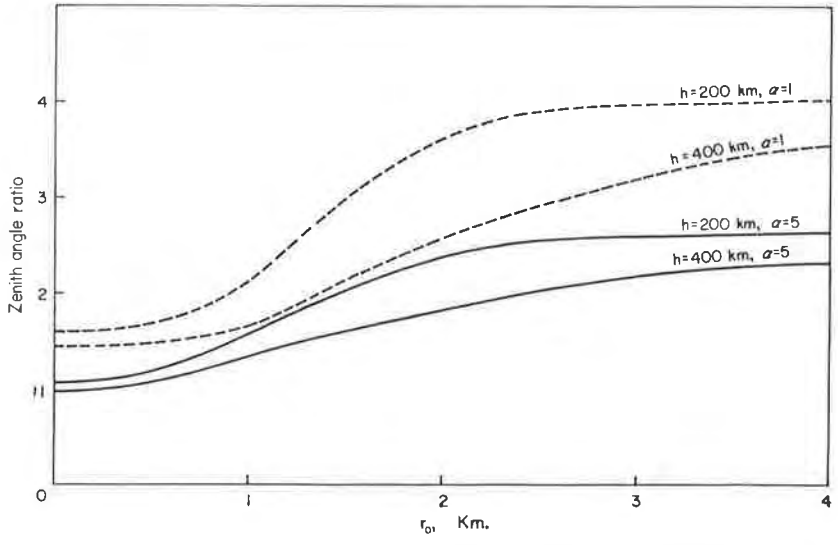

Fig. 7. The ratio of scintillation depth at lower transit to scintillation depth at upper transit for the source Cassiopeia A observed at Cambridge on 38 Mc/s. The solid curves are for anisotropic irregularities with an axial ratio of 5, and the dotted curves for isotropic irregularities.

angle ratio is 4·0 for isotropic irregularities, but only 2·65 for anisotropic irregularities with $\alpha = 5$. The reason for this is easy to see when the particular geometry for this source is considered in relation to the direction of the magnetic field. At lower transit the line of sight to the source is approximately transverse to the field in the F-region, so that the irregularities are viewed "broadside-on". At upper transit, the irregularities are viewed more nearly "end-on" and so the phase deviation is increased (equation (14)). This effect produces a variation in the opposite sense to the usual zenith angle variation, and so reduces the zenith angle ratio. This effect has been discussed by Little, Reid, Stiltner and Merritt (1962), in connection with observations of the same source made in Alaska. There the irregularities are viewed almost exactly "end-on" at upper transit, and the zenith angle variation is almost completely removed.

Experimental values of the zenith angle ratio have been determined from the Cambridge observations, and may be compared with the theoretical results shown in Fig. 7. It is necessary to use a whole year's data to determine the zenith angle variation, in order to remove the solar time variation. The procedure adopted

was to obtain monthly mean curves of the diurnal variation, and to average these in sidereal time by displacing each curve two hours relative to the preceding one. From the resulting variation with sidereal time, the variation with zenith angle can be found, since the zenith angle is a function of sidereal time. Values of the zenith angle ratio determined in this way are shown in Table 1. There is some evidence for a systematic variation with the solar cycle.

Table 1

Year	1950	1953	1954	1955	1956	1957	1958	1959	1960	1961
Zenith angle ratio	3·8	2·6	2·3	2·7	2·7	2·3	2·1	2·8	3·3	3·5

Figure 7 shows that for the most probable values $r_0 = 1$ km and $\alpha = 5$, the calculated zenith angle ratio is only of the order of 1·25, which is much less than the values observed. It seems unlikely that these values of r_0 and α can be grea ly in error since they were determined by other experiments made at Cambridge, using the same source and the same frequency. It therefore seems that the discrepancy is real, and that the observed zenith angle variation is influenced by some other effect. The most probable explanation is that the degree of irregularity of the F-region increases with latitude. For large zenith angles, the line of sight intersects the F-region well north of Cambridge, so that the zenith angle ratio would be increased by such an effect. A similar latitude variation has been suggested for different reasons by Chivers (1960) who observed the same source at Jodrell Bank.

A point which should be mentioned here is that the Cassiopeia A source has an appreciable angular diameter, and this has the effect of reducing the scintillation depth (Briggs, 1961). This reduction is largest when the irregularities are far from the observer, and so the effect tends to reduce the normal zenith angle variation. An approximate correction for this effect was made in evaluating the ratios given in Table 1.

5.3. *The ratio of the scintillation depths for two wavelengths*

We have shown that a direct comparison of the theory with observations is difficult. To obtain a zenith angle variation, the source must be observed for a year, so that solar time and irregular variations can be eliminated. Also, the effect of latitude variations is uncertain. All these difficulties arise from variations of the degree of irregularity of the ionosphere, and hence of ϕ_0, with time and space.

Now the ratio of the scintillation depths on two wavelengths is independent of ϕ_0, provided it does not exceed about 0·7 rad. This suggests that many of the difficulties would be removed if we used this ratio rather than the value on a single wavelength. This ratio will still vary with zenith angle, but this variation is due solely to the changing geometry of the diffraction process. From the observational point of view, the use of this ratio would appear to have great advantages. Since it would be no longer necessary to average large amounts of data, the scintillation

depth S could be evaluated accurately from its definition (17), thus avoiding the use of a semi-empirical "scintillation index" (see Section 8). A zenith angle curve could be obtained in 12 hr. The condition that ϕ_0 is small could always be met by observing on sufficiently short wavelengths.

The use of this ratio also eliminates the main effect of anisotropy of the irregularities. As explained in Section 5.2, this arises from the fact that the irregularities are viewed in different aspects at different zenith angles, thus changing the phase deviation ϕ_0. This effect is therefore removed by using the ratio on two wavelengths. Some effect of anisotropy remains due to the difference between the various curves of Fig. 4, since these control the subsequent diffraction process. However the differences between these curves are not large, and so, to quite a good approximation, we can take the irregularities to be isotropic.

Let the scintillation depth be $S(\lambda_1)$ for a wavelength λ_1 and $S(\lambda_2)$ for a wavelength λ_2. Then from (23) we have

$$\frac{S(\lambda_1)}{S(\lambda_2)} = \frac{\lambda_1}{\lambda_2}\left(1 + \frac{\pi^2 r_0^4}{4\lambda_1^2 z_1^2}\right)^{-1/2}\left(1 + \frac{\pi^2 r_0^4}{4\lambda_2^2 z_1^2}\right)^{1/2}. \tag{25}$$

The variation of this ratio with zenith angle is shown in Fig. 8 for irregularities at a height of 300 km, and for wavelengths $\lambda_1 = 7{\cdot}5$ m, $\lambda_2 = 3{\cdot}75$ m (40 Mc/s and 80 Mc/s). Each curve is for a different value of r_0, and it will be seen that the variation is very sensitive to the value of this parameter. If r_0 is very small, observations are made entirely in the far zone, and for this limiting case (25) gives

$$\frac{S(\lambda_1)}{S(\lambda_2)} = \frac{\lambda_1}{\lambda_2} \qquad \text{(far zone)}.$$

If r_0 is very large observations are made entirely in the near zone, and for this case

$$\frac{S(\lambda_1)}{S(\lambda_2)} = \left(\frac{\lambda_1}{\lambda_2}\right)^2 \qquad \text{(near zone)}.$$

In the present example the curves tend to a limit of 2 when r_0 is small, and 4 when r_0 is large. For intermediate values of r_0 there is a change over from the near zone to the far zone as the zenith angle increases, and the curves cross over from one limit to the other.

The detailed shapes of the curves depend on both the value of r_0 and on the height of the irregularities. This was investigated by calculating curves for other values of the height, but these are not reproduced here. It was found that variations of h produced a family of curves rather similar in form to the family of Fig. 8, so that it is not possible to determine both r_0 and h. However, variations of r_0 produce much larger changes in the curves than variations in h. For example, a variation of h from 200 km to 400 km produces about the same effect as a change of r_0 by ± 15 per cent. The method therefore appears to offer a simple means for determining r_0. Since the irregularities almost certainly lie in the range 200–400 km, at any rate for zenith angles less than 70°, the curves of Fig. 8 can be used, and the resulting error in r_0 will not be more than ± 15 per cent. For the

collection of statistical data on variations of r_0 this is quite adequate, in view of the large variations which may be expected from one occasion to another.

It should be emphasized that the curves of Fig. 8 apply strictly to isotropic

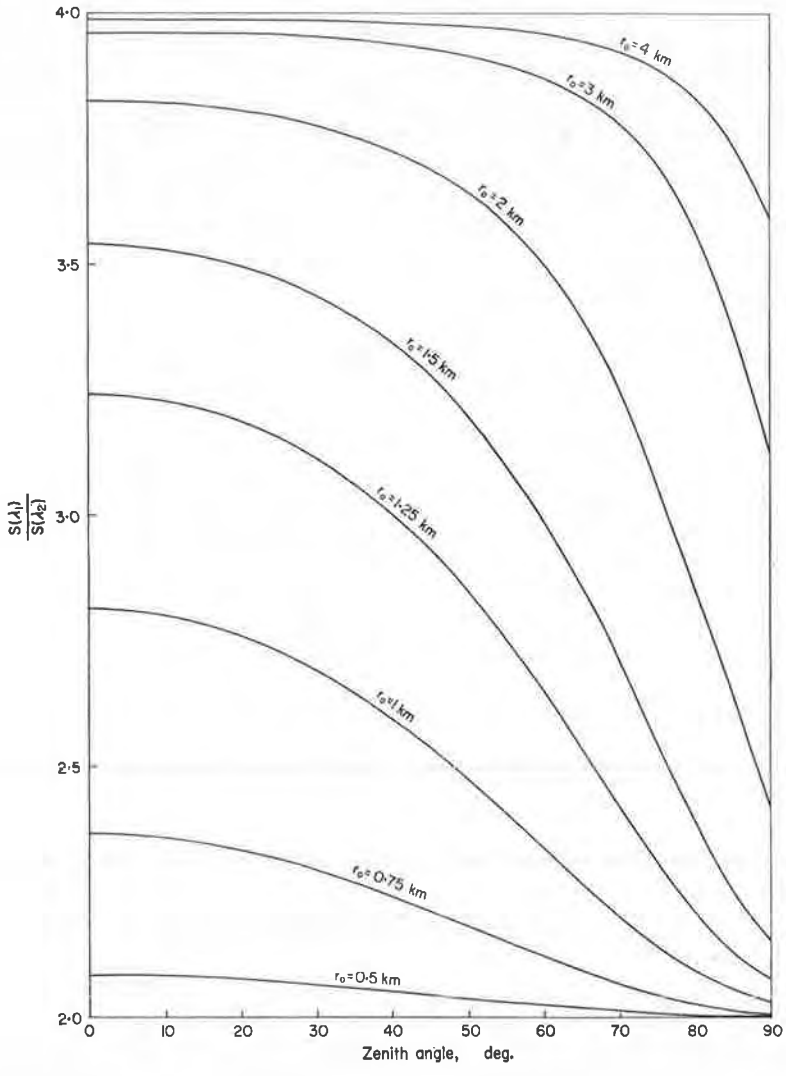

Fig. 8. The ratio of the scintillation depth on 40 Mc/s to the scintillation depth on 80 Mc/s as a function of zenith angle. The curves apply to observations of a radio star, and for irregularities at a height of 300 km.

irregularities, but will be a close approximation even if the irregularities are anisotropic. In the latter case, the value of r_0 which is determined is, of course, the smaller dimension. Also the curves of Fig. 8 will apply, to a close approximation, for any radio star observed at any latitude.

6. The Zenith Angle Variation when the Source is a Satellite

6.1. *Isotropic irregularities*

Again it is useful to consider isotropic irregularities first for purposes of illustration, though the results cannot be expected to be more than a rough approximation when the irregularities are in the F-region.

For isotropic irregularities, the scintillation depth is a function of the zenith angle alone, and is independent of the azimuth angle of the satellite. Universal curves can be given which will apply at any latitude. The calculation is similar to that for a radio star; the only difference is that in equation (19) we must write $z = z_1 z_2/(z_1 + z_2)$ instead of $z = z_1$. This gives, when combined with (15)

$$S \propto \lambda(\sec i)^{1/2}\left[1 + \frac{\pi^2 r_0{}^4 (z_1 + z_2)^2}{4\lambda^2 z_1{}^2 z_2{}^2}\right]^{-1/2}. \tag{26}$$

The factors which vary with the zenith angle θ are i, z_1 and z_2 (equations (1), (2) and (3)). The family of curves shown in Fig. 9 illustrates the nature of the results.

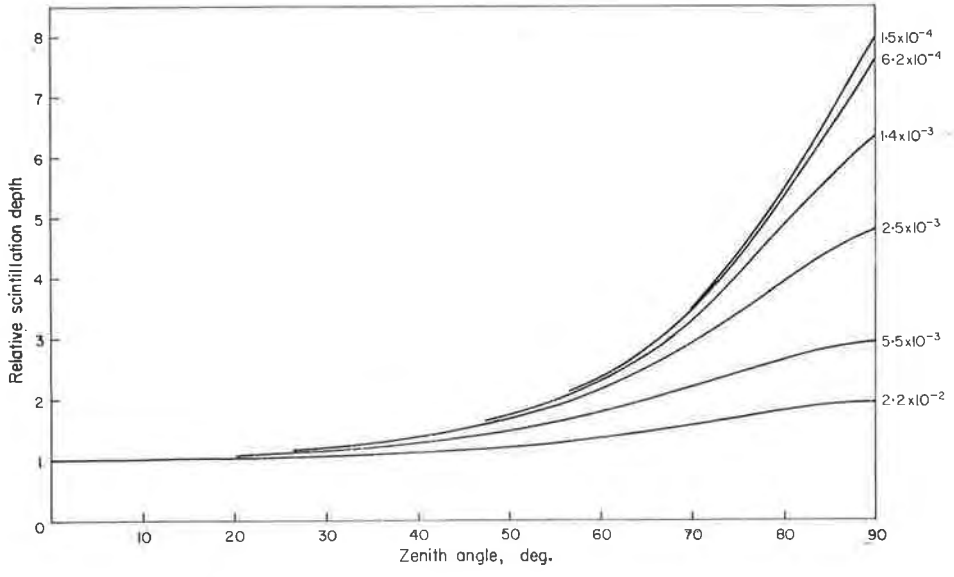

Fig. 9. The scintillation depth S (normalized to unity at the zenith) as a function of zenith angle, when the source is a satellite at a height of 1000 km. Irregularities at a height of 300 km. The curves are for different values of the parameter $\lambda/r_0{}^2$ (km^{-1}).

These curves are for a satellite at a height of 1000 km, and irregularities at a height of 300 km. The quantity $\lambda/r_0{}^2$ is used as a parameter, so that the effect on the zenith angle curve of changing either λ or r_0 can be seen. The curves are similar to those for radio star scintillations (Fig. 5), but different in detail because z_1 and z_2 vary differently with θ.

Singleton and Lynch (1962a) gave theoretical zenith angle curves for observations of Explorer VII made on a frequency of 20 Mc/s. These do not

agree with equation (26), and we believe that they are incorrect. No allowance was made for the fact that the source is at a finite distance, nor for the fact that, at the wavelength concerned, the observer is situated in the far zone. The curves given by Singleton and Lynch would, in fact, be correct for observations of a radio star if the observer were situated in the near zone.

6.2. *Anisotropic irregularities*

If the irregularities are anisotropic, and field-aligned, the scintillation depth depends not only on the zenith angle, but also on the azimuth angle. During a passage of a satellite past the observing station, the zenith angle and the azimuth angle vary in some particular way, and the geometry of each passage is different. It is not possible to investigate the variation of scintillation depth during a single passage, because some averaging procedure is necessary to remove the effects of a possible patchy distribution of irregularities in the horizontal plane. It would be possible to regard the scintillation depth as a function of the two variables, zenith angle and azimuth angle, and to average a large number of observations in such a way that this function was determined. The theoretical form of this function could be determined for any particular observing station from the equations already given, together with the known geometry of the magnetic field. However, this would be a very elaborate procedure, and it is preferable to use a simpler approach.

Following Singleton and Lynch (1962b) we shall simplify the problem by considering only times when the satellite crosses the magnetic meridian plane. It will cross this plane at different zenith angles on different occasions, and the variation with zenith angle for these occasions will show the maximum possible influence of the anisotropy of the irregularities. This is because the irregularities will be viewed exactly "end-on" when the angle of incidence is equal to the complement of the dip angle. In order to calculate the zenith angle variation in the magnetic meridian plane we proceed as follows. For any particular zenith angle, the angle ψ between the line of sight and the magnetic field can be found. The value of ϕ_0 and the axial ratio of the phase pattern on the emerging wavefront can then be found from equations (14) and (11). Then either equation (20) or the curves of Fig. 4 can be used to determine the scintillation depth, remembering that z in equation (20) must be taken equal to $z_1 z_2/(z_1 + z_2)$ where z_1 and z_2 are functions of the zenith angle given by equations (2) and (3). This procedure is then repeated for each value of zenith angle.

As an example of the nature of the results, Fig. 10 shows the curves which apply to observations of the Explorer VII satellite made at Brisbane on a frequency of 20 Mc/s. These can be compared with the observations made by Singleton and Lynch (1962b, Fig. 1). In the actual observations, the height of the satellite was variable, but we have taken a mean height of 820 km. The irregularities were assumed to be at a height of 300 km. Their smaller dimension r_0 was assumed to be 1 km, and curves are shown for values of the axial ratio α of 1, 2·5, 5, 10, 15 and 20. It will be seen that there is a marked peak in the curves at a zenith angle of 33° towards the North, when the irregularities are viewed "end-on". This peak is superimposed on the normal zenith angle variation. The

normalizing procedure used in the observations removed this variation, but showed clearly the peak at 33°N. The amplitude and width of the observed peak can be compared with the theoretical curves, and this comparison shows that there is agreement if the axial ratio α is of the order of 10.

Singleton and Lynch (1962b) gave a different explanation of this effect, based on specular reflection from field-aligned irregularities, following a similar

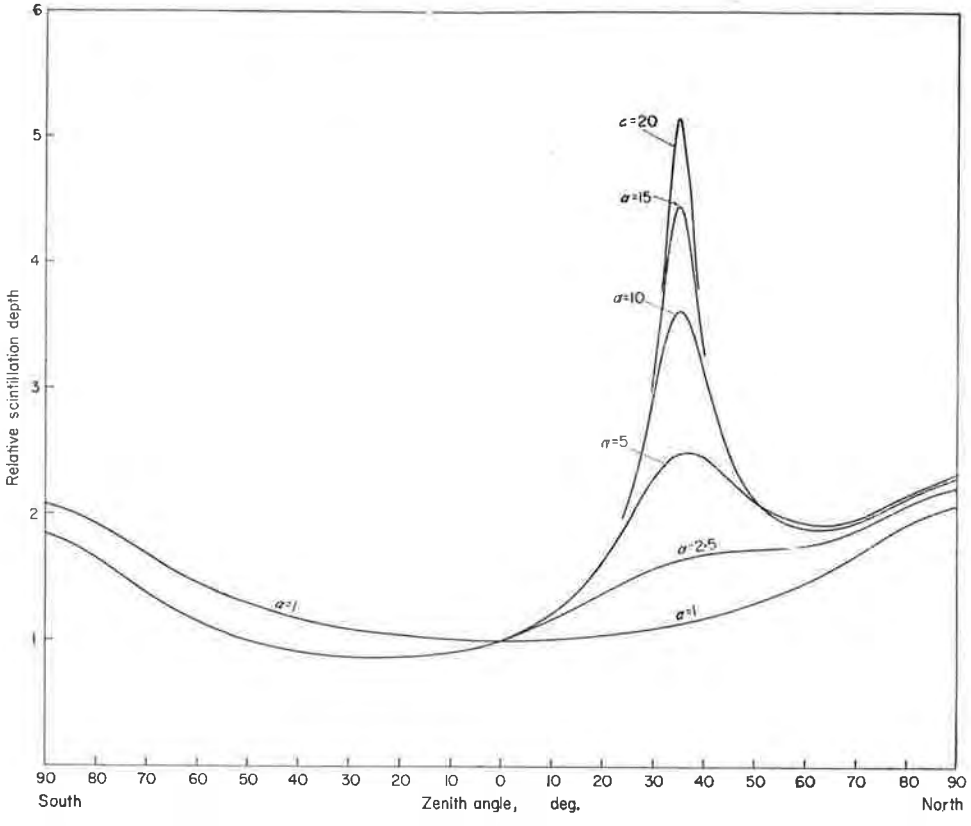

Fig. 10. The zenith angle variation in the magnetic meridian plane for scintillations of the signals from the satellite Explorer VII on 20 Mc/s, observed at Brisbane. The curves are for different values of the axial ratio α, and for irregularities at a height of 300 km. The curves are normalized to unity at the zenith.

suggestion of Rush and Colin (1958) for radio star scintillations. It does not appear to be necessary to invoke a special mechanism of this type, since, as we have shown, the effect is readily explained on the basis of the general diffraction approach used throughout the present paper. So long as the influence of the medium is weak, either a scattering theory or a diffraction theory must include all effects if fully worked out. The specular reflection idea appears convincing if sharply bounded irregularities are assumed. If, however, more realistic irregularities with gradual boundaries are considered, the "reflection" process is seen to

be no more than a process of gradual refraction, which will occur whether the irregularities are isotropic or anisotropic.

Mawdsley (1960) has suggested that the most favourable condition for forward scattering by field-aligned irregularities is when the incident radiation is normal to the field lines rather than along them. This is in direct conflict with the results of our calculations and we believe that the suggestion is erroneous. It is true that the scattered radiation is confined more closely to the forward direction when the irregularities are viewed "broadside-on". The scintillation depth, however, depends only on the ratio of the total scattered power to the power remaining in the unscattered wave, and is independent of the angular distribution of the scattered power. The total scattered power is a maximum when the irregularities are viewed "end-on", because the phase deviation is then a maximum. The angular distribution controls the scale of the pattern formed on the ground, which is, on the average, larger when the irregularities are viewed "broadside-on", because the angular spectrum of the scattered radiation is then narrower.

6.3. *The ratio of the scintillation depth for two wavelengths*

As for radio star scintillations, the ratio of the scintillation depths for two wavelengths is independent of ϕ_0, and this leads to a considerable simplification. It is no longer necessary to average a large number of observations in order to remove the influence of the patchy distribution of the irregularities. Variations with latitude, and the main effects of anisotropy are also eliminated (see Section 5.3).

The expression for the ratio $S(\lambda_1)/S(\lambda_2)$ is the same as equation (25) except that z_1 is replaced by $z_1 z_2/(z_1 + z_2)$. As an illustration we have chosen parameters appropriate to the forthcoming "S66 Polar Beacon Ionosphere Satellite" (Bourdeau, 1962). This will transmit unmodulated signals on 20 Mc/s and 40 Mc/s, two frequencies which would be very suitable for observations of this type. The height of the satellite will be 1000 km. The curves of Fig. 11 show how the ratio of the scintillation depths on the two frequencies would vary with zenith angle, for different values of r_0. The irregularities are assumed to be at a height of 300 km.

In using this method, the variation of S with time would be determined for both frequencies during a passage of the satellite. From the orbital data, the variation of the zenith angle with time would be determined, and the ratio of the scintillation depths would be plotted against zenith angle. This would lead to a value of r_0, the smaller dimension of the irregularities. Although the curves of Fig. 11 are exact only for irregularities at 300 km, the error in r_0 will be less than ± 15 per cent provided the irregularities are in the range 200–400 km. Observations of this type would appear to be very valuable, especially if carried out over a wide range of latitudes, since little is known about the way the size of the irregularities varies with latitude.

It is possible to obtain an independent estimate of the size of the irregularities from the rate of scintillation (Singleton and Lynch, 1962b). However, this method depends rather critically on the height assumed for the irregularities. A combination of both methods may enable the height to be determined.

7. The Weighting Function

Irregularities at different distances are not equally effective in producing amplitude scintillations. In this Section we consider the nature of the "weighting

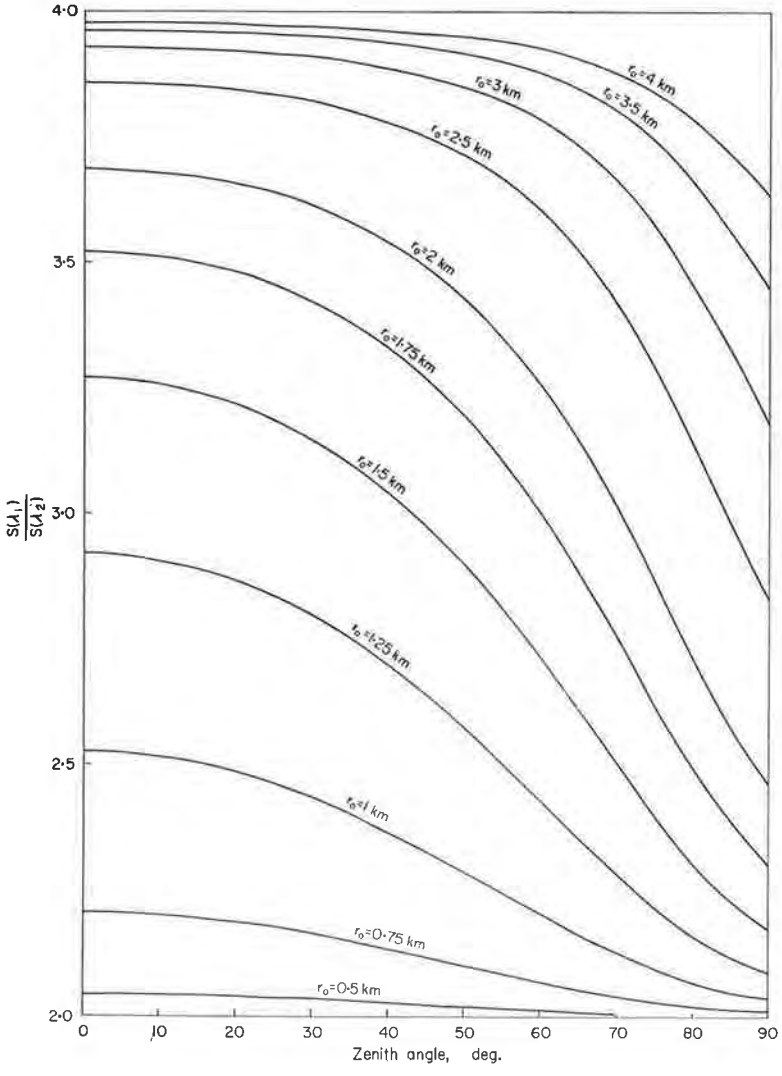

Fig. 11. The ratio of the scintillation depth on 20 Mc/s to the scintillation depth on 40 Mc/s as a function of zenith angle, when the source is a satellite at a height of 1000 km. Irregularities at 300 km.

function" which determines the effectiveness of irregularities at different distances. For simplicity, only the case of isotropic irregularities is considered.

If waves are received from a radio star, the scintillation depth is given by equation (19) where $z = z_1$ is the distance of the irregularities from the observer.

If we imagine the same irregularities to be placed in different positions along the line of sight, ϕ_0 will be constant, and the variation with z_1 gives the weighting function. Thus the weighting function is given by the curves of Fig. 3. Irregularities very close to the observer (z_1 small) are ineffective in producing amplitude scintillations; they produce only phase scintillations. As z_1 increases, the weighting function increases, but finally becomes constant for irregularities at a large distance from the observer.

If waves are received from a satellite, the situation is rather more complicated, since z is now to be put equal to $z_1 z_2/(z_1 + z_2)$. This is zero if $z_1 = 0$ or $z_2 = 0$, so that irregularities very close to the observer or very close to the satellite produce only phase scintillations. The maximum value of z occurs when $z_1 = z_2$, so that the most effective irregularities for the production of amplitude scintillations are those situated half-way between the observer and the satellite. Again, if we imagine the same irregularities to be placed in different positions along the line of sight, ϕ_0 will be constant, and the weighting function is obtained by substituting $z = z_1 z_2/(z_1 + z_2)$ into equation (19). The resulting expression may be regarded as a function of z_1 since $(z_1 + z_2)$ is constant, and equal to the distance of the satellite from the observer. Figure 12 shows the weighting function, regarded as a function of z_1, for a satellite at a distance of 1000 km. The quantity λ/r_0^2 is used as a parameter.

It is important to consider the possible influence of this weighting function in any method for determining the height of the irregularities. If the satellite is so low in height that it actually passes through the irregularities, they will appear to be at a mean height rather less than that of the satellite, because the weighting function is always zero at the satellite itself. For satellites as high as 1000 km the effect is not likely to be serious, because the weighting function has a long flat portion in the range of heights where irregularities are likely to exist (Fig. 12).

8. The Relationship between Various Measures of the Scintillation Depth

Several different measures of scintillation depth have been used in observations of radio star and satellite scintillations. The results of the theoretical calculations made in the present paper cannot be compared directly with experimental data unless the relationship between these various measures is known.

When radio waves are received from a satellite, the deflection of the recorder is normally proportional to the amplitude of the wave. It is therefore convenient to use a measure of the scintillation depth which depends on the deviation of the amplitude from the mean amplitude, divided by the mean amplitude. Two measures are possible, as the mean deviation, or the root-mean-square deviation may be used. These measures will be denoted by S_1 and S_2. They are defined as follows

$$S_1 = \frac{1}{\bar{R}} \overline{|R - \bar{R}|}, \tag{27}$$

$$S_2 = \frac{1}{\bar{R}} \left\{ \overline{(R - \bar{R})^2} \right\}^{1/2}. \tag{28}$$

In the observation of radio star scintillations, the deflection of the recorder is usually proportional to the received power, i.e. to R^2. It is therefore natural to use a measure of the scintillation depth which depends on the deviation of the

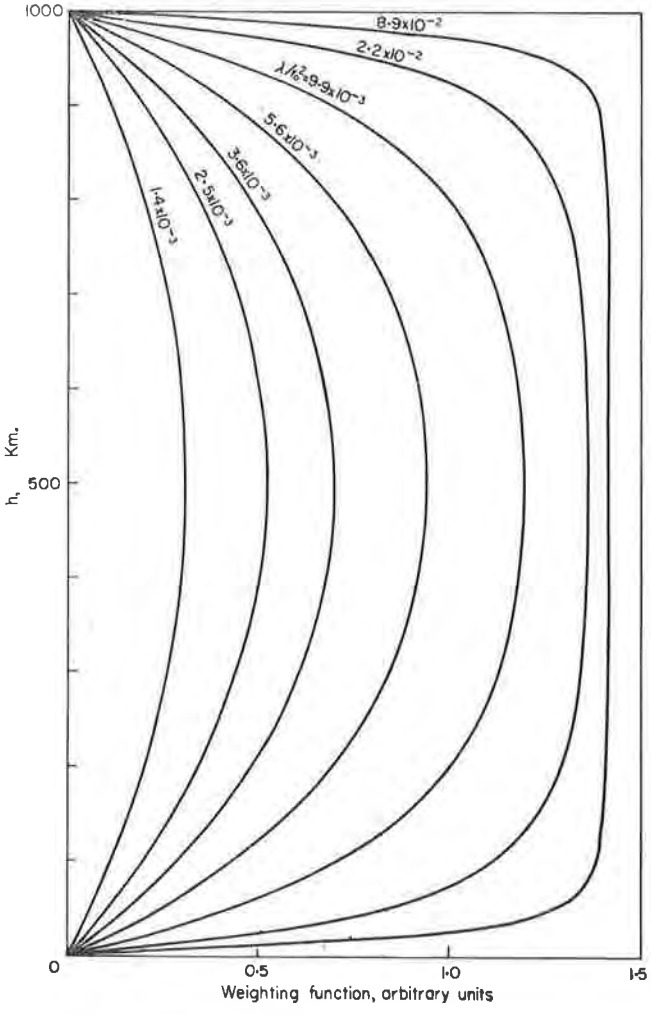

Fig. 12. The "weighting function" which determines the effectiveness of irregularities at different distances from the observer. The source is assumed to be at a distance of 1000 km. The curves are for different values of λ/r_0^2 (km^{-1}).

power from the mean power, divided by the mean power. Again two measures are possible, S_3 and S_4, defined by equations analogous to equations (27) and (28), as follows

$$S_3 = \frac{1}{\overline{R^2}} \overline{|R^2 - \overline{R^2}|}, \tag{29}$$

$$S_4 = \frac{1}{\overline{R^2}} \left\{ \overline{(R^2 - \overline{R^2})^2} \right\}^{1/2}. \tag{30}$$

It is easily shown that S_4 is the same as the measure S used throughout the present paper (cf. equation (17)).

If the probability distribution of R were known, it would be possible to relate S_1, S_2, S_3 and S_4 theoretically. Unfortunately the probability distribution is not, in general, known. Mercier (1962) has shown that far from a random phase screen, when the amplitude fluctuations are fully developed, the distribution of R is one of the "Rice curves" (Rice, 1945). Limiting cases of these curves are a "displaced Gaussian" distribution (when the phase deviation is small) and a Rayleigh distribution (when the phase deviation is large). We are not aware of any similar calculations of the probability distribution of R which apply close to the screen. It is therefore undesirable to make any assumptions about the form of the distribution. The values taken by S_1, S_2, S_3 and S_4 for the limiting case of a Rayleigh distribution are, however, of interest, and these are given in Table 2.

Table 2

Measure	S_1	S_2	S_3	$S_4 \equiv S$
Value for a Rayleigh distribution	0·42	0·52	0·73	1·00

In the absence of definite knowledge of the distribution of R, the safest procedure is to investigate the relation between the various measures experimentally, by evaluating each of them for sample records. Other workers have used this method for particular cases. For example, Lawrence *et al.* (1961) evaluated S_3 and $S_2{}^2$ from sample records of radio star scintillations. The results were given in the form of a graph of S_3 against $S_2{}^2$, using logarithmic scales for both axes. If the results are replotted as a graph of S_3 against S_2 with linear scales, it is found that S_3 is quite accurately proportional to S_2. The maximum observed values of S_2 and S_3 are those expected for a Rayleigh distribution. Also Little *et al.* (1962) have shown that, for all but the largest values of scintillation depth, S_3 is proportional to S_1. These results strongly suggest that all four measures are proportional to each other, within the limits of experimental error. If this is so we might expect the relations between them to be determined by the values which they take for a Rayleigh distribution, which suggests semi-empirical relationships of the form

$$S_1 = 0{\cdot}42\, S_4, \tag{31}$$

$$S_2 = 0{\cdot}52\, S_4, \tag{32}$$

$$S_3 = 0{\cdot}73\, S_4. \tag{33}$$

These results relate the measures S_1, S_2, S_3 to the measure $S_4 \equiv S$ which is used throughout the present paper.

In order to test further the relations (31) to (33) some records of the Transit 4A satellite obtained at Adelaide have been analysed. The frequency was 54 Mc/s. Each sample record contained about 50 fading maxima, and about 150 readings of amplitude were taken at equally spaced time intervals. The quantities S_1, S_2, S_3 and S_4 were calculated for each sample. The results are shown in Fig. 13(a),

(b), (c), in which S_1, S_2 and S_3 are plotted against S_4. The straight lines represent the linear relationships given by equations (31) to (33). It will be seen that the experimental points lie quite close to these lines.

These results show that it is permissible to assume that the four measures of scintillation depth are proportional to each other. It follows that when only relative values are required, it does not matter which measure is used. This is fortunate, since it simplifies the interpretation of earlier work. If absolute values are needed it is necessary to convert the measure used to the one which is calculated in the theory. In future work, it would be desirable to standardize on the use of S_4, since this is most easily calculated in the diffraction theory.

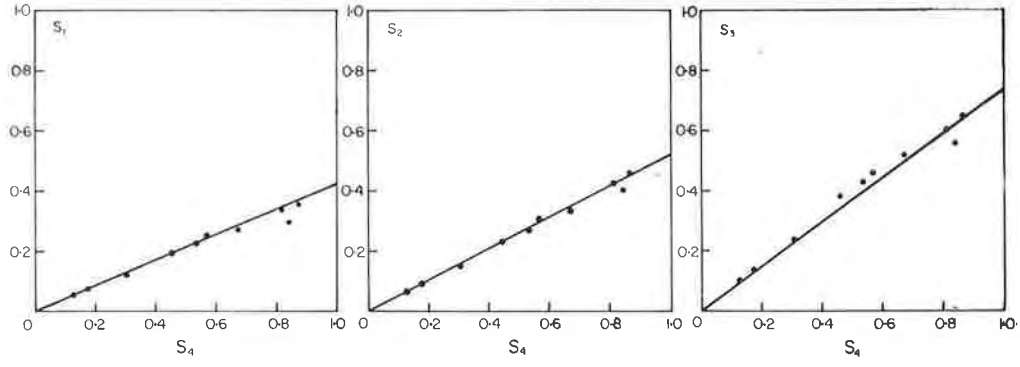

Fig. 13(a),(b),(c). Observed values of the quantities S_1, S_2, S_3 plotted against S_4, which is the measure of scintillation depth used throughout the paper. The relationships given by equations (31) to (33) are shown by the straight lines.

When very large numbers of records are to be analysed, it has been common to use a "scintillation index", assigned to each sample of record by visual inspection, without actual measurement. When this is done, it is very desirable to "standardize" the index by relating it to one of the quantities S_1, S_2, S_3 or S_4 (preferably S_4). This can be done by analysing some sample records by the exact method, and plotting the "index" against the actual value of scintillation depth. MERCIER (1962) has shown that the scintillation index used by the Cambridge workers, which has a scale 0–5, is proportional to S_4. The index used by workers at Jodrell Bank is determined "by assessing visually the mean peak to peak amplitude of the fluctuations . . . (which is) . . . then converted into a percentage of the estimated source intensity" (CHIVERS, 1960). The term "amplitude" is apparently used here in the sense of "amplitude on the chart", and since the record is one of intensity, the index should be proportional to S_3. SINGLETON and LYNCH (1962) define their scintillation index, used for satellite observations, as the amplitude of the signal fluctuations, divided by the mean signal level. This should be proportional to S_1.

In Sections (5) and (6) we compared the various observations with the calculated results, without commenting on the measure used. This is now seen to be justified, since only relative values of scintillation depth were used.

Acknowledgements—This work forms part of the upper atmosphere research programme of the University of Adelaide. This programme is financed jointly by the University and the Radio Research Board of the C.S.I.R.O. One of us (I. A. P.) is indebted to the University for the award of a Research Grant. We are indebted to the Director of the Computing Centre of the University of Adelaide for permission to use the IBM 1620 computer.

References

Booker H. G.	1958	*Proc. I.R.E.* **46**, 298.
Bourdeau R. E.	1962	*Publication No. X*615–62–99. Goddard Space Flight Centre.
Bramley E. N.	1954	*Proc. Roy. Soc.* A **225**, 515.
Briggs B. H.	1958	*J. Atmosph. Terr. Phys.* **12**, 34.
Briggs B. H.	1961	*Geophys. J. Roy. Ast. Soc.* **5**, 306.
Chernov L. A.	1960	*Wave Propagation in a Random Medium*, p. 29. McGraw-Hill, New York.
Chivers H. J. A.	1960	*J. Atmosph. Terr Phys.* **19**, 54.
Chivers H. J. A. and Davies R. D.	1962	*J. Atmosph. Terr. Phys.* **24**, 573.
Hartz T. R.	1955	*Canad. J. Phys.* **33**, 476.
Hewish A.	1952	*Proc. Roy. Soc.* A **214**, 494.
Jones I. L.	1960	*J. Atmosph. Terr. Phys.* **19**, 26.
Lawrence R. S., Jesperson J. L. and Lamb R. C.	1961	*J. Res. Nat. Bur. Stand.* **65D**, 333.
Little C. G., Reid G. C., Stiltner E. and Merritt R. P.	1962	*J. Geophys. Res.* **67**, 1763.
Mercier R. P.	1962	*Proc. Camb. Phil. Soc.* **58**, 382.
Mawdsley J.	1960	*J. Atmosph. Terr. Phys.* **18**, 344.
Ratcliffe J. A.	1956	*Rep. Progr. Phys.* **19**, 188.
Rice S. O.	1945	*Bell Syst. Tech. J.* **24**, 46.
Rush S. and Colin L.	1958	*Proc. I.R.E.* **46**, 356.
Ryle M. and Hewish A.	1950	*Mon. Not. R. Astr. Soc.* **110**, 381.
Singleton D. G. and Lynch G. J. E.	1962a	*J. Atmosph. Terr. Phys.* **24**, 353.
	1962b	*J. Atmosph. Terr. Phys.* **24**, 363.
Spencer M.	1955	*Proc. Phys. Soc. Lond.* B **68**, 493.
Wagner L. S.	1962a	*J. Geophys. Res.* **67**, 4187.
	1962b	*J. Geophys. Res.* **67**, 4195.
Wheelon A.	1959	*J. Res. Nat. Bur. Stand.* **63D**, 199.
Wild J. P. and Roberts J. A.	1956	*Nature, Lond.* **178**, 377.
Wright R. W., Koster J. R. and Skinner N. J.	1956	*J. Atmosph. Terr. Phys.* **8**, 240.

Comments on the Paper by J. D. Lawrence and J. D. Martin, 'Diurnal, Seasonal, Latitudinal, and Height Variations of Satellite Scintillation'

B. H. BRIGGS AND I. A. PARKIN

Department of Physics, University of Adelaide
Adelaide, South Australia

In their paper *Lawrence and Martin* [1964] make the statement (which they attribute to us) that the maximum scintillation depth will be observed when the satellite's distance from the observer is twice the distance of the irregularities from the observer. The statement in this form is not true, and it is not the statement we made.

We did show [*Briggs and Parkin*, 1963] that, if the phase deviation introduced by the irregularities is less than one radian, the scintillation depth is a monotonically increasing function of the quantity $Z^1 = Z_1 Z_2/(Z_1 + Z_2)$, where Z_1 is the distance from the observer to the irregularities, and Z_2 is the distance from the irregularities to the satellite. Thus, if the distance of the satellite from the observer is regarded as fixed (say $Z_1 + Z_2 = H$), and if Z_1 is regarded as being variable, the scintillations depth will be a maximum when Z^1 is a maximum, and this occurs when $Z_1 = \frac{1}{2}H$. In this case, the observer and the satellite are regarded as fixed, and irregularities are considered to be placed at varying positions between the two. It is then true that the maximum scintillation depth occurs when the irregularities are halfway between the observer and the satellite.

This, however, is not the problem considered by Lawrence and Martin. They are concerned with a case in which the irregularities are fixed in position and the satellite's distance changes; i.e., Z_1 is fixed and H is variable. For these conditions, Z^1 has no maximum; it increases monotonically from zero when $H = Z_1$ to infinity when H tends to infinity. The scintillation depth therefore also increases monotonically as the distance of the satellite increases. Thus the maximum which they observed for a certain distance of the satellite (their Figure 4) cannot be explained along these lines.

A possible explanation could be suggested if the phase deviation introduced by the irregularities is greater than one radian. As *Mercier* [1962] has shown, the scintillation depth is then no longer a monotonically increasing function of Z^1, but first increases to a maximum and then decreases, eventually becoming constant (see our Figure 3). This fits qualitatively the form of variation obtained by the authors. The peak at a certain value of Z^1 can be regarded as a kind of rough 'focusing' produced by the ionospheric irregularities acting as 'lenses.' At the frequency used (20 Mc/s) it is quite likely that the phase deviation would exceed one radian on many occasions.

REFERENCES

Briggs, B. H., and I. A. Parkin, On the variation of radio star and satellite scintillations with zenith angle, *J. Atmospheric Terrest. Phys., 25,* 339, 1963.

Lawrence, J. D., Jr., and J. D. Martin, Diurnal, seasonal, latitudinal, and height variations of satellite scintillations, *J. Geophys. Res., 69,* 1293, 1964.

Mercier, R. P., Diffraction by a screen causing large random phase fluctuations, *Proc. Cambridge Phil. Soc., 58,* part 2, 382, 1962.

(Received June 3, 1964.)

Reprinted from the *Journal of the Institution of Telecommunication Engineers*, Vol. 10, No. 8, pp. 299-309

The Study of Ionospheric Irregularities by the Use of Signals from Satellites

B. H. BRIGGS & I. A. PARKIN*

ABSTRACT

A survey is made of the information about ionospheric irregularities which can be obtained by the study of the scintillation of radio waves received from satellites. Special consideration is given to experimental methods, both existing and proposed, which give quantitative information about the size and shape of the irregularities and about the height and the thickness of the layer in which they are situated.

1. INTRODUCTION

THE degree of ionization of the ionosphere is far from uniform. Irregularities or 'blobs' of increased or diminished electron density are usually found at all levels and with a wide variety of sizes. Perhaps the most prominent irregularities of all, with the largest deviation of electron density from the mean, are those often present in the F-region which cause 'spread-F' echoes and scintillations of radio stars. They are observed to be elongated with their long axes in the direction of the earth's magnetic field. They occur mainly at night.

Recently it has become possible to study these irregularities by new methods, based on the use of artificial satellites carrying radio transmitters. Thus 'spread-F' has been observed above the maximum of the F-region by the Alouette 'topside sounder'. Other methods make use of radio signals transmitted right through the F-region from a satellite to the ground. In optical terminology we may speak of the irregularities as forming a kind of random 'diffracting screen' which produces over the ground a random 'diffraction pattern' when 'illuminated' from above by the radio wave. This pattern can be observed in various ways by radio receivers on the ground. In the present paper we shall discuss observations of this type, and the deductions which can be made from them.

The diffraction pattern will be in motion over the ground, due to the motion of the satellite, and so a receiver on the ground will record a fluctuating signal strength. By analogy with the scintillation of radio stars, these fluctuations are usually known as 'scintillations'. The 'scintillation depth' can be measured by calculating, for example, the root-mean-square deviation of the signal from its mean value, and expressing this as a percentage of the mean signal amplitude.

The rapid fluctuations or scintillations must be distinguished from other fluctuations, usually much slower, due to the Faraday effect. Fig. 1 shows a typical record in which both effects can be seen. The Faraday effect (rotation of the plane of polarization) produces the slow changes of amplitude; it will be discussed in more detail shortly.

Manuscript received on 29 *April* 1964.
*Department of Physics, University of Adelaide, South Australia.

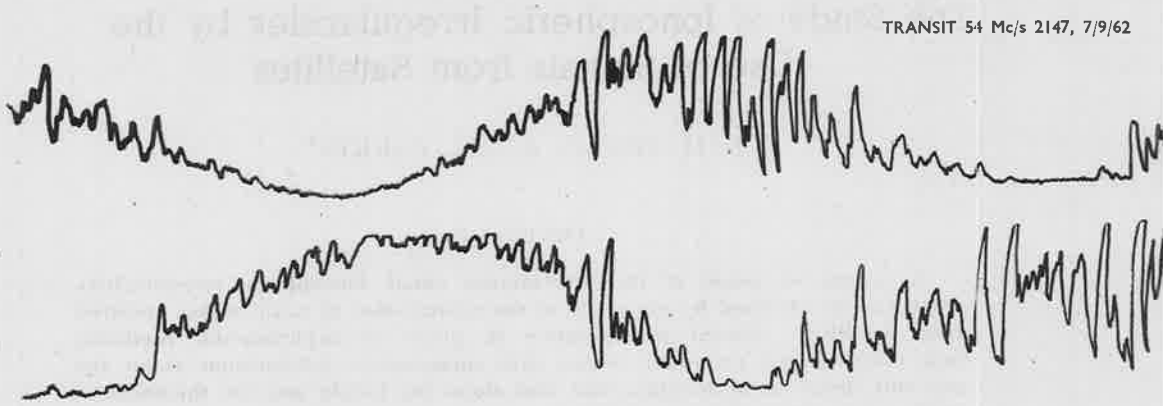

Fig. 1 — Recording of the signal strength received from the satellite Transit IVA on 54 Mc/s. Two
in antiphase at the two aerials. The fast fluctuations

Let us now consider the diffracting screen formed by the ionospheric irregularities in more detail. Satellite transmissions are usually at high frequencies, in the range 20-300 Mc/s. At these frequencies the refractive index of the ionosphere is only slightly less than unity, and refraction of the waves can usually be neglected. Nevertheless, because of the presence of the irregularities the ' optical thickness ' will vary with position and a wave will emerge from the lower side of the ionosphere with random variations of phase across its wavefront. Amplitude variations will be negligible because there is no appreciable absorption of waves of these frequencies in passing through the ionosphere. Thus we may call the diffracting screen a ' phase screen ' in contrast to an ' amplitude screen ', which would be a screen which modified the amplitude but not the phase of a wave passing through it.

If the diffraction pattern formed on the ground by the phase screen were also a ' phase pattern ' it would be difficult to observe. However, it can be shown by diffraction theory that amplitude fluctuations will appear, and will increase in depth as the wave propagates downwards through the free space between the ionosphere and the ground. The theory of this effect has been considered by Mercier (1962), Wagner (1962) and others. Thus over the ground a pattern is formed with fluctuations of both phase and amplitude, but usually only the amplitude fluctuations are recorded.

It is now necessary to discuss the Faraday effect in more detail in order to show that it can be neglected as a cause of the *fast* scintillations. It can be shown that the plane of polarization of a plane-polarized wave rotates as the wave travels through an ionized gas in the presence of a magnetic field, unless the propagation is exactly at right angles to the field. The total angle of rotation depends on the angle to the field and the total number of electrons contained in a column along the ray path. As both these quantities vary as the satellite passes over an observing station, a continuous rotation of the plane of polarization occurs. The voltage induced in a dipole receiving aerial therefore shows periodic fluctuations as shown in Fig. 1. Now if, due to the motion of the satellite, the ray happens to pass through a cloud of increased electron density, the Faraday rotation angle will suddenly increase. If the ray passes through a region of decreased density, the rotation angle will decrease. Therefore, when the

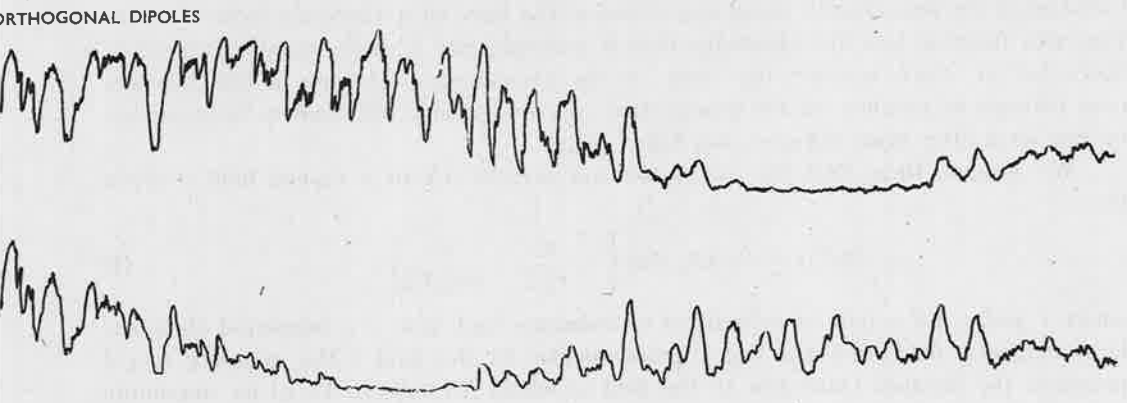

dipoles at right angles were used. The slow variations are due to Faraday rotation and are or ' scintillations ' are in phase at the two aerials.

ionosphere contains irregularities, there should be a rapid ' flicker ' of the plane of polarization in addition to the rotation. When the wave is received on a dipole, this flicker in angle would be converted to an amplitude fluctuation. Thus in principle, the Faraday effect could cause amplitude scintillations, and it may be asked whether this effect might not account for part or all of the amplitude fluctuations which are observed.

While this flicker phenomenon must occur, calculations show that it would be extremely small in most practical cases (probably less than 1 degree), and would therefore make no appreciable contribution to the amplitude fluctuations. This can be confirmed experimentally by using two dipoles at right angles. If Faraday flicker were appreciable, the signal on one dipole should decrease whenever the signal on the other increases. On the other hand, true variations of amplitude of the downcoming wave would have the same sign for both aerials. The records shown in Fig. 1 were obtained using crossed dipoles, and it can be seen that there is close and detailed agreement between the fast fluctuations. This shows that the Faraday effect cannot be important as a cause of scintillations.

We are justified, then, in supposing that the diffraction process outlined earlier is the main cause of the amplitude fluctuations, and we shall now consider what can be deduced from observations of these fluctuations. The objective is to find out as much as possible about the irregularities which cause the effects. We wish to know, for example, their size, shape and height above the ground, and whether they exist uniformly over a large region of the earth, or are distributed in patches. Relatively simple observations using a small number of radio receivers can give this type of information, if the records are analysed by suitable statistical methods.

Before we discuss these methods it is necessary to consider how the ' size ' and ' shape ' of the irregularities are to be specified. Since they are irregular, definitions of a statistical type are needed. Further, we must keep the number of parameters to be determined as small as possible, or we shall find that we have too many unknowns. Considerations of this type, together with the known elongation along the earth's magnetic field, suggest that an ' average ' irregularity or ' blob ' may be taken to have the form of an ellipsoid of revolution with its long axis along the field and with a

variation of electron density along any radius of the form of a Gaussian error function. The error function has the advantage that it contains only a single variable parameter, the value of which specifies the 'size' of the irregularity. The use of this function may perhaps be justified on the ground that any irregularity will tend to approximate to this form after some diffusion has taken place.

We assume, then, that the excess electron density ΔN of a typical blob is given by

$$\Delta N(r, s) = \Delta N_0 \exp\left[-\frac{r^2}{r_0^2/2} - \frac{s^2}{(\alpha r_0)^2/2}\right] \qquad \ldots(1)$$

where r and s are a pair of cylindrical co-ordinates such that s is measured along the local magnetic field direction and r perpendicular to the field. The quantity $r_0/\sqrt{2}$ measures the distance transverse to the field at which ΔN falls to $1/e$ of its maximum value ΔN_0. Similarly, $\alpha r_0/\sqrt{2}$ measures the corresponding distance along the field. The 'axial ratio' is therefore α, which is assumed to be greater than 1.

It can be shown (Ratcliffe, 1956) that if a large number of blobs of the above form are distributed at random so as to build up an irregular medium, then this medium will have an 'auto-correlation function' $\rho_N(r, s)$ given by

$$\rho_N(r, s) = \exp\left[-\frac{r^2}{r_0^2} - \frac{s^2}{(\alpha r_0)^2}\right] \qquad \ldots(2)$$

[The factors of 2 are introduced in (1) for convenience, so that they disappear in (2).]

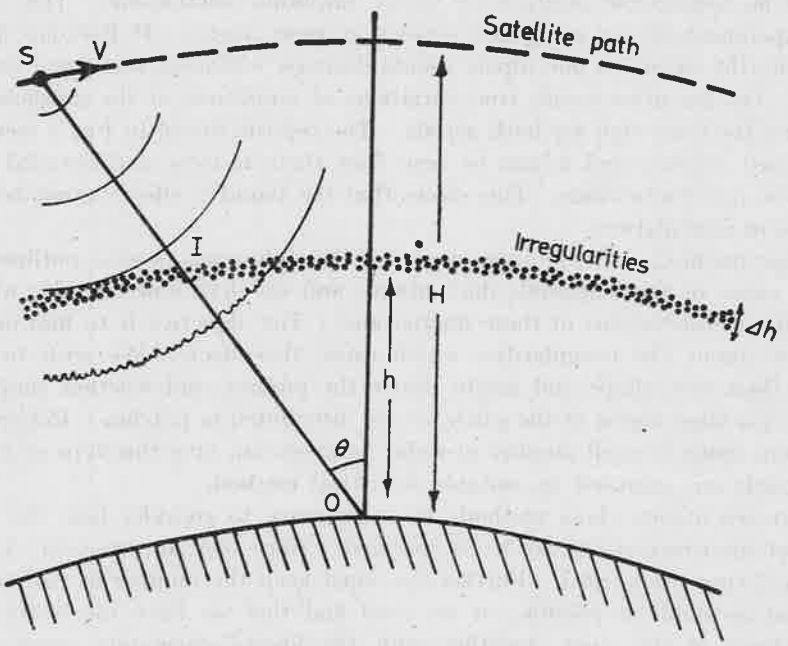

Fig. 2 — A satellite at a height H travels with velocity V over a layer of irregularities at a height h. SIO represents a radio ray travelling from the satellite at S to a receiver at O. Irregularities are impressed on the wavefront near the point I

With these definitions the problem of specifying the 'size' and 'shape' of the irregularities is reduced to the determination of the value of r_0 (the 'size' transverse to the field) and α (the axial ratio). We now consider some possible observations which enable these quantities to be found.

2. VARIATIONS WITH ZENITH ANGLE

As a satellite passes over an observing station, its zenith angle θ is continually changing (*see* Fig. 2). When θ is large the thickness of the irregular layer intercepted by the ray SIO from the satellite is increased. This leads to increased phase fluctuations across the emerging wavefront. Also, when θ is large there is a greater distance IO for amplitude fluctuations to build up as the wave travels to the receiver at O. For both reasons the depth of the amplitude scintillations would be expected to increase with increasing zenith angle. Further, it may happen that for some value of θ the ray SIO is along the direction of the earth's magnetic field. The wave then travels along the 'long axis' of the ellipsoidal irregularities, and this produces the maximum possible phase deviations. Especially strong scintillations would therefore be expected whenever the satellite is viewed in the direction of the magnetic field. This 'aspect-sensitive' effect will be more marked the greater the axial ratio α.

These effects can be worked out quantitatively (Briggs and Parkin, 1963) and some of the results are shown in Fig. 3. Fig. 3(a) shows the variation of scintillation depth with zenith angle in the magnetic meridian plane for observations of the proposed Beacon Satellite S66 made at Adelaide. The peak at an angle of about 25 from° the

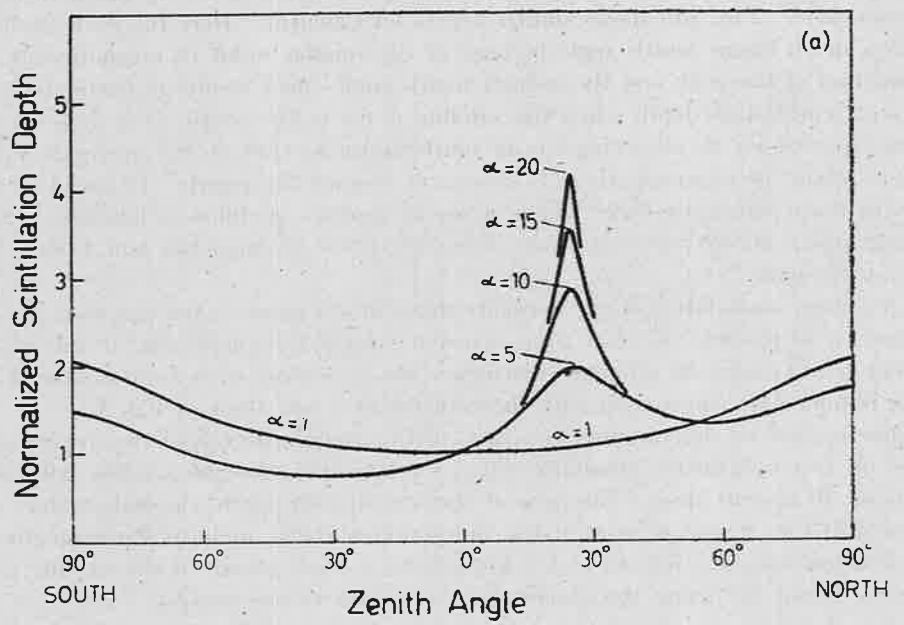

Fig. 3(a), (b) and (c) — The zenith angle variation of scintillation depth in the magnetic meridian plane for observations of a satellite at a height of 1000 km., when the layer of irregularities is at a height of 300 km. The parameter r_0 is taken to be 1 km., and curves are plotted for different values of axial ratio α. The frequency is 20 Mc/s. (a) Adelaide (dip angle = 66°), (b) Calcutta (dip angle = 27°), (c) South India (dip angle = 0). The curves are normalized to the same value at the zenith.

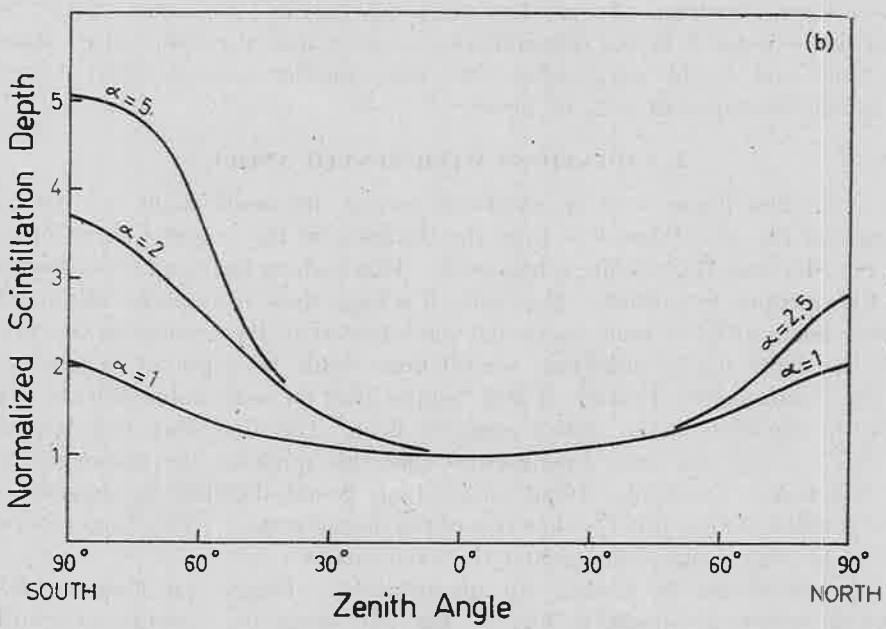

Fig. 3(b)

zenith occurs when the radio wave travels along the direction of the magnetic field in the ionosphere. Fig. 3(b) shows similar curves for Calcutta. Here the peak has moved out to a much larger zenith angle because of the smaller value of magnetic dip. The combination of the peak and the normal zenith angle effect results in particularly large values of scintillation depth when the satellite is far to the south. Fig 3(c) shows the curves expected for an observing site in southern India, close to the magnetic equator. Here, as would be expected, there is symmetry around the zenith. It would be useful to verify these results by observations made at stations at different latitudes. So far, the only observations reporting such effects are those of Singleton and Lynch (1962) made at Brisbane.

Of course, a satellite will not normally move in the plane of the magnetic meridian. However, it is possible to select times when it crosses this plane, and it will do so at different zenith angles on different occasions. By combining such results, a mean curve can be obtained for comparison with theoretical curves like those of Fig. 3.

One method for determining the ' size ' of the irregularities (r_0) is to observe scintillations on two frequencies simultaneously. For example, the S66 satellite will provide signals on 20 and 40 Mc/s. The *ratio* of the scintillation depths depends mainly on r_0, as shown in Fig. 4, and is more or less independent of the angle to the magnetic field. The variation shown in Fig. 4 can be obtained for a *single* transit of the satellite, and so r_0 can be found by fitting the observed ratios to one of the curves.

3. DETERMINATION OF THE HEIGHT OF THE IRREGULARITIES

We assume that the irregularities are situated at a mean height of h and that the thickness of the layer Δh is small compared with h (Fig. 2). The problem now is to

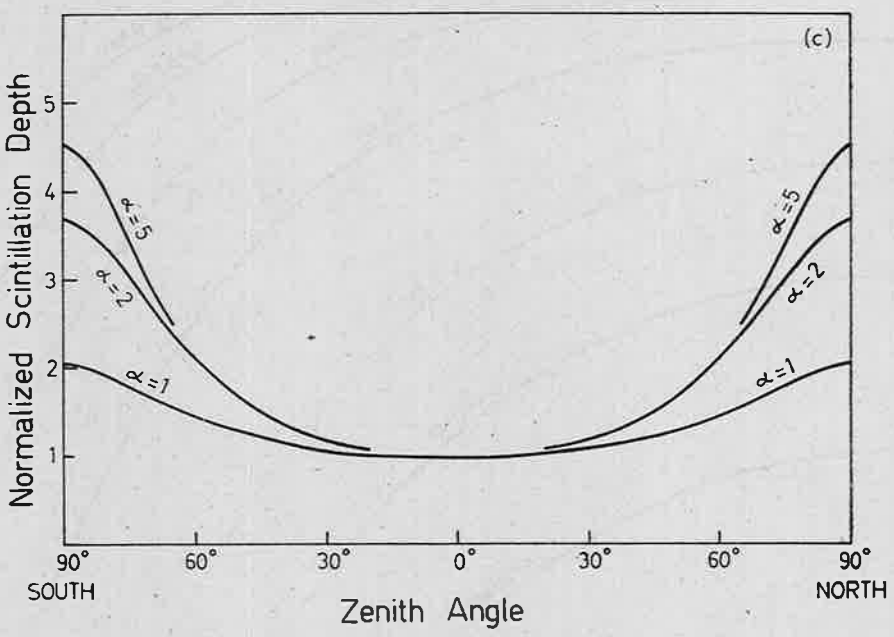

Fig. 3(c)

determine h, and if possible also Δh, from observations made with a number of receivers on the ground.

In one simple method the ray SIO is considered as an optical lever which is instantaneously 'pivoted' at I within the irregular layer. The motion of the diffraction pattern over the ground at O is due principally to rotation of this lever as the satellite S moves, with smaller and usually negligible contributions from movements of the layer tself.

The velocity of the pattern arising in this way is given by

$$v = \frac{-h}{H-h}.V \qquad \ldots(3)$$

for a satellite moving with velocity V near the zenith.

Frihagen and Troim (1960) have made use of this result. They arranged two receivers at a known separation along the path of a satellite so that the diffraction pattern moved parallel to the line joining the receivers. Following the Mitra method (Mitra, 1949), they determined the time delay between the occurrence of a recognizable signal 'shape' at the two receivers and deduced from it the drift velocity of the pattern. This and a knowledge of the altitude and velocity of the satellite enabled them to find the height of the irregular region which they put at about 350 km.

In the analysis of their records Frihagen and Troim found a considerable spread in the values deduced for pattern velocity on any one occasion. Such a spread is due, in the main, to the finite thickness of the irregular layer, the higher parts of the layer contributing to the ground pattern, a structure which moves with a greater speed than that due to the lower parts. The differential form

$$\Delta v = -\frac{HV}{(H-h)^2}\Delta h \qquad \ldots(4)$$

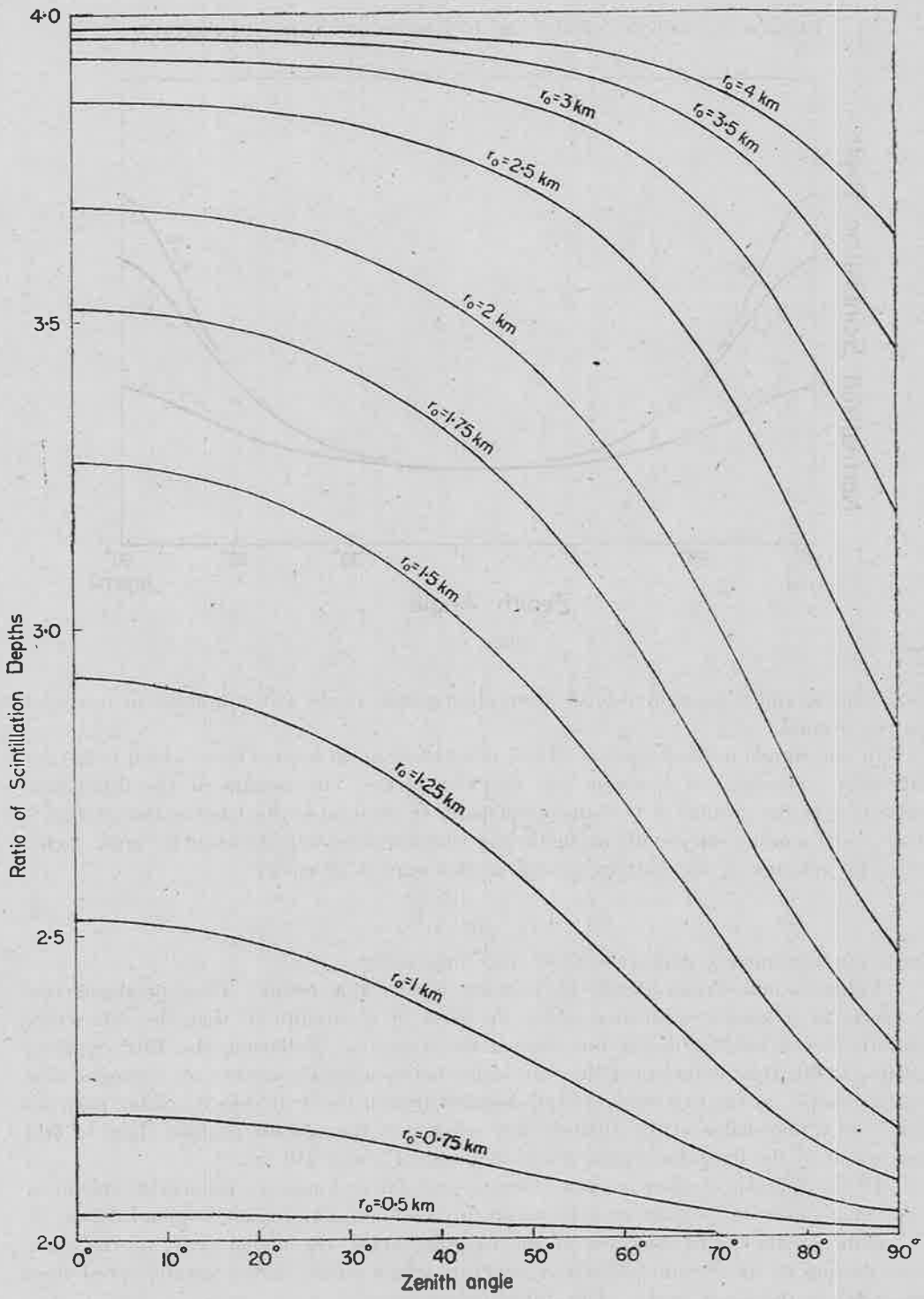

Fig. 4 — The ratio of the scintillation depth on 20 Mc/s. to the scintillation depth on 40 Mc/s. as a function of zenith angle, when the source is a satellite at a height of 1000 km. The irregularities are assumed to be at 300 km., but the curves are not very sensitive to the height assumed

derived from the previous equation, permits an estimate of the layer thickness Δh to be made when the spread in pattern velocity Δv is known.

A rigorous treatment of these methods is to be found in the correlation analysis of Briggs, Phillips and Shinn (1950) and Phillips and Spencer (1955). There well-defined measures of the mean pattern velocity and the velocity spread are determined accurately from the cross-correlation functions of records taken at three spaced receiving points. James (1962) has related these measures theoretically to the height and thickness of the irregular region. His results have not yet been applied in practice.

4. INFORMATION OBTAINED BY FOURIER METHODS

We have seen in Section 2 that the parameters r_0 and α can be determined from the behaviour of the scintillation depth with zenith angle. It is reasonable to expect, in a different approach to the evaluation of these parameters, that the diffraction image on the ground will have spatial dimensions closely related to those of the irregularities. A brief consideration of the diffraction process will outline this relationship.

It will be necessary to define two more correlation functions. The two-dimensional correlation function of the phase variation which appears across a wavefront emerging from the irregular region will be denoted by $\rho_\phi(\xi, \eta)$. At the radio frequencies which concern us the phase deviation at any point is proportional to the integrated electron density along the ray through that point. It follows that the phase fluctuations represent ' projections ' of the electron density irregularities onto the wavefront and in the same sense the two-dimensional function $\rho_\phi(\xi, \eta)$ is the projection of the three-dimensional function $\rho_N(r, s)$ defined in Section 1. $\rho_\phi(\xi, \eta)$ has elliptical contours whose shape and dimensions are directly related to the corresponding characteristics of $\rho_N(r, s)$ (Briggs and Parkin, 1963).

At the ground we define the correlation function $\rho_A(\xi, \eta)$ which describes the spatial behaviour of the two-dimensional pattern of signal amplitude. The ' shape ' of this function is that of a typical structure in the amplitude pattern.

Fourier transformation of the functions $\rho_\phi(\xi, \eta)$ and $\rho_A(\xi, \eta)$ gives the power spectra of the variations they describe. $W_\phi(\nu_1, \nu_2)$ and $W_A(\nu_1, \nu_2)$ are respectively the spatial power spectra of the emerging phase pattern and the ground amplitude pattern.

The relationship between $\rho_\phi(\xi, \eta)$ and its ' image ' $\rho_A(\xi, \eta)$ depends upon the extent to which any sinusoidal phase component is reproduced as a corresponding amplitude component when the wave has travelled to the ground.

This aspect of diffraction theory has been treated by Bowhill (1961). For a screen which produces a shallow irregular fluctuation of phase in a wave, the two power spectra are related by

$$W_A(\nu_1, \nu_2) = W_\phi(\nu_1, \nu_2) \sin^2[\Pi z\lambda(\nu_1^2+\nu_2^2)] \qquad \ldots(5)$$

where z is the distance from the diffracting screen to the plane in which the amplitude pattern is examined.

Application of this result to scattering by a screen of the type defined by our function $\rho_N(r, s)$ leads to an analytic expression for $\rho_A(\xi, \eta)$ which can be written in terms of r_0 and α. Without quoting the expression we can say that the characteristic contour (at the $1/e$ level) of the function $\rho_A(\xi, \eta)$ is approximately elliptical. Its spatial

dimensions do not differ by more than a factor of two from those of the corresponding contour of $\rho_\phi(\xi, \eta)$.

In practice $\rho_A(\xi, \eta)$ is determined from records of signal amplitude taken at spaced receivers. In the correlation analysis of Briggs, Phillips and Shinn (1950), three such records are used. The assumption is made that $\rho_A(\xi, \eta)$ has elliptical contours and the semi-minor axis, the axial ratio and the orientation of the major axis of the characteristic ellipse are found. The first two of these parameters we know to be related to r_0 and α. The last, the orientation of the axis, will give information on the field aligned nature of the irregularities.

The possibility of another interesting experiment arises from a consideration of Eq. (5). The function

$$F(\lambda, z, \nu_1, \nu_2) = \sin^2 [\Pi z\lambda(\nu_1^2+\nu_2^2)] \qquad ...(6)$$

which modifies the power spectrum of the phase fluctuations has circular symmetry and distinctive zeroes at radii given by

$$(\nu_1^2+\nu_2^2)^{1/2} = (n/z\lambda)^{1/2}, \quad n = 0, 1, 2 \qquad ...(7)$$

From a determination of $\rho_A(\xi, \eta)$ over the ground using a large number of receivers, it should be possible by Fourier transformation to obtain enough information to fix the zeroes of $F(\lambda, z, \nu_1, \nu_2)$. The use of Eq. (7) will then provide a value of z corresponding to the height of the irregular region. This should of course agree with the value determined by the method of Section 3.

The results which have been given in this section are only applicable to diffraction by a thin phase screen. The theoretical problem of diffraction by a thick irregular screen has been considered by Tatarski (1961) and Budden (1964).

5. OTHER METHODS

The irregular regions in the ionosphere which cause scintillations often seem to be of limited horizontal extent. Satellite methods are particularly suitable for locating localized ' patches ' of irregularities. It is also possible to determine the sizes and heights of the patches. In this type of observation, the time of onset and cessation of scintillation is observed at several stations separated by a few hundred kilometres. Then by triangulation it is possible to locate the positions in space of the ' edges ' of the irregular regions.

The results of observations of this type seem to show that there is a well-defined boundary at about 54° magnetic latitude, such that irregularities always exist to the poleward side of the boundary and are continuous. On the equatorial side of the boundary, however, irregularities tend to occur in discrete regions with north-south dimensions of a few hundred kilometres, and east-west dimensions probably in excess of 1000 km. (Munro, 1963). The latter results are in agreement with the observed sizes of patches of irregularities which cause spread-F echoes (Briggs, 1958).

CONCLUSION

A number of methods have been described which enable useful information about ionospheric irregularities to be obtained by observing the scintillations of radio signals received from satellites. From the experimental point of view the methods are simple,

as they require no more than a number of radio receivers and chart or film recorders. It would be useful to carry out such observations at many places on the earth.

REFERENCES

1. Bowhill, S. A., *J. Res. Nat. Bur. Stand.*, **65D** (1961), 275.
2. Briggs, B. H., *J. atmos. terr. Phys.*, **12** (1958), 34.
3. Briggs, B. H. & Parkin, I. A., *J. atmos. terr. Phys.*, **25** (1963), 339.
4. Briggs, B. H., Phillips, G. J. & Shinn, D. H., *Proc. phys. Soc.*, **63B** (1950), 106.
5. Budden, K. G., 1964, in press.
6. Frihagen, J. & Troim, J., *J. atmos. terr. Phys.*, **18** (1961), 75.
7. Hook, J. L. & Owren, L., *J. geophys. Res.*, **67** (1962), 5353.
8. James, P. W., *J. atmos. terr. Phys.*, **24** (1962), 237.
9. Mercier, R. P., *Proc. Camb. Phil. Soc.*, **58**, Pt. 2, (1962), 382.
10. Mitra, S. N., *Proc. Instn elect. Engrs*, Pt. III, **96** (1949), 441.
11. Munro, G. H., *J. geophys. Res.*, **68** (1963), 1851.
12. Phillips, G. J. & Spencer, M., *Proc. phys. Soc.*, **68B** (1955), 481.
13. Ratcliffe, J. A., *Rep. Prog. Phys.* Vol. 19 (Physical Society, London) (1956), 188.
14. Singleton, D. G. & Lynch, G. J. E., *J. atoms. terr. Phys.*, **24** (1962), 363.
15. Tatarski, V. I., *Wave Propagation in a Turbulent Medium* (McGraw-Hill Book Co. Inc., New York), 1961.
16. Wagner, L. S., *J. geophys. Res.*, **67** (1962), 4195.